Experimental investigation of heterogeneous nucleation of ice in remote locations

Alessia Nicosia

DOCTORAL COURSE
IN PHYSICS

CYCLE XXXI

Scientific Disciplinary Sector (SDS):
FIS/06

DOCTORAL COURSE
IN GEOLOGY

VERS. 701

Speciality: Atmospheric Physics-
Chemistry and Climate

Doctoral Thesis with joint co-tutorship of:
Università degli Studi di Ferrara and Université Clermont Auvergne
for the obtention of the degree "European Doctorate".

Years 2015/2018

Experimental investigation of heterogeneous nucleation of ice in remote locations.

Candidate
Nicosia Alessia

Supervisor
Prof. Porcù Federico

Supervisor
Sellegri Karine

Co-Supervisor
Belosi Franco

Public defence done the 14th Dec. 2018 in front of the members of the examining committee.

President:

Prof. Guidi Vincenzo	Università degli Studi Di Ferrara

Reviewers:

Möhler Ottmar	Karlsruhe Institute of Technology
Wex Heike	Leibniz Institute for Tropospheric Research
Prof. Hinrich Grothe	TU Wien - Institute of Materials Chemistry

Examining Committee:

Prof. Flossmann Andrea	CNRS - UCA - Laboratoire de Météorologie Physique
Prof. Levizzani Vincenzo	CNR - Institute of Atmospheric Sciences and Climate
Wex Heike	Leibniz Institute for Tropospheric Research
Amato Pierre	CNRS - UCA - SIGMA - Institut de Chimie de Clermont-Ferrand
Sellegri Karine	CNRS - UCA - Laboratoire de Météorologie Physique
Prof. Guidi Vincenzo	Università degli Studi Di Ferrara

Abstract (English Version)

Title: Experimental investigation of heterogeneous nucleation of ice in remote locations.

Keywords: Ice nuclei particles; Heterogeneous freezing; Cimone Mountain; Arctic; Sea Spray.

Heterogeneous ice nucleation is one element inside the overall complexity of the Earth's atmosphere, however, it has a profound impact on our representation of cloud properties: this process affects the optical thickness and lifetime of mixed-phase clouds and cirrus clouds, and it is responsible for a significant proportion of precipitations formed globally. Heterogeneous ice nucleation is related to the presence of specific aerosol particles, named ice nuclei particles (INP), with the unique ability of lowering the energy barrier required for the formation of ice crystals, especially where cloud's temperatures are >-38 °C. In the last decades, significant advancements have been made to the fundamental understanding of ice nucleation, however the lack of knowledge on the cloud ice phase still contributes to major uncertainties in climate model prediction of radiative forcing. This is partly due to limited observational data quantifying INP distributions and properties all over the world, especially in remote locations.

In the first part of this thesis, field observations of ice nucleating particles have been performed at the Italian Climate Observatory "O. Vittori" on Mountain Cimone (2165 m above sea level), in the spring 2014 and autumn 2015, within the Bacchus and Air Sea Lab projects. For the first time we report the results of offline INP measurements, performed at a high altitude site within the Mediterranean basin. In the period 19-29 May 2014, a parallel campaign took place at the low-altitude station San Pietro Capofiume, a rural site in the Po Valley. The two campaigns were concerned, for a few days, by a Saharan Dust transport Event, which was recorded simultaneously at the high and the low-level station. We investigated the ambient number concentration of INP under condensation freezing activation mechanism (at -18 °C and above water saturation).

In the second part of this thesis, we present the observations that were performed during the Arctic campaign Parcs-Maca, in the period of transition among the polar night and the polar day. We could characterise for the first time the ice nucleating and physical/chemical properties of the Arctic Primary Marine Aerosol, in a laboratory-controlled generation approach, that was combined to a mesocosm experiment. The aim of the mesocosm experiment was to adopt a multidisciplinary approach to study the effect of marine pollution on marine emissions. We found a moderate but significant decrease of the ice nuclei concentration in the polluted seawater (with respect to the control seawater) recorded in the freezing range between -8.5 and -19 °C and activated through immersion-freezing. Within the seaspray our measurements have indicated a relation among INP active at warm temperature (above -15 °C through immersion-freezing) and a calcium enrichment detected in PM1 filters (and followed by an apparent Chloride depletion). On the basis of our observations, and the results reported from other studies, a few suggestions on the nature of these marine ice nuclei have been suggested.

In summary, the measurements made for this thesis provide new information on the concentrations of ice nuclei in ambient aerosol particles in remote regions (a high-altitude observatory in the central Mediterranean region) and in relation to a specific source (the Arctic sea spray).

Abstract (Italian Version)

Titolo: Studio sperimentale della nucleazione eterogenea del ghiaccio in zone remote.

Parole Chiave: Nucleatori del Ghiaccio; Nucleazione eterogenea; Monte Cimone; Artide; Spray Marino.

La nucleazione eterogenea del ghiaccio é solo uno dei molteplici fattori che riguardano le complesse dinamiche dell'atmosfera terrestre, eppure il suo impatto sulle proprietà e sull'evoluzione delle nubi é determinante: infatti la formazione del ghiaccio in nube influenza sia le proprietà ottiche che il tempo di vita ed evoluzione delle nubi miste e fredde, ed é legata alla formazione delle precipitazioni su scala globale. La formazione eterogenea del ghiaccio é legata alla presenza di specifiche particelle di aerosol, chiamati nucleatori del ghiaccio (acronimo 'INP' dall'inglese Ice Nuclei Particles), particelle con l'abilità di abbassare la barriera energetica richiesta per la formazione dei cristalli di ghiaccio, e il cui ruolo é influente per temperature di nube >-38 °C. Anche se significativi avanzamenti sono stati fatti negli ultimi decenni nella descrizione dei nucleatori del ghiaccio, la loro comprensione é incompleta e cio' influenza le incertezze sulle stime di forcing radiativo nei modelli climatici. Tutto cio' é legato anche ad una mancanza di osservazioni sulle distribuzioni e proprietà degli 'INP' su scala globale, specialmente in zone remote.

Nella prima parte di questa tesi, misure sperimentali di nucleatori del ghiaccio sono state eseguite all'Osservatorio Climatico Italiano "O. Vittori" sulla cima del Monte Cimone (2165 m sopra il livello del mare), nella primavera 2014 e autunno 2015, nel contesto dei progetti Bacchus e Air Sea Lab. Per la prima volta, si riportano i risultati di misure offline di 'INP' ad alta quota nel bacino del Mediterraneo. Nel periodo 19-29 Maggio 2014, in parallelo é stata svolta un'ulteriore campagna di misura presso San Pietro Capofiume, una zona rurale della pianura Padana. In alcuni giorni entrambe le campagne di misura sono state interessate da un evento di trasporto di polveri Sahariane, registrato contemporaneamente presso le due stazioni. La concentrazione atmosferica di 'INP' é stata valutata rispetto al meccanismo di attivazione detto condensation-freezing (a -18 °C e in condizioni di sovrassaturazione).

Nella seconda parte della tesi, le osservazioni sono state eseguite durante la campagna di misura Parcs-Maca in Artide, nel periodo di transizione fra la notte polare e il giorno polare. E' stato possibile caratterizzare per la prima volta le proprietà nucleanti e fisico/chimiche dell'Aerosol Marino Primario Artico, tramito un approccio di generazione controllata in laboratorio, combinata ad un esperimento di tipo mesocosmo. L'esperimento in mesocosmo ha permesso di adottare un approccio multidisciplinare per studiare l'effetto dell'inquinamento marino sulle emissioni marine. E' stata trovata una moderata ma significativa diminuzione nella concentrazione dei nucleatori del ghiaccio nell'acqua di mare inquinata (rispetto ai campioni di acqua di mare del sistema di controllo) attivati tramite immersion-freezing nell'intervallo di congelamento fra -8.5 e -19 °C. Le misure effettuate sullo spray marino hanno indicato una relazione fra i nucleatori del ghiaccio attivi a temperature più calde (> -15 °C attivati tramite immersion-freezing) e un arricchimento di calcio rilevato in filtri PM1 (e accompagnato da un apparente riduzione di Cloro). Sulla base delle osservazioni effettuate, e dei risultati riportato in altri studi, sono state suggerite alcune indicazioni sulla natura dei nucleatori biologici marini.

In conclusione, le misure fatte durante questa tesi forniscono nuove informazioni sulle concentrazioni di INP per l'aerosol atmosferico di una zona remota (un osservatorio ad alta quota nel bacino centrale del Mediterraneo) e in relazione a una sorgente specifica (lo spray marino Artico).

Abstract (French Version)

Titre: Etude expérimentale de la nucléation hétérogène de la glace en régions éloignées.

Mots clefs: noyaux glaçogènes; nucléation hétérogène; montagne Cimone; Arctique; Spray Marin.

La nucléation hétérogène de la glace est un processus, entre autres, qui concerne les phénomènes complexes de l'Atmosphère terrestre, cependant son impact est déterminant pour les propriétés et le temps de vie des nuages : ce processus affecte l'épaisseur optique et la durée de vie des nuages en phase mixte et froide et il est responsable d'une proportion significative des précipitations à l'échelle mondiale. La nucléation hétérogène de la glace est liée à la présence de particules d'aérosol spécifiques, nommées noyaux glaçogènes (acronyme INP depuis l'anglais), avec la propriété de réduire l'énergie de seuil exigée pour la formation des cristaux de glace, et dont le rôle est influent pour des températures de nuage >-38 °C. Dans les dernières décennies, des avancements significatifs ont été faits dans la description des noyaux glaçogènes, cependant leur compréhension reste incomplète et ceci influence les incertitudes sur les estimations de forçage radiatif dans les modèles climatiques. Il manque un grand nombre d'observations sur les distributions et propriété des 'INP' à l'échelle globale, spécialement en région éloignée.

Dans la première partie de cette thèse, sont présentées des mesures de noyaux glaçogènes faites à l'Observatoire Climatique Italien "O. Vittori" sur la Montagne Cimone (2165 m au-dessus du niveau de la mer), pendant le printemps 2014 et l'automne 2015, sous les projets Bacchus et Air Sea Lab. Pour la première fois des mesures de INP hors ligne, reliés à un site de haute altitude du bassin méditerranéen sont présentées. Pendant la période du 19 au 29 mai 2014, une autre campagne a eu lieu en parallèle à la station San Pietro Capofiume, un site rural de basse altitude dans la Vallée du Po. Pendant quelques jours, les deux campagnes ont été concernées par un phénomène de Transport de Poussière Saharienne, qui a été enregistré simultanément dans la station de bas et de haute altitude. Nous avons examiné la concentration atmosphérique de INP activés à travers une congélation par condensation de vapeur (à -18°C et au-dessus de la pression de vapeur saturante).

Dans la deuxième partie de cette thèse, sont présentées les observations qui ont été menées pendant la campagne arctique Parcs-Maca, dans la période de transition entre la nuit polaire et le jour polaire. Pour la première fois on reporte la caractérisation des propriétés glaçogènes et physiques/chimiques de l'aérosol marin primaire Arctique, dans une approche de génération contrôlée en laboratoire, qui a été combinée à une expérience de mesocosm. Le but de l'expérience de mesocosm était d'adopter une approche pluridisciplinaire afin d'étudier l'effet de la pollution marine sur les émissions marines. Nous avons trouvé une diminution modérée mais significative de la concentration de noyaux glaçogènes dans l'eau de mer polluée (par rapport à l'eau de mer du contrôle) pour des noyaux glaçogènes actives en congélation par immersion entre -8.5 et -19 °C. En ce qui concerne le spray marin, nos mesures indiquent une relation parmi les INP actifs à des températures chaudes (en congélation par immersion et au-dessus de -15 °C) et un enrichissement du Calcium détecté dans les filtres PM1 (suivi par un apparent épuisement du Chlorure). Sur la base de nos observations et des résultats publiés en littérature, quelque indication a été suggéré sur la nature de ces noyaux glaçogènes marins.

En conclusion, les mesures effectuées dans cette thèse fournissent des nouvelles informations sur les concentrations de noyaux glaçogènes pour des particules d'aérosols en régions éloignées (un observatoire à haute altitude dans la région méditerranéenne centrale) et par rapport à une source spécifique (le spray marin Arctique).

Contents

1 Introduction **1**

1.1 The study of atmospheric ice nucleation . . . 3

1.1.1 Homogeneous Freezing . . . 4

1.1.2 Heterogeneous Freezing . . . 5

1.2 Atmospheric aerosols . . . 8

1.3 Atmospheric aerosols and their role in ice nucleation . . . 10

1.4 Instrumental methods and critical aspects . . . 15

1.5 Open questions . . . 16

1.6 Aim and scope of this thesis . . . 20

2 Materials and methods **23**

2.1 Introduction . . . 23

2.1.1 Aerosol Size Distribution . . . 26

2.1.2 Aerosol Mass Spectrometer . . . 28

2.2 Immersion freezing measurement technique . . . 29

2.3 Condensation (and deposition) freezing measurement technique . . . 31

2.3.1 Improvements . . . 35

2.3.2 Operating procedure . . . 36

2.3.3 Instrument validation experiments . . . 37

3 Ice Nucleating Particle Measurements within BACCHUS and Air-Sea Lab **41**

3.1 Methods . . . 42

3.2 Results . . . 44

3.2.1 Ice nucleation rates at Mountain Cimone in May 2014 . . . 44

3.2.2 Ice nucleation rates at Mountain Cimone in October 2015 . . . 46

3.2.3 Ice nucleation rates at SPC in May 2014 . . . 46

3.3 Influence of the saturation ratio versus freezing temperature on the measured INP concentrations . . . 48

3.4 Effect of the Saharan dust event on INP atmospheric concentration . . . 50

3.5 Effect of vertical transport and synoptic circulation on IN concentration at MC 51

3.6 Conclusions . . . 55

3.7 Acknowledgments . . . 57

4 The Arctic measurement campaign PARCS-MACA **59**
4.1 Introduction . . . 59
4.2 PARCS-MACA . . . 61
4.3 Experimental design . . . 63
4.3.1 Sample generation and collection from the control mesocosm . . . 65
4.4 Number of ice nuclei in the seaspray . . . 66
4.4.1 DFPC results . . . 66
4.4.2 FNA results . . . 71
4.4.3 FNA and DFPC result inter-comparison . . . 73
4.5 Ice nucleation rates of seawater . . . 75
4.5.1 Test–retest of bulk seawater immersion freezing tests . . . 76
4.5.2 IN in the bulk seawater . . . 79
4.5.3 The impact of pollutants and external conditions on seawater ice nuclei content . . . 82
4.5.4 Ice nucleation rates of filtered seawater . . . 85
4.6 Sea Spray size distribution and chemical analysis . . . 86
4.6.1 Sea Spray size distribution . . . 86
4.6.2 Chemical composition, inorganic fraction . . . 89
4.6.3 Chemical composition, organic fraction . . . 91
4.6.4 Parameters influencing ice nuclei concentration in the seaspray . . . 93
4.6.5 Comparison with literature . . . 96
4.7 Conclusions . . . 98
4.8 Acknowledgments . . . 101

5 Conclusions and Future Perspectives **103**
5.1 Introduction . . . 103
5.2 DFPC and FNA instruments . . . 105
5.3 Ice Nucleating properties at the GAW station Cimone Mountain . . . 106
5.4 Ice nucleation properties of ice nuclei in the Arctic marine environment . . . 107
5.5 Achievement . . . 109
5.6 Implication of our findings . . . 109
5.7 Perspective . . . 110

A Bergeron–Findeisen process **113**

B Image analysis for dfpc **115**

C Source Code **121**

D Particle Size Distribution from OPC and DMPS **125**

Bibliography **129**

Chapter 1

Introduction

> Water remarkably only accounts for 0.25% of the total mass of the atmosphere. That's equivalent to a liquid layer of only 2.5 cm deep (barely enough to make a global puddle)...almost (99.5%) in the form of vapour.
>
> Stevens and Bony, 2013 [1]

Clouds are essential to all living things. About 70% of the Earth's surface is covered by clouds [2] that contribute to the energy and water cycle of our planet. Not only clouds distribute water across the surface of the globe, being linked to the hydrological cycle, they also play a crucial role for the Earth's climate and weather.

Droplets, simple crystals, snowflakes, graupel and hail are all condensed forms of water that can be found in clouds, at different size ranges, as illustrated in Figure 1.1. Their dimension (with respect to the electromagnetic radiation's wavelength) and their refractive index determine their ability of scattering and absorbing the electromagnetic radiation, thus affecting energy balance and heat redistribution in the atmosphere.

The formation of clouds and precipitations depends on a combination of dynamical, microphysical and radiative processes, which are often entangled. Microphysical processes are also connected to the availability of aerosol particles. Atmospheric aerosols are suspended particulate matter, of typical size between 0.01-10 μm, with a resident time in the atmosphere of at least several hours. It has long been recognised that the formation and evolution of clouds are strongly influenced by aerosol particles [3].

Clouds form when an air parcel rises, expands and cools down, so the water vapours start condensing on aerosol particles and form either liquid droplets or ice crystals. Clouds that contains only water droplets are referred to as *liquid clouds*. In liquid clouds, droplets can grow by condensation in a supersaturated environment and by colliding and coalescing together. When temperatures are low enough, ice crystals nucleate on aerosol particles and grow at the expense of liquid cloud droplets, as described by the *Wegener-Bergeron-Findeisen* process (see page 113).

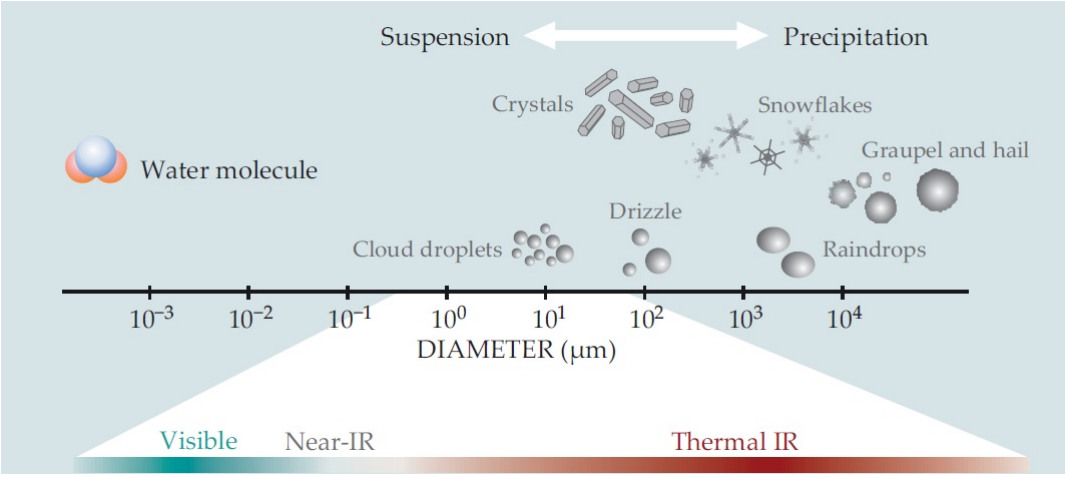

Figure 1.1: Hydrometeors, the condensed forms of water in the atmosphere, come in several sizes. They mostly scatter visible light but absorb over a broad range of the infrared radiation (IR) spectrum. Figure rearranged from Stevens and Bony, 2013 [1].

When liquid droplets and ice crystals coexist, the cloud is named *mixed-phase cloud* MPC; when pure ice crystals are prevalent, the cloud is referred to as *cold cloud* (e.g. cirrus clouds).

To better serve local and national climate adaptation planning and decision-making, there is a clear need for improved understanding and prediction of weather [4] and this came with a better comprehension of the aerosols particles interacting with clouds, which are distinguished in Cloud Condensation Nuclei (CCN) and Ice Nuclei Particles (INP). CCN may constitute typically 10% -varying between 10-80%- of the ambient aerosol number concentration [5] and they are involved in the formation of cloud liquid droplets. INP constitute usually $<10^{-4}$% of the ambient aerosol population ([6] , [5], [7]) and are related to the formation of ice crystals. While knowledge has greatly advanced regarding the formation of liquid droplets on CCN (i.e. the cloud liquid phase), the understanding regarding the formation of ice crystals and the role of INP (the ice cloud phase) is still rather patchy [8], [9].

Cloud microphysics contains, as a sub-topic, research on the partitioning of MPC in its liquid and ice water content. This is an active field of research, which includes a number of in situ aircraft measurements, lidar and satellite retrievals. In this context, a deeper comprehension of the ice cloud phase requires the assessment of the mechanism behind ice crystals formation, also referred to *ice nucleation*. A distinction is made between:

- *Primary ice* which is the first ice formed, either from supersaturated vapour or from supercooled liquid water.

- *Secondary ice* which forms only once some ice is already present.

Evidence for the distinction between primary and secondary ice came initially from field observations. When the concentrations of ice crystals in the mixed-phase region of cold clouds ($-38\ ^\circ\text{C} < T < 0\ ^\circ\text{C}$) agree with the measured concentrations of INP, we suspect that they had primary origins, meaning that each crystal likely formed by the activity of one ice nucleus. By contrast, past studies suggest that ice crystal number concentrations within a cloud may well exceed those of ice nucleating particles (Gultepe et al., 2017 [10]) and in this case, we are left with the conclusion that secondary ice processes must have been active. Describing the

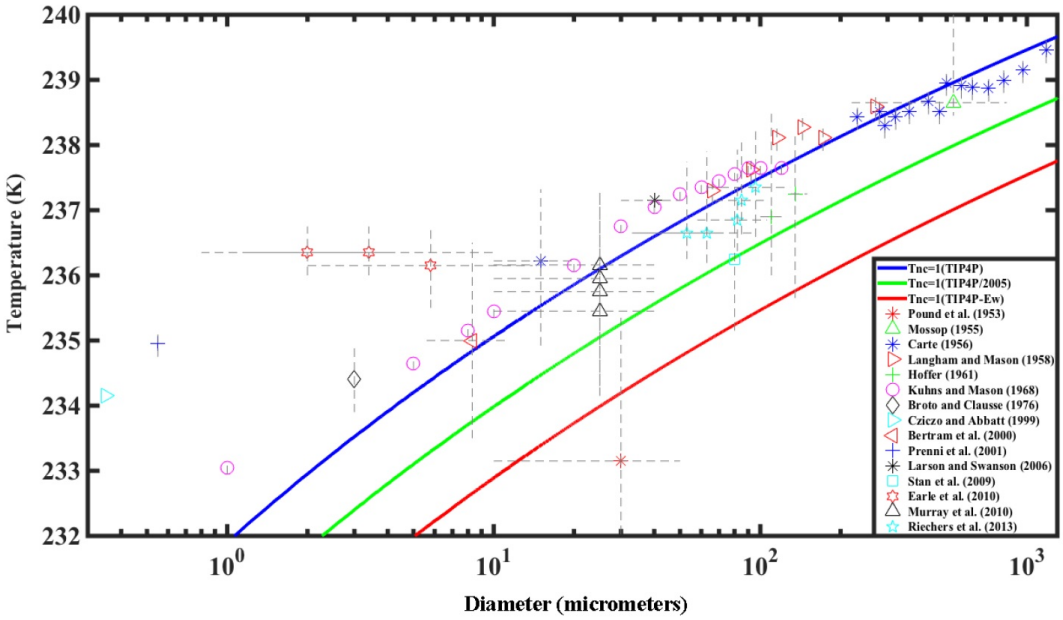

Figure 1.2: Droplet freezing temperature versus diameter for pure water. Comparison between different approximation models (blue line from TIP4P model; green line from TIP4P/2005 model; and red line from TIP4P-Ew model) and several experimental data. Figure taken from O and Wood, 2015 [13]. Refer to the original article [13] for the legend and the experimental studies listed.

contribution of primary ice nucleation to the formation of ice crystals and how this relates to the aerosol particles entering a cloud is the realm of ice nuclei measurements [11].

Primary ice nucleation is dependent on several aspects, and among others, the presence of INP, the height of the cloud top [12], the availability of saturated water vapours, the temperatures and internal cloud dynamic. This field is a cross-community challenge that requires collaboration among different disciplines, such as aerosol science, atmospheric physics, chemistry and biology [4].

Finally, the description of INP is just one element inside the overall complexity of the Earth's atmosphere, however, it has a profound impact on our representation of MPC and cold cloud properties, it is strongly related to the initiation of the ice phase at temperatures warmer than ~ -36 °C [11] and most of all it is connected to the initiation of precipitation.

1.1 The study of atmospheric ice nucleation

Liquid water in household refrigerators is cooled at atmospheric pressure and it freezes when the temperature reaches 0 °C, i.e. at the ice melting temperature. This ice, available in everyday life, has an hexagonal lattice structure, classified with the acronym Ih, in which the molecules of water form an ordered lattice of oxygen atoms while the hydrogens are disordered [14]. But this is not the only solid form of water. In the course of the 20^{th} century other different crystal phases -polymorphs- have been found for solid water (see Vega et., 2011 [14] for a detailed overview). The studying of water in the atmosphere is also surprising and fascinating. Water in

the atmosphere can remain in a liquid state metastable, down to ~ -36 °C (often referred to as supercooled water).

The persistence of liquid water below the melting temperature has been confirmed by both aircraft measurements, e.g. Rosenfeld and Woodley, 2000 [15], and satellite retrievals, e.g. Hu et al., 2010 [16]. This feature is attributed to the small size of liquid water in cloud droplets, also referred to as Super-Cooled Liquid Water Droplets (SCLWD).

A number of theoretical and experimental studies, over the past 60 years, have shown a clear dependence of the freezing temperature upon drop volume, e.g. the study of O and Wood, 2015 [13] reported in Figure 1.2. As mentioned earlier in the introduction, the freezing Temperature (T), together with the Saturation ratio with respect to Water (S_w), and the presence of Ice Nuclei Particles (INP), influence the phase transition of water to the solid phase in the atmosphere, i.e. *primary ice nucleation*.

Primary ice nucleation is formally defined as the process by which the formation of a new daughter phase (e.g. solid) from the parent phase (e.g. liquid) is initiated, Lamb and Verlinde, 2011 [17]. Primary ice nucleation is distinguished in two types of mechanisms: *homogeneous* and *heterogeneous*. In *homogeneous nucleation*, atmospheric ice crystals develop from supercooled water or aqueous solution droplets; while in *heterogeneous nucleation*, the ice phase develops with the help of a pre-existing substrate, i.e. the particle, which initiates the formation of an ice embryo [8]. In presence of , heterogeneous nucleation is the process energetically favoured, as it starts at lower supersaturations and warmer temperatures [8].

1.1.1 Homogeneous Freezing

The homogeneous freezing of a water droplet can be described by the Classical Nucleation Theory (CNT). The phase transition occurs when the free energy of the molecules in the daughter phase, G_{end}, is lower than the free energy in the parent phase G_{start}. The change in the free energy, ΔG_{hom}, caused by the formation of a single cluster, i.e. an embryo, is the sum of two terms: a gain term (volume term) due to the transfer of n_i molecules from the parent to the daughter phase and a loss term (surface term) resulting from the formation of the new interface (Nanev, 2015 [18] and Boose, 2016 [19]):

$$\Delta G_{hom} = \{\underbrace{4\pi r^2 \sigma_{iw}(T)}_{\text{surface term}} - \underbrace{n_i \Delta\mu(t)}_{\text{volume term}}$$

where r is the radius, σ_{iw} is the surface tension between the ice and the water phase, n_i is the number of molecules in the cluster, and $\Delta\mu$ is the chemical potential difference given by the nucleation driving force [18]. The critical cluster size r_c is the minimum size required for the formation of a stable ice germ from the daughter phase. When a cluster arrives at this critical size, then it grows into a macroscopic crystal.

Generally p is calculated as the fraction of frozen droplets to the total number of droplets in a population, over a given time interval.

Wallace and Hobbs (2006) [20] report median freezing temperatures of -41 °C for 1 μm sized water drops and -35 °C for 100 μm. These temperatures are reached in the upper troposphere which is located at approximately 8-16 km depending on latitude [19]. The homogeneous

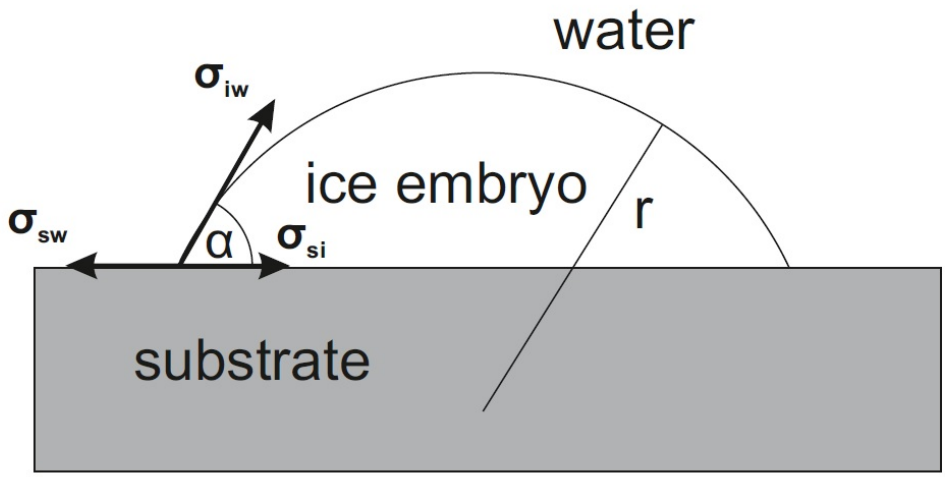

Figure 1.3: Scheme of an ice embryo growing on the surface of an ice nucleating particle, supposed flat for convenience. The contact angle α, the radius of an ice germ, r, and the surface tensions σ between different phases are reported. Picture rearranged from Boose, 2016 [19].

nucleation temperature is further lowered in the atmosphere because drops may contain dissolved salts which leads to a freezing point depression [8]. However, Koop et al., (2000) [21] showed that the homogeneous nucleation of ice from solution droplets is independent of the salt species in the solution and depends only on the water activity. The water activity being defined as the ratio between the water vapour pressure of the solution to that of pure water. Koop et al. (2000) [21] developed a new parameterization in which the effect of solutes are expressed as a function of the water-activity to determine nucleation rates of homogeneous nucleation. In 3-D cloud model, this parametrization may be considered instead of the Classical Nucleation Theory (CNT).

1.1.2 Heterogeneous Freezing

Two different approaches are used to describe heterogeneous freezing theoretically [19] , [22]:

- a *time independent* (also referred to as the *deterministic* [19] or *singular hypothesis* [22])
- a *time dependent* (connected to the Classical Nucleation Theory (CNT), e.g. Fletcher et al., 1962 [23]; Bigg et al., 1953a [24], Bigg et al., 1953b [25])

The *time independent* approach assumes the presence of particular defects on the particle surface, named ice-active sites, Vali, 1966 [26] and Vali, 2015 [27], which reduce the thermodynamic energy barrier to nucleation. They are usually associated with lattice impurities, steps or cracks (Fletcher 1969 [28]; Marcolli et al., 2007 [29]; Marcolli, 2014 [30]). This nucleation approach is independent of time because it assumes that at a constant temperature, the probability of ice formation to take place scales with the surface of the ice nucleating particles. The larger

the surface, the higher is the probability of an active site to occur on a particle. Whether a lattice defect acts as active site depends mainly on the air temperature and the supersaturation conditions. If several particles with active sites are enclosed in a droplet, the freezing is determined by the particle with the strongest active site. This approach has been the basis for a number of parametrisations of heterogeneous nucleation (Connolly et al., 2009 [31]; Lüönd et al., 2010 [32]; Niedermeier et al., 2011 [33]; Niemand et al., 2012 [34]).

The *time dependent approach* is based on the Classical Nucleation Theory (CNT), which assumes ice nucleation as a stochastic process, in which the probability to nucleate ice per surface area is the same for all INP within a sample, under the same thermodynamic conditions. This formulation is time dependent due to fluctuations of temperature and density on a micro-scale [19]. Under these conditions, the Gibbs free energy of heterogeneous nucleation is calculated through a simple modification of ΔG_{hom}. The energy barrier required to form an ice germ heterogeneously ΔG_{het} is decreased by a compatibility function in comparison to ΔG_{hom} of homogeneous freezing, Seinfeld and Pandis, 2006 [35]. This reduction is describe as [23]):

$$\Delta G_{het} = \Delta G_{hom} * f_{\alpha}$$

where f_{α} is a geometric factor. In the simpler case of a planar ice nuclei surface, f_{α} is expressed as:

$$f_{\alpha} = \frac{1}{4}(2 + cos(\alpha))(1 - cos(\alpha)^2$$

where α is the contact angle between the ice embryo and the the surface of the ice nuclei particle, as shown in Figure 1.3. For a particle with a perfect ice nucleating ability f_{α} is set to 0, which represents no energy barrier at all. If the particle does not interact with the nucleating droplet $f_{\alpha} = 1$, which equals the energy barrier for homogeneous freezing.

The contact angle α is derived from the three surface tensions of the ice-substrate (σ_{si}), the ice-water (σ_{iw}) and the water-substrate (σ_{sw}) interface Young, 1805 [36]:

$$cos(\alpha) = \frac{\sigma_{sw} - \sigma_{si}}{\sigma_{iw}}$$

With decreasing size of the ice nuclei particle, the curvature of the surface plays an increasing role and must be considered. In [23] and [8] it is suggested that the nucleation rate decreases rapidly for particles below 0.1 μm. However, Jamieson et al. (2005) [37] showed that the size of an ice nuclei particle only becomes significant when the ice nuclei is of similar size as the critical cluster. The size and the properties that should characterise an active INP particles are still controversial and increases the number of critical aspects (as discussed later in the section *Open Question*). Historically the following requirements were attributed to aerosol particles to be efficient INP [22]:

- highly water-insoluble,
- larger than approximately 0.1 μm,
- crystallographic structure which fit with the ice lattice.

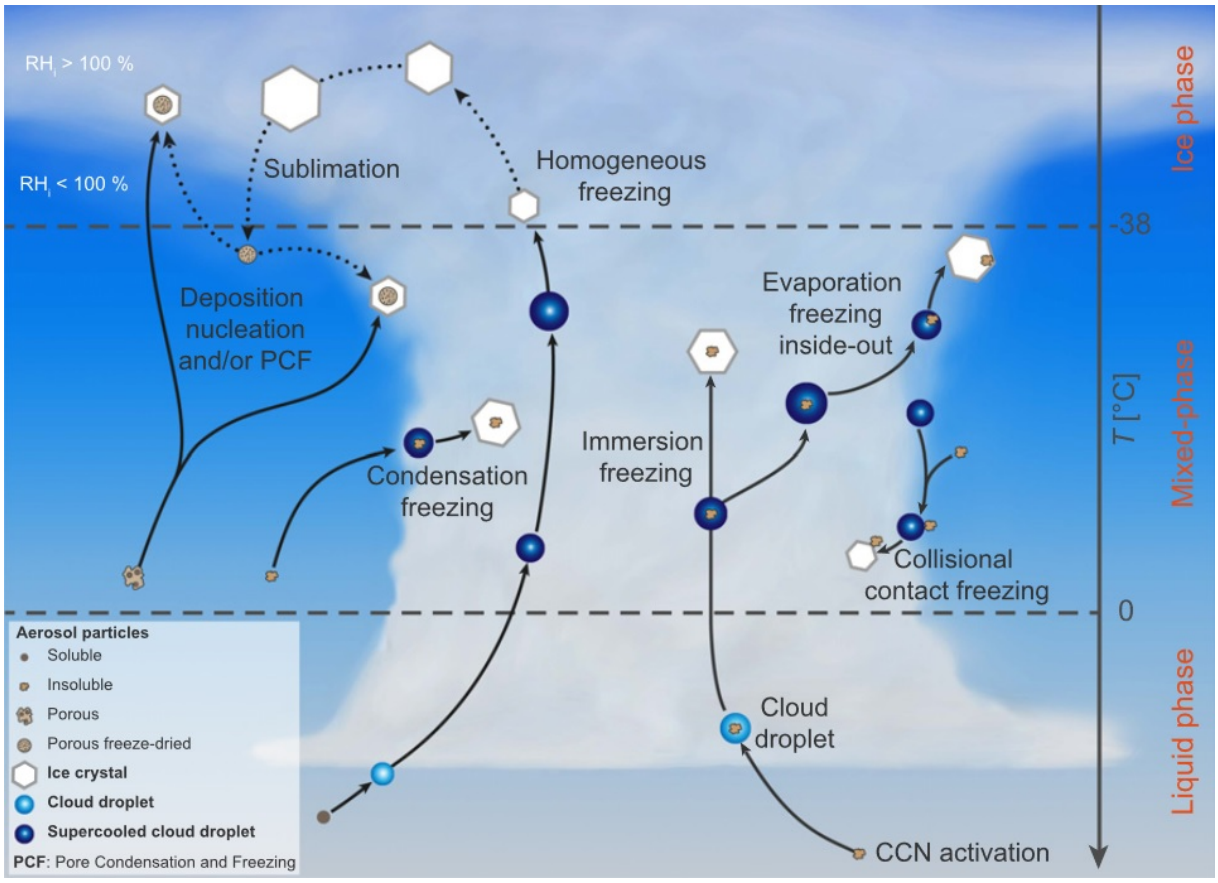

Figure 1.4: Schematic depicting known primary ice nucleation pathways possible in the atmosphere. Figure taken from Kanji et al., 2017 [38].

As reported in [38], these properties are no more considered as mandatory. The most important accepted ice nuclei in the atmosphere, which fulfil the above mentioned requirements, is the group of mineral dust particles (e.g. clays -kaolinite, illite, montmorillonite-, quartz, feldspars, and calcite) described in Zolles et al., 2015 [39]. Within this group, K-feldspar is considered the most important mineral dust for ice nucleation [38].

In addition to the chemical and physical properties of ice nuclei active particle, one may consider that a number of several pathways -in Figure 1.4- have been identified for heterogeneous ice nucleation to take place, Rogers and Yau, 1989[40] and Pruppacher and Klett, 1997 [8]. Historically, the main four pathways, also called *activation modes*, are:

- *deposition nucleation* when ice forms from supersaturated water vapours -with respect to ice- which deposit directly on the ice nucleus surface, at S_i>1;

- *immersion freezing* when the ice nucleus is already immersed in a supercooled aqueous droplet which freeze at the INP activation freezing temperature T_{act}^{imm};

- *condensation freezing* when water vapours condenses on the ice nucleus surface at S_w>1, and then, in a consecutive step, the liquid film freeze at the activation freezing temperature T_{act}^{cond};

- *contact freezing* when ice formation is induced by collision of a supercooled droplet with an ice nucleus, at the activation freezing temperature T_{act}^{cont}.

It is generally assumed that $T_{act}^{imm} \neq T_{act}^{cond} \neq T_{act}^{cont}$, then each mechanism may be distinguished by different and S_w/S_i conditions.

A number of controversy are still open in relation to the activation modes classification. For example, condensation freezing may be included in the immersion freezing mode or another mode. Following [27] it is not fully established if condensation freezing is truly different from immersion freezing or deposition nucleation, at the microscopic scale [38].

In conclusion, a large number of variables and mechanisms need to be considered to describe heterogeneous freezing. Thus the formulation of the number of nucleated ice crystals expected from a population of solid aerosol particles, based on field measurements or nucleation theory (e.g. Meyers et al., 1992 [41]; Phillips et al., 2008 [42]; Hoose et al., 2010b [43]) is still considered a challenging task of current research.

1.2 Atmospheric aerosols

Atmospheric aerosols contribute to the largest uncertainty in the global radiative forcing: on one hand aerosols have the ability to scatter and/or absorb the incoming solar and terrestrial radiation (*aerosol direct effect*); on the other hand, aerosols influence clouds formation and lifetime -as well as their microphysical properties- influencing the precipitation and the radiative budget (*aerosol indirect effect*), as described in Lohmann and Feichter (2004), [44] or Storelvmo et al., 2017 [45].

Aerosol are defined as a collection of solid or liquid particles suspended in a gas. Their size is generally included between 0.01 and 10 μm and their residence time in the atmosphere goes from few hours to several days. Ice crystals and cloud droplets theoretically fall into the definition of aerosol particles, however, they are distinguished because they only occur in relation to a water phase.

Most aerosol particles originate from emissions at the Earth's surface. They are classified depending on their source, in relation to their natural or anthropogenic (human-made) origin and distinguished by their size. Among natural sources we should mention: oceans, volcanoes, forests, forest fires.

Further classifications consider the distinction between:

- primary aerosols which are directly emitted from the source, for example seaspray or mineral dust;

- secondary aerosols which are derived from gaseous emissions and then are converted to aerosol particles by chemical reactions in the atmosphere. For example, gas-to-particle conversion of naturally occurring gases such as sulphur dioxide (SO_2) and some naturally occurring VOC, such as α-pinene.

Among all the possible anthropogenic sources for primary and secondary particle emission we account: industries, transports, home heating, power plants, using fires to clear cropland.

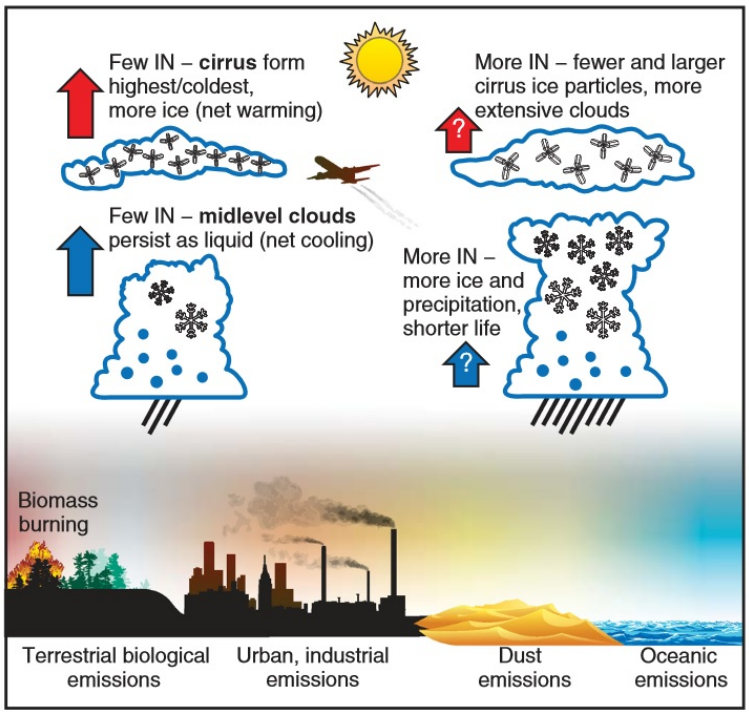

Figure 1.5: Schematic diagram of the effect of ice nuclei from various possible aerosol sources on mid-level precipitating clouds and cirrus ice clouds. The likely but uncertain change in the magnitude of the general cooling impact (blue arrows) of mid-level clouds and warming impact (red arrows) of high cirrus clouds in response to increases concentrations of IN. Figure taken from DeMott et al., 2010 [47].

Aerosols have been broadly studied for air quality control assessment, but they have also a complex effect on clouds and precipitations, as previously explained, and they have been identified as a major research challenge for the implementation, understanding and prediction of weather and climate. Indeed, the current limited representation of clouds and aerosols/clouds interactions results in a wide uncertainty for climate models. In the Intergovernmental Panel on Climate Change report of 2013 it was stated that "clouds and aerosols continue to contribute the largest uncertainty to estimates and interpretations of the Earth's changing energy budget" [46].

It stands to reason that changes in the atmospheric aerosol populations and abundance of CCN and INP, have an immediate impact on the formation of cloud droplets and ice crystals in the atmosphere. However, the magnitude of this impact, is still poorly quantified. A main reason is the competition of the individual particles for water vapour during the cloud formation and the resulting feedback on supersaturation [47].

An increase in the number concentration of hygroscopic particles decreases the maximum supersaturation reached during cloud formation. This can inhibit the activation of weaker aerosol particles and attenuate or inhibit the increase in cloud droplet number and/or ice crystals[22]. This will result in a different cloud typology (i.e. a thin or a more extensive cloud) and then on a different response to solar radiation, as summarised in Figure 1.5 (see [47], [45] for an extensive explication).

Models will be able to provide a reliable quantitative assessment of the susceptibility of cloud droplet and ice crystal number to aerosol changes only if all the physico-chemical properties of

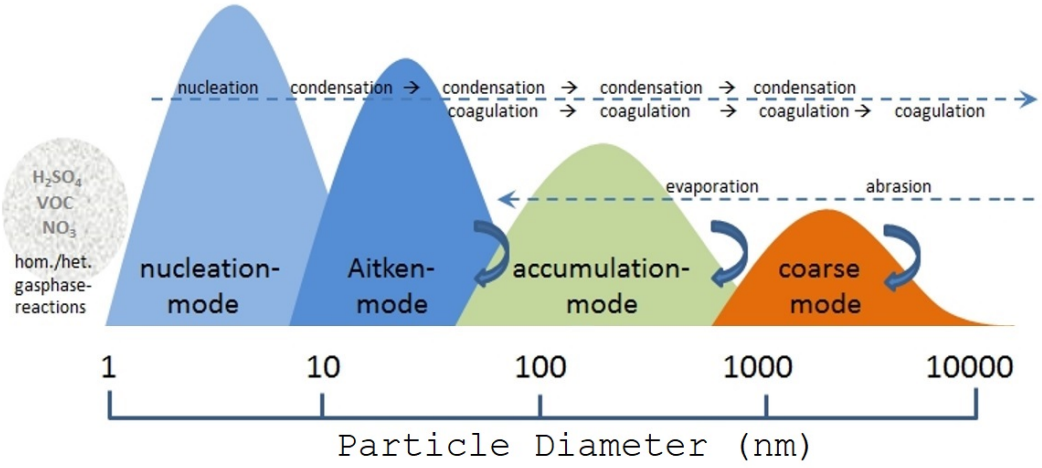

Figure 1.6: Aerosols size distribution segregated into different mode, in relation to their life-cycle, which is influenced by sink and growing mechanisms.

particles that are present during cloud formation will be known.

Additionally to the aerosol properties, the atmospheric conditions have to be considered. Updrafts and the accompanying adiabatic cooling are considered the main source of supersaturation in the atmosphere and therefore crucial for the activation of aerosol.

Finally, the atmospheric water budget must be fulfilled, i.e. on the global scale, the amount of precipitation must balance the amount of evaporation/transpiration. Strongly enhanced precipitation will limit the water vapour available for subsequent cloud and rain formation, whereas a suppression of precipitation can potentially enhance the precipitation formation in the later cloud development [22].

Although the physics governing the nucleation and growth of aerosol droplets to the size of cloud droplets and rain drops is well known, the interaction of aerosol and clouds is still a challenging field of research, because of the complex coupling of the individual processes and the variety of atmospheric conditions. As a result, the potential impact of aerosol on the hydrological cycle and the radiation budget of the atmosphere is poorly quantified.

In summary, various feedback mechanisms between aerosol, clouds, radiation, precipitation, and atmospheric conditions exist, which inhibit a simple classification and general quantification of the aerosol-cloud interactions [45].

1.3 Atmospheric aerosols and their role in ice nucleation

Atmospheric aerosol particles extend in size over more than 4 orders of magnitude (see Figure 1.6) and can be of very different kinds: from freshly nucleated nanoparticles (with a diameter below 10 nm) up to large mineral dust (dp > 1-10 μm) and pollen (dp $\sim$ 20-50 μm). Four modes are distinguished, in relation to different sources and sink mechanisms (Figure 1.6):

- The *nucleation* mode includes the smallest particles forming by gas-to-particle conversion and growing relatively faster through condensation of gases and water vapour.

- The *Aitken* mode includes particles with a diameter between 0.01 - 0.1 μm, growing slowly in size by coagulation and coalescence. These small particles are depleted mainly by coagulation with larger particles.

- The *accumulation* mode, ranging from about 0.1 to 2.5 μm in diameter, which provides most of the aerosol surface area and a great portion of the total aerosol mass (Seinfeld and Pandis, 2006[35]). Particles in this mode have longer residence times, than smaller or larger particles, as atmospheric removal processes are least efficient in this range.

- The *coarse* mode having particles larger than 2.5 μm in diameter for which fragmentation/grinding and evaporation processes act against a further growth. Simultaneously, mechanical sink mechanisms (e.g. sedimentation, deposition/impaction) reduces their number concentration.

In the size spectrum these modes overlap, due to the continuous evolution of particles, which evolve in the atmosphere due to evaporation, condensation, coagulation and sedimentation.

Ice Nuclei Particles usually represents 1 in in 10^3–10^6 of all aerosol particles [47], [48], thus making it difficult to ascertain and predict their type, source, and concentration.

A list of the principal INP species is reported in Figure 1.7 and detailed below. The INAS density parameter -that appears in the y-axis of Figure 1.7- will be detailed in the second chapter. For the sake of synthesis we will not mention all the further subspecies that are usually treated, e.g. volcanic ashes, secondary organic aerosols (forms by atmospheric oxidation and gas-to-particle conversion of volatile organic compounds stemming from biological sources such as trees and plants), soil dust (from grazed and agricultural lands), marine aerosol. For an exhaustive overview of all the IN species classified so far, refer to [38].

- *Mineral and desert dust*

  Mineral dusts and desert dusts are recognised as the most common ice nucleating particle type in the atmosphere, both for their efficiency of activation and their abundance (Hande et al., 2015 [50]). Already Schaefer, 1949 [51] found several naturally occurring mineral dusts to nucleate ice at temperatures < -15 °C. Many other studies have shown dust to be the most representative composition of ice residuals collected in MPC (Cozic et al., 2008 [52]; Kamphus et al., 2010 [53]) and cirrus clouds (Cziczo et al., 2013 [54]). DeMott et al., 2003b [55] found increased concentrations of INP in air masses carrying Saharan dust over Florida, and Creamean et al., 2013 [56] observed dust from the Sahara and Asia to influence precipitation in California. Over Europe, Chou et al.,2011 [57] confirms that Saharan dust events coincided with increased INP concentrations per unit volume under deposition freezing at -31 °C. At the South Pole Kumai, 1976 [58] identified 60 % of ice crystal residuals as clay minerals.

  Dust particles are important on a regional scale but can also undergo long range transport, in many cases influencing ice cloud formation far away from the source.

  As shown in Hoose and Möhler (2012) [49], dust particles are readily activated as ice crystals at T < -15 °C; however, they may be active as INP also at higher temperatures depending on the type, size and most of all composition.

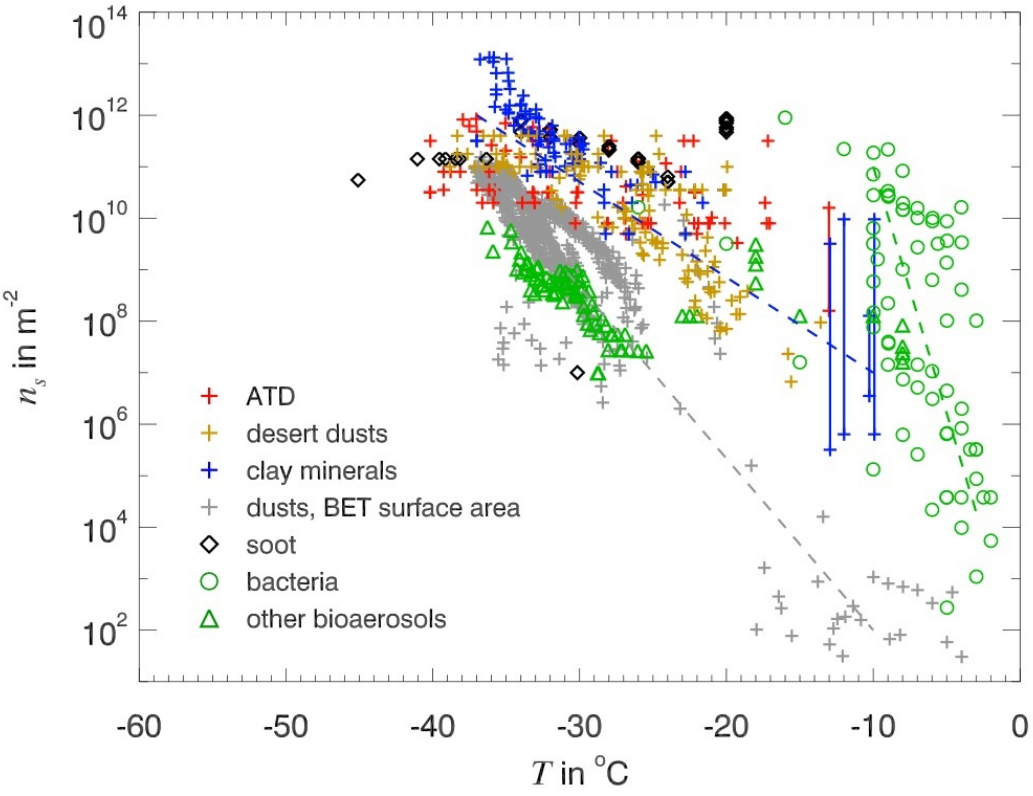

Figure 1.7: INAS densities for ATD, kaolinite, natural desert dusts, soot and bioaerosols explored mainly with immersion freezing, but including also deposition/condensation freezing experiments at or above water saturation. The data sources came from several experiments and were gathered together by Hoose and Möhler, 2012 [49]. The blue line refers to both ATD, desert dusts and clay minerals. The green line refers to highly INP biological aerosols. Lines were inserted to guide the eye. Image taken from [49].

For many years, the ice activity of mineral dust were associated mainly to the effect of clays, due to their high mass fraction in mineral dust. Five years ago, certain potassium feldspars (K-feldspars) have been identified to nucleate ice at warmer temperatures or lower relative humidity than all other typical components of natural mineral dust (Atkinson et al., 2013 [59]; Yakobi-Hancock et al., 2013 [60]). Despite the much lower abundance of feldspar compared to clays in most desert dusts, feldspar may significantly contribute to cloud glaciation in mixed-phase clouds, especially at T ≥ -20 °C, i.e. warmer than the ice nucleation onset temperature of other minerals [19].

- *Metal oxide particles*

  Metallic particles (containing metals such as iron, lead, nickel, and copper) can be found in the atmosphere and they are mainly generated by anthropogenic activities like smelting, aircraft engine ablation, and urban dust.

  Frequent observations of metallic particles inside ice residuals from cirrus clouds are reported in literature, e.g. Cziczo et al., 2009 [61] and Cziczo et al., 2013 [54]). The ice nucleating capability of metal particles depends strictly on their chemical composition. Metal oxides such as aluminium oxide, and iron oxide were found to nucleate ice via deposition nucleation

at temperatures ranging from −45 °C to −60 °C (see Archuleta et al., 2005 [62]). Lead-containing particles were considered as the most efficient INP among the metals tested by Cziczo et al. 2009 [61].

- *Biomass and fossil fuel combustion aerosol particles*

  A large quantities of particles are generated from biomass and fossil fuel combustion presenting a chemically complex composition (both carbonaceous and noncarbonaceous, organics and inorganics, e.g. soots and ashes) and are emitted into the atmosphere. They are almost always of anthropogenic origin (except natural wildfire).

  Belonging to this category there are also soot, consisting of black carbon particles that have either organics condensed onto them or either oxidised surfaces, resulting from incomplete combustion or from biomass burning [38].

  Both soot and ash particles may play an important role as cloud interacting particles given their high emission rates and therefore their high atmospheric concentration. However, it is still unclear if these particles are active as ice nuclei, as laboratory and field observations are contradictory (see Bond et al. 2013 [63]; Brooks et al., 2014 [64]).

  Chou et al., 2013 [65] showed that wood burning particles were ice-active in the condensation mode at T ≤ −35 °C and diesel exhaust particles only at T ≤ −40 °C, i.e. mostly in the cirrus regime. On the other hand, Petters et al., 2009 [66] found biomass burning particles from 9 out of 30 fuels to show significant ice nucleation activity at T = −30 °C in the condensation/immersion mode, i.e. in the mixed-phase cloud regime (however the efficiency varied a lot from the considered fuel with activated fraction $<10^{-4}$ to 10^{-2}). DeMott et al. (1999) [67]; Möhler et al., 2005 [68]; Dymarska et al., 2006 [69] and Kanji and Abbatt, 2006 [70] observed only low ice nucleation activity of different soot samples at temperatures ≥ −43 °C.

  In the cases where soot and ash particles behaved as active ice nuclei, their properties nucleating ability appeared to be linked to their fuel source and mixing state (via chemical aging or coatings). Möhler et al. 2005 [68] found a possible influence of the oxygen to carbon fraction O:C, to the ice nucleating activity thus leading to a wide variety of results.

  In line with these researches, also field observations of ice crystal residuals are controversial: DeMott et al., 2003 [55] found fly ash ice active at cirrus temperatures in the ice residuals collected trhough a research aircraft over United States, while Cziczo et al. 2013 [54] had not found consistent amount of ice active soot and ash particles inside cirrus' ice residuals (from aircraft measurements too).

- Organics

  Research over the last two decades has demonstrated that Organic Matter (OM) is ubiquitous in the atmosphere, present as Organic Aerosol (OA) particles or as coatings on other particle types, [71]. Primary organic particles can be, for example, emitted in marine environments. In Wilson et al., 2015 [72] primary organic material collected from the sea surface microlayer was found to nucleate ice via deposition mode at RHi <120% for T=−40 °C, and via immersion freezing mode at T < −10 °C. "Pure" organics, such as oxalic acid,

citric acid, and maleic acid, were found to promote IN via deposition mode only at T<−40 °C when amorphous glasslike species form (Baustian et al., 2013 [73]; Murray et al., 2010 [74]; Shilling et al., 2006 [75]; Wilson et al., 2012 [76]; Zobrist et al., 2006 [77]). Determining the freezing mechanism of complex organic mixtures seems related to the variable organic composition, and corresponding viscosity of the aerosol particles considered and then also to the particle-generation methods used, as explained in Lienhard et al., 2015 [78].

Investigations to understand which property (degree of oxidation, functional group density, mixing, viscosity/phase) renders organic aerosol components as IN an open field of research, especially with regards to Secondary Organic Aerosol (SOA).

Recently Knopf et al., 2018 [71] has advanced a theoretical model, based on particle water activity, to holistically predict amorphous phase changes and ice nucleation rates of particles coated by Organic Matter.

- Bioaerosols

  Biological aerosol particles (or bioaerosol) are defined as "solid airborne particles derived from biological organisms, including microorganisms and fragments of biological materials such as plant debris and animal dander" [79]. Their size ranges from few nanometers (e.g. viruses) to hundred of micrometers (e.g. pollen, fungi, plant debris). Other example of biological aerosol particles are algae, cyanobacteria, archaea and lichens. Thus the term bioaerosol refers to a wide range of organic material, which have a typical residence time in the atmosphere of several days. Furthermore, bacteria and viruses are often found attached to other aerosol particles and can be transported thousands of kilometers away from their source [79].

  Previous work have shown that biological aerosol particles -or biogenic particles produced from organic matter- might have the potential to initiate heterogeneous ice nucleation in clouds and create precipitation [80] [81], [82] [83], [84]. Moreover, they have been found to be the only naturally occurring aerosol that can lead to significant ice nucleation at temperatures between -2 °C and -10 °C . However, it remains to be seen which role these particles play in the atmosphere, since their abundance is unclear [49].

  Among them, the plant pathogenic bacterium, Pseudomonas syringae, is an important microbial ice nucleator that has been found in clouds, rain, and snow. A handful of fungi have also been reported to be ice nucleators, including species of Fusarium and Mortierella [85]. Representatives of these fungi can be found in soils all over the globe, and [86] showed that they can serve as a reservoir of biological ice nuclei which may be transferred to mineral particles.

  Other genera of ice-nucleating microorganisms have been reported [87], but their relative abundance in the atmosphere and their potential role in atmospheric processes is presently unknown. The study of biological ice nuclei from soil and aquatic sources are two ongoing field of research. Considering that about 70% of the Earth's surface is covered with water, the aquatic sources may represent a biological reservoir of ice nuclei even more important than the soil, however it has been poorly characterised so far.

Research is needed to understand the relative contributions of aquatic and terrestrial sources of ice nuclei [88], [89], and environmental conditions that trigger their release into the atmosphere [90].

1.4 Instrumental methods and critical aspects

Atmospheric physicians have searched, so far, all the possible sources of INP to evaluate their abundance and activation properties. This task included: laboratory studies using different/new techniques; observations from field campaigns to measure ice nucleating particle concentrations; computer simulation either within atmospheric models or either in molecular dynamics simulation of surface structure.

A non exhaustive list of the main techniques used to measure ice nuclei is reported below.

- *Mixing chambers* (Langer, 1973 [91]; Bundke et al., 2008 [92]),
- *Expansion cloud chambers* (Möhler et al., 2003 [93]; Tajiri et al., 2013 [94]),
- *Continuous flow diffusion chambers* (Al-Naimi and Saunders, 1985 [95]; Rogers et al., 2001 [96]),
- *Filter processing methods* (Bigg, 1996 [97]; Klein et al., 2010 [98]; Langer and Rogers, 1975 [99]).
- *Droplet-freezing techniques* (Ardon-Dryer et al., 2011 [100]; Budke and Koop, 2015 [101]; Knopf and Alpert, 2013 [102]; Murray et al., 2011 [103]; Vali, 2008 [104]).

Each device has its advantages and disadvantages. For instance, the continuous flow diffusion chamber (CFDC) cannot detect contact freezing, and aerosol particles larger than about 2 μm need to be removed with an impactor to distinguish ice crystals reliably from background aerosols. In addition, the CFCD provides no information on the size distribution of INP.

The typical techniques for quantifying INP concentrations tend to be highly labour-intensive and are limited in sensitivity to the low number concentration of INP in the atmospheres [48].

As reported by Vali et al., 1978 [105], the measurements of the ice nucleating activity of aerosol particles depend on several elements, among which the device and the operating conditions. For example, the cloud droplet concentration has an important influence upon the number of ice crystals which form by contact nucleation in a cloud chamber. Furthermore, the activity measured in one device (e.g. the filter processing) can not be readily compared with that measured in a different device (e.g., the drop freezing counter), and predicting the activity in a cloud chamber environment from measurements in two different devices may be very difficult [105].

This topic is further complicated by any possible physical/chemical/biological interaction with the surrounding environment. These interactions affect the INP capabilities of a specie and take place both at the source and both along the atmospheric transport (which can be short or long). Depending on the type of reaction (possibility of oxidation, coating, dilution, fragmentation, aggregation with other particles, microbial attacks, etc), the CCN/INP properties can be either deteriorated or either enhanced.

Even a specific inorganic species, as silver iodide, has water affinity and nucleating ability which can be strongly affected by the method of preparation and by the addition of complexing agents. "Pure" silver iodide (Corrin et al., 1964 [106]), is hydrophobic and actually quite a poor nucleating material (threshold activation temperature of about -10 °C). In comparison, complexes of silver iodide with ammonium iodide are hygroscopic and possess rather good nucleation temperatures, with the warmest activity near -10 °C (Davis et al., 1975 and Reischel, 1976).

Then, observed onset conditions for heterogeneous ice nucleation spread over large ranges of temperature and ice supersaturation, due to differences in methodology and non-standardised reported variables [49].

1.5 Open questions

A key point summary of open questions is reported below. This list, non exhaustive, is the summary of articles [85], [38] which focus on the research needs emerged from the most recent workshops on atmospheric ice nucleation.

- *Uncovering the molecular identity of active sites for ice nucleation and identifying the best time (in)dependent parametrisation of heterogeneous ice nucleation.*

  Active sites are more and more studied at a molecular level through computer simulations [107], [108], [109], [110],[111], [112]. This approach has shown that ice nucleation activity is influenced by several independent molecular properties, including surface hydrophobicity [109] ,[113], [114], surface morphology [115], and local electric fields [116], [117], [118].

  The widespread notion that ice nuclei particle have surfaces similar to the crystallographic structure of ice has been questioned [119]. A few experimental observations and computer simulation have showed that even amorphous surfaces may act as good ice nuclei [120] and that the ice can nucleate on surface regions with a large number of defects on feldspar particles [121] . The most recent approaches investigate ice nucleation as a function of different molecular properties, such as water-substrate interactions and surface morphologies.

  However, new researches are needed to fill the gap in fundamental knowledge of surface properties (e.g. the molecular basis for the hydrophilic or hydrophobic character of an interface, the functional groups and/or the chemical composition of an active site).

  Furthermore, new methods of investigation need to be explored to validate and interpret interfacial properties of ice nuclei at a molecular level (as techniques sensitive to the interfacial chemical composition). Experimental observations should be realised in conjunction with numerical modelling calculations to discern the role of different surface functional groups on ice formation.

  Thus, molecular computer simulations will be able to identify the most relevant competing molecular interactions and then to determine which formalism should be developed in order to take the latest into account [85]. Either a *surface thermodynamic approach* may be feasible, based on a free energy balance split into contributions between molecule-molecule and molecule-interface interactions; either *statistical thermodynamic approaches* to account

for the surface enthalpies and surface entropies (2-D for the surface, and standard 3-D for the gas phase) which are amenable to molecular interpretation. Finally, the best time (in)dependent parametrisation should be unravelled.

- *Identifying the classes of heterogeneous nucleation activation modes.*

  Current perception of the four classical freezing mechanisms (deposition ice nucleation, condensation, immersion and contact freezing) was different in the past and might change in the future. Originally, immersion and condensation freezing were combined together and only three ice nucleating modes were assumed to exist (Fukuta and Schaller, 1982 [122]). Today, the current definition of condensation freezing is distinct from immersion. In particular, condensation is supposed to occur when the freezing is initiated concurrently with the formation of a liquid film on the ice nuclei surface at supercooled temperatures [27].

  The current description is based on Vali et al., 2015 [27] and was the product of an open discussion and debate during the peer-review process in the journal Atmospheric Physics and Chemistry.

  However, Vali et al., 2015 [27] also state that it is not fully established if condensation freezing (on a microscopic scale) is truly different from deposition nucleation or immersion freezing and advise further circumspection for its use as a separate mechanism. Wex et al., 2014 [123] have proposed to remove the classification between immersion and condensation freezing, based on a series of experiments using the clay kaolinites. Also Hiranuma et al., 2015 [124] observed identical ice-nucleating efficiency -for condensation and immersion freezing experiments performed in a cloud expansion chamber for microcrystalline cellulose aerosol particles- and they suggested the formal identity of both mechanisms.

  Considering the possible existence of further activation methods, Marcolli et al., 2014 [30] hypothesises that a *pore condensation followed by freezing process* (PCF) might takes place in cavities -such as cylindrical pores, capillaries or interstices- where water is trapped and freezes at relative humidities (with respect to water) below 100% (see Figure 1.4). This mechanism could be mistaken for *deposition*, which in turn, occurs when ice nucleates from supersaturated vapours directly on the surface of the INP, at RHi $> 100\%$. The two mechanisms should be distinct as in deposition liquid water is presumed to be absent.

  Observations reported in Wagner et al., 2016 [125] investigated the PCF mechanism, although [125] called it "preactivation". Wagner et al., 2016 [125] investigations suggest that ice may form homogeneously inside the pores at sufficiently low temperatures. Then, the ice might be retained in the cavities at decreasing RHi $<100\%$ and increasing temperatures, up to -13 °C. Subsequently, if RHi is increased to values slightly above saturation, a macroscopic ice growth can be induced.

  It is therefore unclear to what extent data reported as deposition INP in the past truly occur directly via the vapour phase or from water trapped inside cavities, and what role this plays for interpretation of atmospheric processes [38].

  Further on, speculations followed also the contact freezing activation mode. Traditionally, contact freezing is initiated when an ice nuclei approaches the air–water interface from the

outside of a droplet (e.g., via a collision). Controversy concerns the occurrence of an *inside out* process, in case when the ice nuclei touches the droplet surface from within the droplet (see Figure 1.4). Evaporation of a droplet could lead to inside-out contact freezing and particle collisions may provide the energy required for freezing, from the impact of the ice nuclei with the droplet surface [38]. Recent developments in the experimental techniques deployed to examine contact freezing [126], [127], [128], have reported the probability of ice nucleation to be proportional to INP surface area. This result challenges the concept that contact freezing is triggered by the first point encountered between the droplet and the ice nuclei. However, the same studies show that contact-initiated freezing efficiency dominates over immersion freezing in the laboratory studies described, thus questioning the involvement of the entire particle in contact freezing [38]. The frequency with which these two mechanisms -outside and inside out- occur and their relative importance in the atmosphere remains poorly understood, but its contribution could be relevant to MPC (Seifert et al., 2011 [129]).

- *Examining the role of aging in ice nuclei.*

  Aerosol particles can be modified chemically and physically after being released into the atmosphere through a variety of *aging* processes occurring in the troposphere. Such processes include chemical modification by reaction with gases (e.g. coating, oxidation, functionalization, oligomerization) and physical modification arising from collision or from changes in temperature and humidity (e.g. agglomeration/fragmentation, drying/wetting, freezing/melting/sublimation) see Figure 1.4. Ice nucleation sites might be altered, destroyed or enhanced because of aging processes. The effect may also depend on the activation mechanism which is considered.

  A number of tests with ATD, kaolinite, illite, and K-feldspar dust particles treated with HNO_3 have shown a suppression of INP activity in the deposition mode, and unaffected ice formation in the condensation mode, e.g. [130], [131]. However, coating with H_2SO_4 have shown a suppression of IN activity in both the deposition and in the immersion mode for ATD, K, and Na/Ca feldspar, kaolinite, illite, motmorillonite, alumina silicates, and quartz [130]. A number of reasons have been adduced for this suppressed effect in sulphate-coated particles, especially for the immersion mode. Among others, it has been suggested that coating might be followed by surfaces modification, resulting in a degradation of the ice-active nuclei sites.

  Other treatments, such as montmorillonite exposed to NH_3 (Salam et al., 2007 [132] and kaolinite exposed to ozone (Kanji et al., 2013 [133]), have shown an enhancement of the ice forming capabilities for T>-36 °C in both deposition and immersion condensation modes. An explanation may be related to an increased hydrophilicity at the particle surface, due to the treatments performed.

  Even more recently, Kumar et al., 2018 [134] showed both an enhancement and a decrease ice nucleation efficiency of the microcline immersed in NH_3 and NH_4 solutions. The enhanced or decreased behaviour depended on the dilution degree of the solution. Authors suggested a possible aggregation and/or coagulation of the particles present in the dilution.

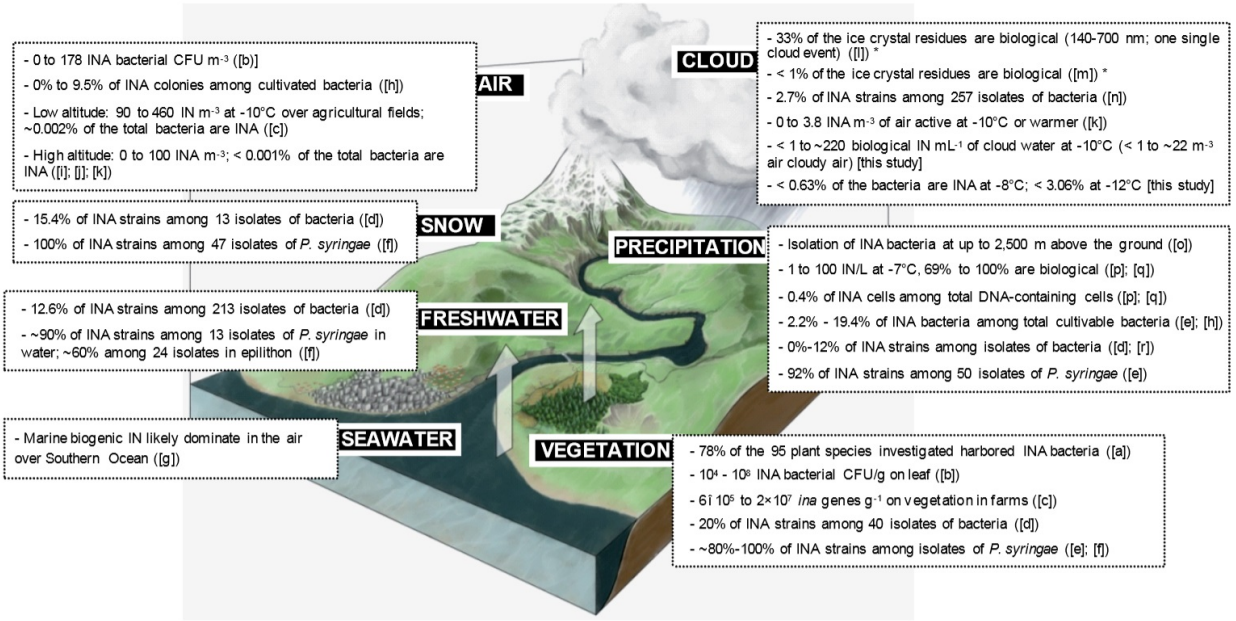

Figure 1.8: Figure taken from Joly et al., 2014 [136] summarising current knowledge about the abundance of biological INP active at temperatures above −10 °C in different environments links to the water cycle. Refer to the original article [136] for the references of the experimental studies listed in the brackets.

Indeed, aggregation and coagulation reduce the total surface area available for ice nucleation and they decrease the heterogeneous frozen fraction.

While the effect of aging on mineral ice nuclei has been investigated so far [19], the influence of chemical aging on biogenic ice nuclei and/or ice-nucleating macromolecules [135] is still an open topic.

- *Identifying and quantifying contributions of biological ice nuclei from natural environments*

  Recent studies indicate a higher contribution and importance of biological ice nuclei than previously assumed. Amato et al.,2015 [137] have observed that the IN activity of airborne bacteria did not change over time for at least several hours after aerosolization. In nature, this time may be enough for an INP active cell to be transported to high altitudes and get incorporated into a cloud. Several authors [138], [89], [139], [140], adduced that biological ice nuclei had developed the capability to induce freezing of supercooled droplets, in order to selectively prime their own redeposition (thus being able to trigger precipitations).

  As indicated by O'Sullivan et al., 2016 [86] nano-ice nucleating biological particles might be much more effective INP and wide spread in the environment than supermicron particles such as bacterial cells, fungal spores and pollen grains. Biogenic ice-nucleating macromolecules such as protein complexes and polysaccharides can exist detached from their original carrier/source and still nucleate ice at temperatures as high as -4 °C [141], [142], [143], [135], [144], [145]. These ice-nucleating macromolecules may also be associated to soil dust particles and then they could contribute to cloud glaciation indirectly [141], [86], [143].

O'Sullivan et al.,2016 [86] showed observations of the proteinaceous ice-nucleating macromolecule from the fungus Fusarium avenaceum and showed that it was able to confer its ice nucleation activity to the mineral particles of kaolinite -a common soil clay mineral- in which it is adsorbed. Similar observations are reported by Augustin-Bauditz et al. [146], who investigated the ice nucleation behaviour of particles consisting of a mixture of illite-NX and biological material washed of birch pollen grains.

Furthermore, [147] demonstrated that nanometer-sized particles of biological and inorganic origin were found to be the most abundant particles in snow sampled from different ecosystems.

All these researches have recently put the theory of *biology-driven precipitation* back on the limelight of the international scientific community. *Bioprecipitation theory* was first suggested by Hamilton and Lenton, 1998 [148] and is represented schematically in Figure 1.8. In this theory, microbes from soil or aquatic sourced are aerosolised, transported into the troposphere by updrafts, and after travelling long distances within clouds, they expel an ice nucleating protein able to induce ice nucleation (which helps deposing a layer of frozen water vapour on their surfaces). The consequent cocoon of ice protect them from solar radiation and allow them to fall down. The hypothesis that bacteria are advantaged if they can travel distances in clouds and then fall down with precipitation was first developed by Lenton developed and further developed by Hamilton, later on merging into the Gaia idea. The *Gaia theory* holds that living and non-living parts of the Earth are a complex interacting system, in which living things have a regulatory effect that promotes life overall.

Within this field of research, understanding the relative contributions of biological ice nuclei from aquatic environments remains a priority and an open field, as well as the taxonomic, genetic, and functional diversity of biological ice nuclei, and their possible evolution during atmospheric aging processes [85].

1.6 Aim and scope of this thesis

Ice nucleation on aerosol particles is a fundamental atmospheric process, which governs precipitation, cloud lifetimes, and climate. Despite being a basic atmospheric process, our current understanding of heterogeneous ice nucleation in the atmosphere is poor. One reason is that the concentration of particles able to catalyse cloud glaciation are scarce -only around 1 out of 10^6 particles in the atmosphere nucleate ice at ~ -20 °C [6]- making it challenging to identify their composition and sources. Furthermore, the properties needed for a surface to be efficient as an ice nucleating site are not well understood.

Despite the common use in models of ice nuclei parametrisations based on aerosol concentrations, such as the ones reported in Figure 1.9, experiments show that nucleation mechanisms and INP habits are broader. Uncertainties on the privileged mechanism of activation and INP availability still persist, especially in remote locations, where such uncertainties heavily affect models [149], [150]. In the previous section we reported a list of the main questions that seek answers in this field and that affect INP parametrization on cloud dynamic. To explore a part of these ideas, a cooperation among the Italian CNR and the French CNRS was promoted and two

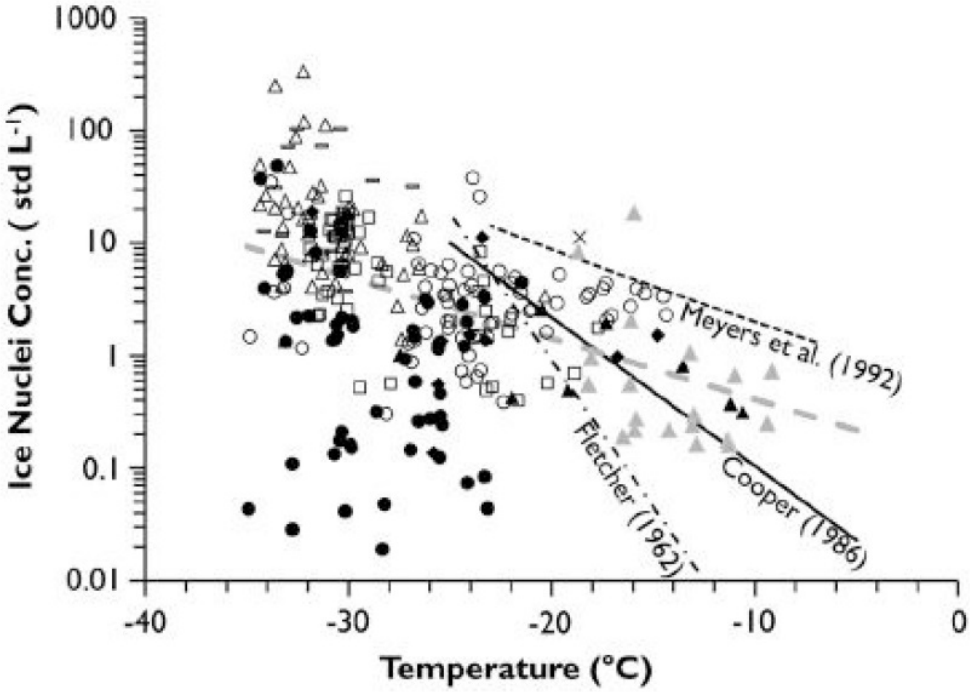

Figure 1.9: Ice nuclei number concentrations as a function of temperature (activated at water saturation or above). Figure is taken from DeMott et al., 2010 [47]. Three parametrisations are also reported, and among them, Meyers et al., 1992 [41] has been largely considered. These data demonstrate the large variability in INP concentrations at a single temperature and emphasise the small subset of total atmospheric aerosol concentrations that IN represent.

main instruments were employed for this study (Figure 1.10): the Dynamic Filter Processing Chamber, from ISAC-CNR in Bologna, and the Freezing Nucleation Apparatus replica based in Clermont-Ferrand. Then 3 out of 4 freezing activation methods could be considered. The principle strength of the two methods is the coupling to an easy aerosol collection, that allows for operations in remote environments.

The original aim of this dissertation was to characterise INP sources in different locations and period of time, by means of the above mentioned established instrumental techniquesand mainly to nourish database, such as the BACCHUS and the Research In Svalbard portal database, which are essential to run climate models and increase our understanding of aerosol/clouds interactions.

The experimental methods considered in this study, together with a list of concomitant instruments employed, are reported in *Chapter 2*. Then *Chapter 3* summarise the results obtained from 5 field campaigns belonging to the projects BACCHUS and AIR SEA LAB. These results have already been published in 2017 and are the result of the analysis and data treatment of a rich set of samples, collected from different sites -a rural, a mountain and a marine location- which fulfilled the first part of the present PhD research project (2015-2016). All the aerosol sources were considered in this task, in order to privilege the relative importance of the location and period of the year. In the meanwhile, an increased visibility of the bioprecipitation theory turn the scientific community towards the urgency of estimating INP of biogenic origin. Suggested

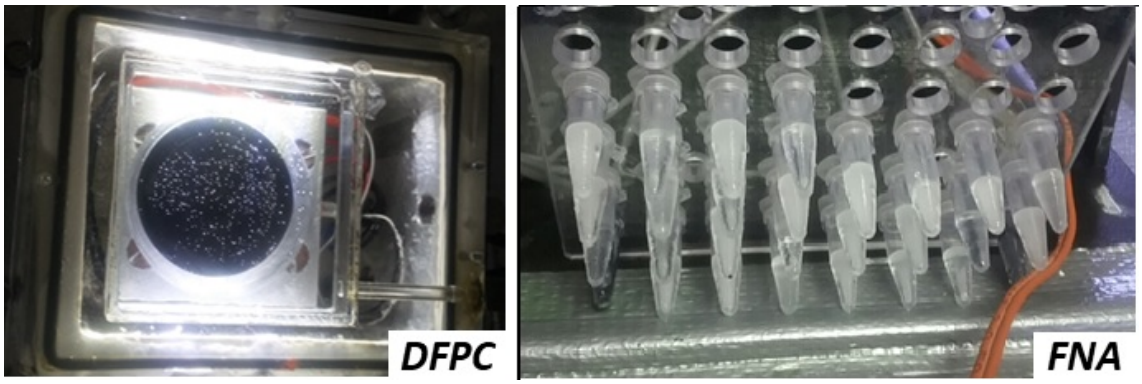

Figure 1.10: The two methods used to detect ice nuclei particles in this study: a filter based processing chamber (DFPC) and a droplet freezing apparatus (FNA).

by many authors -[89], [139], [140]- the bioprecipitation hypothesis starts from the idea that ice nuclei active cell can induce freezing of supercooled droplets and trigger precipitation. This capability may have been naturally selected to advantage the species able to induce their own re-deposition (thus reducing their residence time in the atmosphere). The modelling study [151] confirmed that the atmospheric residence time of singularly airborne bacterial cells is highly reduced if such bacteria act as ice nuclei by favouring the growth of ice crystals in clouds. Others numerical simulations suggest that the impact of biological ice nucleation on precipitation might be negligible at the scale of the planet [43]; [152]. However, an increasing amount of measurement data [137],[141], [86], [72], [153], [154] seems to indicate that we can not exclude biological sources, especially the ones from soil and aquatic sources.

Subsequently, from a general evaluation of the spatial and temporal variability of the overall ice nuclei species's concentrations, this study turned toward the characterisation of a more specific ice nuclei population, of biogenic origin. Because of the limited time, and in relation to the main interests of the two research groups involved in this PhD, we omitted the study of soil and we focused only on marine sources. This decision was performed during the PhD, and it seemed to answer to a need expressed by several climatologists [150]. Actually, this dissertation is neither a manuscript on climatology neither in marine biology, but it aims to provide information which are important for both climate model and both bio-geochemistry science. Then the second part of the manuscript is focused on a number of measurements performed entirely on primary marine aerosol emissions and seawater.

Chapter 4 gathers the results performed in the Arctic during the experimental campaign MACA. In this second part of the thesis, INP properties of marine aerosols were not investigated in ambient air, instead, a state of art marine aerosol generator was considered to laboratory generate the primary marine aerosols. The observations on marine INP species have not been published yet and they will be detailed thoroughly. Considering that marine ice nuclei is an ongoing field of research, a number of unsolved questions arose from our research, opening a variety of possible experiments for the future, that will be discussed. Conclusions and future work are given in *Chapter 5*.

Chapter 2

Materials and methods

> Historically, the measurement of ice nucleating activity has been found to be stubbornly difficult. Ice nucleation is sensitive to a large number of complex variables, so that the requirement that measurements reflect the reaction of the nuclei to the state of those variables in natural clouds is indeed a demanding one.
>
> Vali, 1976 [155]

2.1 Introduction

Laboratory experiments have shown that the freezing of very pure water droplets occurs at about -41 °C for droplets of 1 μm in diameter and at about -35 °C for droplets of 100 μm in diameter, as reported by Mason 1971 [156]. Hence, in the atmosphere, homogeneous freezing (i.e. the formation of ice crystals from pure water and haze droplets) is relevant only for high level clouds, as for example cirrus, cirrostratus and cirrocumulus. For mixed phase clouds, the formation of ice crystals is mainly related to the presence of specific aerosol particles called Ice Nuclei Particles. As explained in the first chapter, these nuclei provide a substrate capable to lower the energy barrier required to create a thermodynamically stable crystalline phase starting from supersaturated water vapours or supercooled droplets (also referred to as metastable liquid water).

These particles may act as *deposition nuclei* during the direct passage from the vapour state to the solid state, or as *freezing nuclei* during the passage from the liquid metastable phase to the solid phase. Three additional sub-cases are distinguished for the freezing nuclei: *immersion-freezing* the direct freezing of supercooled water by a nucleus contained within the droplet; *condensation-freezing* the condensation of water vapour on the nucleus surface and the subsequent freezing; *contact-freezing* the collision between a nucleus and a supercooled droplet with the subsequent freezing.

Which of the mentioned processes -deposition, immersion freezing, condensation freezing and contact freezing- is the most relevant, may depend on the meteorological conditions and the specific nucleus, its chemical composition and dimension.

Field campaigns in addition to cloud models indicate that immersion and condensation freezing are relevant activation modes within mixed-phase clouds, when supercooled water droplets and ice particles coexist. DeMott et al., 2010 [47] assumed that water-supersaturated condition reflect the maximum ambient INP number concentrations spontaneously active in mixed-phase clouds at temperatures warmer than -35 °C activated mainly by condensation and immersion freezing. Hoose et al., 2010 [43] indicated immersion freezing as one of the most important mechanisms, accounting for the 85% of ice formation in clouds that contain supercooled droplets. However, the relative importance of the particles' physico-chemical properties (i.e. size, composition, solubility, hygroscopicity, cloud condensation nuclei (CCN) activity, ice nucleation active sites, surface charge and/or crystallographic structure) for immersion freezing is not yet well known (Hiranuma et al., 2015 [157]; Murray et al., 2012 [158]). Several efforts have been made to clarify these aspects, and a large variety of techniques have been developed (see section 1.4). However, due to the fact that no existing instrument can explore the four activation methods at the same time, the characterisation of INP generally includes several order of magnitude.

For example, in the work of Hiranuma et al., 2015 [157] 17 immersion freezing measurement techniques have been compare to characterise illite NX particles. The instruments deviated within a range of about 8 °C in terms of temperature, and by 3 orders of magnitude with respect to the size equivalent Ice Nucleation Active Surface-site density (n_s).

The size equivalent Ice Nucleation Active Surface-site density has been introduced to parameterize the relevant properties in relation to atmospheric cloud models, as described by Connolly et al., 2009 [31].

This parameter results from the combination of others metrics previously adopted:

- the number of INP per unit volume of air, n_{IN}, summarised in Figure 1.9 and largely used inside models, it is expressed in m^{-3} or L^{-1};
- the activated fraction AF, that represents the fraction of particles activated, and is calculated as the number of ice crystals $n_{IN}(T)$, grown at T freezing temperature, divided for the total number of aerosol particles considered. It is dimensionless.

Surface active site densities, n_s, are usually calculated from the geometric aerosol surface areas, under the assumption of spherical equivalent diameters. Following Hiranuma et al. (2015) [157], for $n_{IN} <\sim 10\%$, n_s can be approximated as:

$$n_s \cong \frac{n_{IN}(T)}{S_{tot}}$$

where S_{tot} is the average total surface area of aerosols particles. Equivalently, this parameter is sometimes expressed as [159]:

$$n_s \cong \frac{AF}{A_{aer}}$$

where A_{aer} is the average total surface area of aerosols particles per unit volume (by considering the same diameter range used to calculate AF).

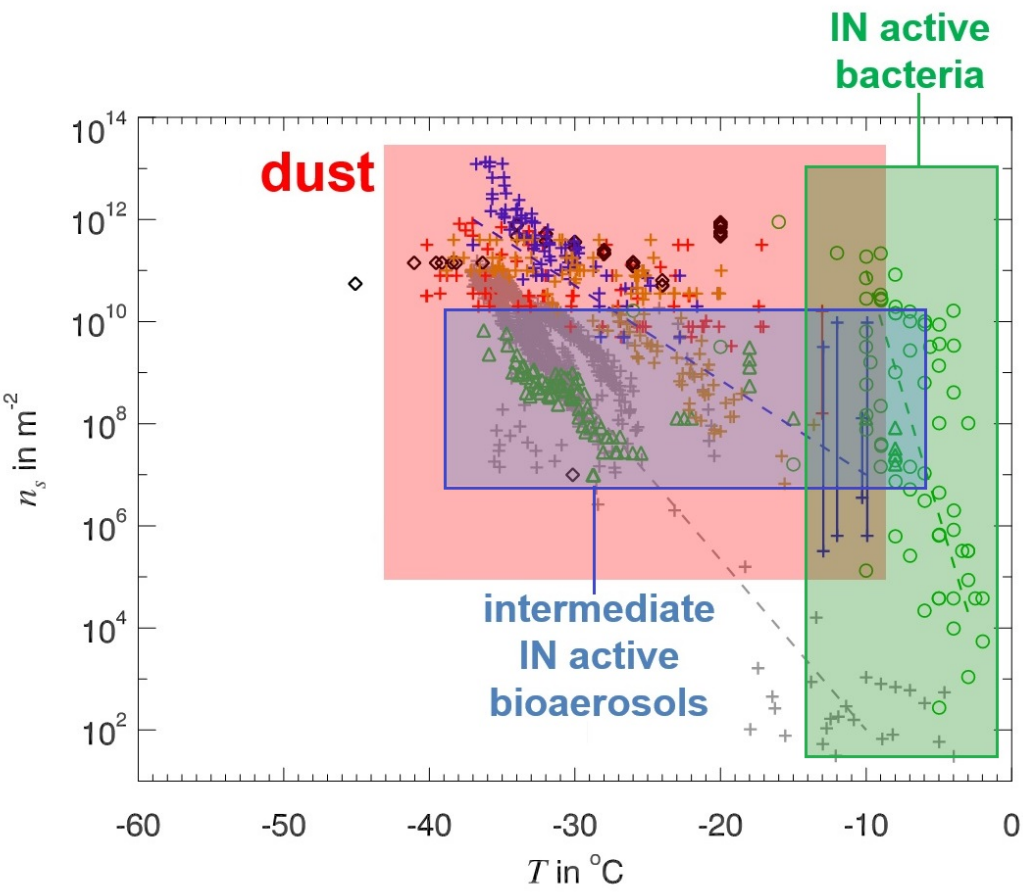

Figure 2.1: Image 1.7 modified to highlight the region of activation of different species. From C. Hoose presentation at the Summer School on Aerosol-Cloud Physic Interaction, Trieste, 2016.

A fundamental assumption of n_s metric is that one species of insoluble aerosol has a number of active INP approximately proportional to the total surface area of its aerosol particles (i.e. the active sites have a certain probability of occurrence per unit area of the surface of a given ice nuclei material). The n_s parameter can be modified to consider also an active site density per unit mass, n_m, instead of density per unit surface,

$$n_m \cong \frac{n_{IN}(T)}{m_{tot}}$$

in relation to the parameterization introduced by Wilson et al., 2015 [72] and used to calculate the ice nuclei contribution of marine aerosols (see Huang et al., 2017 [150]).

Traditionally, two different metrics were used to express the capability of an aerosol species to nucleate ice:

- the number of ice crystals detected per unit volume of air (L^{-1} or m^{-3}), for a considered set of temperature T and supersaturation with respect to water S_w or ice S_i.
- the Activation Fraction (f_{in}) calculated as the number of ice crystals detected in a unit volume, to the total particle number concentration measured in the same unit volume. This parameter is dimensionless and it is considered the basic measurement value (any other value is derived from that).

The first metric lacks of information on the number of aerosol particles contained in the considered air volume, and might be influenced by the availability of aerosol particles in a certain region/period of time, however it is still considered in field campaign observation and to compare with past studies. To characterise different aerosol species, the Activation Fraction or size equivalent Ice Nucleation Active Surface-site density parametrisation are mostly employed.

In [49] an overview of the results obtained in the past on different INP species and with different freezing techniques is reported (Figure 2.1). It can be seen that inorganic particles -e.g. clay particles, volcanic ash, soil dust- present the highest n_s in the region of temperatures above -25 °C. Instead organic materials -such as bacteria, pollen, lichen, fungi, decaying vegetation material, marine bacteria associated with plankton- are effective ice nucleators at fairly high temperatures (below -4 °C) (see Figure 2.1).

The uncertainty related to n_s) is affected by the particle surface area, which has to be derived from the particle number size distributions. This information is usually obtained from an Optical Particle Counter possibly combined with a Mobility Particle Sizer Spectrometer.

Aerosols Mass Spectrometer may also be considered to estimate the aerosol mass and the chemical composition of the aerosol, to extrapolate the fraction of organics and their relative contribution. Details on the operating principle of the OPC, MPS, AMS instruments are provided in the next section.

The freezing device used in this study are Dynamic Filter Processing Chamber and Freezing Nucleation Apparatus. These apparatus might be combined with the filter processing method, which is one of the most versatile, largely used in the past for its convenience and simplicity, and employed in a number of field campaigns and remote regions observations. With this method, aerosol particles are first collected on a filter substrate, and then conserved and transported. Inside the laboratory, a number of instruments exist to process the filter, in order to explore different activation modes, and to distinguish the IN from the remaining aerosols collected. The Dynamic Filter Processing Chamber is one of these instruments and it allows the control of supersaturated water vapour S_w and temperature T conditions, in order to explore either the deposition or the condensation-freezing activation mode. Another possibility, is to to extract the particles from the filter, to dilute them in solution with ultrapure water and to distribute this solution in a droplet freezing apparatus to explore the immersion freezing activation mode. Description of the principle of operation of DFPC and FNA, together with the benefit obtained with respect to other similar techniques, are provided in section 2.2 and 2.3.

2.1.1 Aerosol Size Distribution

As explained in the introduction, atmospheric aerosol particles have dimensions spreading over several order of magnitude. Due to their broad size range it is not possible to characterise the entire particle spectrum with only one method, and at least two different principles of operation have to be considered. Figure 2.2 displays the two ranges of operation of the main instruments used to characterise aerosol particle size-distribution, as reported by Sabbagh-Kupelwiese et al., 2011 [160]). Particle size distributions in this study were obtained using the following two types of instrumentation:

- *Optical Particle Counters (OPC)* for particles larger than ~ 0.2 μm. Their principle of

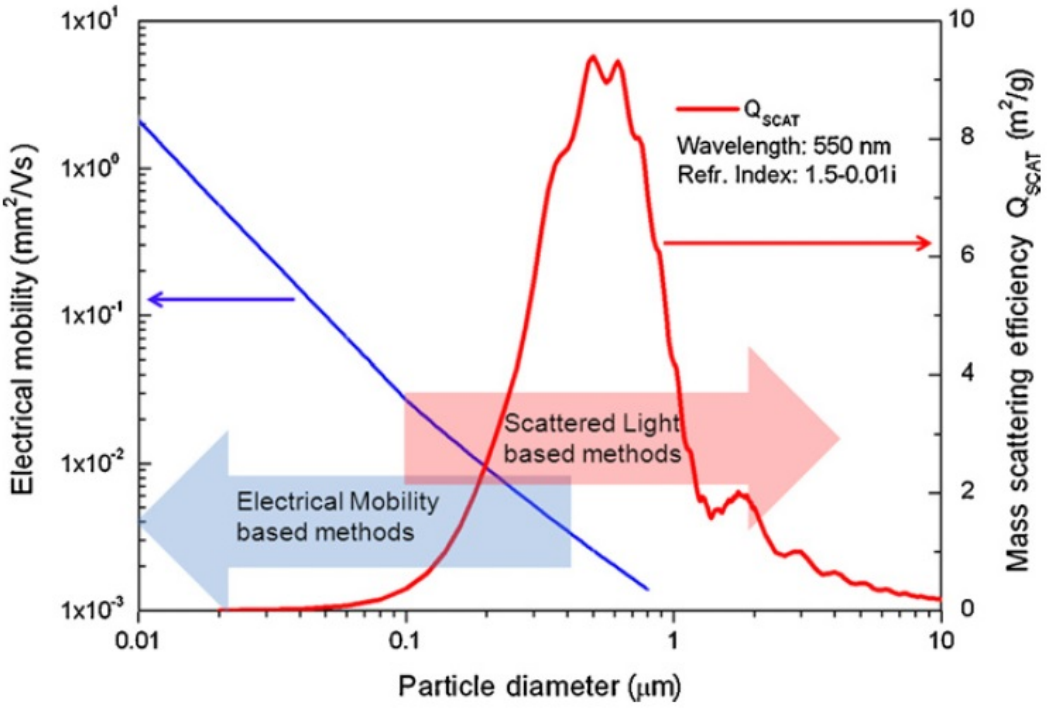

Figure 2.2: Relation of optical and electrical properties of airborne particles. The electrical mobility of a charged particle in a given electrical field increases logarithmically with the decreasing particle size. That property offers evidently an excellent possibility to detect and characterise nanoparticles. In turn, nanoaerosol particles well below 100 nm in size cannot be directly measured by optical means using elastic light scattering. From Sabbagh-Kupelwiese et al., 2011 [160].

operation is based on measuring the light scattered when aerosol particles are irradiated through a diode laser and embedded in a narrow (∼1 mm) and focused laminar flow. Individual particles are assumed to be spherical and homogeneous and the light scattered is attributed to size ranges, based on Mie theory. The scattering signal of a multitude of particles is attributed to size ranges by a pulse-height analyser which is calibrated with commercially available particle standards.

- *Mobility particle size spectrometers* for sub-micrometric particles and mostly used for the size range from 10 to 500 nm. Their fundamental principle is the separation of particles in an electric field, based on different electrical mobilities. Particles are first conditioned, through a neutralizer, to obtain a known aerosol charge distribution (often referred to as the Fuchs distribution). This is usually done by exposing the particles to a stream of beta or alpha radiation. Then particles enter the differential mobility analyzer, which consists of a cylinder, with a charged central rod, thus setting up an electric field in the space between the walls and the rod. Varying the capacitor voltage sequentially help selecting different electromobilities (corresponding to different particle diameters). Successively counting the voltage-dependent electromobility classes with a condensation particle counter yields the number electromobility spectrum. Finally the number size-distribution is retrieved from

the electromobility spectrum in the data inversion processing, assuming a known aerosol charge distribution at the inlet, obtained via aerosol conditioning through a neutralizer.

A non radioactive source was employed in this study as neutraliser (the X-ray Advanced Aerosol Neutralizer 3088 from TSI). The measurements with the MPS were operated with a desiccator at the inlet (silicagel powders) used to reduce aerosol relative humidity to less than 40%. This step is mandatory for the correct functioning of the neutraliser (both radioactive and non radioactive). In the Bacchus-AirSeaLab campaigns, the Optical Particle Counter was a Grimm Aerosol Technik GmbH - Aerosol Spectrometer 11A, described in Grimm and Eatough, 2009 [161]. The particles which are detected with this instrument have an optical diameter in the range 0.25 μm a 32 μm. A MPS was available at the ISAC-CNR laboratory (a Grimm SMPS, which employs a ^{241}Am radioactive source). In the PARCS-MACA campaign the MPS was a laboratory home made (named scanotron) combined to a non radioactive source (TSI 3088) and the OPC was the Welas digital 2100 sensors. For all these instruments, the calibrations were regularly performed under the routine maintenance and/or with commercially available test aerosol (e.g. suspension of calibrated polystyrene latex spheres).

Side-by-side comparison with a reference instrument or different models were also performed under occurring inter-comparison campaigns. Within this context, the results obtained by comparing three MPS (TSI and Grimm brands) equipped with different aerosol neutralizers have been recently published in Nicosia et al., 2017 [162].

2.1.2 Aerosol Mass Spectrometer

The chemical characterisation of aerosol particles is currently one of the central topics in atmospheric science. Indeed, a better understanding of particle sources can only be achieved with detailed knowledge of their constituents. Typical anthropogenic sources -such as industrial emissions, traffic exhaust, and biomass burning- as well as natural sources -such as sea salt and dust resuspension- are characterised by specific chemical compositions. Their determination helps to better elucidate the sources of aerosol particles in the atmosphere. In line with this trend, a Compact Time of Flight Aerosol Mass Spectrometer (C-Tof-AMS) is considered in this study (Chapter 4). The principles of operation of an Aerosol Mass Spectrometers (AMS) can befoundin Jayne et al. 2000 [163]; Jimenez et al. 2003 [164]; Allan et al. 2003 [165].

Briefly, considering a C-ToF-AMS, this instrument consists of an aerodynamic inlet, a Particle Time-Of-Flight (PTOF) chamber, and a vaporiser/ionizer that is interfaced to a time of flight mass spectrometer. The sample air is aspirated through a critical orifice -diameter 100 μm- that maintains a constant flow rate (generally of 1.4 cm^3 s^{-1}). A narrow particle beam is generated by focusing the aerosol particles with diameter from 60 to 800 nm. A chopper wheel delivers a slug of particles into the time of flight vacuum region, where their speed is proportional to their size. This chopper blocks the aerosol beam to only allow a small number of particles to pass on to the vaporiser. The aerodynamic diameter is calculated from the time of flight of the aerosol particles to the vaporiser. The vaporiser -typically heated at 600 °C- and a filament with a relative electrical potential of 70 eV are placed at the end of the sizing chamber, yielding a flash vaporisation of the particles followed by electron impact ionisation of the evolved gas molecules. The ions for a particular mass-to-charge (m/z) ratio are then detected using the

ToF-AMS. Since only non-refractory PM1 (NR-PM1) is vaporised below 600 °C, the aerosols measured by the C-ToF-AMS are referred to as non-refractory PM1 (NR PM1). Therefore, the C-ToF-AMS provides mass concentrations of the size resolved organic carbon, sulphate, ammonium and nitrate (in the size range between ≈ 50 and 600 nm). The mass spectral signals are usually treated following the recommendations of Allan et al., (2004) [166].

2.2 Immersion freezing measurement technique

The immersion freezing technique considered in this study is a "droplet freezing assay", also referred to as the Freezing Nucleation Apparatus (FNA) or the LED based Ice Nucleation Detection Apparatus (LINDA). The FNA has been developed at the Department of Environmental Sciences, University of Basel, Switzerland by Lukas Zimmermann and Franz Conen in 2012 (see FNA-Basel Web Page). Together with the related software, the Freezing Nucleation Apparatus is Open Source, disposable at the page http://azug.minpet.unibas.ch/ lukas/FNA/FNA-OSHW.html.

Replica of the original apparatus have spread to a few French laboratories, in Avignon and Clermont-Ferrand. These replica are all based on the Basel design and have been used in [167]; [168]; [136]; [137]; [135]; [169]; [170], in which FNA was applied to rain samples, snow, bacteria, birch pollen and fungal species, at temperature relevant for biological INP species. In Chapter 4 we will combine for the first time immersion freezing analysis on both seawater and sea spray (by means of FNA). Indeed, the simple design and operation of FNA renders this method suitable for monitoring observations of a large variety of INP biological species.

FNA has been described carefully in Stopelli et al., 2014 [171]. Briefly, the FNA consists of a thermostat (JULABO FP40) with a 16 L cooling bath, a camera, 4 thermocouples, and a plastic tray with the eppendorf tubes to be analysed. Each droplet is enclosed inside an eppendorf tube to prevent external contamination. A schematic of the instrument is shown in Figure 2.3.

The number of frozen droplets can be distinguished from liquid droplets since they reflect incident light differently, and therefore appear much darker.

The relative change in the red light intensity is recorded by an USB CMOS Monochrome Camera. Each droplet is enclosed inside a translucent vial which allow reliable detection of the phase change from liquid to ice. The choice of a red light beam is related to the fact that radiative transfer of visible light, through ice water, is increasingly reduced the longer its wavelength. The presence of air bubbles and brine pockets included in the ice is responsible of the scattering (as reported by Perovich, 2003 [172]). Considering that this inclusions are rarely present in pure iced water, the addition of a small amounts of NaCl is indicated as a possible solution to create impurities which further increase the scattering of light, an help distinguish among liquid and solid samples. Stopelli et al., 2014 [171] have shown that the addition of small amounts of NaCl (up to 0.9 % final concentration, equal to physiological solution) had no noticeable impact on freezing temperatures. Much lower NaCl concentrations are insufficient for reliably detecting change in light transmission. Through this method, the phase change from liquid to ice is clearly detectable by a sudden decrease in transmitted light recorded by the camera (see Figure 2.4).

For the analysis, as explained in [171], it is first calculated the frozen fraction at a certain temperature T, and then this fraction is reduced to the number K_T of INP per unit volume, similarly to [173]:

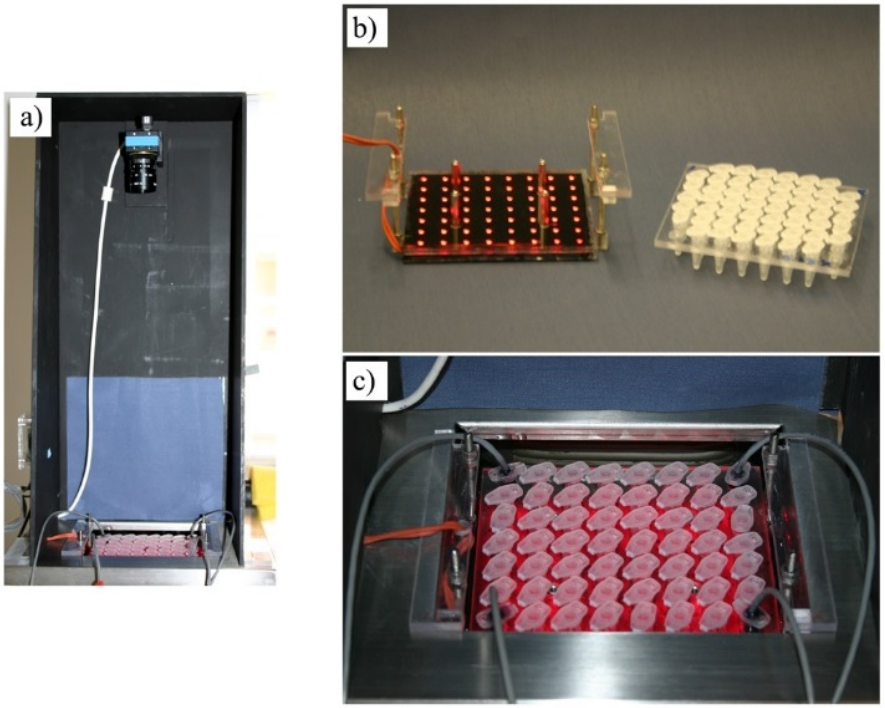

Figure 2.3: (a) Cold bath set-up, ready for analysis with camera recording from above; (b) LED array and polycarbonate plate holding 52 sample tubes; (c) detail of tubes and Pt1000 sensors in the corners of the grid inside the cooling bath. Figure taken from [171].

$$K_T = \frac{[ln(N_{total}) - ln(N_{unfrozen})]}{a}$$

where N_{total} is the total number of droplets (corresponding to the total number of Eppendorf tubes in which the sample is distributed), $N_{unfrozen}$ is the number of tubes still unfrozen (liquid) at the observation temperature T, and a is the volume associated to each droplet.

The upper limit for the number of INP detectable is determined by the total number of aliquots analysed and the smallest volume that still results in a clearly detectable change in light transmission when changing from liquid to frozen. The droplet volume considered in previous studies was 500 μL in [167]); 400 μL in [170] and [171]); 50 μL in [135]. The modification of the aliquots determine the lower and upper quantification limits of the number of INP per unit volume. In our study we will consider a droplet volume of 200 μL for the studying of seawater and sea spray samples, which in our set up is associated to an upper detectable limit of 162.9 INP mL^{-1} and a lower detection limit 1.96 INP mL^{-1}. The upper detectable limit can be extended by orders of magnitude through proper dilution. Concerning our study, we prefered to avoid dilution in order to unmodified the salinity of our samples, based on seawater.

In any case, the freezing apparatus is conceived in a way that the Eppendorf tubes containing the droplets are always fully surrounded by the cooling liquid. However, depending on the operational, the background determined on blank may vary. [171] has reported that the blank due to container characteristics, water quality and working environment could become an issue at temperatures around -15 °C or lower (while working with droplets of 400 μL each).

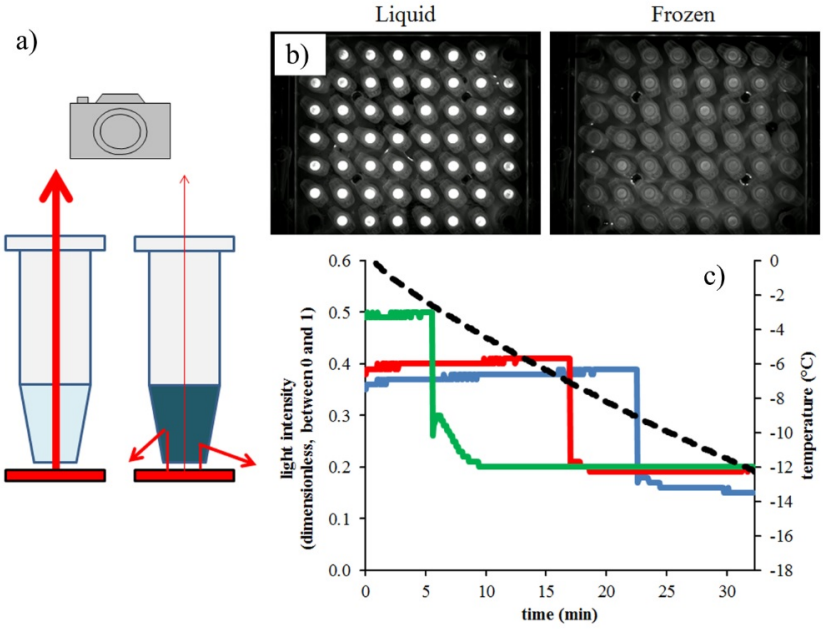

Figure 2.4: (a) FNA principle of operation: freezing detection by a decrease in light transmission associated with the passage from liquid water (light blue) to ice (dark blue);(b) images taken by the camera at the beginning and the end of a test run when all samples were liquid (left panel) and frozen (right panel); (c) time record of temperature (black dashed line) and light intensities of three tubes (coloured solid lines) showing the sudden and sharp decrease in recorded light intensity (full line), associated with ice nucleation. Figure taken from [171].

The precision of the apparatus has been associated to 0.2 °C by considering 1 standard deviation when calibrating the instrument with measuring reference substances of known freezing temperature range [171].

2.3 Condensation (and deposition) freezing measurement technique

The Dynamic Filter Processing Chamber is a replica of the Langer dynamic developing chamber [99], housed in a chest freezer and used to detect and determine the concentration of aerosol particles active as INP at different saturations S_w and temperatures T. The experimental method used to measure the IN activated fraction comprises three main steps.

- First the aerosol is collected on a filter (e.g. nitrocellulose membrane, Millipore HABG04700, nominal porosity 0.45 μm, see Figure 2.6 left) through a common sampling line which combines a filter holder, a pump and eventually a cyclone or a particulate monitoring sampling head (as 1- and 10-μm cut point Standard EN 12341, TCR Tecora). The sampling is done in parallel with the monitoring of aerosol properties through an Optical Particle Counter (OPC) and/or a Mobility Particle Sizer Spectrometer (MPS).
- Secondly, the filter is pretreated at the laboratory, by filling its pores with paraffin (see Figure 2.6 right). More specifically, the filter is placed on a metallic support covered with a smooth layer of paraffin. Then the paraffin is slightly heated (depending on the sample

Figure 2.5: Phase 1: Aerosol sampling.

the heating temperature is around 80-60 °C) for few seconds and rapidly cooled in order to penetrate deeper inside the filter pores (bringing out the particles from the inner pores to the surface). The main goal of this pretreatment is to modify the colour of the filter (from white to black) and most of all to enhance the thermal conductivity between the filter and the supporting substrate. Filter heating is carried out for a very short time (10 s), in order to prevent any degradation of the heat-labile material which may act as ice nuclei. In fact, experiments on "INP thermally liable materials" are carried out at higher temperature (95C/100C) and most of all for a longer time (at least 10 minutes) [72]. Our heating protocol is so rapid that we do not foresee any effects on INP.

- The filter is processed inside DFPC, by placing the sandwich (metal plate plus paraffin plus filter) on a Peltier cooler plate. Inside DFPC, the filter is continuously swept by humid and cold air. Ice nuclei which are activated generate an ice crystal which growth up to ∼0.4 millimetre and that can be visually detected to determine the concentration of INP.

- Finally a photo is recorded and analysed to count the number of white dot on the black background. This information is crossed with the sampling conditions (volume of air passed through the filter, total number of particles counted, total aerosol surface distribution) to estimate the Activation Fraction and size equivalent Ice Nucleation Active Surface-site density.

Figure 2.7 reports the instrumental set-up of DFPC which can be divided into three sections: the air pneumatic circuit (section I), the supersaturation control level (section II) and the filter temperature control (section III). In section I, the air is filtered and forced by a pump to flow

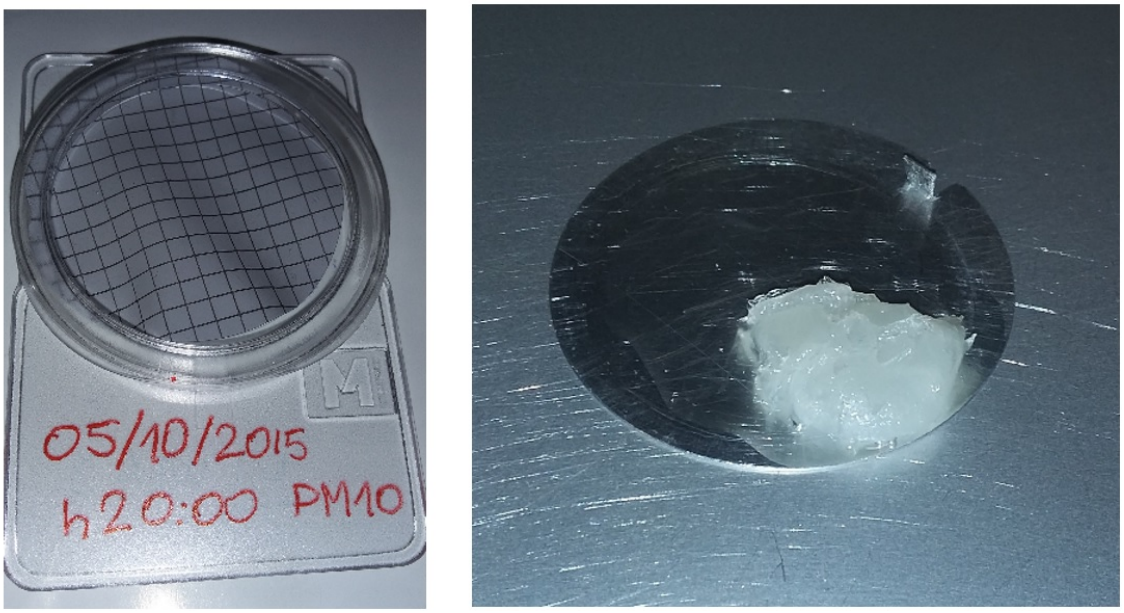

Figure 2.6: Phase 2: pretreatment. A metallic support (at right) is covered with a thin layer of paraffin and then the filter (at left) is superposed onto.

through the remaining sections in a closed loop. Section II is filled with minced ice, which is cooled by the base plate, while section III allocates a Peltier cooled plate, where the filter is placed. Air spreading inside the ice bed (section II) becomes saturated with respect to ice, and then enters in the following section (III) in which borders on the filter.

The values of T and S_w are measured before approaching the filter with a thermo-hygrometer (HD 9216 model by DeltaOhm) and verified theoretically from vapour pressures of ice and water at the considered temperatures [17].

By varying the different temperatures inside the chamber and the vapour supersaturation with respect to liquid and/or ice, it is possible to activate the INP both in the deposition and in the condensation-freezing modes. Ice can form by deposition provided that the air is supersaturated with respect to ice, for example, at S_w=0.92 or by condensation-freezing if the air is supersaturated with respect to both ice and water such as, for example, at S_w=1.02.

Blanks (unsampled filters) are analyzed in a similar way to account for possible contamination during the IN quantication procedure, and the results are corrected accordingly.

Finally, the INP activated fraction f_{IN} can be derived from the number of crystals grown on the filter and the initial sampling conditions (i.e. the volume of sampled air and the concentration measured by the OPC and/or the MPS).

The DFPC set up is housed at the Institute of Atmospheric Sciences and Climate of the Italian National Research Council in Bologna, Italy. Because it is associated to a temperature controller and a large chest freezer, it is not possible to transport it. Therefore it is considered a fixed apparatus. Similarly, the FRankfurt Isothermal static Diffusion chambEr (described in [98] and [174]) is another fixed apparatus with an analogous principal of operation and an experimental method quite close to DFPC. In particular, FRIDGE pairs electrostatic precipitation of aerosol particles on Si-wafers with the subsequent analysis of the substrates. Ice crystals grow on INP and are photographed and counted [174]. The main results from the last intercomparison between

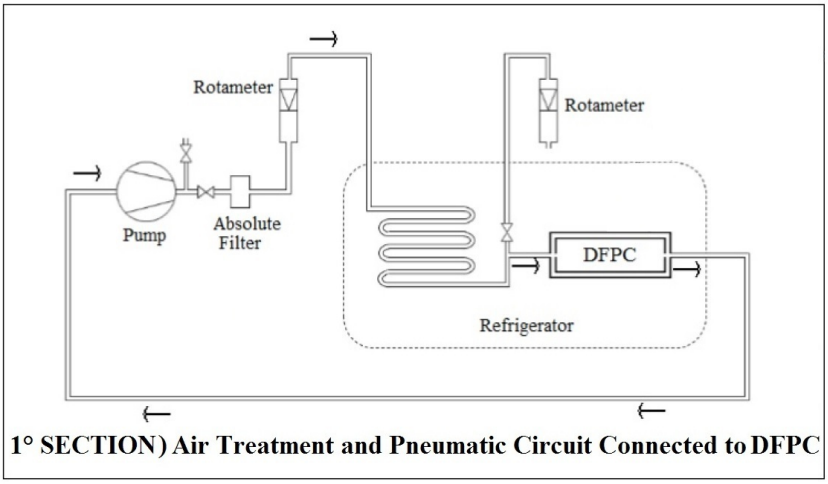

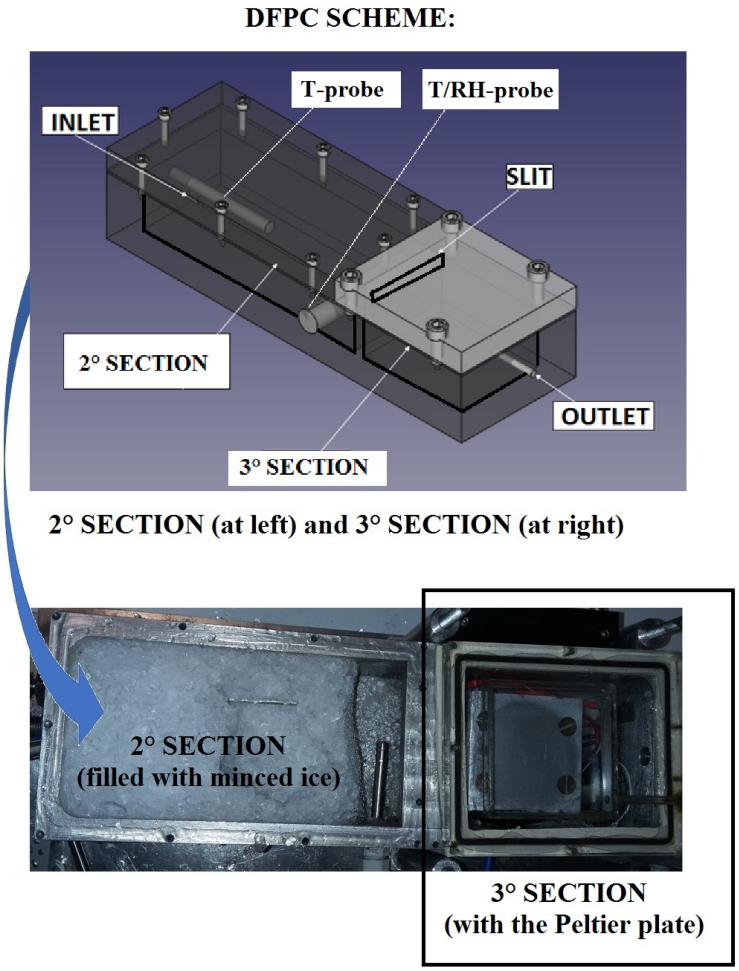

Figure 2.7: Phase 3: processing inside DFPC. The scheme reproduces: the air treatment and pneumatic circuit connected to DFPC (section I in the text); the detail of the DFPC chamber that allocate minced ice at left (section II) and has a Peltier at right.

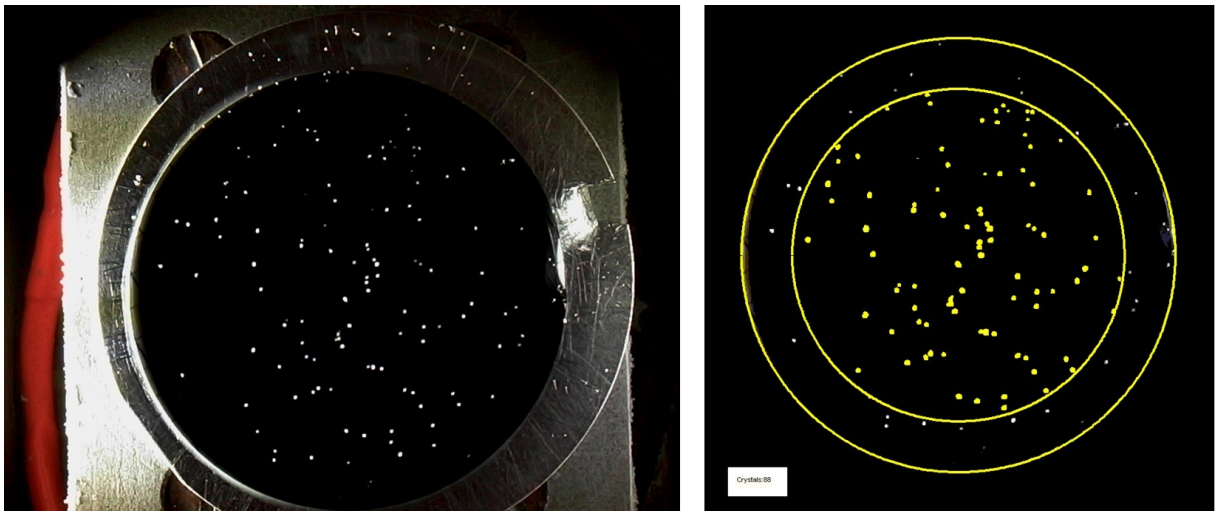

Figure 2.8: Phase 4:Countings

FRIDGE and DFPC is reported at the end of the chapter.

DFPC has been used for several measurement campaigns (Belosi et al. [175]; [176]; Rinaldi et al., 2017 [177]; Nicosia et al., 2017 [178]; McCluskey et al. 2018 [154]), intercomparison studies (DeMott in press [179]) and most of all theoretical studies (see Santachiara et al. [180], [181], [182] and Belosi et al. 2018 [159]).

2.3.1 Improvements

The DFPC was developed by Gianni Santachiara and Franco Prodi in the nineties for the activation, growth and counting of ice nuclei collected on substrates. It is based on the design by Langer and Rodger (1975) [99], but uses state of the art equipment. In the last 5 years DFPC has known a number of improvements, detailed below in a list of points:

- An ice chamber controller has been developed by Pollution Analytical Equipment to pilot the chest freezer's temperature and at the same time to monitor all the other temperatures involved (the air entering the chamber, dfpc walls, the ice, the Peltier unit). The ice temperature is the privilege parameter that needs to be monitored, and the probe used for this purpouse is the GHM greisinger GMH 3700 series Pt100 thermometer high precision. Before the ice chamber controller, different monitors have to be visually inspected to deduce the operative T and Sw. Now the temperatures are easily piloted and the time spent to set each configuration has been reduced.

- A new chamber has been built in order to enlarge the ice section (i.e. more ice is allocated and the resident time of air inside this part is augmented). In the ice section, an air injection has been added to distribute the air flow all over the ice granular ice.

- After the ice section, the amount of saturated water vapour are now monitored through an additional probe to verify carefully the air temperature and its relative humidity prior to the filter. This probe is a thermo-hygrometer from Delta Ohm (model HD 2101.2).

- In the new DFPC chamber, the air slit has been raised in order to be exactly at the same level as the filter and then it considers both the high of the Peltier, the metal support and the filter itself.

- New metal plates have been built, together with a specific utensil which help coating the paraffin on the metal plate, thus automatizing the longest part of the pretreatment process.

- To count the number of ice crystals, a photograph of the filter is taken with a high resolution camera sensor (model DP-M17 USB digital microscope from Conrad electronic international) and analyzed with an image analysis software (e.g. ImageJ).

- Two new Peltier cells have been located to replace the old ones.

To account for all these modifications, a complete calibration of the temperature probes was performed through a calibrated LLG-Precision (non-mercury filled) glass thermometer for low temperatures (from -25 up to -5 °C) having a 0.1 °C graduation interval. The DKD-calibation certificate was furnished by Exacta+Optech Labcenter SpA at the purchase. A special attention was dedicated to the measure of the filter temperature by considering the operative conditions and by placing the temperature probe directly between the metal plate and the filter (see Figure 2.9). An offset of around 0.3 °C has been estimated (with respect to the set temperature of the Peltier cooler plate) and considered to correct the setting of the freezing temperature T (which always refers to the temperature of the particles contained inside the filter, which are at the equilibrium with the filter temperature).

ImageJ was traditionally used to treat the image, by reducing the noise, selecting the area of interest, and counting the visible crystals. Briefly, the figure was select to account only for the filter area (through the Oval Selection Tool) and to erase the background. The diameter usually selected ranged between 505 and 515 pixels. Then the selected area was cut (Ctrl+X) and pasted (Ctrl+V) on a new frame (600 X 600 pixel) in a RGB format. The disc was automatically placed in the centre of the new frame by the software. If necessary, the threshold function was used to reduce the noise.

During the image treatment, it was important to excludes the external corona of the filter (which is pressed by the filter holder during the aerosol sampling and in which the air does not pass through). In 2016, an algorithm has been coded to this purpose under Matlab (R2008a) to automitise these step. Figure 2.8 reports an example of the ice crystals grown on the filter and the subsequent image processing and counting of the software. Appendix B reports further information on the strategy adopted for the image analysis. Appendix C reports the code, working under Matlab 2008.

2.3.2 Operating procedure

Prior to each experiment a sealing test is performed. Only if the results is a leak-free test, the experiment is started. During the approximately 30 min of cooling time of the DFPC walls, a cleaned air stream is flushed through the tubes to removes the ice needles which may arise during DFPC inactivity periods. Subsequently, the air pump is running continuously to provide a clean flow of 200 L h^{-1} inside the chamber. Prior to each experiment, the ice is regularly

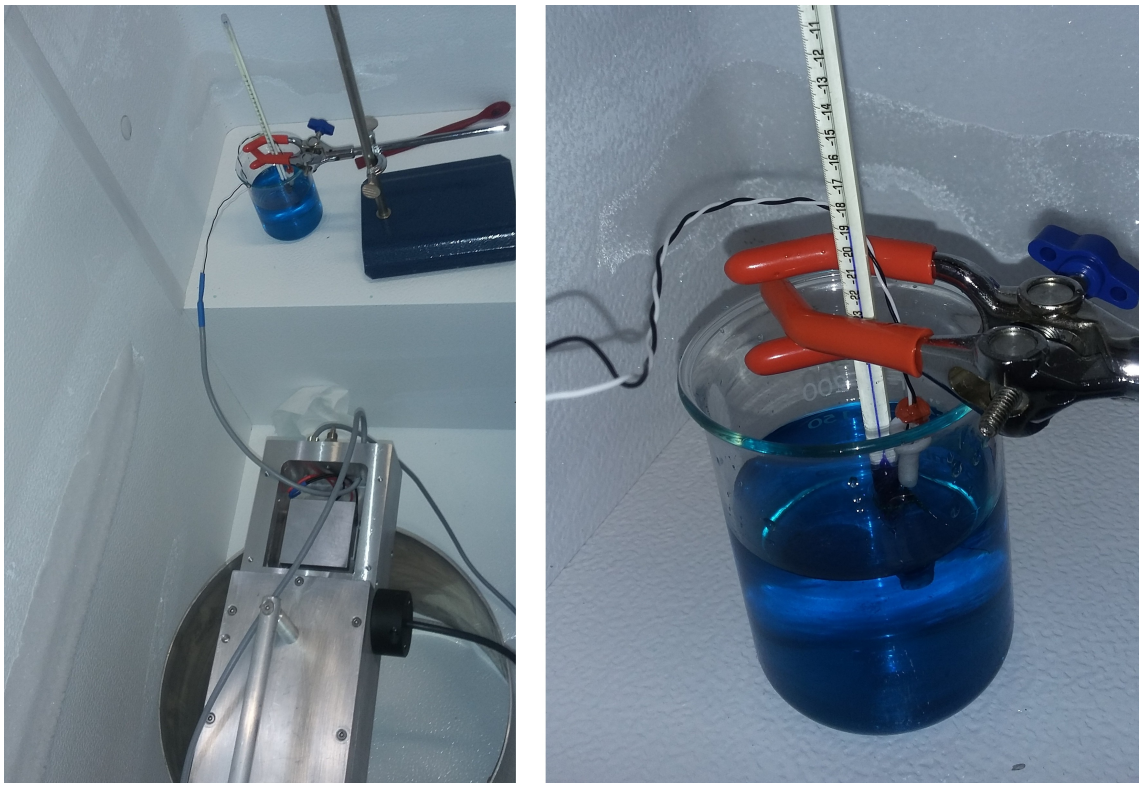

Figure 2.9: Temperature calibration of the thermocouples was performed by recording the different values measured by the probes temperature when place in thermal contact with the reference thermometer. The thermal contact was obatined by plunging the probes in ethylene glycol and inside the freezer chest. At least three different temperatures were considered to trace the calibration curve.

smashed through an ice crusher to maintain a fine size of the granular bed, which accounts for a better functioning of the water vapour source. The water vapour source is a rectangular, thermostatically controlled stainless steel chamber containing ice. The temperature controller is fixed to the aimed value, and it pilots the chest freezer. The DFPC walls and the ice stabilise to the freezer chest temperature. Experience has shown, that the ice temperature stabilise on the DFPC wall temperature (which in turn is fixed by the chest freezer temperature). Also the air spreading inside the ice reduce its temperature until an equilibrium with the surroundings.

The limit of detection (LOD) equals the error of the background or one standard deviation, i.e. the 68 % confidence interval minus the background mean, which is approximately the square root of the mean counts. The background range from 1 to 10 crystals for filter. To diminish the background counts, the water vapour source (i.e. the ice granular bed) is regularly regenerated with new ice -based on ultrapure Milli-Q water- and the chamber is cleaned once a week to remove residuals of particles.

2.3.3 Instrument validation experiments

Validation of the DFPC set up was conducted under controlled laboratory conditions to calibrate S_w and T (as explained in the previous calibration section) and further validated through the test experiments of the second phase of the Fifth International Ice Nucleation Workshop (FIN-02) at

the Karlsruhe Institute of Technology's Aerosol Interactions and Dynamics of the Atmosphere facility. The result of this intercomparison are reported in DeMott et all. (in press [179]). Experimental methods involved sampling of aerosol particles by online ice nucleation measuring systems from the same volume of air in separate experiments using different ice nucleating particle types, and collections of aerosol particle samples onto filters or into liquid for sharing amongst offline measurement techniques. During FIN-2, a total of nine mobile IN instruments directly sampled from AIDA aerosol chamber. Among them, two diffusion chambers FRIDGE and DFPC have partecipated, by sampling off line the filters taken and addressing deposition and condensation nucleation modes.

Past intercomparisons have shown a highly variability (upon 2 order of magnitude) for different instrument working at the same S_w conditions (Jones et al., 2011 [183]). The problem of water depletion was historically addicted as one of the main responsible for differences in static chambers.

In these comparisons, the AIDA expansion chamber measurements were taken as reference, considering that it is expected to be the closest representation to INP activation in atmospheric cloud parcels, due to exposing particles freely to adiabatic cooling. The aerosol types tested were: minerals Illite NX and K-feldspar, two natural soil dusts representative of arable sandy loam (Argentina) and highly erodible sandy dry land (Tunisia) soils, respectively, and a bacterial INP (Snomax®).

During the workshop, temperature uncertainties were inferred to be a key factor in determining INP uncertainties. Collection onto filters versus directly into liquid in impingers made also a little difference. For offline methods that activated single particles on a substrate at a controlled humidity at or above water saturation, agreement with immersion freezing methods was good in most cases. For illite NX the comparison among DFPC-ISAC at -20 °C and the upper bound values of FRIDGE-STD shown to be consistent with the parametrization found by Hiranuma et al., (2015) [157] to represent immersion freezing measurement data. Furthermore, it was seen that both DFPC-ISAC and FRIDGE-STD were mostly consistent with the immersion freezing data.

Results from FRIDGE and DFPC are shown as INP concentration at T=-20 °C and saturation ratios of 0.95 and 1.01 with respect to water, in Figure 2.11 INP concentrations and n_s density were in agreement between the two instruments for all mineral dusts (R_2=0.927). Furthermore, size equivalent Ice Nucleation Active Surface-site density for mineral dusts were in agreement with the published data (Hoose et al.,2012 [49]).

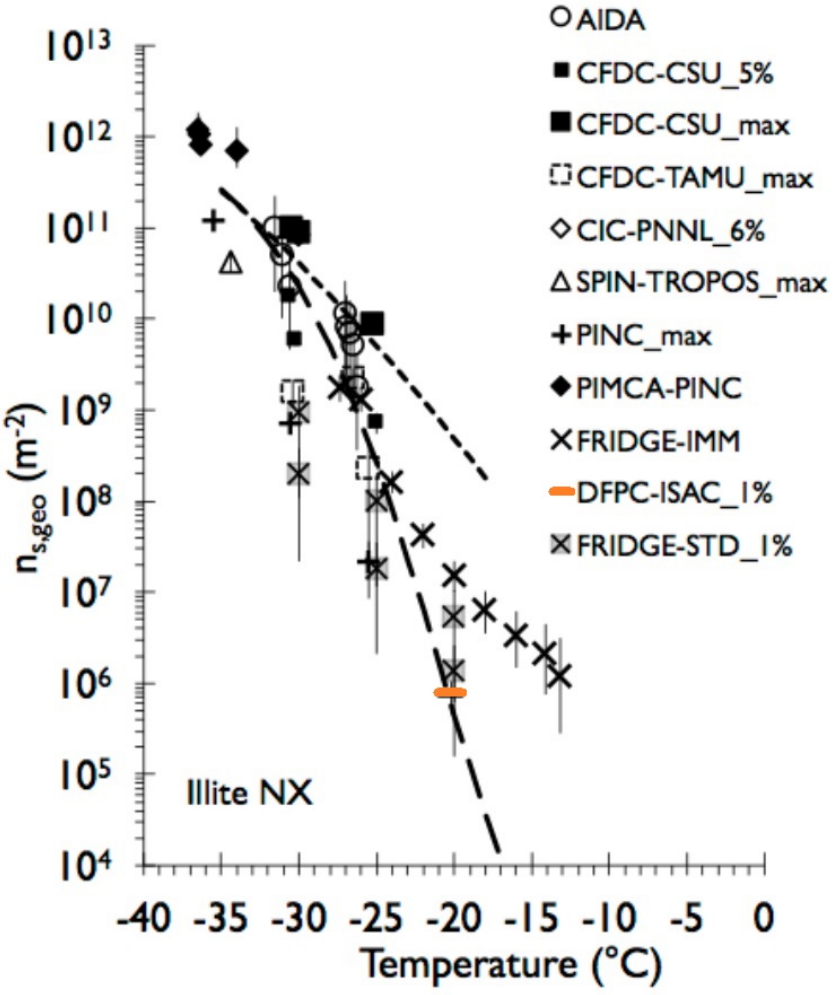

Figure 2.10: Geometric surface active site density parameter, ns,geo from multiple experiments performed on illite NX aerosols sampled directly from the AIDA chamber (FIN-02 AIDA experiments). The term "max" means the highest RHw achieved in a scan (102-110 %) by portable instruments. Fit curves for illite NX are from Hiranuma et al. (2015). Figure taken from DeMott 2018 and modified to highlight DFPC (in the text referred to as DFPC-ISAC).

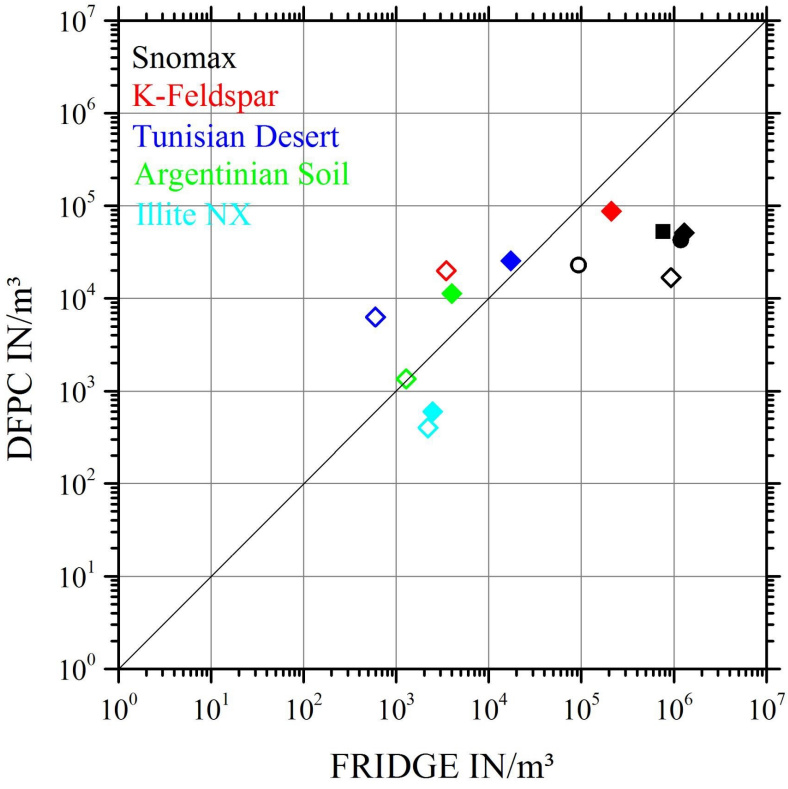

Figure 2.11: INP concentration at −20 °C obtained with FRIDGE and DFPC (m-3). Open symbols: saturation ratio 0.95; filled ones: saturation ratio 1.01 in [184].

Chapter 3

Ice Nucleating Particle Measurements within BACCHUS and Air-Sea Lab

High elevation sites are useful to investigate tropospheric baseline conditions, long-range transport and vertical mixing processes, by which atmospheric boundary layer pollutants are mixed into the free troposphere (Baltensperger et al., 1997 [185]; Bonasoni et al., 2000 [186]; Lugauer et al., 2000 [187]; Marinoni et al., 2008 [188]). These sites offer the possibility to make prolonged observations of free-tropospheric and in-cloud conditions (warm and mixed-phase clouds), impractical with research aircrafts. This is particularly useful for studying INP, as observations can be made at altitudes closer to those at which cloud formation generally occurs.

Results from INP measurements around the world have been published in the past few decades, however, only few of them regard the Mediterranean region. Recently, Schrod et al. (2017) [189] measured the vertical distribution of IN over the East Mediterranean by unmanned aircraft. In addition, a few ground observations are available for the Eastern Mediterranean region (Gagin, 1975 [190]; Levi and Rosenfeld, 1996 [191]; Ardon-Dryer and Levin, 2014 [192]). However, concerning the central Mediterranean basin, the only INP ground measurements were reported by Santachiara et al., 2010 [180] for San Pietro Capofiume station, a rural area in the Italian Po Valley, near Bologna.

In this chapter, we report the results of offline INP measurements, performed for the first time at the Italian Climate Observatory "O. Vittori" (Mountain Cimone, 2165 m above sea level) in the northern Apennines. In the period 19-29 May 2014, the measurements took place not only at Mountain Cimone but also at the low-altitude station San Pietro Capofiume. During these two parallel campaigns, the sites were mainly reached by air masses from the South. In the period between the 21^{st} and the 23^{rd} of May, a Saharan Dust transport Event (SDE) took place and it was recorded simultaneously at the high and the low level station. In a second campaign performed during October, only at Mountain Cimone, air masses were mainly from North-East and West, and results are also described in this chapter.

The main aim of the present work is to investigate INP levels and transport processes over the central Mediterranean region, to lay the foundations of a better understanding of the aerosol-climate interactions over this climate hot spot. The results presented in this chapter were obtained through the freezing detection apparatus Dynamic Filter Processing Chamber

Figure 3.1: Location of Mountain Cimone and San Pietro Capofiume, where the described field campaigns took place. The samples were analysed in Bologna city, which hosts the ISAC-CNR laboratory. A picture of the Italian Climate Observatory "O. Vittori" is also reported.

(DFPC), during the first eighteen month of the present doctorate research program. Samples were collected previously -in 2014 and 2015- during several measurements campaigns that were organised under the funding projects: European FP7-ENV-2013 Project BACCHUS (grant no. 603445); and CNR funded bilateral project "Air-Sea Lab: Climate air pollution interaction in coastal environment". In detail:

- the aim of the EU project was to investigate the importance of biogenic versus anthropogenic emissions and to understand the key regulators of biosphere-aerosol-cloud-climate feedbacks that occur via emission and transformation of biogenic volatile organic compounds, primary biological aerosols, secondary organic aerosols and dust;
- the aim of the AIR-SEA LAB project was similar to BACCHUS but more focused on the coastal environment and concerned mainly the study of aerosol physico-chemical properties and aerosol-cloud interactions at the air sea interface.

Results have already been published in Nicosia et al., 2017 [178], Belosi et al., 2017 [176], Rinaldi et al., 2017 [177], and presented at the international European Geosciences Union General Assembly in 2017 [193]. A summary of the data and the main conclusions obtained will be reported in this chapter.

3.1 Methods

Mountain Cimone (MC) is the highest peak of the north Italian Apennines. The top of MC (44°11′ N, 10°42′ E; 2165 m a.s.l.) hosts the Italian Climate Observatory "O. Vittori" that is part of the Global Atmospheric Watch (GAW) program of the World Meteorological Organisation (WMO). The station is situated at the southern border of the Po Valley, which is a highly populated and industrialised area, also characterised by intense agricultural activities.

Also considered in the present study is San Pietro Capofiume (SPC), a rural site located at about 30 km north-east of Bologna, in the eastern Po Valley (44°39′16.33″N; 11°37′22.28″E), which hosts the "Giorgio Fea" Meteorological Station.

For both MC and SPC campaigns the experimental method is describe above.

- Aerosols were sampled by using two different sampling heads in parallel (1 μm, and 10 μm cut-point, Standard EN 12341, TCR Tecora) in front of the filters. The aim was to size segregated PM10 and PM1 aerosol fractions, i.e., particles with aerodynamic diameter lower than 10 μm and 1 μm. Each fraction was collected on individual nitrocellulose membrane filters (Millipore HABG04700, nominal porosity 0.45 μm) twice or three times a day (indicatively one in the morning, one in the afternoon and one at night) to capture different stages of the planetary boundary layer evolution.

- Sampling occurred with a mean flow rate of 38.3 L min^{-1} and a sampling time of 15 min for each filter. The short sampling time was necessary to avoid filter overloading, which makes INP counting unfeasible. The measurements were performed at ambient humidity conditions (i.e. any drier was included to the sampling line, thus reducing particle losses along the lines).

- The experimental campaigns that will be considered in this study, were carried out in the following periods:

  - from 19 to 29 May 2014, named *MC1*, in Mountain Cimone;
  - from 19 to 30 May 2014, named *SPC*, in San Pietro Capofiume;
  - from 5 to 12 October 2015, named *MC2*, in Mountain Cimone.

  Sampling occurred at 3.5 m above ground level for MC1 and MC2 and at 2 m above ground level for SPC .

- Aerosol particle size distribution was measured by means of an Optical Particle Counter (OPC, Model 1.108, Grimm Aerosol Technik GmbH). In the following text, N_{X-Y} will indicate the number of particles with diameter comprised between X and Y μm obtained from the Grimm OPC.

- Meteorological data (air temperature, relative humidity and atmospheric pressure) were recorded by an integrated automated weather station (Rotronics and Technoel), while wind speed and direction were recorded by a sonic anemometer (Vaisala WS425).

- Back-trajectories were calculated through the NOAA HYSPLIT model, while dust model forecast (Nickovic et al., 2001; Pérez et al., 2006) were obtained through BSC-DREAM from the Barcelona Supercomputing Center (BSC).

- During MC campaigns, the time series of cloud amount estimate were also considered. This information, provided as the fraction of celestial dome covered by all clouds, was provided by the Italian National weather Service (Italian Air Force) by using the manual methodology recommended by WMO (2014). Reactive gases (O_3, CO, NO_x) were also

monitored at MC in the framework of WMO/GAW programme. The experimental method used for the gases analyses can be found in Cristofanelli et al. (2016) [194].

For all the campaigns, INP concentrations were analysed through the DFPC device -described in the second chapter- that belongs to the offline category of the "membrane filter techniques" (Bigg, 1990b [195]; Bigg et al., 1963 [196]; Lala and Jiusto, 1972 [197]; Stevenson, 1968 [198]). INP concentrations were detected at different temperatures and water saturations. In detail, measurements were carried out at -18 °C (and -22 °C for a few samples), while Sw was 1.01 (and 0.96 for a few samples). As explained in the second chapter, measurements with DFPC below water saturation (Sw<1) are considered representative of deposition nucleation, while above water saturation (Sw>1) are representative of condensation-freezing.

In a few cases (3 over 35 samples), the IN_{PM_1} concentrations were higher than the corresponding $IN_{PM_{10}}$ concentration. It is known that INP measurements performed by off-line methods include a complex procedure (sampling of aerosols on filter, preparation of the filter and detection of INP, as described in the second chapter) and that the technique holds intrinsic uncertainty. Repeated analysis of simultaneously sampled filter can yield some spread in the number of observed INP (as reported by Schrod et al., 2016 [174]). Furthermore, it is an open question if repeated deposition/condensation experiments at the same temperature and water vapour saturation ratio provides the same results (Knopf and Koop, 2006 [199]; Wang and Knopf, 2011 [200]; Wang et al., 2012 [201]). Given these reasons, we have decided to provide all the results obtained from the measurements, avoiding manipulations of the datasets, to provide a measure of the uncertainty associated to the presented observations. In any case, these uncertainties do not invalidate the obtained results and the conclusions derived from them.

3.2 Results

3.2.1 Ice nucleation rates at Mountain Cimone in May 2014

Figure 3.2 reports the atmospheric concentrations of INP, detected in the PM1 and PM10 fractions and named respectively IN_{PM_1} and $IN_{PM_{10}}$, during MC1 campaign. INP were activated at Sw = 1.01 and T = -18 °C. The associated particle number concentration, named $N_{0.5-1}$ and N_{1-10}, was extrapolated from the Grimm optical counter respectively INP the intervals 0.5-1 μm and 1-10 μm. This is also indicated in Figure 3.2.

The observed INP levels ranged from 10 to 135 particles m^{-3}, in the PM1 fraction, and from 30 to 220 particles m^{-3}, in the PM10 fraction. The average INP concentration was 86±40 IN m^{-1} for the PM10 and 64±49 IN m^{-1} for the PM1, thus leading to an average 67% contribution of the PM1 fraction (where IN refers to Ice Nuclei). In this campaign, the contribution of INP in the aerosol fraction larger than 1 μm (i.e. the coarse fraction) was the 33 %.

During this campaign, a significant correlation (p-value<0.05, n = 16) was observed between INP concentrations and aerosols concentrations, in both the IN_{PM1} fraction (R = 0.75 correlating to $N_{0.5-1}$) and $IN_{PM_{10}}$ fraction (R=0.61 correlating to N_{1-10}). The correlation between coarse INP and the related aerosol concentration ($IN_{PM_{1-10}}$ versus N_{1-10}) was significant only during the Saharan dust event (R = 0.59, $p < 0.05$, n = 8).

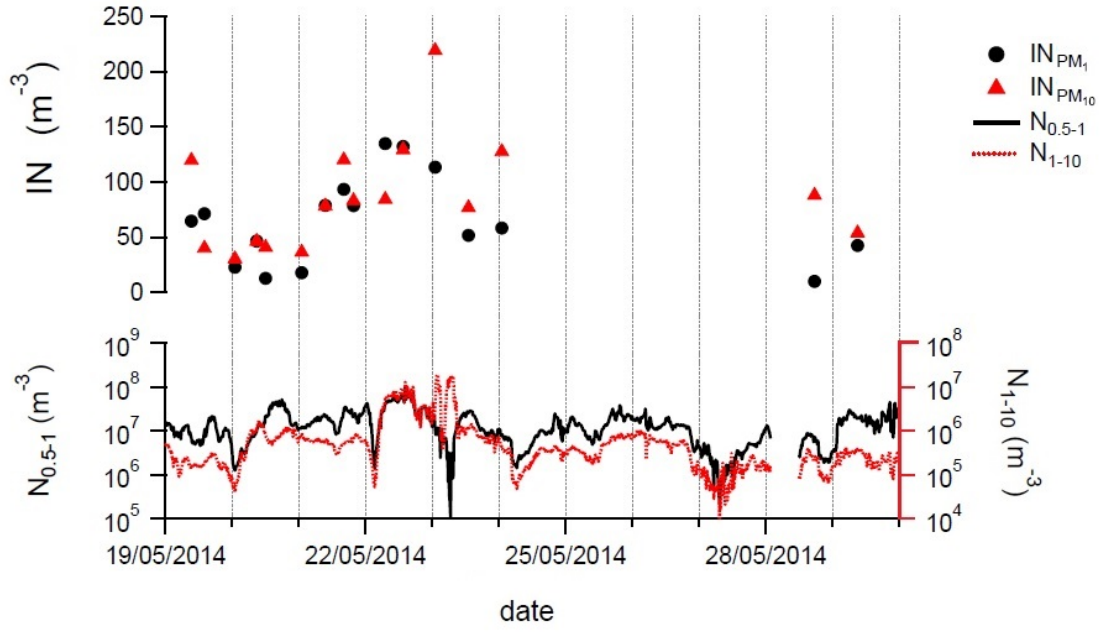

Figure 3.2: Atmospheric concentration of INP, in the PM1 and PM10 fractions, and particle number concentration, in the 0.5–1 μm ($N_{0.5-1}$) and 1–10 μm (N_{1-10}) size ranges, observed during MC1 (T=18 °C, SW=1.01).

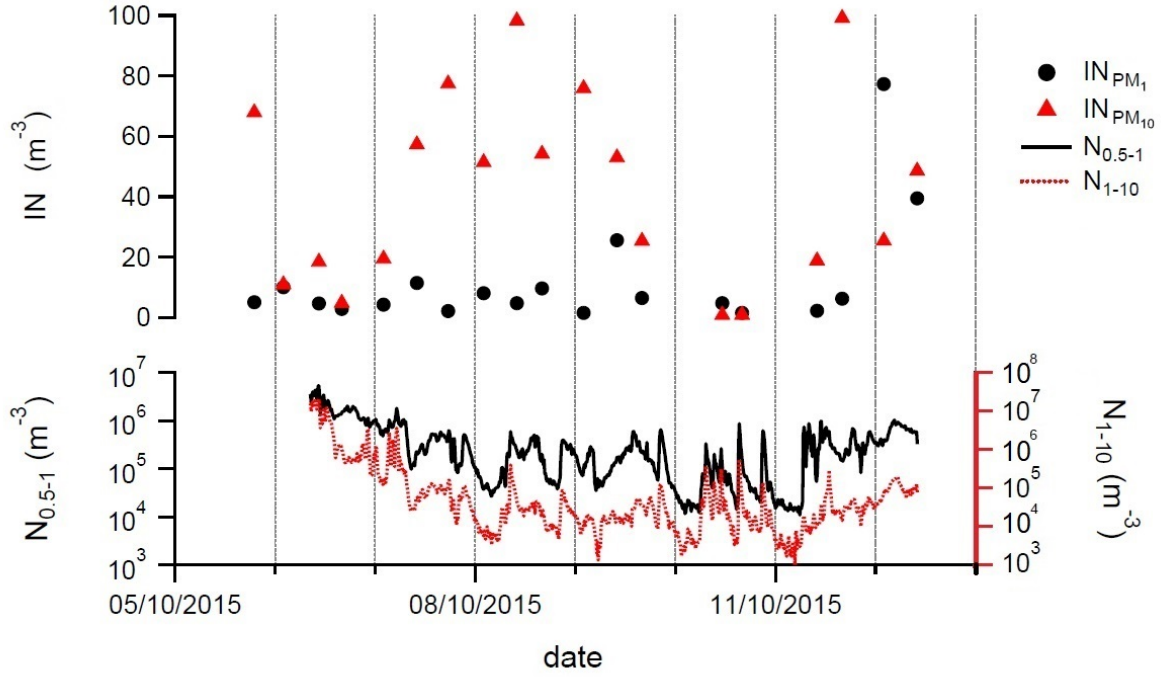

Figure 3.3: Atmospheric concentration of ice nuclei (IN), in the PM1 and PM10 fractions, and particle number concentration, in the 0.5–1 μm ($N_{0.5-1}$) and 1–10 μm (N_{1-10}) size ranges, observed during MC2 (T = −18 °C, SW = 1.01).

Considering as metric the activated fraction (AF), the average value, obtained from PM10 filters analysis, was (4.3±4.5) 10^{-5} at Sw = 1.01 and T = −18 °C. In this calculation, AF is the ratio among the number of ice crystals grown on the filter, at Sw = 1.01 and T = −18 °C, and the number of aerosol particles collected on the filter (estimated from the Grimm OPC and considering optical diameters >0.5 μm).

3.2.2 Ice nucleation rates at Mountain Cimone in October 2015

Considering CM2 campaign, the time series of INP and aerosols concentrations are reported in Figure 3.3 and refer to the same thermodynamic conditions of activation than MC1.

During MC2, the average number concentration of INP was lower than in MC1, for both IN_{PM10} (43±32 m^{-3} versus 86±40 m^{-3}) and IN_{PM1} (12±19 m^{-3} versus 64±49 m^{-3}). The IN_{PM_1} levels remained constantly lower than <20 ice nuclei m^{-3}, made the exception of the last two days, while the $IN_{PM_{10}}$ varied to a great extent (around two orders of magnitude). Overall, INP levels were in the range 1–77 m^{-3} for PM1 filters and 1-99 m^{-3} for PM10, thus lower than MC1 campaign (as reported in Figure 3.5).

The average contribution of the coarse fraction to the INP population was relevant (the 72% in MC2 with respect to the 33% in MC1). No correlation between INP number concentration per unit volume and total particle number concentration was observed during MC2.

Considering the average activated fraction (AF), in PM10 filter, MC2 shows a higher value (2.4±3.2) 10^{-4}, almost 5 times the AF detected in May, suggesting a seasonal change in the composition of the INP population and/or in background aerosols.

3.2.3 Ice nucleation rates at SPC in May 2014

Figure 3.4 reports the atmospheric concentration of particles, in the PM1 and PM10 fractions, and the related time series of INP concentration during SPC campaign. The average INP concentrations, activated at Sw=1.01 and T=−18 °C, are 172±72 m^{-3} for the PM10 and 108±52 m^{-3} for the PM1. In this campaign the contribution of the coarse fraction $IN_{PM_{1-10}}$ is 37%, thus slightly higher than MC1 (the 33%).

When comparing the INP concentrations, MC1 is about a half of that at SPC (see Figure 3.5). Excluding situations characterised by high altitude transport of dust plumes, a decrease of INP with altitude is generally reported in literature, coupled with a decrease of aerosol concentration (Schnell et al., 1982 [202]; Jiang et al., 2014 [203]; Conen et al., 2015 [204]). By comparing the activated fractions -in PM10 filters- we found comparable values: (4.9±4.0)x10^5 for SPC and (4.3±4.5)x10^5 for MC1.

In a previous campaign (see Santachiara et al., 2010 [180]) performed at SPC in the period 09–12 July 2007, at close thermodynamic conditions (Sw = 1.00 and T=−19 °C), the contribution of the coarse fraction was 49% (close to the value of 37% reported here for SPC in Mai 2014). In the July 2007 campaign, the average IN concentration was 171 m^{-3} for the PM10 and 101 m^{-3} for the PM1, these values are also correspondent to the average found in May 2014 (and obtained at closed thermodynamic conditions).

During SPC campaign, in May 2014, a few days were characterised by frequent precipitation events (period 26–30 May) and during them we noticed a slightly higher concentration of aerosols

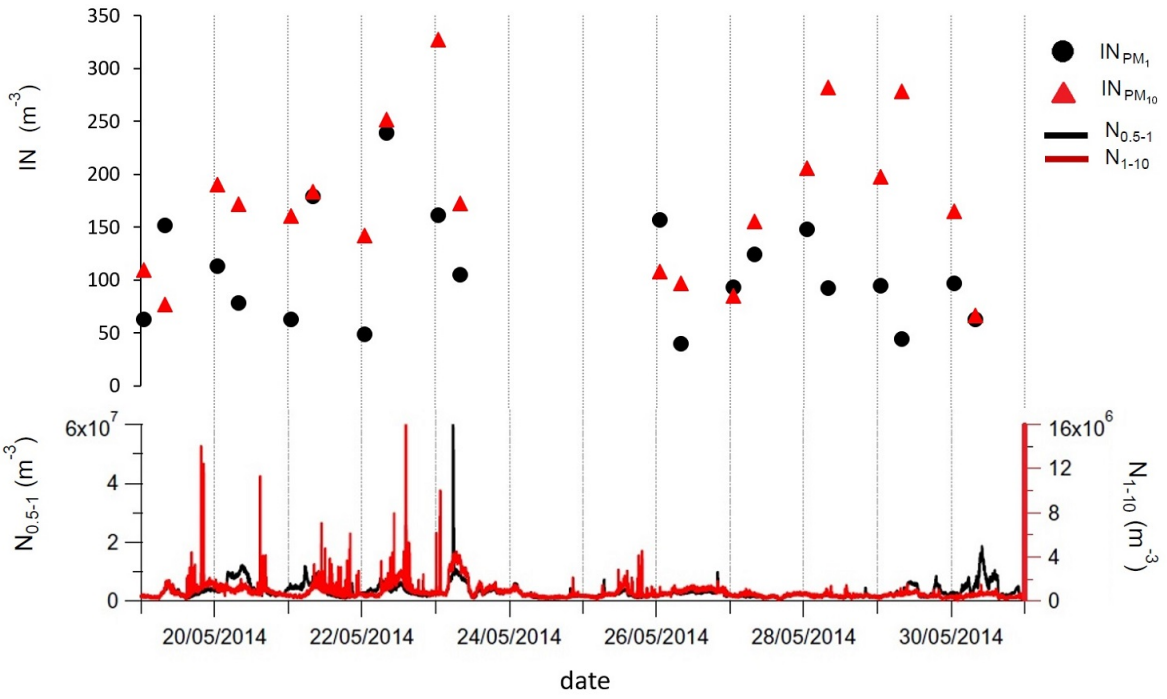

Figure 3.4: Time series of INP and particle number concentrations during May 2014 at San Pietro CapoFiume.

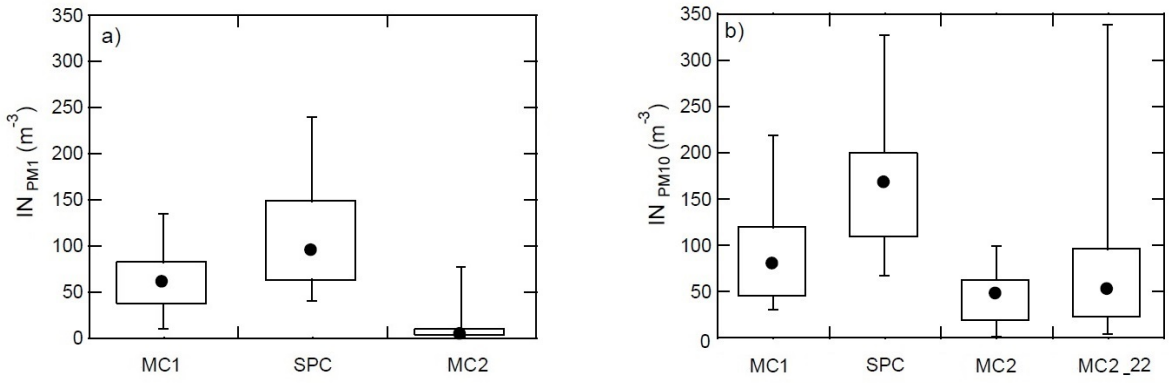

Figure 3.5: Box and whiskers plot for INP concentration (m^{-3}) for the PM1 (a) and PM10 (b) size fractions at T=−18°C and Sw =1.01, made the exception of $MC2_{22}$. $MC2_{22}$ indicates measurements performed at −22 °C. Each dot represents the median value, while the box represents the 25^{th} and 75^{th} percentiles, and whiskers are minimum and maximum values.

in the range 0.5–10 μm, with respect to days with no precipitation (6.80x10^6 m^{-3} and 3.81x10^6 m^{-3}, respectively). On the overall, the rainfall intensity was low ($\sim$0.4 mm h^{-1}). Only in a few cases, we noted a remarkable INP decrease in the PM10 fraction (26 May, 8 a.m. and 1 p.m.; 27 May, 1 p.m.) concomitant to precipitation events.

The non regular relationship between INP concentrations and precipitations is often related to the complexity of the aerosol scavenging processes and the possible combination of other phenomena (e.g. droplets evaporation in clouds or near the ground) as reported in previous studies (Cotton and Field, 2002 [205]; Field et al., 2001 [206]; Rosinski and Morgan, 1991 [207]).

A fall in INP concentration before and after precipitation has been reported by several authors associated with high rainfall event (Bertrand et al., 1973 [208]; Bigg and Miles, 1964 [209]; Jiang et al., 2015 [210]). Hobbs and Locatelli (1970) [211] observed that in many cases rain showers occurred without being accompanied by any significant modification in ice nucleation. In turn, several authors reported an increase in INP concentration at ground level at the onset of rain (Ryan and Scott, 1969 [212]) probably due to release of ice nuclei by the evaporation of small drops between cloud base and ground or during fog dissipation. Bigg et al. (2015) [213], Huffman et al. (2013) [214] and Prenni et al. (2013) [215] showed that the ground level INP concentrations in a forest ecosystem were enhanced during rain events, and that a fraction of these were biological. A similar result was obtained by Hara et al. (2016) [216] in a forested site in Japan. Biological particles, which become a source of INP, can be released during precipitation and during periods of high humidity through mechanisms such as spore release from fungi, mechanical ejection of bacteria and spores from leaf surfaces, and pollen release and fragmentation during wet weather. Wang et al. (2012) [201] performed irrigation experiments of soil surface and found that intensive water impaction is sufficient to cause ejection of airborne soil organic particles from the soil surface. The importance of soil organic matter as strong ice nuclei has been reported in laboratory and field studies (Schnell and Vali, 1972 [217]). In our case, the rainfall intensity was low, and we did not measure any increase of INP during these events. Therefore, we conclude that soil (and associated bio-particles) emission, triggered by precipitation, was not an important source of INP during the SPC campaign.

3.3 Influence of the saturation ratio versus freezing temperature on the measured INP concentrations

Samples collected during MC2 underwent analysis at two different activation temperatures (T=$-$18 and T=$-$22 °C) and saturation ratio (Sw = 0.92 and Sw = 1.01). Figure 3.6 shows the averaged INP concentrations for MC2 as a function of the thermodynamic conditions. We observed that the INP concentrations (calculates as number of INP per unit volume) generally increases by increasing the saturation ratio and by decreasing the freezing temperature. By considering PM10 filters, tested under constant saturation ratio (Sw=1.01), the average concentration of INP was 43 m^{-3} at T=$-$18 °C and 71 m^{-3} at T=$-$22 °C. The temperature dependency, inferred from the difference between measurements performed at $-$18 and at $-$22 °C, is consistent with the one presented by DeMott et al. (2010) [47], even though the concentration range of our measurements is about one order of magnitude lower than those reported in the cited paper (see

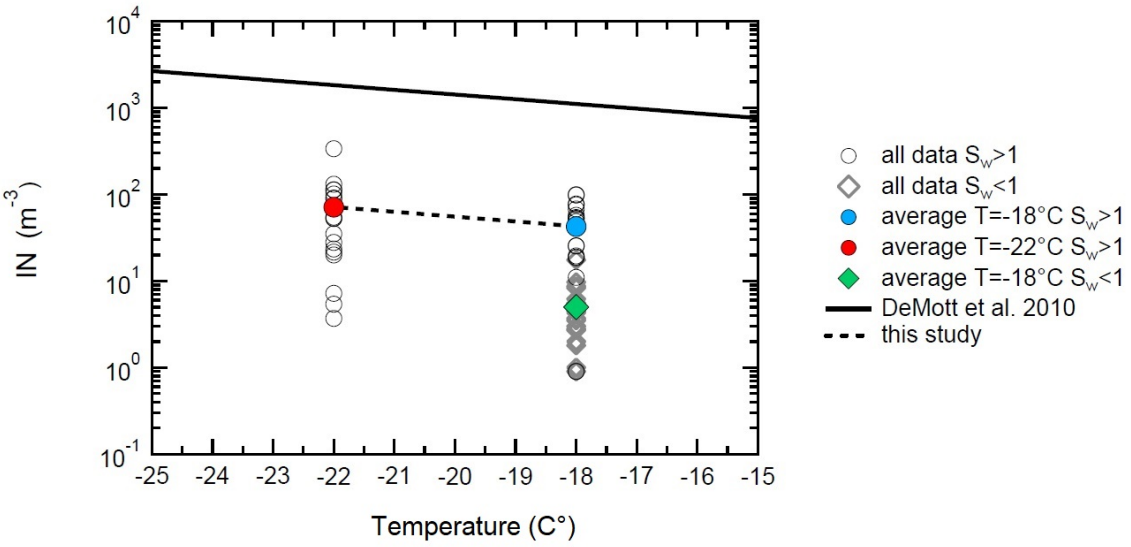

Figure 3.6: INP concentrations (single samples and average values) measured during MC2 in the PM10 size fraction, as a function of the activation temperature and of Sw. The dashed line represents the exponential fitting of the average INP concentrations obtained at −18 and −22 °C. The INP versus Temperature parametrization by DeMott et al. (2010) [47] is also reported for comparison purposes.

the solid and dashed lines in Figure 3.6). However, most of the data collected by DeMott et al. (2010) [47] were made at water relative humidity between 101% and 104% (while it was mainly 101% in this study) and the considered aerosol size distribution was between 0.5 and 1.6 μm.

By considering a constant temperature (T= −18°C), the average concentration of INP increased from 5.1 m^{-3} at Sw = 0.92 to 43 IN m^{-3} at Sw = 1.01. Therefore, with the considered set of samples originated from MC2 campaign (only PM10 filters), the transition from sub-to super-saturated conditions appeared to have a greater influence than the decrease of temperature from −18 °C to −22 °C.

Further analysis were performed with DFPC to explore the influence of saturation ratio versus freezing temperature on different samples (generated from laboratory and field campaigns) and have reported in Belosi et al., 2018 [159]. The supersaturations are calculated theoretically from the ice and filter temperatures, and vapour pressure saturation of ice and water (Buck, 1981 [218]). Taking into account the accuracy of the air and sample temperature sensors, and the temperature control system, an experimental uncertainty of about 10% for Sw was estimated.

During our study (detailed in Belosi et al., 2018 [159]), there was a general increase of all INP parameters (number concentration per unit volume, activated fraction AF and ice nuclei surface density n_s) from water sub-saturated conditions (Sw =0.96) to super-saturated conditions (Sw = 1.02). This increase, noticed in all the samples, is tied to the transition from deposition nucleation to condensation freezing.

By considering the variations from Sw = 1.02 to the even higher sur-saturation Sw = 1.1, it was observed a variable answer, in relation to the sample analysed. In detail, the increase of AF and n_s was higher for samples influenced by urban aerosols (collected in Bologna city) and for samples influenced by mixed air masses (sampled in SPC) and it was lower for sample

representative of marine aerosols (collected at the coastal site of Capo Granitola station, in the south of Italy). Our study (reported in [159]) highlights the atmospheric interest in performing measurements of ice nucleation for continental aerosol even at supersaturation higher than 1/2%, a value typically associated with clouds.

3.4 Effect of the Saharan dust event on INP atmospheric concentration

In this section we will focus only on the dataset obtained during May 2014 at Mountain Cimone (MC) and San Pietro Capofiume SPC within the campaigns named MC1 and SPC (see Belosi et al. (2017) [176] for a more detailed description of the event). Between 21 and 23 May 2014, a Saharan Dust transport Event (SDE) took place influencing both MC1 and SPC. The SDE was detected also in the Swiss Alps (as mentioned in Boose et al., 2016 [19]), confirming a transport event that has virtually affected the whole Italian peninsula, from South to North, including the Po Valley. Table 3.1 summarizes the INP results from PM10 filters, by separating days interested by the SDE or not (non-SDE) for activation under condensation freezing at Sw=1.01 and T=−18 °C.

	n	IN_{PM10} m^{-3}	$N_{0.5-1}$ m^{-3}	AF
MC1 (SDE)	8	103 ± 55	(1.1 ± 1.1) x 10^7	(2.0 ± 1.5) x 10^{-5}
SPC (SDE)	6	218 ± 70	(7.2 ± 4.1) x 10^6	(4.6 ± 4.6) x 10^{-5}
MC1 (Non-SDE)	8	68 ± 38	(1.6 ± 1.4) x 10^6	(6.7 ± 5.4) x 10^{-5}
SPC (Non-SDE)	14	163 ± 60	(4.3 ± 2.7) x 10^6	(4.9 ± 4.0) x 10^{-5}

Table 3.1: Average INP concentration and AF during MC1 and SPC campaign, gathering together the results concomitant to the Saharan Dust transport Event (SDE) and the others (Non-SDE). $N_{0.5-1}$ indicates the total particle concentration between 0.5 and 10 μm, while n is the number of point analysed.

Particle concentration $N_{0.5-1}$ (in the size interval 0.5–10 μm) increased during the SDE at both sites; nevertheless, particle number concentration increased almost by one order of magnitude at MC against an increase of around 2 at SPC . As a result, much greater particle number concentrations were observed at MC with respect to SPC during the SDE, while in background conditions the average concentration at SPC (5.0 x 10^6 m^{-3}) is about three times higher with respect to MC1 (1.6 x 10^6 m^{-3}). These data indicate that desert dust travelling in lofted layers can significantly impact aerosol concentrations and IN levels at high elevations. During the SDE, the average INP concentration was higher with respect to non-SDE at both CM and SPC. The ratio between INP concentration at CM during the SDE and in non-SDE conditions is about 1.5, lower than the aerosol number concentration increment discussed above, resulting in a lower AF with respect to non-SDE conditions. This implies that, during the investigated event, the mineral dust transported from the Sahara region was apparently characterised by a lower ice nucleating capability (at the activation condition probed in this work) with respect to aerosol particles affecting CM in typical conditions. The reduced nucleating properties of desert dust particles reaching CM might be due to the modifications of their surface properties during

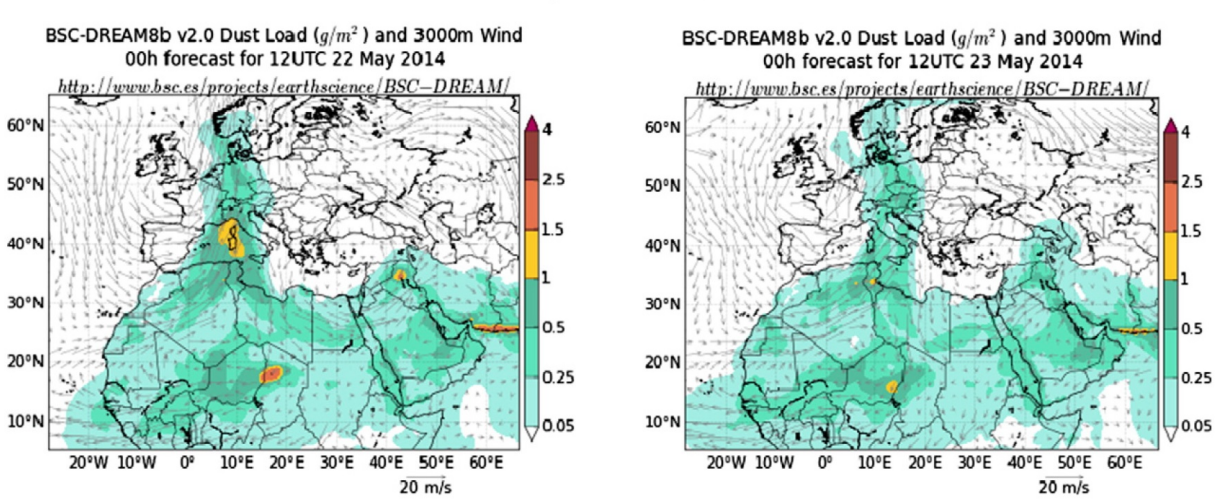

Figure 3.7: Dust load distribution over the Mediterranean region on 22 (left) and 23 May 2014 (right) at 12 a.m. UTC.

transport in the atmosphere ("aging processes"), according to Prospero, 1999 [219] and Levin et al, 2005 [220]. Nevertheless, it is worth highlighting that the activation process was performed at -18 °C, a relative high temperature for the activation of mineral dust, which may have led to an underestimation of the ice nucleation properties of Saharan mineral dust.

AF at the two sites in background conditions (non-SDE) are comparable. This suggests homogeneous aerosol sources at the rural and high altitude site during the 2014 campaign, and that IN were transported along with the total aerosol population between the two sites (with a net transport from the boundary layer to the high altitude site). The influence of vertical transport from lower tropospheric layers on the INP concentration at MC will be further discussed in next Section.

3.5 Effect of vertical transport and synoptic circulation on IN concentration at MC

To investigate the effect of vertical transport on the INP concentration at the high altitude station, we calculated the daily relative increase RI in the specific humidity SH for each day of the two campaigns. SH can be used as a tracer of air masses transport at high altitudes (Henne et al., 2005 [221]). This approach, introduced by Prévôt et al. (2000) and Henne et al, 2005 [221] for two sites in the Alps, was already applied to MC station by Carbone et al., 2014 [222] and Rinaldi et al., 2015 [223].

$$RI = \frac{[SH_{aft}(MC) - SH_{nig}(MC)]}{[SH_{aft}(SPC) - SH_{nig}(MC)]}$$

where SH_{aft}(MC) is the average specific humidity measured in the afternoon at Mt. Cimone, SH_{nig}(MC) is the average specific humidity measured during the night at Mountain Cimone and SH_{aft}(SPC) is the average specific humidity measured in the afternoon at the rural background

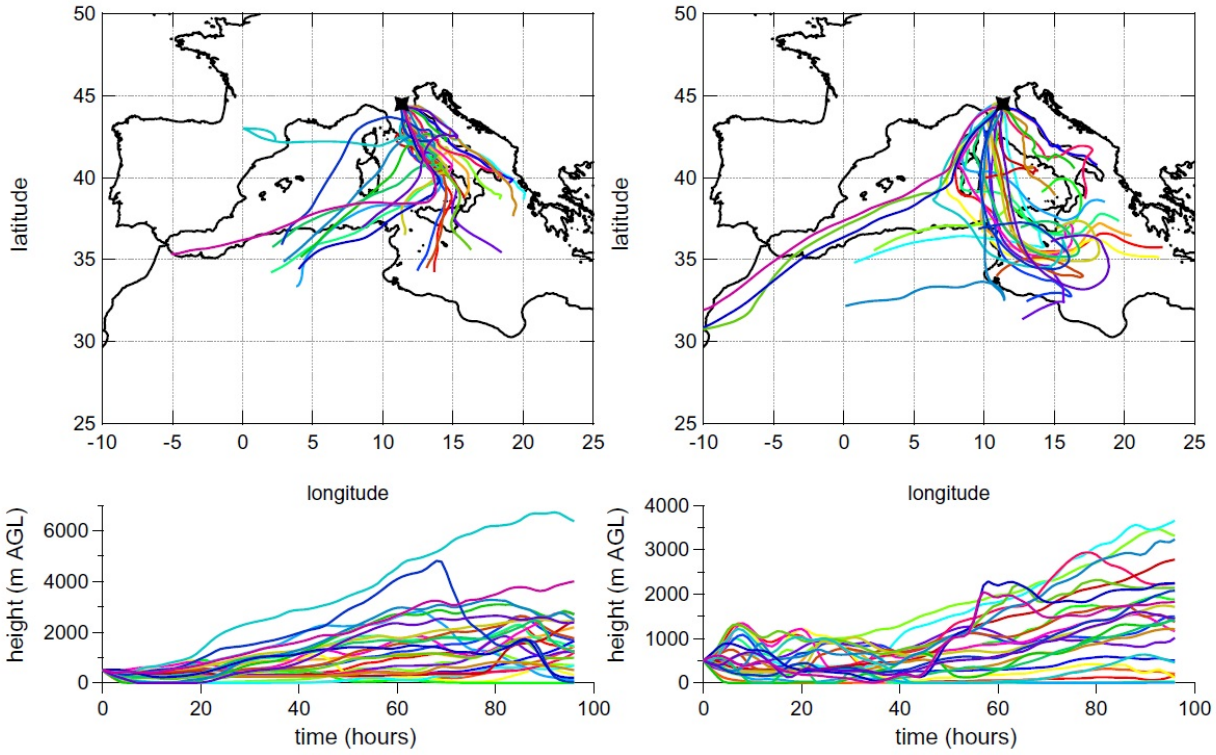

Figure 3.8: The 4-day backward trajectories of air masses arriving at SPC at 500 m AGL at 1 p.m. UTC on 22 (left) May and 23 May 2014 (right), calculated by the NOOA HYSPLIT model.

		T	RH	WS	P	SH	O_3	CO	NO_x	O_3/NO_x	CO/NO_x
CM1 (May 2014)	IN_PM_1	**0.69**	0.01	0.37	0.13	**0.56**	**−0.54**	−0.20	-	-	-
	IN_PM_{10}	0.19	−0.16	**0.72**	−0.38	0.08	−0.30	−0.14	-	-	-
	$IN\_PM_{1\text{-}10}$	−0.38	−0.39	**0.66**	**−0.66**	−0.43	0.17	−0.33	-	-	-
	$N_{0.5\text{-}1}$	**0.71**	−0.03	0.14	0.15	**0.57**	**−0.77**	−0.44	-	-	-
	$N_{1\text{-}10}$	0.33	0.17	**0.82**	−0.32	0.39	**−0.56**	−0.22	-	-	-
CM2 (Oct 2015)	IN_PM_1	−0.07	−0.18	−0.22	0.33	−0.15	**0.72**	−0.19	−0.34	**0.52**	**0.45**
	IN_PM_{10}	0.20	**−0.58**	−0.18	**0.65**	−0.02	−0.05	−0.09	**−0.45**	0.21	0.31
	$IN\_PM_{1\text{-}10}$	0.22	**−0.51**	−0.10	**0.54**	0.03	−0.39	0.02	−0.19	−0.11	0.01
	$N_{0.5\text{-}1}$	**0.60**	0.27	−0.31	0.11	**0.75**	−0.21	−0.17	−0.26	0.11	0.09
	$N_{1\text{-}10}$	**0.53**	0.21	−0.24	0.10	**0.65**	−0.24	−0.08	−0.16	0.04	0.03

Figure 3.9: Pearson's correlation coefficient between aerosol data, meteorological parameters and gas tracers during MC1 and MC2. Bold values are statistically significant ($p<0.05$, $n=16$ for MC1, $n = 19$ for MC2).

station of SPC. Here SPC is assumed to be representative of meteorological conditions at the foot of the MC mountain station, although it is about 90 Km far from it.

This assumption holds considering that the Po Valley is characterised by a general good air mixing within its boundaries (Ricciardelli et al., 2017 [224]). Moreover, SPC can be considered a more suitable station compared, for example, to Bologna (which is closer to MC), as it is not perturbed by local influences (e.g., urban heat bubble).

A *RI* of 1 virtually corresponds to a complete replacement of the high altitude air by boundary layer air, while no vertical motion yields zero relative increase. The average *RI* for the MC1 campaign was 0.46 ± 0.45, while a smaller relative increase index (0.24 ± 0.21) was found in October 2015. This indicates that the sampling site was significantly more influenced by vertical uplift of boundary layer air from lower altitudes during the first campaign than during the second one. This is in agreement with the lower INP and particle number concentrations observed in October 2015 (even excluding the SDE). Indeed, IN_{PM10} of MC2 was 43±32 while IN_{PM10} of MC1 -excluded the SDE- was 68±38.

Correlation analysis between INP and meteorological parameters or gaseous tracers measured at MC (Figure 3.9) shows that IN_{PM1} concentration (Sw = 1.01) correlated with *SH* during the first campaign, confirming that the sub-micrometer INP concentration was regulated by the PBL dynamics and pointing to important IN sources from the PBL during that period. Conversely, IN_{PM1} shows a negative correlation with *SH* during the second campaign, while correlating with the O_3/NO_X and CO/NO_X ratios. These ratios are often used to evaluate the photochemical age of air masses, which increases at the increase of the ratios.

In particular, the median O_3/NO_X ratio (∼360) of the October 2015 campaign is typical of very aged background air masses (Morgan et al., 2010 [225]). In summary, the concentration of sub-micrometer INP, during the second campaign, seems regulated more by the advection of aged air masses and therefore by aerosol sources likely located at remote distances from the measurement station and from the Po Valley itself. Correlations with coarse-mode $IN_{PM_{1-10}}$ are always weaker, likely indicating a lower influence of PBL dynamics and synoptic circulation.

During MC1, coarse INP and particle concentrations were positively correlated with wind speed (WS), while during MC2 coarse INP were negatively correlated with relative humidity (RH). Furthermore, cloud coverage observations by the Italian Air Force at MC show that in-cloud conditions were frequent during MC2 and that the prominent peak of coarse IN (7–10 October 2015) characterising the campaign coincides with the major off-cloud period. This suggests that coarse INP may have been scavenged by cloud droplets during MC2. No such effect was observed during MC1, although in-cloud periods were reported, and for IN_{PM1} in both campaigns.

These observations suggest that coarse INP concentration may be more influenced by local meteorological conditions. In the case of MC1, the link with local wind speed may also suggest a relation with local aerosol sources. The time series of the main meteorological parameters (including occurrence of in-cloud conditions derived from visibility data) are reported in Figure 3.10 and 3.11.

In order to investigate the influence of synoptic circulation on the INP concentration at MC, 96 h back-trajectories were calculated by means of the HYSPLIT model provided by the NOAA Air Resources Laboratory (Stein et al., 2015 [226]; Rolph, 2017 [227]) for each sample, and the

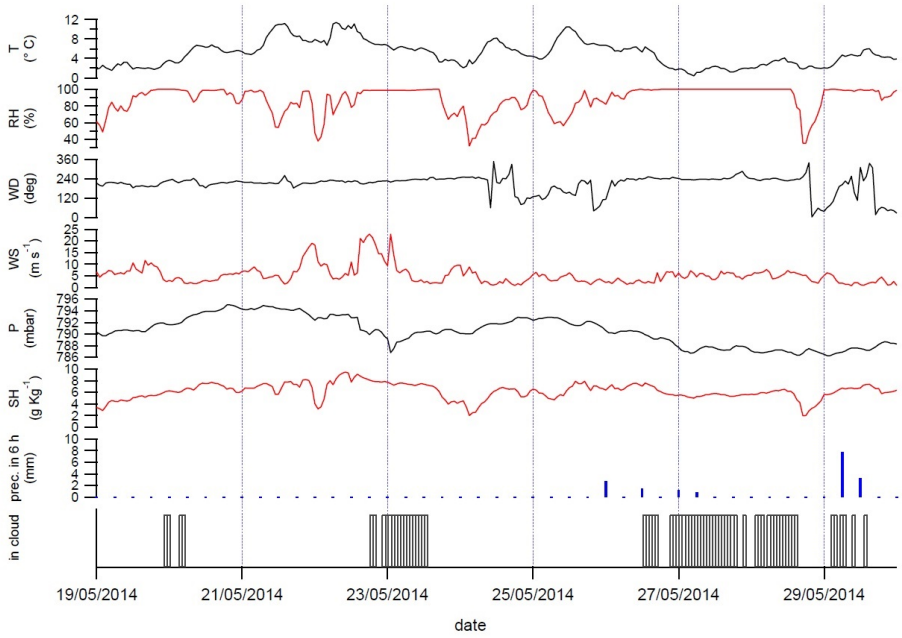

Figure 3.10: Time trend of the main meteorological parameters during MC1. T = Air Temperature, RH = Relative Humidity, WD = Wind Direction, WS = Wind Speed, P = Air Pressure, SH = Specific Humidity.

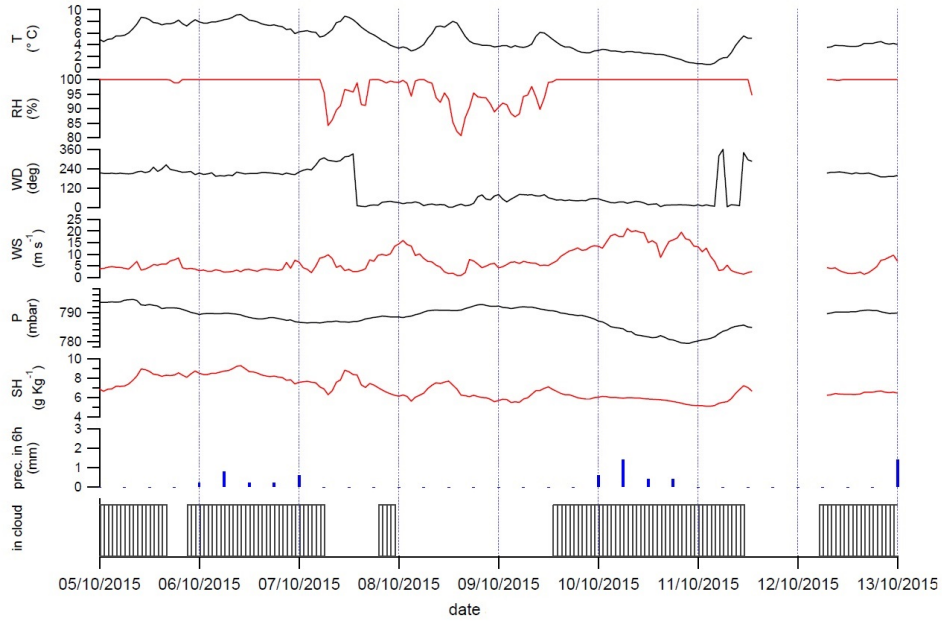

Figure 3.11: Time trend of the main meteorological parameters during MC2. T = Air Temperature, RH = Relative Humidity, WD = Wind Direction, WS = Wind Speed, P = Air Pressure, SH = Specific Humidity.

samples were grouped based on air mass origin. Samples collected during the MC1 campaign originated from three main sectors: Africa (Afr, 11 samples), which coincides mostly with the SDE, West Europe and the Atlantic Ocean (WE-Atl, 3 samples) and Central Europe (CE, 2

samples).

The MC2 campaign presented air masses from *WE-Atl* (12 samples) and *CE* (7 samples). The lowest INP concentrations (Fig. 5), in the PM1 size fraction, were associated with *WE-Atl* air masses in both campaigns (37.1 ± 24.6 and 6.0 ± 3.2 m^{-3}, respectively). In the first campaign, *Afr* and *CE* air masses presented a higher INP concentration than *WE-Atl* ones (air pressure < 0.1) and were characterised by similar average values. Also during the MC2 campaign *CE* air masses carried significantly (air pressure < 0.03) more INP than *WE-Atl* ones. A higher AF of sub-micrometer particles was associated to *CE* air masses in both campaigns (Figure 3.13), with a statistically significant difference in the first campaign (P value < 0.05). This analysis shows that air masses from central Europe are enriched in sub-micron particles that act as better INP than those from *Afr* and *WE-Atl*, at an activation temperature of −18°C. No appreciable difference in the INP concentration as a function of the air mass origin can be observed, instead, looking at PM10 data (Figure 3.12).

Comparison of INP concentration in samples with homologous origin shows systematically higher values during the first campaign than the second, particularly for the PM1 size fraction, which may be reconciled with the different PBL influence characterising the two campaigns, as detailed above.

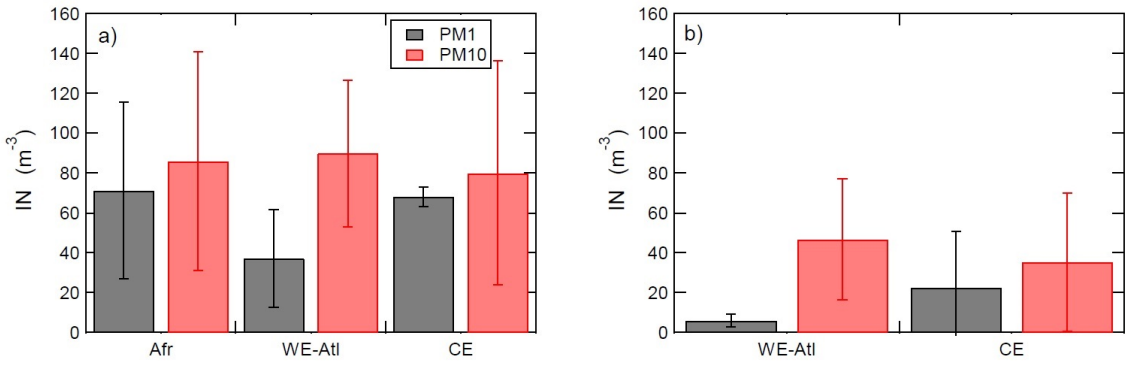

Figure 3.12: Average INP concentration as a function of the air mass origin for (a) MC1, May 2014, and (b) MC2, October 2015. Error bars represent ± one standard deviation.

In conclusion, the sub-micron INP concentration observed at MC is likely contributed by long range transport of aerosol particles from remote sources (synoptic scale), mid-distance sources which affect the measurement site depending on the intensity of vertical mixing due to PBL dynamics (well represented by aerosol sources located within the Po Valley basin) and minor local sources (few kilometers scale). The latter source may be likely more important for super-micron INP concentration, under certain meteorological conditions. Local meteorology seems to affect more coarse INP than the fine fraction.

3.6 Conclusions

This chapter has reported offline measurements of INP and particle number concentration at the high altitude observatory Monte Cimone (MC1: May 2014; MC2: October 2015) and at the low

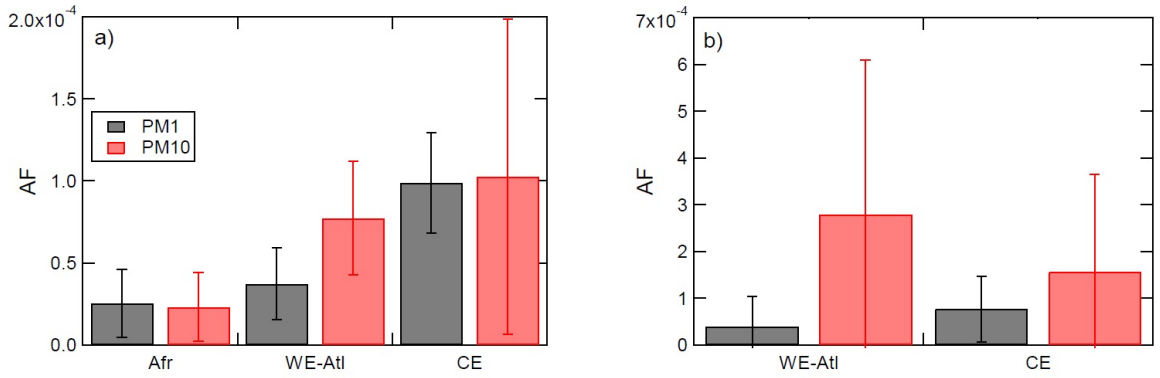

Figure 3.13: Average AF as a function of the air mass origin for (a) MC1, May 2014, and (b) MC2, October 2015. Error bars represent ± one standard deviation.

altitude rural area of San Pietro Capofiume (SPC: May 2014). Presented IN data are the first ever published for a high altitude site within the Mediterranean basin.

The main conclusions of the campaigns can be summarized as follows:

- During the parallel measurement campaigns held in May 2014, the average INP concentration was roughly double at SPC than at MC. Systematically higher concentrations (factor of 2–5, according to the size fraction) were observed at MC during the MC1 campaign with respect to the second MC2. The activated fraction of MC1 was comparable to the one of SPC. In turn, a significantly higher AF characterised the October 2015 campaign MC2, suggesting a seasonal change in the composition of the INP population and/or in background aerosol.

- Considering INP activated at Sw = 1.01, T = −18 °C (i.e. condensation freezing), super-micrometer IN contributed for about 30% in the May 2014 campaign (both MC1 and SPC1) and for about 70% in the October 2015 campaign MC2. These results show the importance of super-micrometer particles in the INP population. A significant correlation between INP and particle number concentration, in both the PM1 and PM10 size fractions, was observed during MC1, while no correlation was noticed for MC2. This is in line with the variability of results published in literature.

- The examination of the dependency of INP concentration on measurement temperature and water supersaturation, performed on PM10 samples during MC2, confirms that the INP concentration increases by increasing the saturation ratio and decreasing the activation temperature. In particular, the transition from sub-to super-saturated conditions showed a higher influence than the increase of temperature, in the considered range of T and Sw. The observed temperature dependency was consistent with that reported by DeMott et al. (2010) [47].

- During the SDE that occurred in May 2014, a reduction of the AF was observed at MC and, to a lower extent, at SPC, suggesting, for this event, a limited ice nucleating activity for Saharan dust particles. This might be due to modifications of the Saharan dust surface

properties during transport in the atmosphere ("aging processes"), or likely to the fact that the measurements were performed at a relatively high temperature for the activation of mineral dust (−18 °C).

- In SPC campaign, the results confirmed the conclusion obtained in a previous campaign (09–12 July 2007). On the whole, the results show that the freezing activity of aerosol diameters larger than 1 μm should not be neglected to obtain the entire INP population.

- Precipitation events influence the aerosol concentration at SPC. Days characterised by frequent precipitation events (period 26–30 May) showed an average aerosol number concentration in the range 0.5–10 μm, slightly higher with respect to days with no precipitation. Predominantly the rainfall intensity was low. Only in a few cases of precipitation, a sharp drop in INP in the PM10 fraction was noticed at Sw = 1.01 (26 May, 8 a.m. and 1 p.m.; 27 May, 1 p.m.).

- Analysis of meteorological parameters, gaseous tracers concentrations and backwards trajectories suggests that the INP population at MC is contributed by: (1) long range transport of aerosol particles from remote sources, regulated by the synoptic circulation, (2) by mid-distance sources, which affect the measurement site depending on the intensity of vertical mixing and (3) by local sources. The latter is likely more important for the super-micron fraction of the INP population, which shows also higher dependency on local meteorology, while it is likely a minor source of sub-micrometer IN.

A further extension of INP observations at MC station, obtaining a wider temporal coverage, would be desirable in order to strengthen the conclusions derived in this work.

3.7 Acknowledgments

This work was funded by FP7-ENV-2013 Project BACCHUS (grant no.603445) and by the CNR funded bilateral project 'Air-Sea Lab: Climate air pollution interaction in coastal environment'.

We gratefully acknowledge the NOAA Air Resources Laboratory (ARL) for the provision of the 'HYSPLIT transport and dispersion model', used in this work.

Chapter 4

The Arctic measurement campaign PARCS-MACA

> The inability of regional models and global climate models to reproduce Arctic clouds and the Arctic radiation budget may be due to inadequate parameterizations of ice nuclei.
>
> Prenni et al., 2007 [228]

4.1 Introduction

Arctic Amplification is the fast increase of the near-surface temperatures, at a rate which is greater in the Arctic than anywhere else on the planet. The Arctic Amplification is peculiar of the behavior of the Earth's climate system and has a number of known potential causes [229]: sea ice loss, albedo feedback, horizontal heat flux convergence, changes in cloud cover and water vapour content, enhanced concentrations of black carbon aerosols. Among these different processes, the feedbacks from enhanced atmospheric water vapour and cloud coverage are gaining increased attentions [230]. A greater humidity content is expected to additionally trap the infrared radiation emitted by the Earth and enhance the warming of the surface. Changes in the Arctic cloudiness might also have a net warming effect of the surface in all seasons except for a portion of the summer, as reported by Curry et al.,1993 [231] and Walsh and Chapman, 1998 [232]. Given the scarcity of records - documenting Arctic clouds changes and their radiative properties - it is still an open question whether changes in cloudiness will represent a minor or a relevant contribution to Arctic amplification (Screen and Simmonds, 2010 [233] and Ghatak and Miller, 2013 [234]).

Understanding cloud feedback mechanisms and clouds changes in the Arctic is particularly challenging, and it requires a synergy between observations and modelling approaches. So far, models strive to reproduce correctly the observed drastic changes. Models difficulties may be related to inaccuracies in the representation of Arctic clouds, especially concerning the

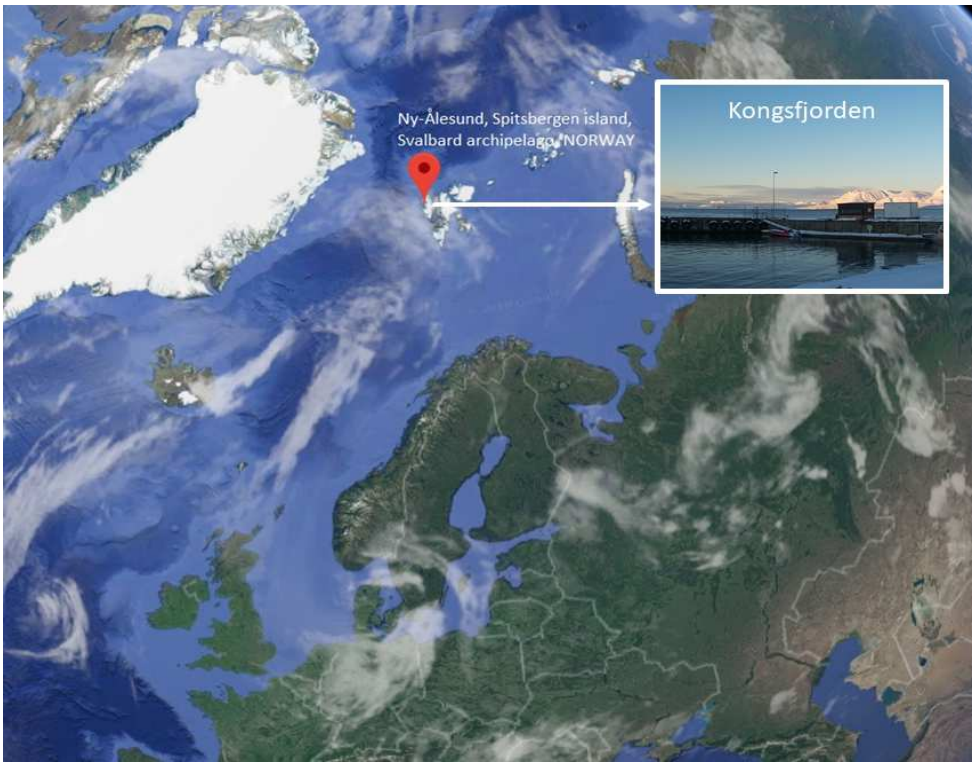

Figure 4.1: Locations of the campaign presented in this chapter.

parameterization of ice nucleating (IN) particles [228]. Notably, a small percentage of Arctic clouds are glaciated, while 50 to 80% are liquid and consists of persistent stratiforms, where supercooled liquid water has been measured down to −20 °C [235].

A possible explanation for the large number of *mostly liquid clouds* and their *persistence* in the Arctic could be related to a decreased number of IN in the atmosphere, as explained in [228] and [235], even though the overall aerosol concentration is comparable to the mid-latitude [235]. In fact, a lack in the available IN concentration diminishes the number of processes that trigger the liquid to solid transformation of cloud water. Such absence can explain also the persistence of Arctic cloudiness, as a decrease IN concentration can lengthen cloud lifetime and invigorate cloud circulations [228]. On this point, the observation of Arctic IN sources is crucial, especially for the group of biogenic macromolecules which are ice active down to -20 °C. To evaluate such biological IN (e.g. bacteria or lichen from soil, marine biota as micro-algae) it is essential to evaluate the exchanges of particles at the interface. Recently, a German research consortium named Arctic Amplification: Climate Relevant Atmospheric and Surface Processes, and Feedback Mechanisms (AC3) has been investigating the coupling of clouds and aerosol in the transition zone between open ocean and sea ice over the Arctic [236]. However, the exchanges between open ocean and the Arctic atmosphere remains to be largely characterized and represent an ongoing field of research.

Given the current concerns for the Arctic Amplification, and the need of observations at the atmosphere/oceans interface, a measurement campaign took place in Ny-Ålesund (Spitsbergen, Svalbard), in order to characterize marine IN sources and improve cloud models. The field campaign took place in March 2017, a period when light intensity and the seawater phytoplanktonic


Figure 4.2: Mesocosms installation in Svalbard. Photo credit Karine SELLEGRI (LaMP).

activity are increasing.

Within this campaign, named PARCS-MACA (presented in the following section), we could collect samples from the Kongsfjorden (Figure 4.1), and we studied the ice inducing capability of the Arctic primary marine aerosol, using a sea spray generator and a Pelagic mesocosm experiment. Primary marine aerosol refers to particles directly emitted in the atmosphere from the seawater. These particles are supposed to possess Ice Nucleating properties [72], whereas their origin and concentration remain unclear. The above mentioned *pelagic mesocosm* (described in the next section) refers to an enclosed environment, in which a large volume of seawater is isolated and at the same time it is immersed in the water column, so that the mesocosm water temperature follows the natural variation during the day/night period as well as during the several weeks of experimentation. Primary aerosol emissions were characterized off-line by artificially generating aerosols from a wave-breaking laboratory device, filled using the seawater taken from the mesocosms.

4.2 PARCS-MACA

PARCS-MACA is a joint mesocosm experiment based on the following two funding projects:

- Pollution in the ARtic System (PARCS) work package 3: impacts on marine ecosystems;
- Marine Aerosol impact on Clouds in the Arctic (MACA), supported program 1187 of the French polar institute IPEV and number 10713 of the research in Svalbard database.

PARCS-MACA is included in the French Initiative Chantier Arctique and has been financially supported by: CNRS, INSU, IPEV. In addition, the campaign is incorporated in the international network *Surface Ocean–Lower Atmosphere Study* and it is listed in the 2017 *SOLAS* French initiatives [237]. PARCS-MACA addresses two major research objectives:

- To identify the marine sources of ice nuclei and cloud condensation nuclei particles in the Arctic atmosphere (Svalbard), their relations to the biogeochemical properties of seawater and their impacts on cloud microphysical properties.

- To assess the impact of pollutants on marine ecosystems and their repercussion on the concentration of ice nuclei and cloud condensation nuclei emitted in the marine atmosphere.

The influence of the oceanic biogeochemistry on aerosols and ultimately cloud properties is especially important in the Arctic, where the environment is very sensitive to climate change. To these purposes, a few Pelagic mesocosms were intentionally contaminated with artificial precipitations of different levels of pollutants (sulphate, ammonium and nitrate) that will likely increase in future years in the Arctic's atmosphere. The aim of this study was therefore to assess if potential perturbations in nutrient cycles and micro-organisms concentrations may impact the sea to air emissions of aerosols and gases.

In PARCS-MACA, the experimental approach has combined: (1) process studies in semi-controlled environments (the so called Pelagic mesocosms), (2) in situ field measurements, and (3) laboratory controlled generation of sea spray. Three mesocosms were employed: a control mesocosm (unchanged) and two mesocosms modified with different amount of atmospheric pollutants. Through these mesocosms, also a portion of air above the seawater was isolated, in order to study gas emissions and secondary marine aerosols (i.e. molecular clusters that may be formed from the photo-oxidation of the gas-phase species). The mesocosms used during PARCS-MACA were specifically designed to study sea-to-air fluxes, such emissions were measured directly in the head-space of the mesocosms, from a mobile laboratory station settled down in the harbour, closed to the mesocosms.

The multidisciplinary approach of PARCS-MACA was realised through the cooperation of several international partners, with strong track record in the Arctic and complementary expertise. The main group involved are listed below:

- *Medimeer* (MEDIterranean platform for Marine Ecosystem Experimental Research, UMS-3301 CNRS - Université Montpellier 2, Montpellier, France) for the biogeochemical characterisation of the seawater, and the logistical handling of the mesocosms;

- *LaMP* (Laboratoire de Météorologie Physique, UMR 6016 CNRS - Université Clermont Auvergne, Observatoire de Physique du Globe, Clermont-Ferrand, France) for the design of the experiment, the characterisation of the primary marine aerosols (size distributions, CCN and IN) and the detection and size distribution of nucleated particles in the mesocosm headspace;

- *IRCELYON* (Institut de recherches sur la catalyse et l'environnement de Lyon, 5256 CNRS - Université de Lyon, France) for the online chemical analysis of primary marine aerosols;

- *ISAC-CNR* (Institute of Atmospheric Sciences and Climate, Italian National Research Council, Bologna, Italy) for the characterisation of the ice nuclei in the deposition and condensation freezing activation mode;

- *ICCF* (Institut de Chimie de Clermont-Ferrand, France) for the characterisation of the ice nuclei in the immersion freezing activation mode;

- *UOH* (University of Helsinki, Finland) for the chemical characterisation of the secondary marine aerosols.

Figure 4.3: A part of the PARCS/MACA team in Svalbard. Back row, from left to right: D. Picard (LaMP), S. Mas (Medimeer), R. Valdes (Medimeer), P. Villani (LaMP), C. Rose (University of Helsinki). Front row from left to right: K. Sellegri (LaMP), A. Nicosia (LaMP), B. D'Anna (IRCELYON). Picture taken from the official project page. Credit K. Sellegri (LaMP).

For the purpose of the present work, we will focused mainly on the characterisation of the primary marine aerosol, since measurements performed on the gases and the secondary marine aerosols, as well as the biological analysis of the seawater, are still under data treatment.

4.3 Experimental design

The mesocosm experiment was carried out from the 5^{th} to the 22^{nd} of March 2017 in the harbour of Ny-Ålesund research station (78°55'42.5"N 11°56'13.3"E) and it was supervised by the Marine Ecosystem Experimental Research (MEDIMEER) scientists S. Mas and R. Valdes. Given the time of the year, the mesocosms were settled in the harbour to protect them from the close icebergs that could break their walls. Each mesocosm was 3 m high, 1.2 m wide, and made of a thick polyethylene film (UV-transparent Ethylene Tetrafluoroethylene). Each mesocosm was held at the surface of the seawater by floating structures (Figure 4.2), the top was covered with the same polyethylene material [238] and the headspace was continuously flushed with cleaned air (filtered from preexisting particles). Mesocosm headspace served to isolate a portion of atmosphere above the sea surface, in order to monitor the composition of gases and aerosols derived from the sea to air fluxes. The UV transparent film allowed radiation (including UV) to penetrate in both the seawater and the headspace enclosures, allowing photo-chemical processes to occur, in line with the natural environment.

Three mesocosms were simultaneously filled on the 4^{th} of March 2017 with screened (<1000 μm mesh) natural seawater taken from the Arctic Kongsfjorden. Each mesocosm had a maximum water column depth of 2 m and contained 2260 Liter of seawater in thermal contact with the surroundings. Among the three deployed mesocosms, one remained unmodified, as control, and two were modified by seeding with:

- 3.1 mg of $(NH_4)_2SO_4$ and 1.08 mg of NH_4NO_3 to the so called "polluted mesocosm";

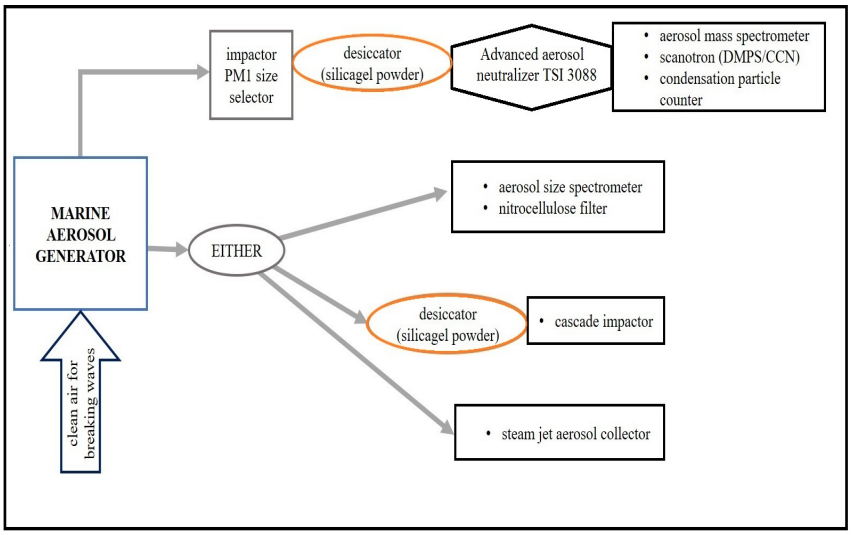

Figure 4.4: Experimental set up of the PARCS-MACA campaign dedicated to the primary marine aerosol generation, collection and analysis.

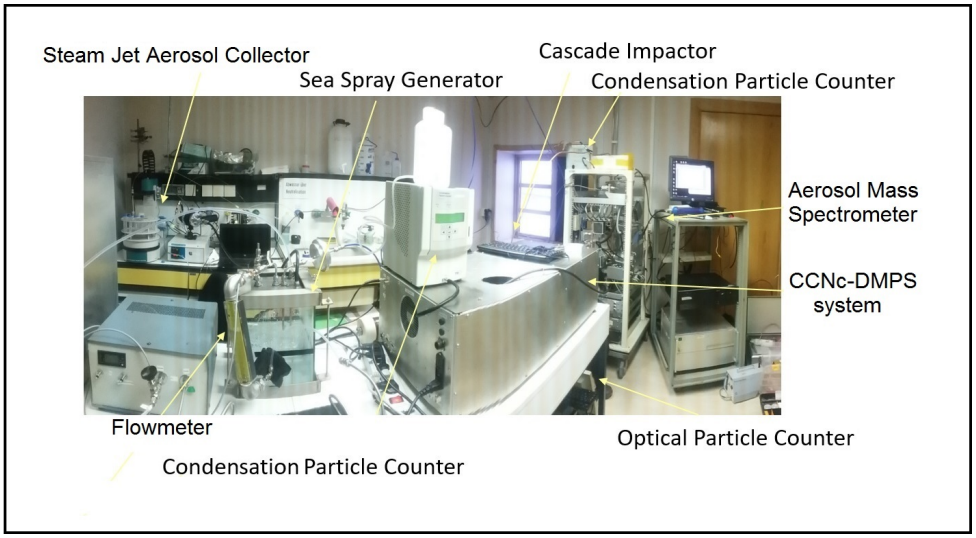

Figure 4.5: At the laboratory for the experiments on primary emission.

- 6.2 mg of $(NH_4)_2SO_4$ and 2.16 mg of NH_4NO_3 to the so called "highly polluted mesocosm".

Seeding was applied the night between the 5^{th} and the 6^{th} of March 2017. All mesocosms were sampled daily from the 5^{th} of March to the 22^{nd} of March, made exception from the 10^{th} and the 11^{th} due to severe weather conditions. Collection of samples were performed in the early morning using 20 Liter polycarbonate carboys, cleaned with ultrapure water. Aliquots to measure the seawater ice nuclei content were taken from these polycarbonate cans, as well as the portion necessary to feed the marine aerosol generator, for the subsequent sea spray production and analysis.

4.3.1 Sample generation and collection from the control mesocosm

The marine aerosol generator (MAG) used in this study, and the related experimental protocol, have already been described in [239] and [240]. Briefly, the MAG consists of a glass tank - 20 x 20 cm and 25 cm high- which is filled with 3.6 L of seawater, in order to obtain a water depth of 10 cm. In the remaining volume, purified air is flushed to maintain a constant over-pressure. The air flush ensures the absence of ambient room particles. Inside the MAG, seawater is forced to recirculate using a water pump, pass through eight small nozzles and forms vertical plunging jets. Such plunging jet creates an air/bubble entrainment that finally reproduce the bubble bursting process and generate the sea spray. The water flow rate was set to 1.8 L min^{-1}, the height of the jets above the water surface was 9 cm and the penetration depth of the jets was around 7.5 cm. These operative conditions reproduce the ones reported in [241].

To minimize an increasing seawater temperature, due to the constant circulation of seawater, each bubble bursting experiment was performed for no longer than 60 min. In case of longer measurements, the seawater inside the tank was exchanged. To prevent cross contamination, prior to all experiments the MAG internal surfaces was rinsed thoroughly with Ultrapure water (resistivity >18 MΩ cm) and this cleaning water was re-circulated throughout for 10–15 min to clean also the water pump and the connections. Blank measurements were performed during the first 10 min of each experiment to verify a zero aerosol concentration in the particle-free air flushed tank. Experiments performed on the mesocosm waters were analyzed on line and offline to investigate the generated sea spray.

For the online measurements, the instruments employed were:

- CCNc-DMPS (LaMP custom-made system, also referred to as scanotron), consisting in a differential mobility particle sizer (DMPS) and miniature continuous-flow stream-wise thermal-gradient CCN chamber (CCNc) to determine particle cloud condensation nuclei (CCN) activation properties and ultrafine size distribution [242].

- Compact Time-of-Flight Aerosol Mass Spectrometer (C-TOF AMS, Aerodyne Research, Inc) for the aerosol chemical composition (see Müller et al., 2011 [243]);

- Condensation Particle Counter (CPC 3010 from TSI) for the monitoring of the total particle concentration;

- Scattered-light aerosol spectrometer system (Promo2000 model equipped with Welas digital 2100 sensors, from Palas GmbH) to monitor the size distribution of particles > 0.2 μm.

Prior to the above systems -except the aerosol size spectrometer- the aerosol flow was passed through a diffusion drier, an impactor with cut-off diameter of 1 μm and a neutralizer (Advanced Aerosol Neutralizer 3088 from TSI), as reported in Figure 4.4.

For the off line measurements, the systems employed were:

- Cascade Impactor at three stage (Dekati Ltd.) for ion chromatography and chemical analysis. Aluminum foils were used for PM2.5/PM10 stages and a quartz fiber filter for the PM1 stage;

- Nitrocellulose membrane filters (Millipore HABG04700, nominal porosity 0.45 μm), for the ice nuclei measurements with DFPC;
- TEM grid for observations at microscope;
- Steam Jet Aerosol Collector -abbreviated SJAC- for the ice nuclei measurements with FNA.

In relation to the SJAC, we used a modified version of the Particle Into Liquid Sampler (PILS, Metrohm), for which we considered only the growing chamber. Inside this unit, the aerosol is mixed with supersatured water vapours, the particles grow to droplets, and are subsequently collected on the surface of an impactor plate. This impactor is surrounded by a stainless steel wicking mesh in which the collected droplets are mixed with carrier Milli-Q water. A vacuum air pump attached to the SJAC drew the sample through the whole system at 16.7 L min^{-1} (corresponding to 1 m^3/h). Sea spray aerosol was converted into liquid samples directly through the SJAC and gathered in sterile tubes (Corning Falcon 15mL Conical Tubes) that were initially stored in the dark at +4 °C. A small portion was analyzed for the immersion freezing -through the FNA instrument- directly at the Vaskeri laboratory in Svalbard. The remaining lot of samples were frozen at −20 °C and thawed before the analysis.

Before presenting the results for seawater samples, we will discuss the concentration of ice nuclei measured in the seaspray.

4.4 Number of ice nuclei in the seaspray

4.4.1 DFPC results

The physico-chemical characterization of atmospheric marine aerosol, together with its CCN/IN capabilities, its an ongoing field of research. Few measurements have been published in relation to the number of INP from laboratory generated marine aerosol emissions and to mesocosm experiments, [244], [245],[246], [247], [248]. In our study the primary marine aerosol was collected on nitrocellulose filter substrates at a mean flow rate of 8 L/min. All the particle sizes were considered. Samples were sent frozen to the Italian Institute of Atmospheric Sciences and Climate (ISAC-CNR) in Bologna, and they were processed within two months with the Dynamic Filter Processing Chamber (DFPC). The DFPC allows estimate the number of INP by counting the ice crystals that develop upon the substrate when it is exposed to freezing temperatures and saturated water vapours. Also, it allows the processing of the collected aerosols in both the deposition and the condensation freezing activation mode and it allows measurements of aerosol activation in all size ranges. The processing conditions for the activation temperature and saturation fraction are reported in Table 4.1. To explore all the four conditions, each filter was tested four times (with the coldest test at -25 °C as the last one).

The saturated vapour pressure of ice and water is calculated following [249], that refers to [218]. Taking into account the accuracy of the temperature sensors and control system, an experimental uncertainty of about 1% is associated to estimations of the saturation ratio with respect to water, Sw, as reported in [159]. Table 4.2 shows the number of INP activated under the conditions reported in Table 4.1. Only a subset of samples were tested at the colder temperature of -25 °C. The lowest value of one crystal count was considered as blank and subtracted to all

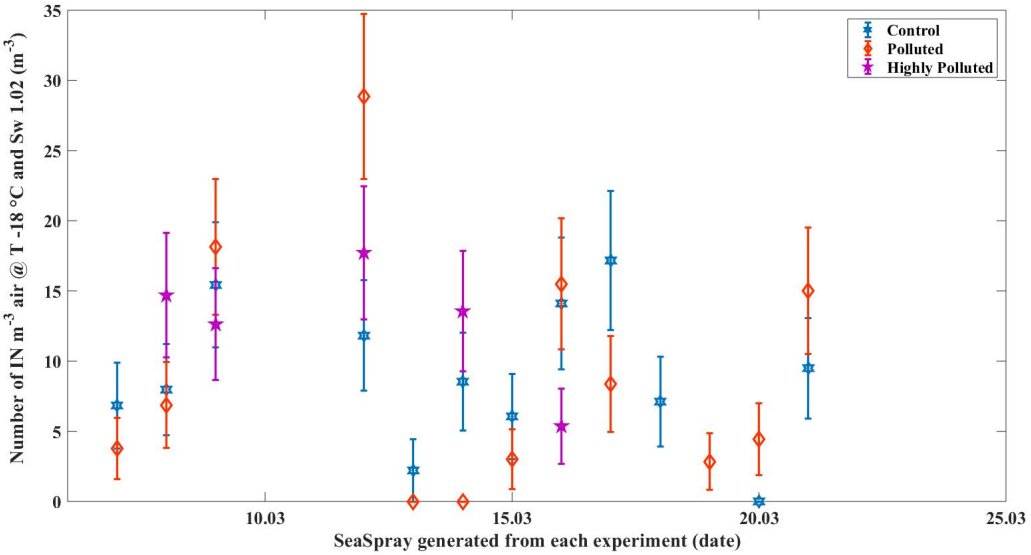

Figure 4.6: Freezing properties of sea spray generated from different seawater samples and activated through condensation freezing at −18 °C. Differences among Control and Highly Polluted are not significant, as verified by the Wilcoxon-Mann-Whitney test (that is always 0 with a p-value of p= 0.23 among Control and Highly Polluted; and p=0.66 among Control and Polluted).

data, as noise correction. This value was the lowest obtained for each measuring condition (when evaluating the overall PARCS-MACA set of samples).

Activation Mode	Filter Processing Temperature, T (°C)	Saturation ratio with respect to water, Sw
Deposition freezing	−18	1.02
Condensation freezing	−22	0.96
Condensation freezing	−22	1.02
Condensation freezing	−25	1.02

Table 4.1: DFPC processing conditions

The test of Wilcoxon-Mann-Whitney was performed through the function *ranksum* under Matlab R2018a, to compare the differences among the median values of control and (highly) polluted sea spray samples. The tests were null almost all the times, except the dataset at −25 °C where the Control was higher than the Polluted (p-value=0.01) but the number of points is lower. Therefore, the majority of our data fail to demonstrate that pollution in seawater affects IN population in seaspray, with the exception of condensation freezing at colder temperature.

Figure 4.10 reports the mean INP number -per unit volume- obtained from each activation mode, by averaging together the INP of control, polluted and highly polluted seaspray. The resulting time series have no specific trends, but oscillate around a central value. All the series showed increasing number of INP at the beginning, and are followed by a series of maxima and minima (made the exception of condensation at −25 °C, which is either missing or in disagreement). All the observations (deposition at −18 °C and condensation at −18 °C/−22 °C/−25 °C) agree on a minimum reached on the 19^{th} of March. Others minima are present

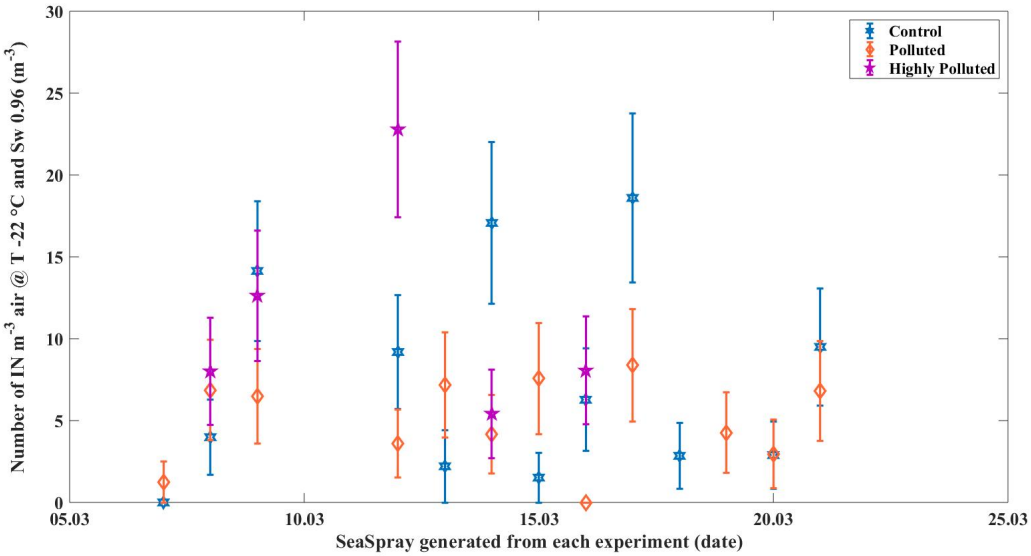

Figure 4.7: Freezing properties of sea spray generated from different seawater samples and activated through deposition at −22 °C. Differences among Control and Highly Polluted are not significant, as verified by the Wilcoxon-Mann-Whitney test (that is always 0 with a p-value of p= p=0.28 among Control and Highly Polluted; and p=0.73 among Control and Polluted).

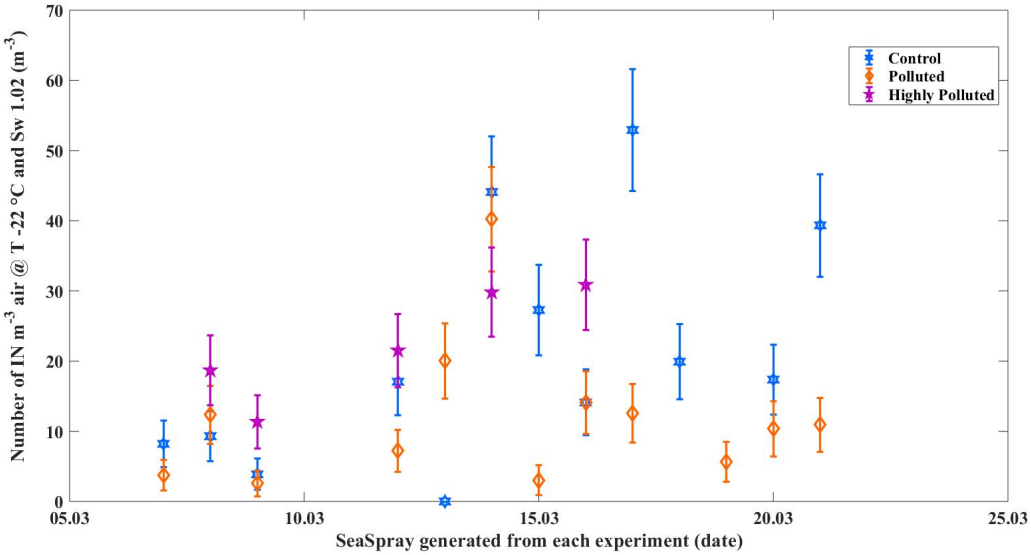

Figure 4.8: Freezing properties of sea spray generated from different seawater samples and activated through condensation freezing at −22 °C. Differences among Control and Polluted are not significant, as verified by the Wilcoxon-Mann-Whitney test (that is always 0 with a p-value of p=0.51 among Control and Highly Polluted; and p=0.13 among Control and Polluted).

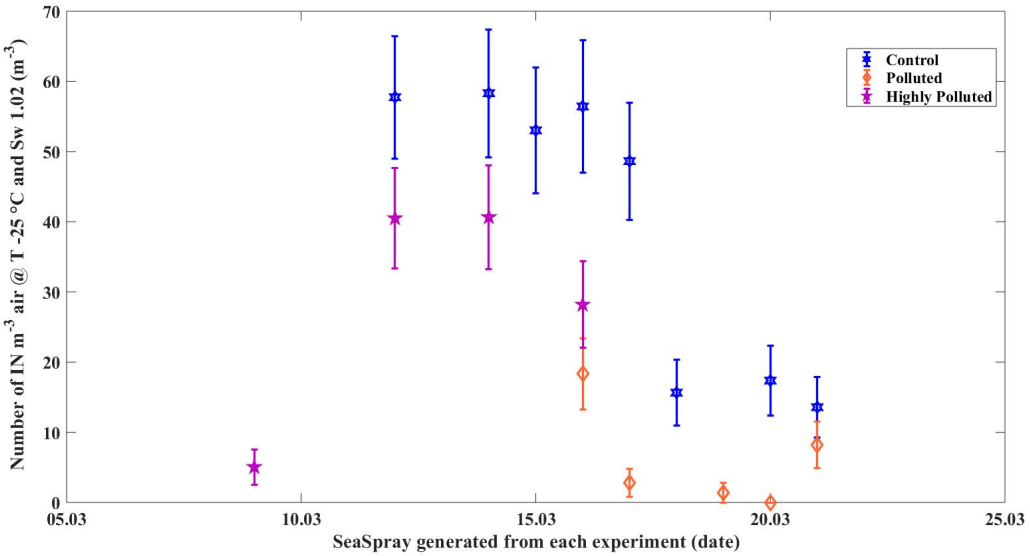

Figure 4.9: Freezing properties of sea spray generated from different seawater samples and activated through condensation freezing at −25 °C. Differences among Control and Polluted are significant, as verified by the Wilcoxon-Mann-Whitney test, that is 1 (p=0.01) among Control and Polluted and 0 (p=0.28) among Control and Highly Polluted.

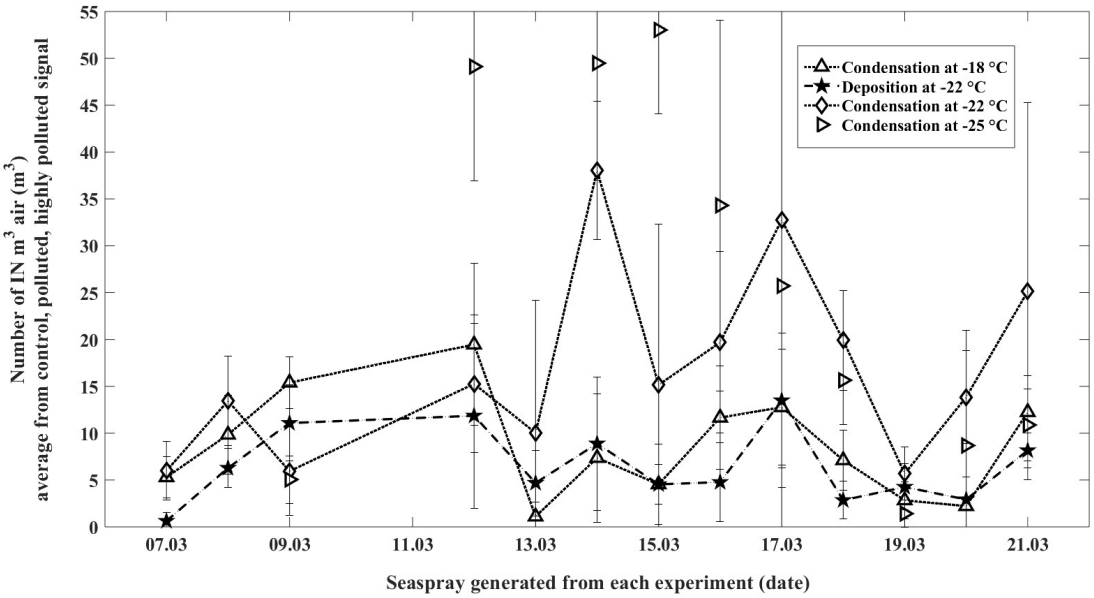

Figure 4.10: Time series of the ice nuclei number -per unit volume- obtained for each activation mode explored with DFPC. Each point is the average of the number of INP measured from control, polluted and highly polluted seaspray. Through this average it is possible to appreciate the fluctuations of IN at different days.

on the 7^{th}, 13^{th} and 15^{th} of March (but they are not confirmed by condensation at −25 °C). Maxima were reached on the 12^{th}, 14^{th}, 17^{th} of March for the majority of freezing activation modes (except for condensation at −25 °C which has a maximum on the 15^{th}). The shape of the oscillation is very closed for deposition activation mode (at −18 °C) and condensation freezing (at −18 °C).

The ratio among the maximum and the minimum measured for each freezing activation mode in figure 4.10 is: 18, 22, 7 and 37 (for, respectively, deposition at −18 °C and condensation at −18 °C / −22 °C / −25 °C). Considering that the seaspray was generated and sampled in an identical way during each experiment, the spread of results should be attributed only to the individual properties of the seawater used to generate the seaspray. Furthermore, our work considers only the seawater collected from the three mesocosms, and then we exclude any possible exchange of material from the surrounding ocean or the atmosphere. Finally, this work provides indications of the variability of seaspray's ice nuclei in relation to seawater conditions, eluding the influence of wind, oceanic currents or others external variables.

Sample Name	Sampling Volume m^3	−18 °C (S_w: 1.02) IN/m^3	−22°C (S_w: 0.96) IN/m^3	−22°C (S_w: 1.02) IN/m^3	−25°C (S_w: 1.02) IN/m^3
07.03 Control	0.731	7±3	0±1	8±3	
07.03 Polluted	0.797	4±2	1±1	4±2	
08.03 Control	0.753	8±3	4±2	9±4	
08.03 Polluted	0.728	7±3	7±3	12±4	
08.03 Highly Pltd.	0.749	15±4	8±3	19±5	
09.03 Control	0.778	15±4	14±4	4±2	
09.03 Polluted	0.772	18±5	6±3	3±2	
09.03 Highly Pltd.	0.792	13±4	13±4	11±4	5±3
12.03 Control	0.762	12±4	9±3	17±5	58±9
12.03 Polluted	0.832	29±6	4±2	7±3	
12.03 Highly Pltd.	0.79	18±5	23±5	22±5	41±7
13.03 Control	0.453	2±2	2±2	0±1	
13.03 Polluted	0.698	0±0	7±3	20±5	
14.03 Control	0.703	9±3	17±5	44±8	58±9
14.03 Polluted	0.721	0±1	4±2	40±7	
14.03 Highly Pltd.	0.738	14±4	5±3	30±6	41±7
15.03 Control	0.66	6±3	2±2	27±6	53±9
15.03 Polluted	0.661	3±2	8±3	3±2	
16.03 Control	0.638	14±5	6±3	14±5	56±9
16.03 Polluted	0.71	15±5	0±0	14±4	18±5
16.03 Highly Pltd.	0.745	5±3	8±3	31±6	28±6
17.03 Control	0.699	17±5	19±5	53±9	49±8
17.03 Polluted	0.716	8±3	8±3	13±4	3±2
18.03 Control	0.703	7±3	3±2	20±5	16±5
19.03 Polluted	0.705	3±2	4±2	6±3	0±1
20.03 Control	0.691	1±1	3±2	17±5	17±5
20.03 Polluted	0.677	4±3	3±2	10±4	0±1
21.03 Control	0.737	9±4	9±4	39±7	14±4
21.03 Polluted	0.733	15±5	7±3	11±4	8±3

Table 4.2: DFPC results, blank corrected.

4.4.2 FNA results

Primary Marine Aerosol (PMA) was directly sampled in a liquid solution through the SJAC to be tested under immersion freezing. The apparatus FNA had been set up following the design described in [167] and [171], in line with the tests performed on bulk seawater (described in section 4.5). The concentration K_T of ice nuclei contained in 1 m^3 of air and activated in the immersion freezing mode at a certain temperature T was calculated similar to [173] as:

$$K_T = \frac{[ln(N_{total}) - ln(N_{unfrozen})]}{a}$$

where N_{total} is the total number of droplets (in our study it corresponds to the total number of Eppendorf tubes in which the sample is distributed), $N_{unfrozen}$ is the number of droplets still unfrozen (liquid) at the observation temperature T, and a is the volume of sampled air associated to the liquid volume of each droplet [167]. To estimate a from our set up, we considered that:

- SJAC could convert 1 m^3 of air containing aerosol into 11 mL of solution (0.1 mL of liquid sample are related to 0.009 m^3).
- in our experiments, each droplet volume was 0.2 mL, so "a" is 0.018 m^3.

Through this conversion, the number of IN mL^{-1} was expressed in number of IN m^{-3}. When all the droplets got frozen, is not possible to establish furthermore the ice nuclei concentration. This limit varies for each sample, depending on the IN concentration and affects the colder detection temperature for each test. In a few cases, to visualise the data in the same range in the graph, we made an exponential fit and extrapolate the values that weren't directly measurable with our operating conditions (this extrapolation is indicated by dashed line in the graphs).

Initial attempts to quantitatively estimate blanks from the generation of synthetic sea salts in ultrapure water, directly on the field, were not successful. Unfortunately we had no access to sterilization methods while in the Arctic, and no matter what procedure we could apply (bursting of the salts, filtration of the solution) there was contaminants affecting our estimations. Blanks performed in France were irrelevant down to $-17/-20$ °C (below this temperature, the influence of droplet volume on the water freezing temperature should be accounted for). In order to consider all the possible artefacts influencing the measures in Svalbard, due to the difficult working conditions, we have calculated the blank as the lowest value of frozen tubes detected at each temperature, by comparing all the IN time series. This blank corresponds to: 1 frozen tube from -16 °C to -16.2 °C; 2 frozen tubes from -16.3 °C to -20 °C. We subtracted the blank in the data treatment, prior to the conversion in IN m^{-3}.

Samples 08.03, 09.03, 15.03, 16.03, 17.03, 21.03 (originated from control seawater) were analyzed directly in Svalbar while the remaining were analyzed in France. We made the assumption that no degradation occurred during transport for sea spray samples. No repeated tests were performed in sea spray samples with FNA. The blank-corrected data are reported in in Figure 4.11.

By focusing on a particular temperature, as for example -15 °C, it is possible to appreciate the time series evolution of the number of IN, as represented in Figure 4.12. The first period of the campaign is characterised by an increasing number of INP, with a maximum reach on the

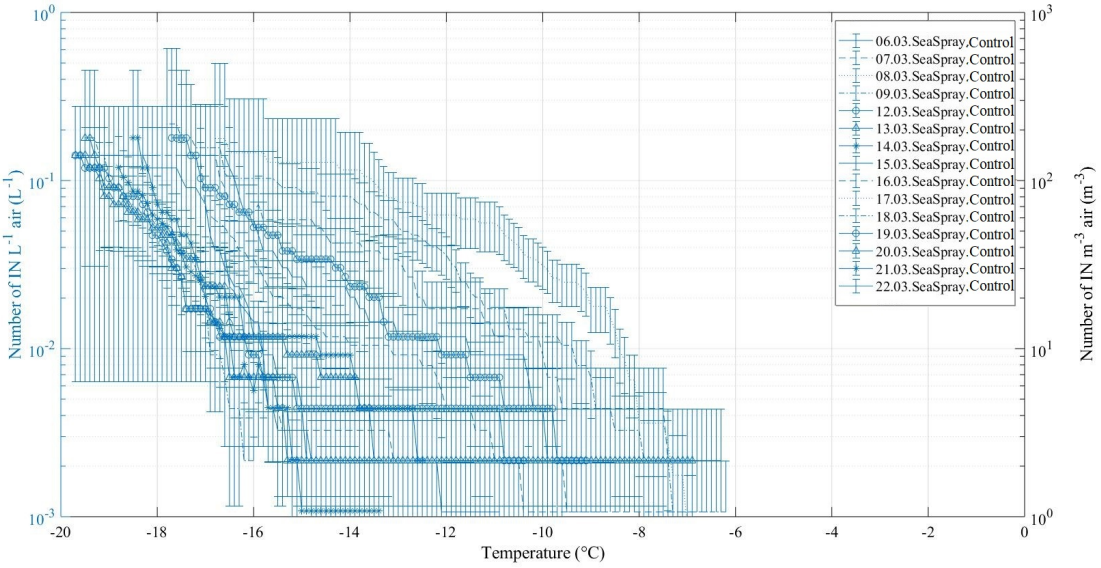

Figure 4.11: Freezing properties of sea spray generated from different seawater samples and immersed in ultrapure Milli-Q water and detected with the analytic technique FNA.

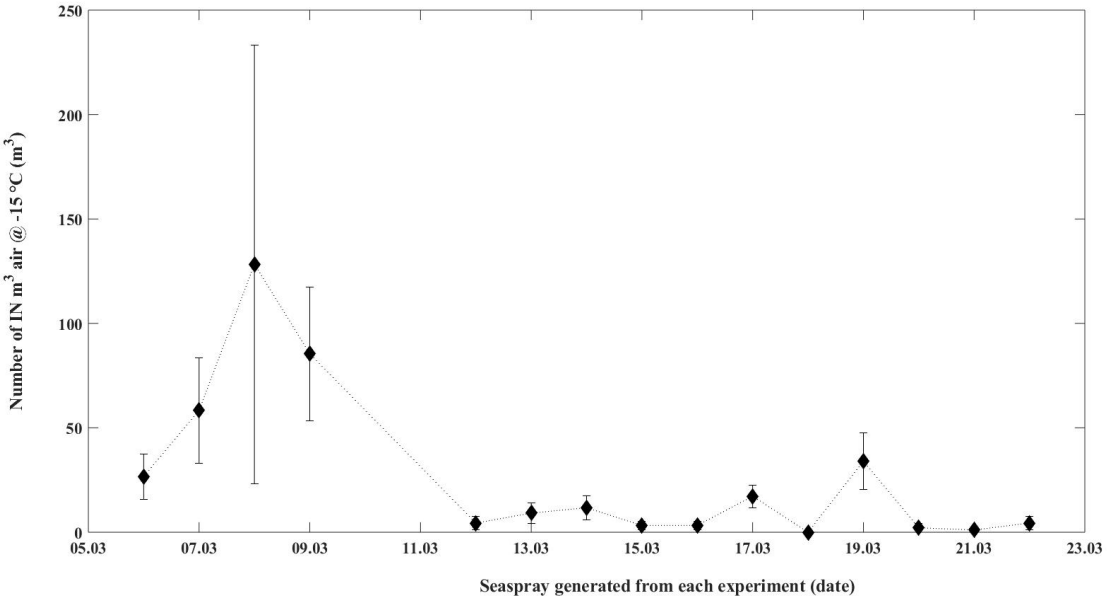

Figure 4.12: Detail of the number of ice nuclei for unit volume in the seaspray, activated at −15 °C through immersion freezing with FNA.

8^{th} of March and followed by a decreased concentration. Others maxima appear on the 14^{th}, 17^{th} and 19^{th} of March. As for DFPC, a large spread -among the maximum and the minimum detected value- distinguishes the population of marine IN observed.

Seaspray samples generated from (highly) polluted seawater and tested directly in Svalbard did not present significant differences from the control, as reported in Figure 4.13 for immersion freezing at −15 °C, thus confirming the results obtained with DFPC at −18 °C and −22 °C.

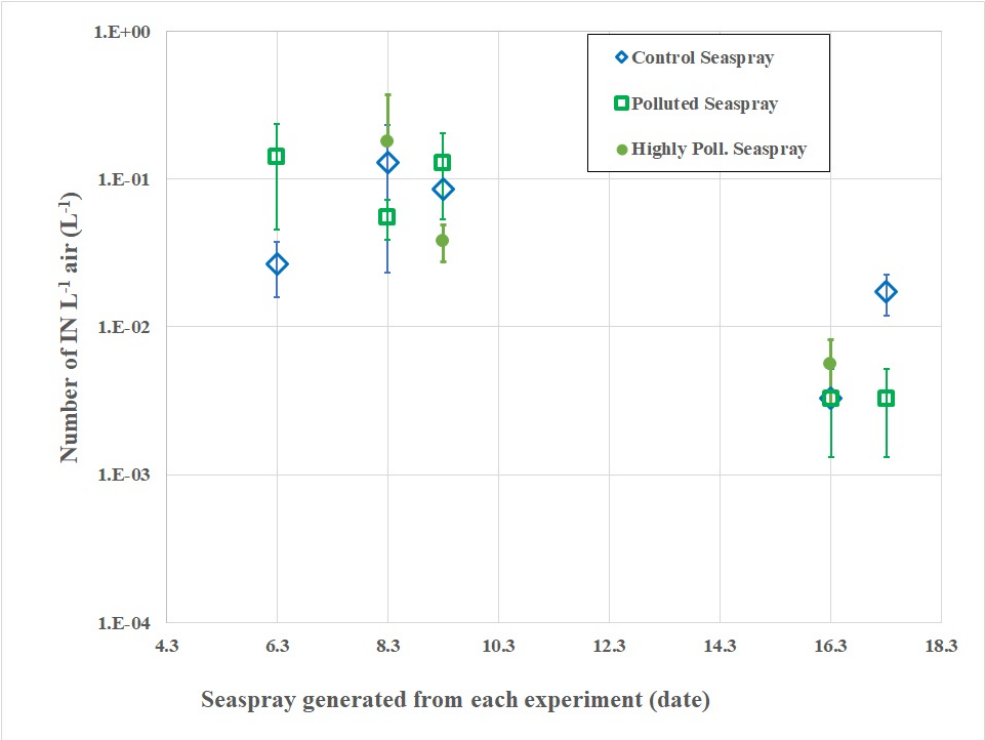

Figure 4.13: Ice nuclei activated at −15 °C in the seaspray generated from from control, polluted and highly polluted mesocosm seawater. Immersion freezing measurements performed in Svalbard, directly after generation and collection of the seaspray.

4.4.3 FNA and DFPC result inter-comparison

In previous works a few authors have assumed that condensation freezing represents also immersion freezing, following the discussion of Vali et al. (2015) [27] and that condensation freezing and immersion freezing are not distinguishable or distinct. This is still a matter of debate (Dymarska et al., 2006 [69]), however the results of Wex et al. (2014) [123] and Hiranuma et al. (2015) [124] support the hypothesis that they might basically be the same process.

Then, by assuming that DFPC conditions at Sw 1.02 represent also immersion freezing [154], we compared the results obtained by DFPC at −18 °C (downer temperature limit) and FNA at −15 °C (upper limit unaffected by blank). By comparing all the common samples, the Pearson's linear correlation coefficient was 0.39, with a corresponding p-value of 0.10. These results indicate a weak correlation among the two techniques. In addition, during the first part of the campaign (before the 12^{th} of March) immersion freezing (FNA) overestimates condensation freezing (DFPC) of about one order of magnitude. In the second part of the campaign, FNA and DFPC present comparable values. Higher differences have been reported in past studies -[124], [179]- up to two-three orders of magnitude while comparing different freezing apparatus. Then, our differences are reasonable, especially considering that it is still difficult to find an overall accuracy of current IN measurement techniques.

We suggest that the different sampling technique -steam jet aerosol collector versus filter aerosol collection- have also played a role in our work. Considering the scatter plot in Figure 4.14 we made the hypothesis that there were two types of IN during the campaign, a first type (better preserved by the SJAC and prevalent during the first part of the campaign) and a second type

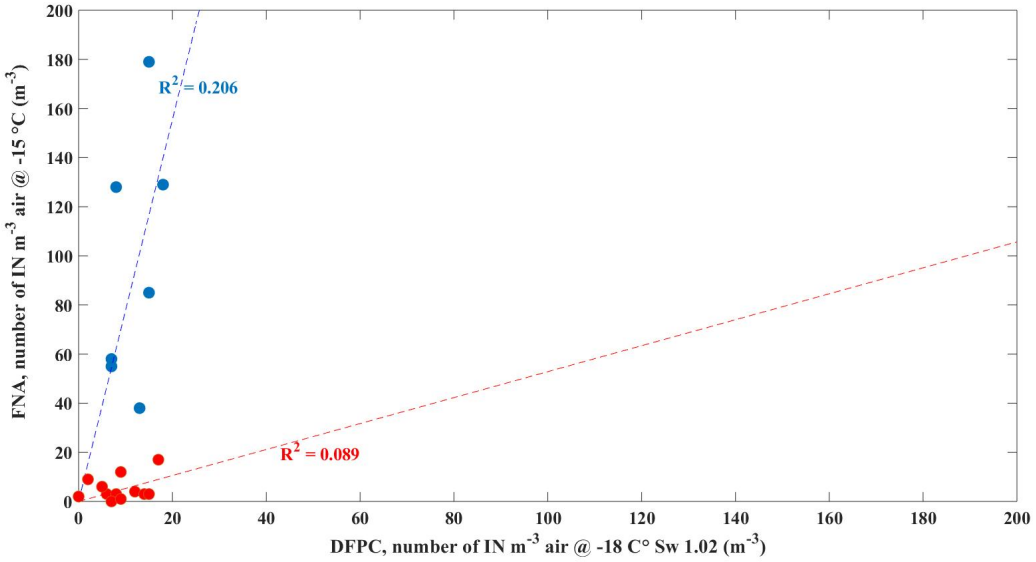

Figure 4.14: Scatter plot DFPC versus FNA. Blue points refers to samples obtained in the first part of the campaign -before the 12^{th} of March- while red points refers to the second part of the campaign.

Sample Name:	condensation freezing at−18 °C (Sw 1.02) IN/m^3	immersion freezing at−15 °C IN/m^3
SEASPRAY FROM CONTROL 07.03	7	58
SEASPRAY FROM CONTROL 08.03	8	128
SEASPRAY FROM POLLUTED 08.03	7	55
SEASPRAY FROM HIGHLY POLLUTED 08.03	15	179
SEASPRAY FROM CONTROL 09.03	15	85
SEASPRAY FROM POLLUTED 09.03	18	129
SEASPRAY FROM HIGHLY POLLUTED 09.03	13	38
SEASPRAY FROM CONTROL 12.03	12	4
SEASPRAY FROM CONTROL 13.03	2	9
SEASPRAY FROM CONTROL 14.03	9	12
SEASPRAY FROM CONTROL 15.03	6	3
SEASPRAY FROM CONTROL 16.03	14	3
SEASPRAY FROM POLLUTED 16.03	15	3
SEASPRAY FROM HIGHLY POLLUTED 16.03	5	6
SEASPRAY FROM CONTROL 17.03	17	17
SEASPRAY FROM POLLUTED 17.03	8	3
SEASPRAY FROM CONTROL 18.03	7	0
SEASPRAY FROM CONTROL 20.03	0	2
SEASPRAY FROM CONTROL 21.03	9	1
Correlation coefficient: 0.3882 P-value: 0.1005		

Table 4.3: Comparison of the results obtained through DFPC and FNA in different seaspray samples. These data are also visualised with a scatter plot in Figure 4.14 by distinguishing among samples collected before and after the 12^{th} of March.

(detectable by both the two techniques and present during the whole campaign). These categories can be related to different soluble-insoluble IN species, as our steam jet aerosol collector (i.e. a modified version of the particle into liquid sampler) is considered to be effective in the sampling of soluble aerosols (refers to Orsini et al., 2003 [250] for the collection efficiency curves of the instrument).

4.5 Ice nucleation rates of seawater

Subsamples of the bulk seawater were stored in 15 mL sterile Falcon tubes frozen at −20 °C for a maximum of 6 months before ice nuclei analysis. A few group of samples were analyzed immediately on site for concentration of IN active between −2 and −18 °C in a drop freeze assay with the FNA device loaded with an array of fifty-two Eppendorf Safe-Lock tubes containing 200 μL of sample each, as described in [171] and [169]. *Blanks* were determined through additional tests of ultrapure water with the addition of sodium chloride (Sigma-Aldrich, 99%, AR grade, product reference 433209) in a 3.5% weight of solute per final solution weight. The number concentration of ice nuclei, N_T, contained in the bulk seawater was determined from each freezing experiment by the following equation, similar to [173], [153]:

$$N_T = \frac{[ln(N_{total}) - ln(N_{unfrozen})]}{V}$$

where N_{total} is the total number of tubes used in the experiment (52), $N_{unfrozen}$ is the number of unfrozen tubes at the temperature T, and V is the liquid volume of each Eppendorf tube analyzed. This equation accounts for the possibility of multiple IN contained in a single tube. The FNA instrument was originally conceived for the detection range < -15 °C, in relation to biological IN species in rain water samples (see section 2.2), working with aliquots of 500 μL in [167]) or 400 μL (in [170] and [171]).

For a 400 μL droplet volume the upper detectable limit -determined through the number of aliquots analysed with FNA- is 98.8 IN mL^{-1} [171] which can be extended by orders of magnitude through proper dilution [170]. Concerning our study, we preferred to avoid dilution in order to preserve the salinity of our seawater samples.

To extend the upper detection limit (and to reduce the noise due to the droplet volume effect) we used aliquots of 200 μL (as in [136]). Thus we could measure IN concentrations up to 162.9 IN mL^{-1}, and freezing temperature down to −20 °C, without a significant background influence. To this purpose, blank tests were performed with solutions of ultrapure water and NaCl in a ratio comparable to the ones of seawater (3.5 g per Liter).

At colder temperatures (below −18 °C), seawater samples were often highly concentrated in IN -more than the upper detection limit of 162.9 IN mL^{-1}- and then the values expressed in our graphs should be considered lower limits (i.e. the IN concentrations may be higher than the ones reported, as it is not possible to go on with the measurement when the entire set of droplets is frozen).

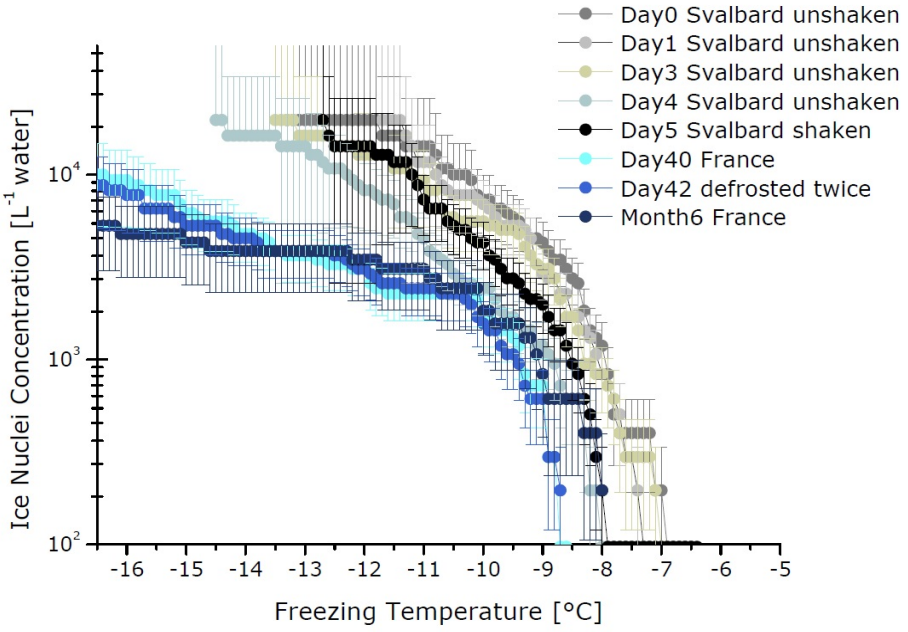

Figure 4.15: Test–retest reliability of immersion freezing measurements performed on the same seawater sample, collected on the 15^{th} March 2017 from control mesocosm.

4.5.1 Test–retest of bulk seawater immersion freezing tests

Figure 4.15 report the comparison among the immersion freezing measurements performed in Svalbard and the measurements performed in France from an identical seawater specimen collected on the 15^{th} of March 2017 from the control mesocosm. A specimen was tested immediately on the 15^{th} of March 2017 (day 0), and then re-tested on the followings days: +1, +3, +4, +5. These aliquots were preserved in the dark at +4 °C, while other aliquots were frozen at −20 °C and thawed once transported in France for further testing. A vial was defrosted and tested in April (+40 days after the initial collection) and another one in September (+6 months after the initial collection). Figure 4.16 shows an exponential decay during the first days followed by a slower degradation. Therefore, it is not possible to exclude a possible degradation related to the passing of time for the adopted storage conditions.

This degradation may result also by the frosting-thawing and the sedimentation. Considering this last point, it should be considered that no method for sample homogenisation was mechanically adopted at the beginning (tests done on days 0, 1, 3, 4). On the contrary, during the test performed on day 5, the sample was vigorously shaken and it showed results comparable to the third day. Considering the differences among the shaken test -on day 5- and the unshaken test -on day 4- we deduced that sample homogenisation (e.g. shaking/mixing) is relevant. Hereinafter -from the 20^{th} of March- all the samples were mechanically shaken, and to this purpose, a Mini-Vortex Mixer was used to ensure an efficient mixing and avoid any possible heating of the sample.

Similar experiences of test-retest reliability were performed on other specimens and are reported in Figure 4.17. For these samples the signal's degradation is not uniform, in certain

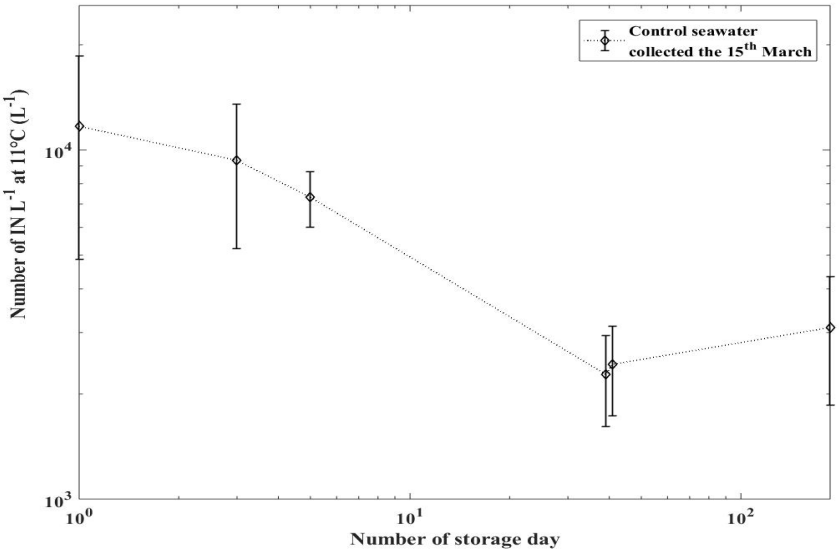

Figure 4.16: Number concentration of Ice Nuclei L^{-1} activated at -11 °C for control mesocosm seawater collected on the 15^{th} of March 2017 and tested at different days.

cases the INP number concentration is slightly reduced (e.g. sample collected the 8 and the 12^{th} of March 2017) in other cases it is highly diminished (e.g. samples collected the 17^{th} and the 21^{st} of March 2017).

Similar conclusions were reported by Schnell and Vali, 1975 [251]. In their work, seawater samples were kept at room temperature for seven months and their freezing nucleus contents were measured periodically. Different levels of degradation were recorded, with one sample showing a two steps deterioration: a huge decrease (down to one per cent of the initial value) after three weeks and a lower decrease in the consecutive period (down to the lowest detected value after seven months from the initial sampling). Another group of sub-samples, stored at room temperature and showing low IN concentration, were related to no change at all. Another group of sub-samples, stored frozen, presented no loss of freezing nucleus activity after the same considered period of seven month. Then, Schnell and Vali [251] suggested that in frozen seawater samples, the ice nucleating properties do not significantly change within seven months, while modifications occur at room temperature in a group of sub samples.

In the study of Irish et al., 2017 [153], samples were stored in Nalgene bottles frozen at -80 °C, for a maximum of 9 months before IN analysis. In this study, homogenisation was performed by inverting at least 10 times each sample.

In the study of Wilson et al., 2015 [72] samples from the Netcare campaign were kept frozen at -20 °C after collection, and before the experiment they were thawed and stored at $+4$ °C in the dark. All the samples stored at $+4$ °C in the dark were analysed within 10 days.

In our study, we initially stored the samples at $+4$ °C in the dark then we froze them at -20 °C and we thawed them the day of the analysis. The article of Schnell and Vali [251] does not provide any indication of the possible degradation at $+4$ °C in the dark, and any study specify the best freezing conditions for the storage (among -20 °C and -80 °C).

On the 15^{th}, 17^{th} and 21^{th} we could analyse seawater samples immediately after the collection

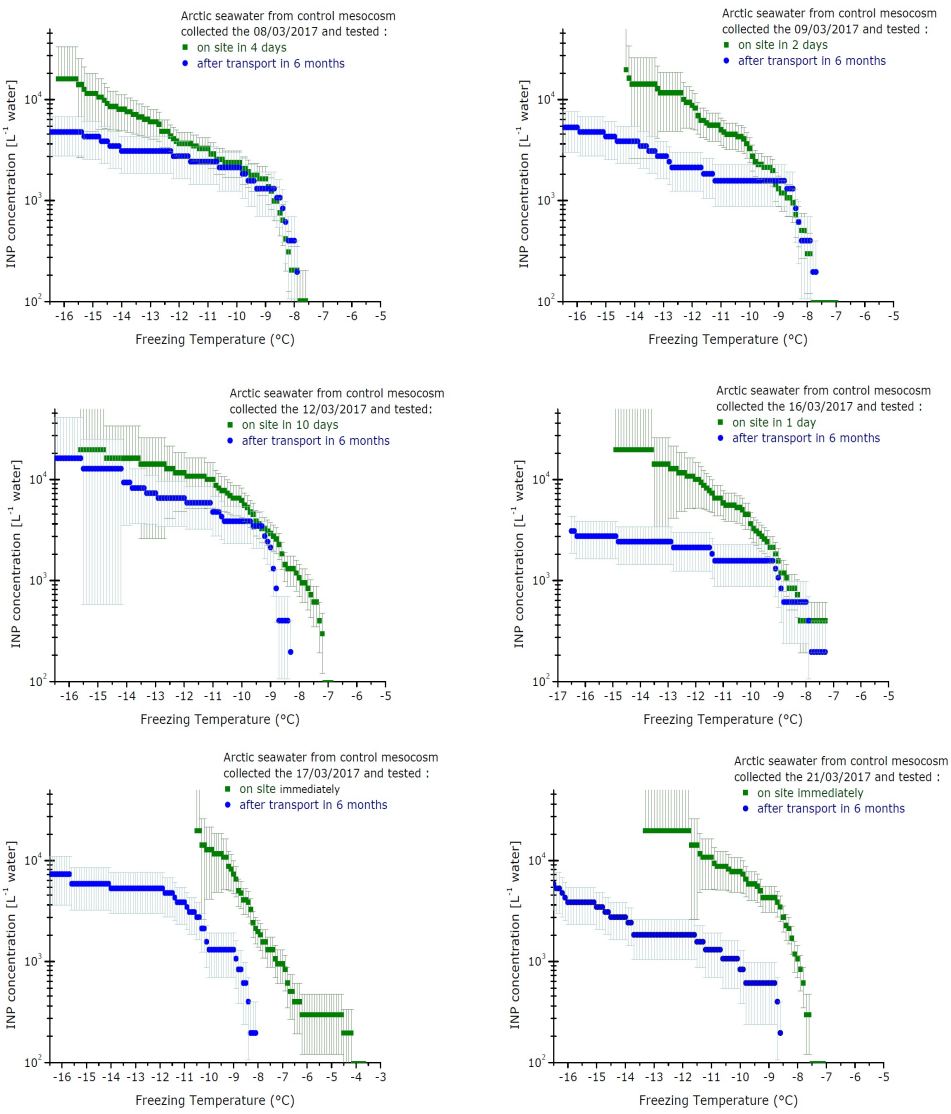

Figure 4.17: Test–retest reliability of immersion freezing measurements on several seawater samples from control mesocosm. Green curves refer to tests performed in Svalbard with samples stored in a refrigerator. Blue curves refers to tests performed in France, few months later, after the transport and the cooling of the samples.

in the harbour (day 0). By comparing immersion freezing performed in situ -at day 0- with immersion freezing performed in France six month later, we reports the scatter plot among the non degraded versus degraded signal in Figure 4.18. Around one tenth of the original number of ice nuclei per Liter is preserved six months later. The high correlation coefficient says that at least the temporal variation are preserved.

Resolving the longevity of IN particles could not be achieved within the timeframe of the present study. At least, these tests show that the hypothesis of an increase of IN due to freezing-thawing is unlikely to occur. In literature, a possible increase of IN due to freezing-thawing was justified by:

- 1) cell breaking fragments, that could follow the freezing-thawing of biological material, could mulitply the number of IN;

- 2) pre-activation phenomena, when cracks occur at the substrate surface during subsequent freezing cycles (cracks may hold ice at lower vapour pressures than ice saturation, or at temperatures above the melting point of bulk ice).

Our tests indicates that the above mentioned effects did not occur and that there is a transformation with time of IN properties -in the dark at +4 °C- reinforcing the hypothesis of a possible biological origin of marine IN species. It may also be worth mentioning that in analogous studies (e.g. [72], [153]) samples are rarely analysed right away after collection, or after thawing. Therefore, also other works may be affected by degradation.

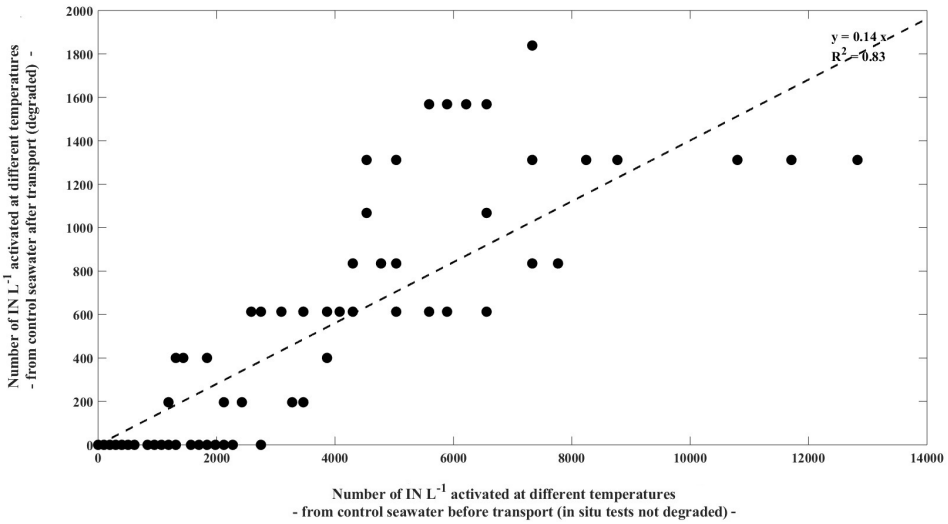

Figure 4.18: Scatter plot of the ice nuclei number per unit volume (L^{-1}) detected before transport (non degraded signal obtained in situ at Svalbard) and after transport (degraded signal obtained in the French laboratory six month later).

4.5.2 IN in the bulk seawater

The majority of samples were transported to the French LaMP/ICCF laboratory and analyzed in a short period of time at the end of September 2017. In order to perform close measurements, we halved the number of droplets for each test, in order to half the time required for each measurement. Therefore in France we used an array of 26x200 μl droplets (instead of an array 52x200 μl adopted in Svalbard). This protocol affected the upper detection limit of the FNA instrument, as explained in paragraph 4.5.

Figure 4.19 reports the time series evolution at -15 °C (as in the case of the sea spray reported in Figure 4.12). The first period of the campaign is characterized by an increasing number of IN in the seawater, with a maximum on the 12^{th} of March for the degraded signal (named after transport A.T.) and the 17^{th} of March for non degraded data (named before transport B.T.). Minor maxima appear on the 8^{th} and 15^{th} for the degraded signal.

The range of concentrations observed in our study is reported in Figure 4.20. However, due to the restricted detection limits of our instrument, the curves obtained in this study cannot catch the all region defined by [72] and [153] down to -30 °C and beyond 2x10^4 IN L^{-1}. Dashed lines

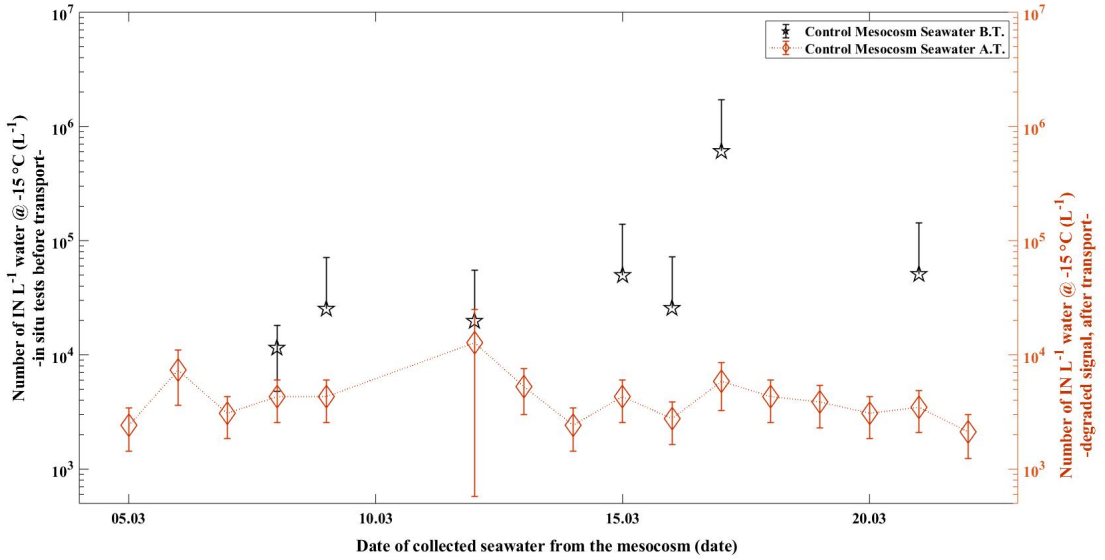

Figure 4.19: Ice nuclei concentrations in the bulk seawater from control mesocosm (after transport A.T. and before transport B.T.). Data are not corrected for freezing point depression due to the presence of sea salts.

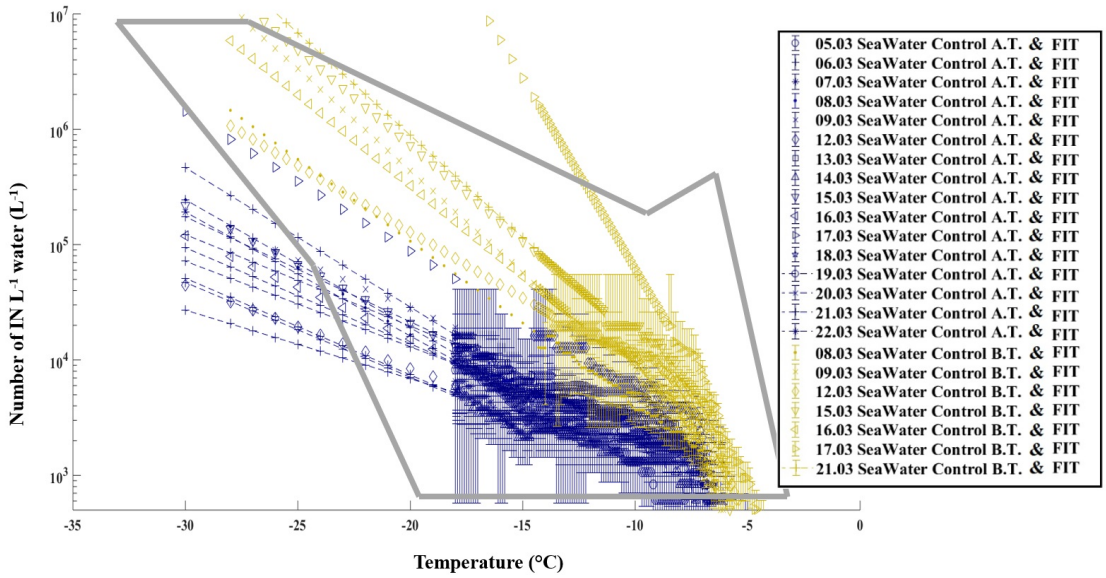

Figure 4.20: Ice nuclei concentrations in the bulk seawater collected from the control mesocosm on different days. Measurements were performed partially on site (before transport B.T.) and then at the laboratory (after transport A.T.). These data are corrected for freezing point depression to compare with literature. Each curve corresponds to a single test on bulk seawater. The uncertainty in temperature is not shown but is ±0.3 °C. The grey line refers to previous studies reported in Figure 4.21.

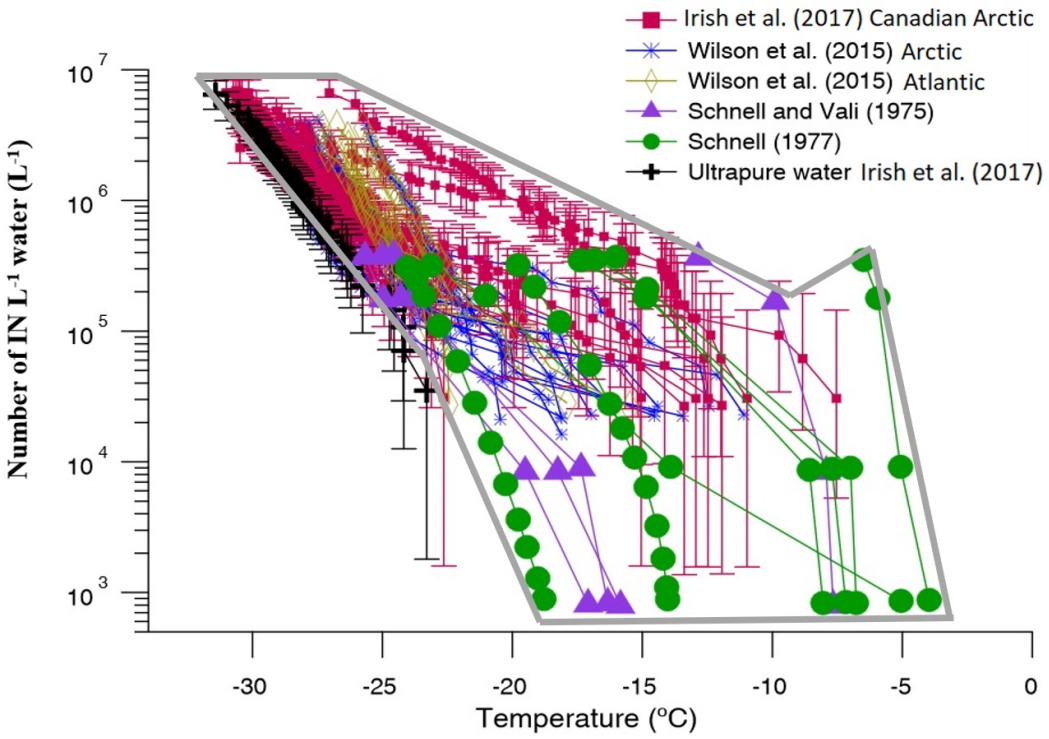

Figure 4.21: Published results of ice nuclei concentrations in the bulk seawater (photo credit Irish et al.,2017 [153]). All data are corrected for freezing point depression due to the presence of sea salts. The grey line define the region of ice nuclei activation that has been defined so far in literature.

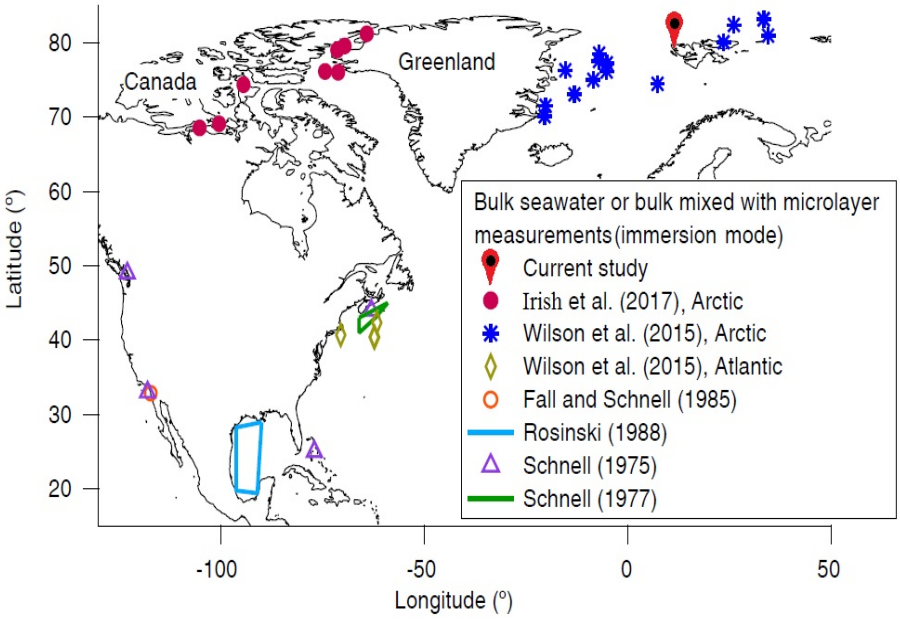

Figure 4.22: Map of IN field measurements (immersion freezing) for the study of bulk seawater or a mixture of bulk seawater and microlayer. Photo credit Irish et al., 2017 [153].

are extrapolated to −30 °C by exponential fit through Matlab R2018a (in the unique purpose to better visualise the trend of our data). Included in Figure 4.20 and detailed in Figure 4.21 is the IN concentration range obtained from other similar studies, that considered samples of bulk seawater or samples containing a mixture of the microlayer and bulk seawater.

These studies are corrected for the freezing point depression, which represents the effect of sea salts, lowering down the freezing temperature of water (when compared to an equivalent sample deprived of these salts). The effect of the freezing point depression correction is an horizontal translation of the freezing curve by applying a 2 °C correction [153], [252], and [246]. For the comparison, we applied the same correction to our data, in Figure 4.20.

Figure 4.22 reports a map with the sampling sites. IN measurements in the Arctic seawater were performed by Wilson et al., 2015 [72] during July–August 2013 and Irish et al., 2017 [153] during July-August 2014, by means of a cold stage apparatus.

We report both our degraded data (after transport to France) and the data obtained in situ (before transport). The range of concentrations observed in our study agrees well with the range defined by past studies, and in particular the degraded data are consistent with the concentrations reported by Wilson et al., 2015 [72] obtained in situ, near Svalbard during summer. The non degraded data are higher and are almost in agreement with Irish et al., 2017 [153].

To explain the differences among our in situ data and [72] possible causes are: i) the published data of [72] were also affected by degradation ii) seawater IN are more concentrated during springtime than during summer iii) coastal seawater may be different than open ocean in relation to IN content. Indeed, [72] was on an oceanographic cruise campaign, relatively far away from the coast, while our research considers the seawater used to fill the mesocosms that was next to the coast. All together, our results indicate that sample degradation -due to storage and transport conditions- could contribute to the differences which are generally attributed to the state of the ocean, the period of the year, the place, or the freezing technique.

4.5.3 The impact of pollutants and external conditions on seawater ice nuclei content

Figure 4.23 presents the average ice nuclei concentration of bulk seawater from the control and the polluted mesocosms. Data belong to the tests performed in France (degraded values). The signal from the polluted system is lower than the unpolluted one (named control) and the differences are included in the respective error bars.

To appreciate the influence of pollution on the modified mesocosm IN population, we investigated whereas the two medians belonged to the same distribution or not, through a non-parametric test. The Mann-Whitney rank sum test is suitable for distributions having unequal number of observables and it is reported in Figure 4.23. Rank sum test was calculated with Matlab R2018a and resulted positive, with a p-value inferior to 0.01 for freezing temperature below −19 °C. We deduce that the differences among the two distributions are significant and that pollution has a negative impact on seawater IN population.

We wonder whether a reduced number of IN in the seawater might affect the number of IN in the seaspray (except if the pollutants are ice active nuclei themselves). Our results on seaspray have shown a weak but significant difference between the control and polluted experiments only

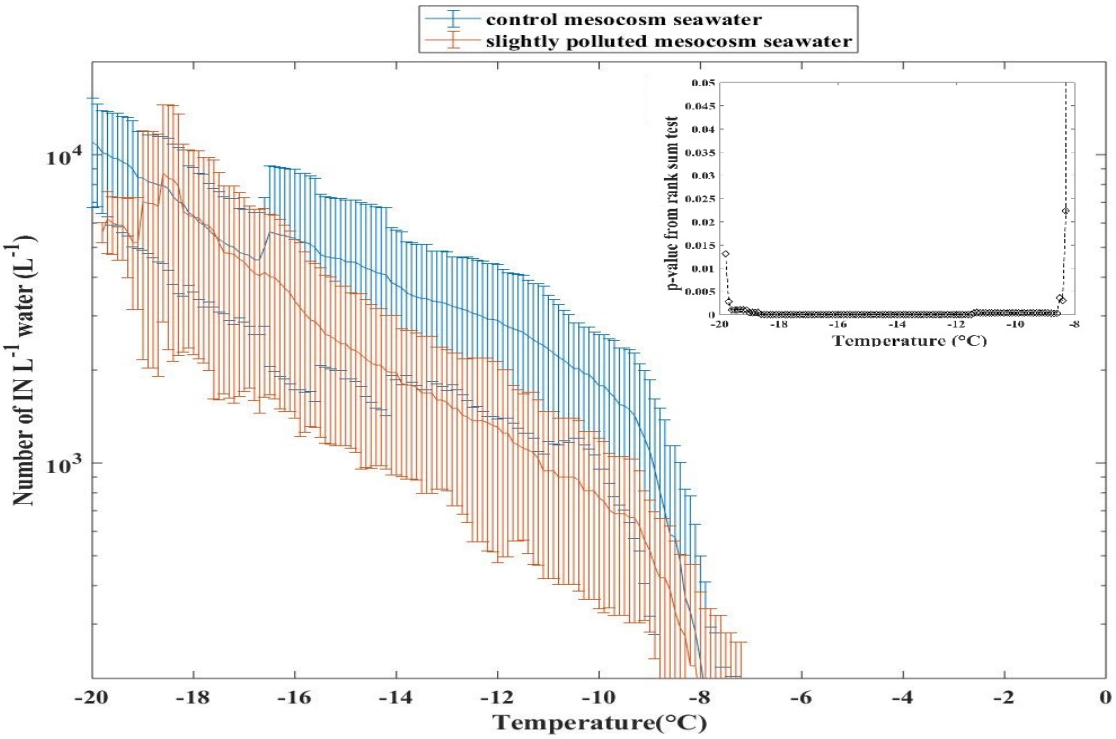

Figure 4.23: Average number of ice nuclei in the bulk seawater of control mesocosm and polluted mesocosm. The rank sum test performed on the two distribution is positive in the temperature interval between −8.3 °C and −19 °C. Both the p-value, < 0.05, and h = 1 indicate the rejection of the null hypothesis of equal medians at the default 5% significance level.

at the coldest freezing temperature of −25 °C with condensation freezing activation mode (tests with DFPC shown in Figure 4.9). For warmer temperature, with both DFPC and FNA we could not appreciate significant difference in the seaspray of control and (highly) polluted samples (see Figure 4.6, 4.7, 4.8, and 4.13). The lack of knowledge on the mechanisms governing IN fluxes, from seawater to seaspray, limits our conclusions to the present mesocosm experiment.

Furthermore, by analysing the time series evolution of IN number concentration in the seaspray (for both immersion freezing and condensation freezing tests) in search of a connection with the time series of IN in the seawater (immersion freezing tests), no correlation was generally found, with the exception of values reported in Table 4.4.

Seaspray Ice Active Nuclei, condensation freezing at −22 °C	R	p-value	N
Seawater Ice Active Nuclei (before transport) at −9 °C	0.98	0.00	7
Seawater Ice Active Nuclei (before transport) at −10 °C	0.98	0.00	7
Seawater Ice Active Nuclei (before transport) at −11 °C	0.88	0.01	7
Seawater Ice Active Nuclei (before transport) at −12 °C	0.85	0.02	7
Seawater Ice Active Nuclei (before transport) −13 °C	0.83	0.02	7
Seawater Ice Active Nuclei (after transport) at −10 °C	-0.46	0.13	12

Table 4.4: Correlation analysis between the number of seaspray ice nuclei activated at −22 °C with DFPC and the number of seawater ice nuclei activated at warmer temperature with FNA). We report only moderate/high correlations that are statistically significant.

Table 4.4 correlations have been calculated among: seaspray condensation freezing tests at

−22 °C and seawater immersion freezing tests between −9 °C and −13 °C. A positive correlation appears only with the non-degraded seawater signal.

The large region occupied by each error bar in Figure 4.23 seems determined by a large variability of the ice nuclei concentration related to each species, if collected on a different day. By focusing on one specific activation temperature, as the average temperature T_{freeze} between T5 and T95 (i.e. the temperatures at which 5% and 95% of droplets had frozen), it is possible to appreciate these fluctuation day by day. Figure 4.24 shows the time evolution of T_{freeze} for both control and polluted mesocosms. To understand the temporal variability, we investigated any possible correlations with external ambient conditions.

As reported in previous mesoscosms experiments [238], the temperature has a major influence on the physiology of marine organisms and their metabolic processes. Some species, like autotrophic organisms, increase their growth rate with temperature, while other species, like heterotrophic bacteria, have shown reduced abundance under warming [238]. In the work of [252], [246] heterotrophic bacteria has been indicated as possible responsible for the ice nucleating properties of seawater. Therefore, we would expect that decreasing temperature would favourite heterotrophic bacteria proliferation and increase the ice nuclei concentration. This hypothesis seems confirmed by our measurements (Figure 4.24).

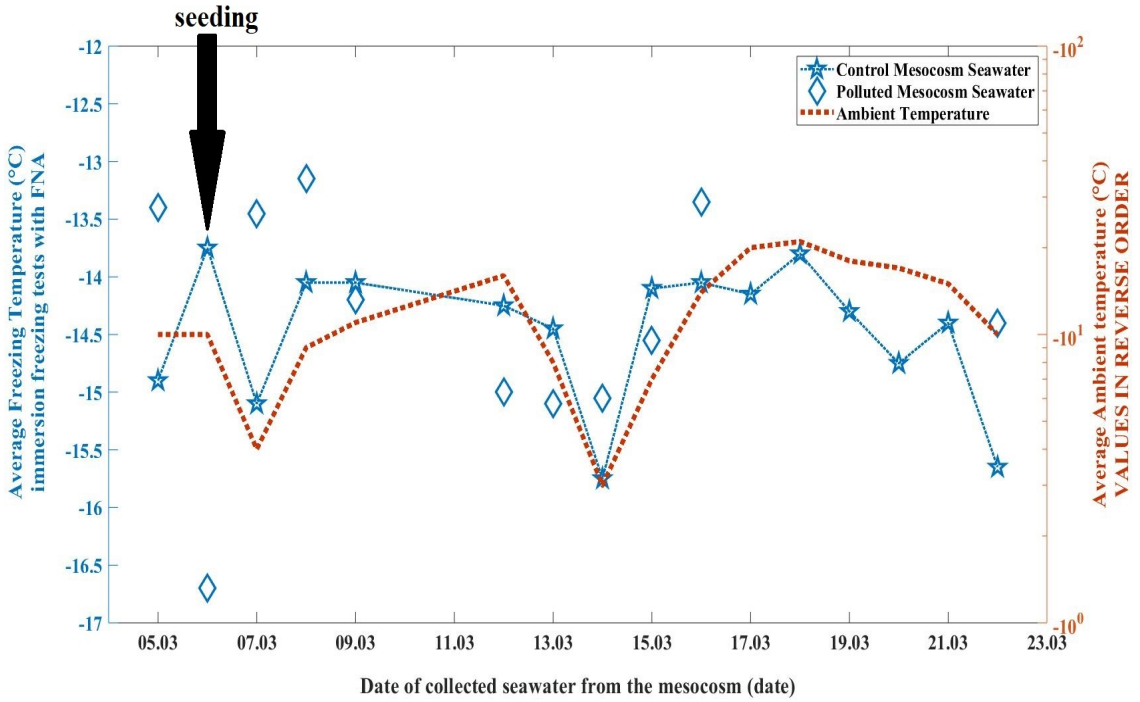

Figure 4.24: Average freezing temperature calculated from T5 and T95, i.e. the temperature at which the 5% and the 95% of ice nuclei have been activated. Ice nuclei were activated through immersion freezing with FNA during the tests performed in France (after transport). Ambient temperature refer to the average daily temperature at Ny-Alesund. No correction for freezing point depression.

A weak but significant anticorrelation (R=-0.50, pvalue=0.05) with ambient temperature seems to indicate a response of seawater ice nuclei concentration to chilling. We suggest that

temperature fluctuations have affected IN concentration in addition to the seeding with ammonium nitrate and sulphate.

4.5.4 Ice nucleation rates of filtered seawater

To identify the nature of marine ice nuclei, tests on the filtered seawater were also considered. Knowledge of particle size distributions provides useful information while identifying a source/species in both atmospheric physics and marine science. To this purpose, filtration is frequently used for separating particles from their gas or liquid carrying medium and segregating them.

Filtration techniques have been used widely in marine science for distinguishing between particulate and dissolved materials (a distinction arbitrarily defined by retention on a filter of 0.45 μm pore size, as reported by Johnson and Wangersky, 1985 [253]).

Following [72], the bulk seawater samples were passed through filters of 0.2 μm pore size (Millex, 0.2 μm pore size). The frozen fraction curves for both the unfiltered and filtered bulk seawater samples are shown in Figure 4.25. The freezing properties of filtered seawater are always lower than the unfiltered samples, as expected. However, filtered samples still contains some IN since the frozen fractions are not negligible. Therefore, some particles <0.2μm in diameter (defined in the biologists community as dissolved material) can act as IN, as already shown by [72]. Past studies [72], [252], [246] have suggested that this IN population of small material might be related to extracellular matter from phytoplankton, or bacteria (exudate), or viruses, or ultramicrobacteria. This suggestion is reinforced by observations of a reduced IN activity of samples heated at temperatures up to 100 °C.

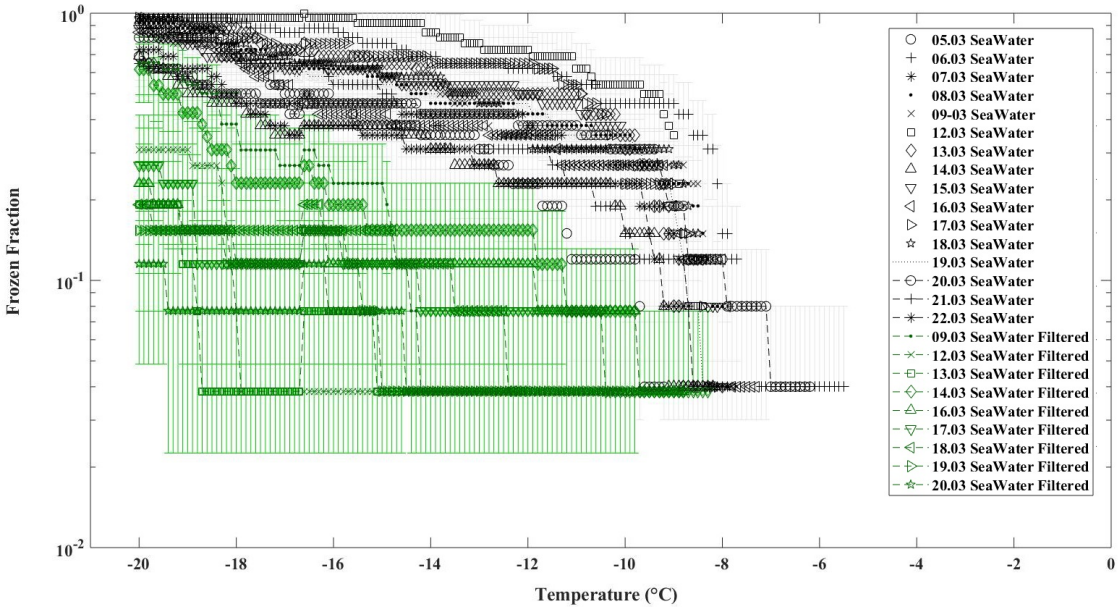

Figure 4.25: Frozen fraction curves for both the unfiltered and filtered bulk seawater from control mesocosm. All data are corrected for the blank, and freezing point depression has not been applied.

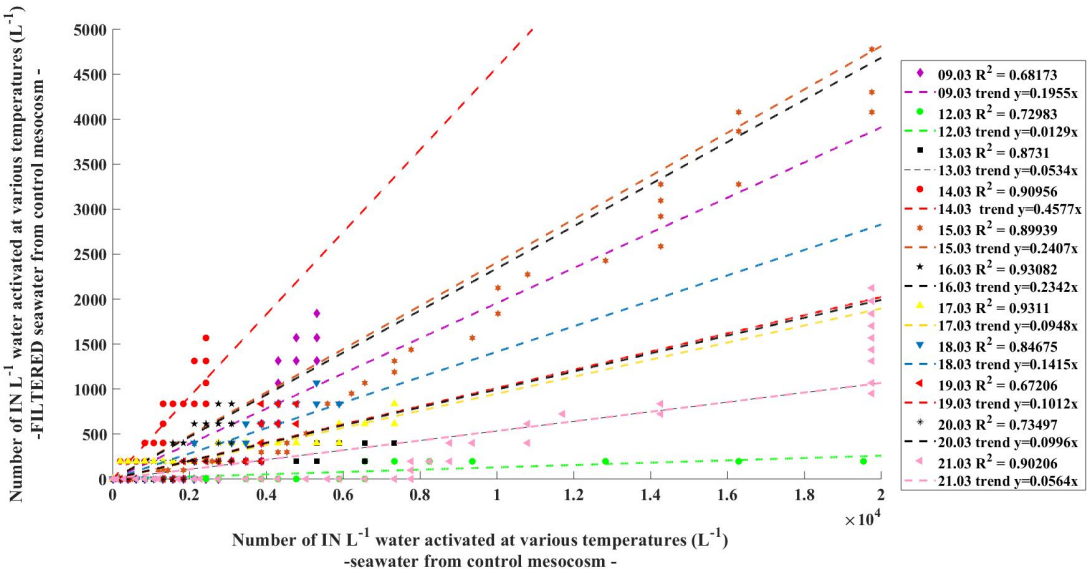

Figure 4.26: Scatter plot among the filtered and unfiltered seawater signal. Each point represents the IN number concentration for unit volume (L^{-1}) activated at a specific temperature through immersion freezing with FNA. X-axis is the value detected in the seawater, while y-axis refers to the value detected in the associated filtered seawater. The majority of data refers to the experiments performed in France (after transport) except the 15^{th} and the 21^{th} of March (tests performed in situ). Data were not corrected for salt freezing depression.

Figure 4.26 reports the scatterplot of the number of IN per Liter in the filtered (y-coordinate) and unfiltered (x-coordinate) seawater samples, together with the R-squared coefficient (that is included between 0.6 and 0.9). The 15^{th} and 21^{th} of March refer to in situ measurements (for both the filtered and unfiltered component), while the others were obtained in France six months later. The mean ratio among unfiltered and filtered seawater is 0.15±0.12, calculated from the average of the trendline equations in Figure 4.26. Then, in the bulk seawater analysed, the contribution of ultrafine IN species (particles smaller than 0.2 μm) is inferior to 20% but is not negligible. Therefore, in this work, the majority of IN should be related to the presence of entities larger than 200 nm. This conclusion is in contrast with the work of Wilson et al., 2015 [72] which found a significant population of ice active nuclei passing through a 0.2 μm filter when considering surface microlayer. We couldn't collect surface micro layer in the Arctic, and then we can not discern if our conclusion is a peculiarity of the bulk seawater when compared to surface micro layer (or a specificity of the place/period of the year).

4.6 Sea Spray size distribution and chemical analysis

To further investigate the parameters governing the ice nuclei activity of PMA, this section considers the physico-chemical characterization of the generated sea-spray.

4.6.1 Sea Spray size distribution

Researchers have investigated primary marine aerosol (PMA) properties both in the field [241], [254] and in the laboratory [255], [256], [257] [258], [259], [260]. Plunging-water jet experiments

were found to mimic the size distribution of ambient primary marine aerosol with the advantage of generating sufficient aerosol for characterization analysis [241] .

Past studies have shown that PMA size distribution and chemistry depend on both: the wave breaking dynamic (i.e. surface wind speed, wave height, wind history, friction velocity, and viscosity, as reported by [261] and [262]); and the organic matter content (see [263], [241], [254]).

The PMA chemical composition is characterised by: i) sea salt particles (associated mainly to the supermicron aerosol fraction) ii) submicron particles which also contain sea salt but may contain as well a fraction of organic matter as colloids and aggregates of exudates from marine microorganisms, gels, and viruses [264], [263], [254].

In this study, aerosol size distributions were measured using a DMPS (custom made by LaMP-CNRS) combined to a soft X-Ray aerosol neutraliser, used to reach a steady state aerosol charge distribution. The use of a non-radioactive source, instead of a radioactive one, can affect MPS measurements (as published in Nicosia et al., 2017 [162]). Then, our post processing inversion algorithm was adapted to correct the data accordingly to the presence of the non-radioactive neutraliser. The aerosol size distributions remained fairly stable throughout the campaign, with

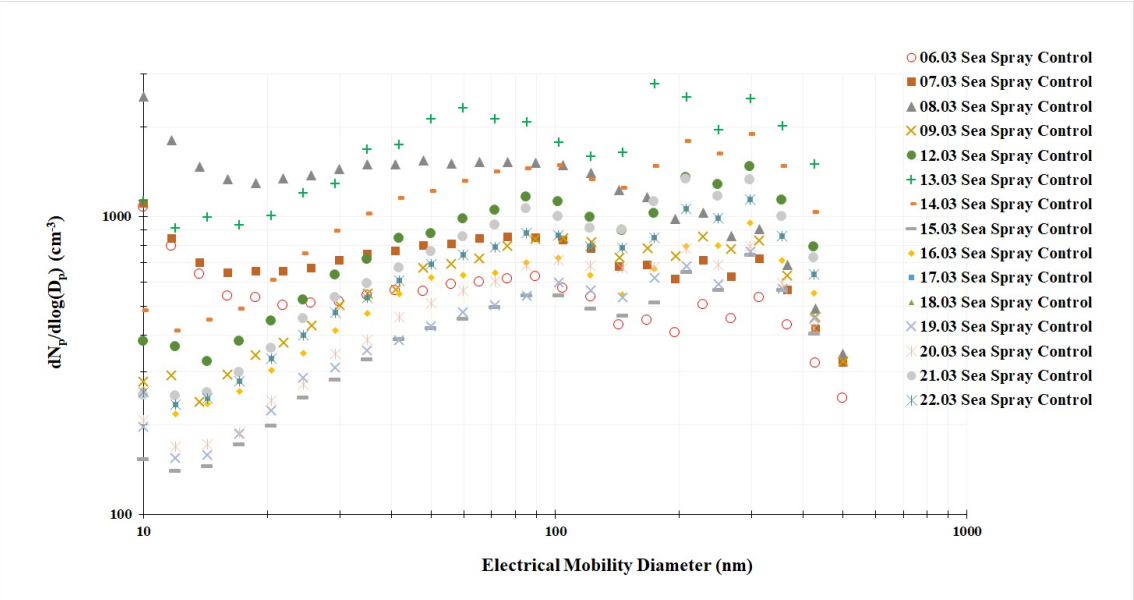

Figure 4.27: Particle Size Distribution of the primary marine aerosol generated from control mesocosm seawater in relation to the day of sampling.

a similar distribution shape, see Figure 4.27. On the 6^{th}, 7^{th}, 8^{th}, 13^{th} and 14^{th} an increased concentration toward smaller size, below 0.02 μm was observed. Figure 4.28 reports the total particle number concentration per unit volume, in cm^{-3}, calculated as the median and standard deviation from the one hour generation experience, recorded by OPC, CPC and DMPS, during each day. OPC shows a stable concentration, around 600 p cm^{-3}, while CPC and DMPS shows larger fluctuations. On the 13^{th} of March the concentration was higher due to a bad regulation of the generator (the intersection of the air exhaust and the plunging jet were not positioned as usual at 90°) that however occurred only in this experience.

No significant correlation was found between these oscillations and the IN number concentration measured in the seawater or the seaspray, except a weak anticorrelation between the

median total particle concentration of CPC and the IN number concentration activated through condensation freezing at −22 °C (R −0.55; p-value 0.06).

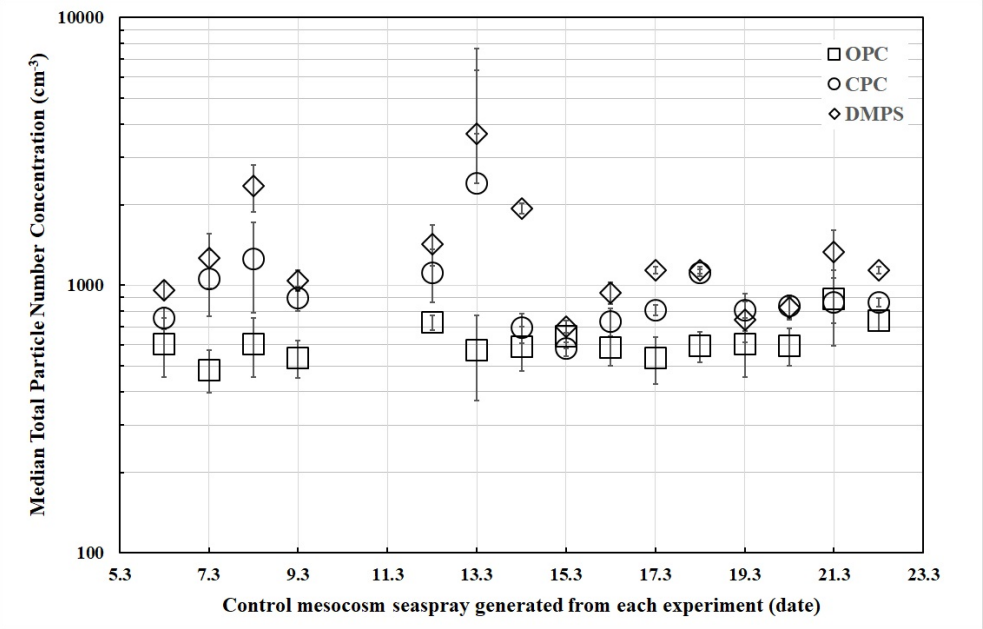

Figure 4.28: Total particle number concentration mediated for each generation experiment (from control seawater). At the inlet of CPC and DMPS, there was a drier and a PM1 impactor, while the sampling line was preserved as short as possible for the OPC. Then, CPC and DMPS could detect only particles smaller than 1 μm. The DMPS custom made (by LaMP-OPGC) was configured to detect particles in the interval 0.01-500 μm; CPC TSI 3010 could detect particles from 0.02-1 μm (and partially from 0.01-0.02 μm); the OPC Welas detect particles in the range 0.2-20 μm (and partially from 0.017-0.02 μm).

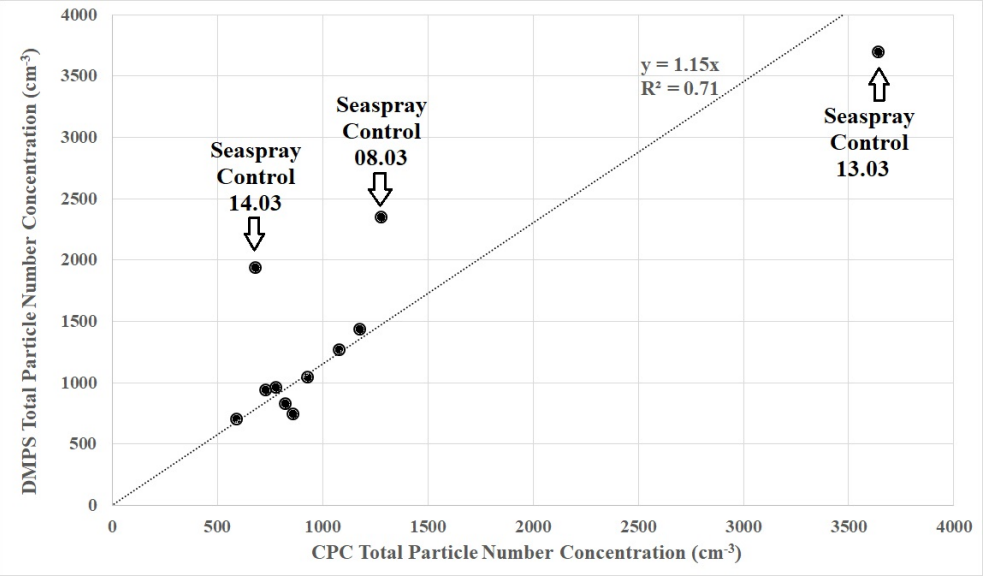

Figure 4.29: Scatter plot of the total particle number concentration (above 0.010 μm diameter and below 1 μm) measured by CPC and by DMPS. The CPC used in this study has a decreasing particle detection below 0.020 μm diameter (50 % of counting efficiency at 0.010 μm). Data-set refers to the sea spray aerosol generated from control mesocosm seawater.

The CPC device (operating in the range 0.010-1.00 μm) was employed to monitor the total particle number concentration measured by DMPS (operating in the range 0.010-0.50 μm). The two instruments are compared in Figure 4.29. Differences registered on the 8^{th} and 14^{th} of March can be attributed to the influence of nanoparticles smaller than 20 nm, that were highly concentrated these two days (as shown in Figure 4.27). It should be considered that the DMPS inversion is more uncertain for particles smaller than 20 nm and this could explain the higher discrepancy with the CPC.

Large particle (>200 nm) number concentration were also measured by OPC without any pre-treatment of the seaspray. Because losses in the drier might be relevant, and supermicron particle concentration are lower than submicron particle concentration under the adopted MAG, we decided to sent the original undried aerosol to the OPC inlet. The particle size distribution obtained by OPC is shown in Annex D. Particles larger than 0.5 μm accounts for less than 3% (with respect to the total particle number concentration counted by OPC).

4.6.2 Chemical composition, inorganic fraction

Determination of the major ionic constituents was conducted by ion chromatography analysis of the PM1 filters sampled in the cascade impactor. Figure 4.30 presents the inorganic mass of aerosol particles <1 μm generated in the sea spray chamber for each day of measurement. The average fraction of inorganic chemicals with respect to the total inorganic mass detected is given in Table 4.5. These fractions are calculated from the average of 15 individual samples (generated from the control mesocosm seawater) and three blanks. The inorganic composition of Arctic sea spray reported in this study is a little bit different from the composition of seawater reported in [35]. We notice a close resemblance to the values reported in [240], apart a lower ratio of sulphates and a higher calcium fraction. However, the study [240] concerns the Mediterranean Sea region, that is warmer and saltier.

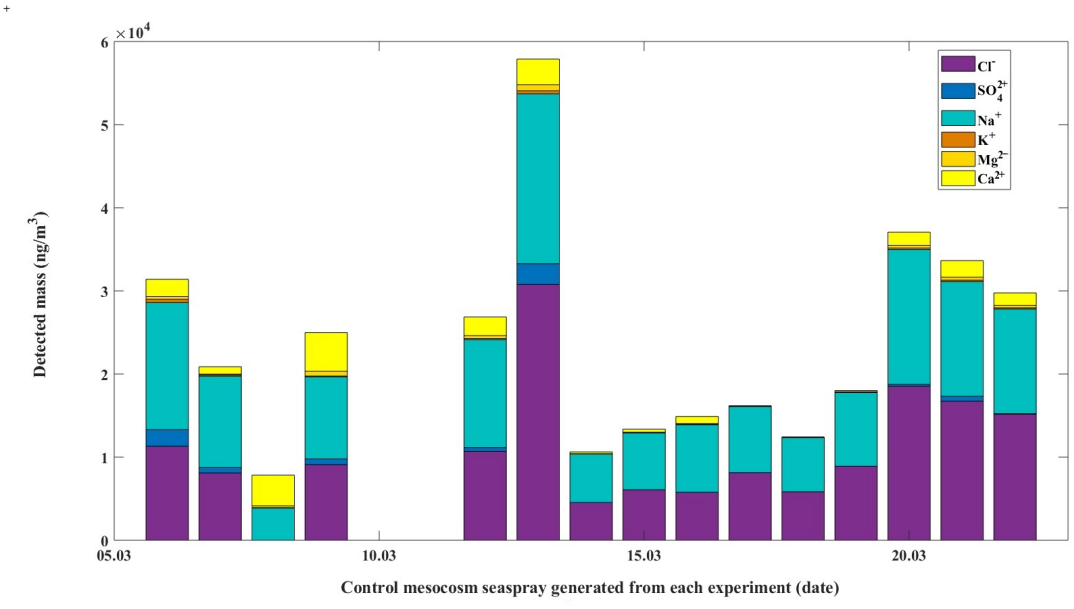

Figure 4.30: Filters samples: speciation of the inorganic fraction PM1.

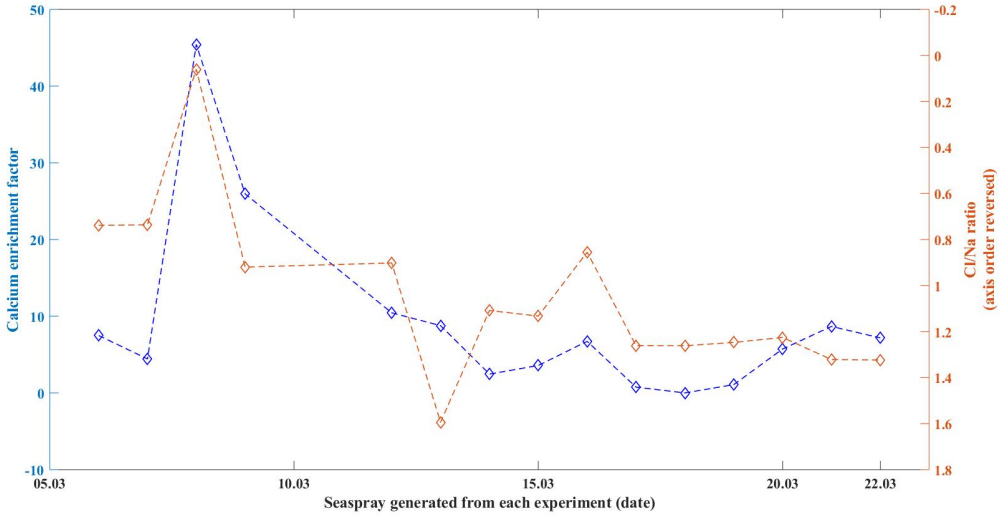

Figure 4.31: Calcium enrichment factor and Cl/Na ratio in the PM1.

To facilitate comparison between seawater sources and particle composition it is common practice to present the observations as enrichment factors relative to sodium [265],[266]. The enrichment factor, EF, is calculated as the ratio of the concentration of a substance X to the concentration of one of the major constituents (e.g. Na^+) in the seaspray divided for the same ratio evaluated in the bulk seawater:

$$EF(X) = \frac{([X]/[Na+])_{SeaSprayAerosol}}{([X]/[Na+])_{Seawater}}$$

The enrichment factor calculation assumes that sodium is a conservative species that does not experience significant chemical reaction in the aerosol phase. By considering for seawater composition the values listed in [35] and reported in Table 4.5, it results that the calcium average enrichment factor is of the order of 9, for the present study. Calcium enrichment in the PM1 primary marine aerosol has also been reported previously, however it was mainly connected to a crustal contribute intrusion, while a minor amount of studies reports the possible marine origin of Ca^{2+} enrichment [265] and [266]. Considering that our study is based on bubble-produced primary marine aerosol, generated from seawater sampled in a fjord surrounded by snowed mountains and connected to a mesocosm experience, a marine origin of Ca^{2+} is expected in our study. Considering that the sea spray generation process was the same for all the 15 experiences, the modification in the Ca^{2+} concentration of our sea spray are probably related to the biogeochemistry of seawater. Whatever the reason, several implication have been associated to calcium and magnesium enrichment in seawater, as they potentially influence bacterial adhesion [267], and are critical for biofilm architecture. What we could observe from our study, in Figure 4.31, is a significant anticorrelation among the calcium enrichment factor and the ratio Cl/Na (R=-0.722, pvalue=0.002).

A "chloride deficit", resulting from Cl/Na ratio < 1 in the sea spray, has already been described. As reported by [35], seawater contains a large amount of sea salts (around 3.5% by weight), which are first emitted in the sea spray. The sea spray composition is close to that of

seawater but reactions during transport in the atmosphere may modify its chemical composition; for example, sodium chloride reacts with sulfuric (/nitric) acid to produce sodium sulphate (/sodium nitrate) and hydrochloric acid vapour, leading to an apparent "chloride deficit" in the marine aerosol [35]. A Cl/Na mass ratio of 0.67 was reported by [268], which is much lower than the seawater ratio of 1.8. Also Wilkniss and Bressan (1972) [269], during bubble-produced sea-salt particles experiences, obtained that the Cl/Na ratio was slightly lower than the value in seawater (for the aerosol particles below 1 μm radius) and they suggested a possible fractionation and/or possible loss of chloride from the jet and film drops after injection into the air [269]. Our data, depicted in Figure 4.31, shows huge deficit of Chloride (Cl/Na ratio of 0.06) concomitant to deep Ca enrichment (around +45%). Similar correlation among chloride deficit and Ca^{2+} enrichment in the sea spray has been presented in [240]. In this work, an enrichment of calcium (around +500%) was concomitant to a deficit in chloride (around −36%) in the submicron PMA mass compared to the literature inorganic composition of the seawater. [240] suggested that the chloride deficit and calcium enrichment were linked to biological processes, as they were found to be stronger in the concerned period.

Mass Fraction	Cl^-	SO_4	Na^+	K^+	Mg^{2-}	Ca^{2+}
Seaspray (present study)	0.46±0.39	0.05±0.05	0.41±0.29	0.00±0.01	0.01±0.01	0.07±0.07
Seaspray [240]	0.47±0.06	0.07±0.02	0.39±0.03	0.00±0.00	0.02±0.00	0.05±0.05
Seawater [35]	0.55	0.08	0.31	0.01	0.04	0.01

Table 4.5: Mass fraction of the main inorganic components in PM1 sea spray with respect to the total inorganic mass. Measures refers to PMA generated from 15 samples originated from control mesocosm. Reported are also the mass fraction of a similar study performed in the Mediterranean Sea [240] and the main inorganic ions in seawater reported by [35].

4.6.3 Chemical composition, organic fraction

The organic fraction of the primary generated aerosol was addressed using an Aerosol Mass Spectrometer (Compact Time of Flight Aerosol Mass Spectrometer of Aerodyne Research Inc) for real-time measurements of aerosols, which is referred to as AMS. Measurements and data processing were made by scientist Barbara D'Anna and Marc Mallet (part of IRCELYON and now member of LCE-CNRS and LISA-CNRS respectively).

The AMS provides size-resolved chemical composition of non-refractory submicron aerosols, with an integration time of the order of seconds/minutes [163], [164], [270]. In front of the AMS inlet, silica gel desiccator was used to remove the moisture of the generated sea spray, reducing the relative humidity to less than 40%.

With AMS, the presence of organic matter is described by an abundance of the organic spectra type, under typical operating conditions. For marine aerosols, the total sampled organic mass distribution cannot be derived so easily, as the AMS is not designed to detect refractory components (such as sea salts). Different organic species, with different electron ionization fragmentation patterns, may contribute to the total organic mass in different amounts and in different size ranges; therefore, the organic mass concentration should be extrapolated as the sum of all fragments after subtracting all identified artifacts, originated by inorganic compounds, such

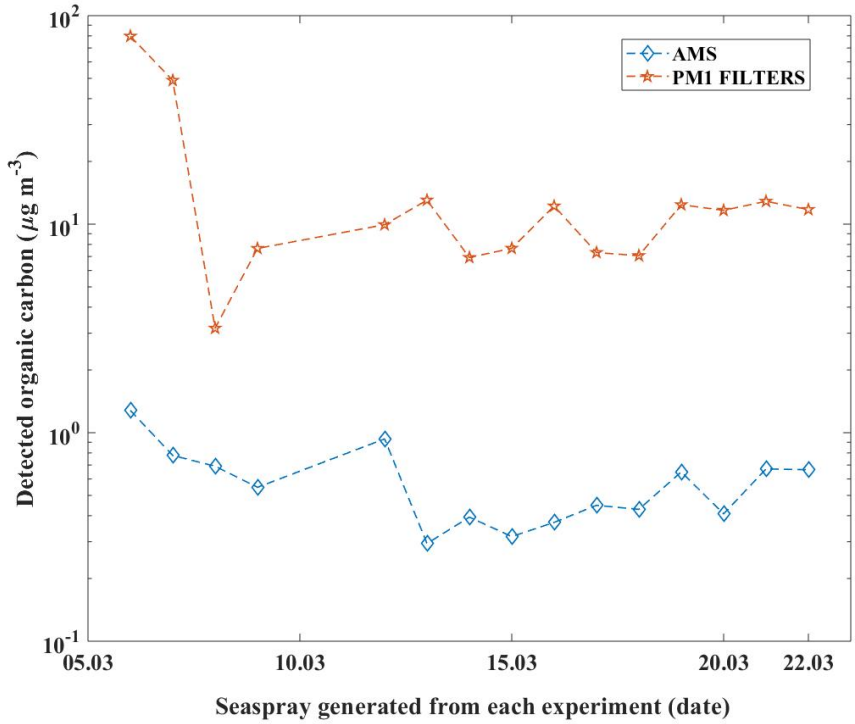

Figure 4.32: Detected organic carbon from the present study (bubble-produced sea-spray experience in the Arctic from control mesocosm).

as sodium ions (Na^+) [165]. Then the organic fraction can be calculated relatively to the total analytical mass, with a significant uncertainty on the NaCl concentration as it is not volatile at the 600 °C operation's AMS heater. During the 15 samples of PMA generation, the organic matter content estimated from the AMS measurements was very similar, with an average fraction of around 6% with respect to the total PM1 aerosol mass, and an average concentration of 0.83 μg m^{-3}.

Because of this uncertainty on OM measurments by the AMS, the analysis of organic carbon (OC) was also conducted through a thermo-optical transmission method following the protocol EUSAAR-2 (European Supersites for Atmospheric Aerosol Research) as reported by [271] on filter samples. All the 18 quartz filters (15 samples and 3 blanks) collected using impactor sampling for particles below 1 μm were analyzed by a Sunset Laboratory Inc. (Oregon) carbon analyzer [272]. Results were blank-corrected. The ratio of organic carbon (with respect to the total PM1 mass) was 26% in average and the concentration 13 μg m^{-3}, so one order of magnitude higher than the one found from the AMS. Figure 4.32 depicts the organic carbon series for the two techniques. Conversion among organic carbon/organic matter were made in accord to [273]. This conversion considers that the organic mass can be obtained by applying a factor of 1.4 to the concentration of organic carbon (to account for the contribution of oxygens and hydrogens to the organic mass). The correlation among the two dataset in Figure 4.32 is significant (R= 0.7352, p= 0.0018) but the difference in the absolute values is high.

Also comparing the total mass concentration detected online by AMS and offline by PM1 filters, a significant correlation is found (R=0.66, P=0.01) but, again, AMS underestimates the

total mass per cubic meter to about one third of the mass revealed by filters. The discrepancy may be related to difficulties in volatilizing NaCl, as already mentioned, but also due to the particle size detection limits of AMS, which has a decreased detection efficiency for aerodynamic diameters larger than 800 nm, while filters have measured the all PM1 range. Considering the Particle Size Distribution reported in D.1, we notice that the concentration in the 800-1000 nm range is not negligible and has certainly contributed to lowering AMS concentrations with respect to filters.

Furthermore, EUSAAR protocol is not well characterized with respect to the interference by carbonate [274]. Therefore, if the aerosol was enriched of carbonate ions (for example in the form of calcium carbonate $CaCO_3$, which constitute the skeleton of some phyto-planktonic species) then estimates of organic carbon may be erroneous. Under most conditions, significant bias of this nature are generally excluded, as reported by [266], but our measurements could be affected. By analyzing the discrepancy among the organics measured offline (filters) and the organics measured online (AMS) we notice an anticorrelation with the Ca^{2+} enrichment factor, meaning that the bias among the two instrument is lower when the calcium enrichment is higher.

Ca^{2+} concentrations were negligeable on the 17th, 18th and 19th of March 2017. In this short set of experience, Cl/Na were 1.26, the organic ratio on PM1 filters was 36% and the related organic carbon concentration was 8.27 μg m^{-3}. The ratio of organics with respect to PM1 mass is highly variable in literature, however our data are close to the ones reported in Facchini et al., 2008 [254] for ambient measurements. The two timeseries reported in Figure 4.32 and the associated ratio with respect to the total PM1 mass did not present any significant correlation to the IN series per unit volume of sea spray (in any of the activation modes explored).

The only exception appears considering the second part of the campaign (from the 12th March). A significant correlation emerges from OM/PM1 ratio (AMS) and IN activated at -15 °C with FNA (R=0.901, p-value 0.0002, N= 11), thus strengthening the hypothesis of a different species of IN during the first and the second part of the campaign.

4.6.4 Parameters influencing ice nuclei concentration in the seaspray

Pearson correlation analysis was applied to many of the variables measured in this study to compute correlation coefficients (R) between IN time series obtained with DFPC/FNA and the following variables:

- NaCl, organics, sulphates, nitrates, total detected aerosols mass, ratio among organics/total detected mass (all from AMS measurements)
- Cl, SO_4, Na, K, Mg, Calcium enrichment, Chloride depression, organic carbon, total aerosols mass, ratio among organics/total detected mass (all from PM1 filters measurements);
- time series of the number of IN activated with FNA in the filtered seawater (from -9 to -15 °C); time series of the correlation coefficient (or the ratio) among IN concentrations in the filtered and unfiltered seawater (values are reported in the legend of Figure 4.26);
- total particle number concentration from OPC, DMPS, OPC;
- average ambient temperatures;

- time series of the number of IN per unit water volume in seawater (from −9 to −15 °C) performed in situ and in France after transport.

In Table 4.6, 4.7, 4.8, 4.9 we report the parameters showing a moderate to strong correlation, following the scheme from Dancey and Reidy (2002) in which correlations with R absolute values of 0.1-0.3, 0.4-0.6, and 0.7-0.9 are classified respectively as weak, moderate, and strong, respectively. P values were also calculated to determine if the correlations were statistically significant at the 95% confidence level (i.e. p <0.05). For small dataset (inferior to 10) we considered an 85% confidence level (i.e. p <0.15).

Seaspray Ice Active Nuclei, immersion freezing at−9 °C	R	p-value	N
Seaspray Ca Enrichment Factor	0.91	0.00	15
Seaspray ratio Na/Cl	0.95	0.00	15
Seaspray Ca content	0.56	0.03	15
Seaspray Cl content	-0.44	0.10	15
Correl. coeff. among ice nuclei conc. in filt. vs unfilt. SW	-0.69	0.02	11

Table 4.6: Correlation analysis between the number of ice nuclei m^{-3} activated at −9 °C with FNA and the chemical/physical properties of seaspray. We report only moderate/high correlations that are statistically significant. SW acronym stands for seawater. The correlation coefficient among ice nuclei concentration in filtered versus unfiltered seawater are reported in Figure 4.26.

Seaspray Ice Active Nuclei, immersion freezing at −15 °C	R	p-value	N
Seaspray Ca Enrichment Factor	0.84	0.00	15
Seaspray ratio Na/Cl	0.77	0.00	15
Seaspray Ca content	0.59	0.02	15
Seaspray Cl content	-0.43	0.10	15
Correl. coeff. among ice nuclei conc. in filt. vs unfilt. SW	-0.62	0.04	11

Table 4.7: Correlation analysis between the number of ice nuclei m^{-3} activated at −15 °C with FNA and the chemical/physical properties of seaspray. We report only moderate/high correlations that are statistically significant.

Seaspray Ice Active Nuclei, condensation freezing at −18 °C	R	p-value	N
Seaspray K content	-0.54	0.07	12
Seaspray Cl content	-0.48	0.11	12

Table 4.8: Correlation analysis between the number of ice nuclei m^{-3} activated at -18°C with DFPC and the chemical/physical properties of seaspray. We report only moderate/high correlations that are statistically significant.

All the IN concentration in the seaspray seems related to the concentration of calcium and chloride. In particular, IN species active at temperature colder than −16 °C appears anti correlated to calcium, magnesium and potassium in the seaspray. For these species a significant correlation wasfoundwith IN availability in the bulk seawater. This may be indicative of a specific type of IN that is efficiently transferred to the atmosphere from the bulk seawater.

In turn, IN sea spray species active at temperatures warmer than −16 °C are positively correlated to calcium and they increase when sea spray shows an enrichment of calcium (and a

Seaspray Ice Active Nuclei, condensation freezing at −22 °C	R	p-value	N
Seaspray Ca content	-0.63	0.03	12
Seaspray Mg content	-0.58	0.05	12
Seaspray Ca Enrichment Factor	-0.45	0.14	12
Seawater Ice Active Nuclei (before transport) at −9 °C	0.98	0.00	7
Seawater Ice Active Nuclei (before transport) at −10 °C	0.98	0.00	7
Seawater Ice Active Nuclei (before transport) at −11 °C	0.88	0.01	7
Seawater Ice Active Nuclei (before transport) at −12 °C	0.85	0.02	7
Seawater Ice Active Nuclei (before transport) −13 °C	0.83	0.02	7
Seawater Ice Active Nuclei (after transport) at −10 °C	-0.46	0.13	12
Seawater Total Particle Concentration (from CPC)	-0.55	0.06	12
Correl. coeff. among ice nuclei conc. in filt. vs unfilt. SW	0.57	0.09	10

Table 4.9: Correlation analysis between the number of ice nuclei m^{-3} activated at −22 °C with DFPC and the chemical/physical properties of seaspray (or bulk seawater). We report only moderate/high correlations that are statistically significant.

chloride depletion). IN active at warmer temperature are likely to be of biological origin, and we suggest a possible connection either (i) with the carbonaceous shell of certain phytoplanktonic species (as Emiliana Huxleyi) or (ii) with the dynamic of marine micro-gels.

In relation to our first hypothesis, the article of Trainic et al., 2018 [275] show the unique aerodynamic structure of coccoliths'shell (which is made on $CaCO_3$). Trainic et al., 2018 [275] also demonstrate that these shells might be efficiently transferred to the atmosphere, especially after a virus attack that might induce apoptosis of a number of Emiliana Huxleyi (in order to preserve the remaining community). Thus, these shell might also contain the virus and/or the bacteria that has attacked the coccoliths and that might be related to the ice nucleating capabilities of sea spray (as suggested by McCluskey [252] in relation to marine heterotrophic bacteria).

In relation to our second hypothesis, we consider the article of Orellana et al., 2011 [264] that describe the unique dynamic of Arctic marine microgels. These gels are based on polymers chains which are stabilised by Ca^{2+} ionic bonds. In particular, Arctic marine gels can undergo a fast reversible volume phase transition from a swollen or hydrated phase to a condensed and collapsed phase depending on the surrounding environment (e.g. alkalinity, the concentration of DMS and DMSP, the availability of organics and soluble calcium element). Orellana et al., 2011 [264] highlight that this behaviour is faster in the Arctic (<1 min) than previously reported studies for oceanic waters. Then, our hypotheses -among others- considers Calcium enrichment -in the seaspray- as a possible proxy of the efficient transfer of marine gels to the atmosphere. Such gel (also referred to as Transparent ExoPolymers Particles, TEP) have been indicated as possible IN in the work of Wilson et al., 2015 ([72]. Because Orellana et al., 2011 [264] and similar studies (e.g. [265]) show that without Calcium the marine gels might desegregate -thus loosing their 3 dimensional structures- their labile attitude might probably explain the discrepancy between DFPC and FNA results (and/or the effect of the dry/wet storage condition of the related seaspray analysed).

The study of nascent sea spray, together with its chemical and physical characterization is an ongoing field of research. As reported by Oppo et al., 1999 [265] following Berg and Winchester

1978, a different chemical composition of the nascent sea spray would affect the binding capacity of its components. In addition, several stages of reorganization could affect the hydrated structure of the nascent SSA particles (e.g. as dehydration and aging under laboratory conditions).

4.6.5 Comparison with literature

Figure 4.33 reports the comparison among the average number of IN per unit Liter measured in the present study and the measurements recently published in McCluskey et al., 2017 [276] that refers to ambient aerosols measured during oceanographic cruise campaigns.

Our results are fully included in the interval range provided by McCluskey et al., 2017 [276] for the condensation mode freezing measurements. For the immersion mode freezing measurements, our results are larger than the ones reported by Mc Cluskey.

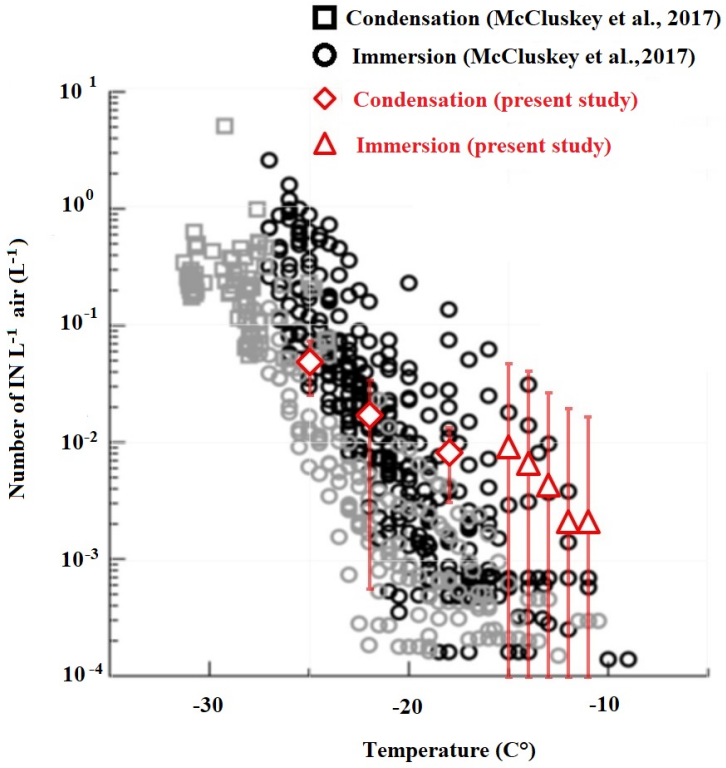

Figure 4.33: Figure taken from McCluskey et al., 2017 [276]. Black values refer to ambient seaspray sampled in the North Hemisphere; grey values refer to ambient seaspray sampled in the South Hemisphere; red values represent the median and standard deviation from the present study (bubble-produced sea-spray experience in the Arctic from control mesocosm).

The activation fraction parameter is reported in Figure 4.34 and in Figure 4.35. This parameter has been calculated as the number of IN activated with respect to the total number of particles detected. Figure 4.34 considers for the total number of particles the measurement made by DMPS instrument, which was validated by CPC instrument, and that refers to the dried aerosols. Particles losses by Brownian diffusion inside the drier, and the entire instrument, were taken into account with the DMPS inversion algorithm, following the indication of [277]. In turn, Figure 4.35 reports the same method of calculation that has been performed in the third

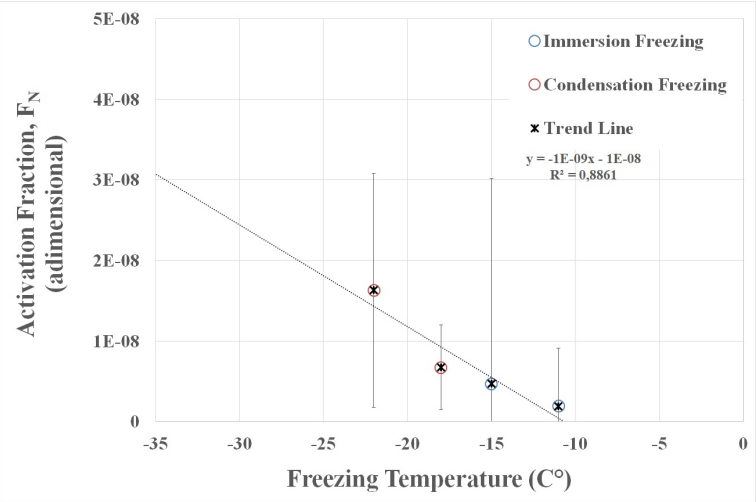

Figure 4.34: Activated fraction of the considered Arctic seaspray (bubble-produced sea-spray experience in the Arctic from control mesocosm). Blue values refer to immersion freezing tests while red values refer to condensation freezing. For the calculation it has been considered the total particle number concentration measured by the DMPS and reported in Figure 4.28.

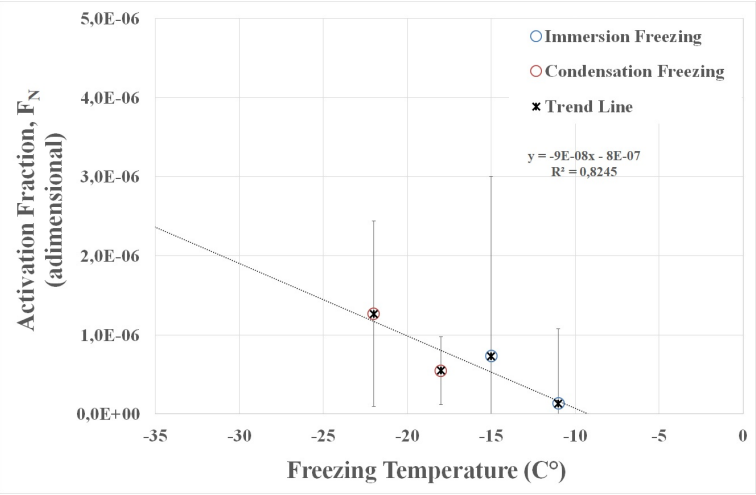

Figure 4.35: Activated fraction of the considered Arctic seaspray (bubble-produced sea-spray experience in the Arctic from control mesocosm). Blue values refer to immersion freezing tests while red values refer to condensation freezing. For the calculation it has been considered the total particle number concentration measured with the optical particle counter from 0.5 μm and reported in Figure 4.28.

chapter and that considers the un-dried aerosol detected through the OPC and that counts only particles larger that 0.5 μ.

The spectrum of ice-nucleating properties is also often represented with the parameter Surface Active Site Density, n_s, expressing the number of active sites with respect to the total aerosol surface area.

This parameter is commonly used to compare the efficiency of different IN particles species, and excludes from differences in the total aerosol number concentrations. Figure 4.36 reports the median n_s obtained from our study and compared it to literature. The total surface area, considered here, refers to the one extrapolated from a dried aerosols. For the purpose of the

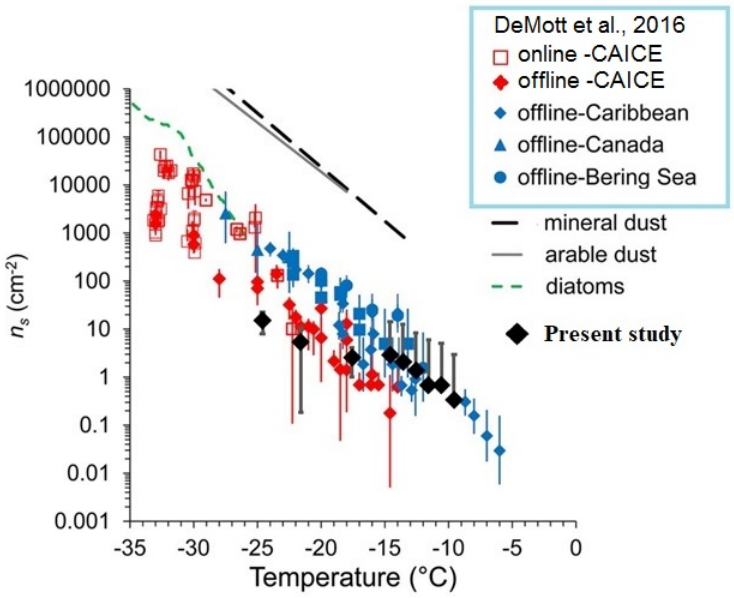

Figure 4.36: Figure taken from DeMott et al., 2016 [245] resuming several field campaigns. Black diamonds are the median and standard deviation from the present study (bubble-produced sea-spray experience in the Arctic from control mesocosm). In order to esteem n_s the total aerosol surface has been calculated from the DMPS. To this purpose we have considered the average particle size distribution of the dried aerosols, that is reported in Figure D.2, blue line.

comparison, we have considered only the average particle size distribution of the dried aerosol, and than the one measured by the DMPS (the blue line reported in D.2). Values are in agreement with DeMott et al., 2016 [245]. The comparison in Figure 4.36 shows that ambient measurements in several parts of the world over oceans (blue dots) -and other similar bubbling experiments (red dots)- show basically the same IN activity as our study (black dots). We suggest that in ambient marine areas, IN come mainly from the seaspray (and not from transported dust or pollution) especially at freezing temperature > -15 °C. This hypothesis seems consistent with the agreement among the black and the blue dots above -15 °C (presumably IN of biogenic origin). In turn, for colder temperatures < -15 °C, our measurements are: (i) below the blue ambient measurements (recorded by DeMott et al., 2016 [245]), (ii) in agreement with the similar generated seaspray experiments of [245] in red. We can not exclude that, for these temperatures, there my be a larger contribution from other sources of aerosols.

4.7 Conclusions

The number concentration of IN has been reported for both the Arctic seawater and the related nascent seaspray that was laboratory generated. The experimental strategy has consisted in:

- *the use of mesocosm for studying the fate of pollutants in the Arctic marine environments as well as providing the ability to conduct controlled manipulative experiments;*
- *the use of a sea spray generator that mimic bubble bursting and wind for the studying of primary marine aerosol and relate its properties to the ones of seawater.*

The experiments were performed in the Arctic village of Ny-Ålesund, during the dark/light transition from the polar night to the polar day.

In the Arctic seawater, measurements of ice nucleating active particles have shown concentrations ranging over two order of magnitude. The spreading of data was mainly related to the degradation of the signal that undergoes an exponential decay during the first days, even if the samples were preserved at +4 °C in the dark. We could not verify such degradation for seaspray samples, but we exclude such effect because data obtained in Svalbard and in France were more consistent (spreading on 1 order of magnitude for each immersion technique). Also for other analytic measurements, degradation is often higher for liquid samples (seawater) than for dry samples (aerosols).

However, even the degraded signal, from control mesocosm, showed immersion freezing concentrations in agreement with Wilson et al., 2015 [72], that analysed Arctic seawater and surface microlayer during summer. Our analysis has considered also the seawater degraded values, obtained from the frozen and thawed samples, once transported to the French laboratory. Indeed, the time variation of transported samples resulted correlated to the one of non transported samples, as shown in Figure 4.18. Thus, we included also the study of the degraded signal in our analysis, in order to investigate how the seawater IN properties might influence the seaspray IN properties.

A weak but significant anticorrelation (R=-0.50, pvalue=0.05) among seawater IN levels and ambient temperature has been reported (see Figure 4.24). We suggested a possible response of seawater ice nuclei concentration to chilling. This hypothesis might be strengthened by the suggestion that marine heterotrophic bacteria can represent a part of the IN marine population (see McCluskey et al., 2017 [252]). In this case, the 'temperature effect' would represent the physiological response of these marine organisms to their environment, where warming temperatures are associated to a decrease growth rate. An analogue observation were performed by Bigg, 1996 [97] during an Arctic campaign. In this work, it is reported that concentration of ambient IN (mainly influenced by oceanic air masses) increased by a factor of 4.5 for a 5°C fall in temperature. However, it should be considered that Bigg observed this effect in the ambient air -during an icebreaker voyage to the North Pole- while we could observe such effect only in the seawater collected from the mesocosm experiment.

Indeed, each mesocosm experience allowed the observation of a large volume of Arctic seawater in thermal contact with the surrounding environment. Average ambient temperatures ranged from −3 °C to −20 °C, and were followed by few episodes of snow storms that hindered the measurements on the 10 and 11^{th} of March. Overall, these temperature variations could explain a few IN fluctuations observed in both the control and the polluted seawater samples.

By comparing IN levels in the polluted and control seawater samples (reported in Figure 4.23), we found significant differences among the two medians, as confirmed by the rank sum test, in the freezing range between −8.5 °C and −19 °C. These differences showed a moderate decreased of ice nuclei concentration in the polluted seawater. This effect was partially observed in seaspray samples, and only for condensation freezing tests at -25 °C.

Globally, the comparison of the IN time series measurements in the seawater and in the seaspray were not correlated, made the exception of the parameters reported in Table 4.4, that

refer to seaspray condensation freezing tests at -22 °C and the non-degraded signal of seawater for immersion freezing between -9 and -13 °C.

With respect to condensation freezing activation mechanism at -22°C (Sw 1.02), the sea spray showed an activated fraction around 10^{-8} IN p^{-1} (see Figure 4.34). This means that around 10^8 particles need to be generated to find at least one ice nuclei in the sea spray. This value (together with the n_s parameter shown in Figure 4.36) is certainly inferior to the values reported for mineral dusts, however, it should not be neglected. INP of marine origin might be relevant in remote locations over the oceans (e.g. the Southern Hemisphere) where antropogenic emissions are scarce. As reported by Vergada-Temprado et al., 2017 [278] marine organic aerosol might be a dominant source of INP at southern high latitudes during Austral autumn to spring. Vergada-Temprado [278] also found marine organic aerosol to be the more dominant source of INP compared to dust (K-feldspar) on 10-30 % of days in the Northern Hemisphere.

Furthermore, a large variability of primary marine aerosol (PMA) production has been observed in relation to wind speeds over the sea, and peculiar conditions of the ocean state (e.g. phytoplanckton bloom which increase surface-active organic material at the sea surface).

In addition, a number of studies have reported concentration of organic carbon (Gershey, 1983; Hoffman and Duce, 1976) and bacteria (Blanchard, 1989) in sea spray aerosol enriched hundreds of time with respect to corresponding concentrations in bulk seawater. To explain such enrichment, it should be considered that bubble bursting takes place at the air to sea interface, which is particularly reach of chemical and biological material (mainly known as the sea-surface micro-layer).

It should be noticed that our experiments have employed a marine aerosol generator operated under the same operative conditions for the whole campaign. This generator can be related to similar PMA distributions found in marine environments for wind of about 10 m/s [239]. During the PARCS-MACA experiments, only bulk seawater was considered, hence the role of the surface microlayer, in which organic matter is likely enhanced, could not be taken into account. Despite these limitations, the current study has pointed out that:

- a number of ambient conditions -as a severe drop in temperatures- can affected the seawater INP population together with the effect of pollution during the one month of observations on the control and polluted mesocosms;

- the measurement of seawater INP can undergo degradation in relation to storaging/transport conditions; while the measurement of seaspray INP seems more stable and we supposed that it was not affected by degradation;

- a lack of correlation among INP levels and organic matter/total carbon measurements in the seaspray (suggesting that the parametrisations based on seawater measurements, as the one proposed by Wilson et al., 2015 [72], can not be extended to seaspray INP).

- INP in the bulk seawater are partially linked to the INP in the seaspray (only for lower temperatures).

- discrepancies among FNA and DFPC results affect only one part of the campaign. It can not be excluded that these differences were affected by the sampling technique (i.e. dry/wet

preservation of the sample), however they suggest that at least two different types of INP are present in the seaspray. One of them should be related to bulk seawater INP content as we found a correlation among seaspray INP levels at -22 °C and seawater INP levels in the range between -8.5 and -13 °C (but only for the non-degraded signal).

- seaspray INP active at warmer temperature >-15 °C (most probably of biological origin) is related to a calcium enrichment and chloride depletion. This may be linked to the bonding of some surface active organics or to the presence of carbonaceous shells from certain phytoplankton communities.

Further measurements are required to enhance these conclusions. On the basis of such considerations, future experiments should foresee the measurement of seawater INP directly on site (or foresee the freezing of the samples immediately after collection and transport them under cold conditions). To this purpose, a duplicate of FNA has been recently assembled at LaMP including a number of modifications functional to its transport. This duplicate preserves the advantage of the original instruments that are:

- less contamination with respect to the majority of immersion freezing techniques (e.g. droplet freezing) because samples are enclosed in a sterile environment during tests;
- capability to detect low values of INP by regulating the unit droplet volume in which the sample is distributed (this advantage belongs to all immersion freezing techniques when compared to condensation freezing techniques).

In the meanwhile of further investigations, the current database provides a basis for comparisons and suggest a few hypothesis on the possible nature of marine ice nuclei.

4.8 Acknowledgments

This work was funded under the French initiative PARCS and by the French institution IPEV. We gratefully acknowledge Barbara D'Anna and Marc Mallet for the sharing of their data obtained with the AMS, and the French "Institut des Géosciences de l'Environnement - UMR 5001" in Grenoble, for the analysis of the inorganic and organic fraction of PM1 filters. We thanks Sébastien Mas and Remy Valdes (Medimeer) for the enriching discussions on marine biology and the technical support during the measurements.

Chapter 5

Conclusions and Future Perspectives

> [..] despite a high temporal and spatial variability of ice nucleating particles, one conclusion from BACCHUS project was that most ice nucleating particles are of natural origin and are dominated by mineral dust and biological particles, such as pollen, bacteria and marine organic carbon. Land use changes due to human activities could therefore affect clouds through changes in emissions and properties of ice nucleating particles.
>
> Deliverable D5.8, European Project BACCHUS "Impact of Biogenic versus Anthropogenic emissions on Clouds and Climate: towards a Holistic UnderStanding", 31.05.2018 [279]

5.1 Introduction

Ice nucleation is only one line of research inside cloud microphysics and atmospheric sciences but the inherent literature has steadily increased in the last decade. Scientists have focused on a number of different aspects: the characterisation of INP sources; the identification of major and minor INP activation mechanisms and the parameters -T, Sw- governing them; the development of new instrumental techniques (offline, on line, portable, large fixed instruments, compact portable ones); dedicated experiments in atmospheric simulation chambers; the preferable metric to quantify ice nuclei content for models (e.g. number of ice nuclei for unit volume, activated fraction, active surface density, number of ice nuclei for unit mass).

Ice nucleation research is very active at the moment also due to its several interconnections with: applied sciences (including knowledge exchange with industrial partners in the fields of cryopreservation, freeze drying, aviation safety), with weather forecasting and most of all with climatology.

After a period of quiescence -around the nineties- a renovated interest has appeared about a decade ago, as shown by Bodenschatz et al., 2010 [280] and De Mott et al., 2011 [11]. A number of essays and workshop aimed to reawake the scientific community toward the field of ice nuclei measurements, mainly because our incomplete knowledge of ice-containing clouds -and in general aerosol-cloud interactions- are a primary source of uncertainty in projections for future climate.

Just over five years ago, the global coverage of ice nucleating particles measurements was still insufficient, especially in remote locations (likely to be less influenced by antropogenic emissions) limiting our understanding of ice formation and ice cloud evolution in different environments. In addition, the information on INP species such as natural biogenic (fungal spores, bacteria, pollen, sea-spray gels, marine bacteria and viruses) and dust particles needed to be better characterised. One of the prominent open question concerned "the importance of biogenic versus anthropogenic emissions on ice nuclei population" [279] -and in general on cloud properties- which is needed to describe the key cloud-aerosol interactions and feedback mechanisms related to climate.

Since then, understanding of nucleation processes has advanced enormously, through a number of projects that have been financed from national and international organisations. Among them, the international European project Bacchus, concluded 2018, has largely helped the harmonisation of INP observations and the compilation of geographic differences between locations such as the Arctic, northern and central Europe, Atlantic, tropics, Mediterranean and Amazon forest. Other projects, funded by national initiatives, helped answering related aspects, as the French campaign PARCS-MACA, which has focused on the Arctic environment. In particular, PARCS-MACA had the overall goal to improve the understanding about the impacts of pollution in the Arctic climate system, and notably, to characterise its influence on primary and secondary marine aerosols properties.

The present PhD was involved and contributed to both: Bacchus together with the related Italian national initiative Air Sea Lab (during the first eighteens months), and PARCS-MACA (during the second half of the PhD).

Our researches have characterised for the first time the IN concentration at the Observatory Cimone Montain (Italy) which is part of the Global Atmosphere Watch (GAW) programme. The Observatory is dedicated to long term measurements for the monitoring of the atmosphere, but the characterisation of INP just started with our researches. Within the Bacchus perspective, we also compared these data to a closed rural site (San Pietro Capofiume in the Po valley). These data have already been published and integrated in the Bacchus INP database. They are summarised in the third chapter.

During PARCS-MACA, we could characterise for the first time the Arctic primary marine aerosol in the period of transition among the polar night and the polar day. We combined a laboratory controlled generation approach to a mesocosm experience, to discern the possible effect of pollution in both seawater and seaspray INP populations. With respect to the strategy performed during Bacchus -in which we considered the overall aerosols- in the Arctic we focused

only on one specific source, the primary marine emission, and its possible connections to pollution. These last data -presented in the forth chapter- have not been published yet and are the more recent. We supported them with information on aerosol size distributions and chemical analysis, that are also presented here.

This fifth chapter aims to present the summary of the main results obtained in this thesis, the implications of our findings and an outlook for future scientific experiments.

5.2 DFPC and FNA instruments

In our research we deployed two established techniques -the Dynamic Filter Processing Chamber (DFPC) and the Freezing Detection Apparatus (FNA)- to increase the mapping of INP concentrations in remote locations.

- To explore deposition freezing and condensation freezing modes we considered DFPC instrument. DFPC was first described in Santachiara et al., (2010) [180] and Belosi et al., 2014 [175]. Since these publications, a number of significant improvements have been made. As part of the thesis, DFPC's measurement routine and data analysis have been addressed. In addition, an evolution of the first prototype has been created, with a larger vapour saturator and the possibility to go down to -25 °C freezing temperature. This work includes a detailed description of the image analysis process (second chapter) and proposes solutions for its improvement -second and third annex- as a code to avoid fake counting of crystals developed in a close region, which are now better distinguished and counted as two single units. Chapter 2 also presents the experimental procedure for temperature calibration, together with the main results from the latest intercomparison campaign FIN-02 (see DeMott et al., 2018 [179]).

  During this thesis, a number of additional tests -not included in this dissertation- have also been performed to assess the influence of saturation ratio (Sw) on the ice nuclei activation and has been reported in Belosi et al., 2018 [159]. In this work ([159]) the dependency of INP concentration on freezing temperature and water supersaturation was explored for both laboratory generated samples and filters from field campaigns. These tests confirm that INP concentrations increase by increasing the saturation ratio and by decreasing the activation temperature. In particular, the transition from sub-to super-saturated conditions showed a significant relevance of Sw with a variable intensity in relation to the INP species. The observed temperature dependency was consistent with that reported by DeMott et al. (2010) [47].

  In the last 4 years DFPC has been successfully deployed during a number of field campaigns performed within the scope of BACCHUS and AIR SEA LAB projects (at Cimone Mountain, San Pietro Capo Fiume, Mace Head, Capo Granitola) and PARCS-MACA project (at Ny Ålesund). Only a minor part of them is included in this dissertation, for brevity reasons. However, this thesis has also contributed to the data analysis of Mace Head and Capo Granitola campaigns (reported in [154], [281], and [282]).

- To explore immersion freezing we have considered FNA instrument. FNA has been characterised in Stopelli et al., 2014 [171] and in the past it has been applied to the study of biological species from rain, snow and soil samples. In the past, similar immersion freezing techniques (e.g. cold stage) were applied to the study of samples from marine environments, and so we applied FNA also to the study of seaspray and seawater samples. Most of all, we succeeded in coupling FNA with a steam jet aerosol collector -for the sampling of seaspray- via a modified version of the particle into liquid sampler (PILS by Metrohm), as described in the forth chapter.

We compared the two devices in the forth chapter. It should be noticed that although the measurements we discuss for DFPC at vapour pressures exceeding water saturation are considered to include the immersion freezing mode, they do not involve freezing in macroscopic droplets (as done with FNA). During PARCS-MACA the data obtained with DFPC at -18 °C were in average lower, but consistent, with respect to FNA at -15 °C. A higher agreement appeared in the second part of the campaign, showing that differences might be affected by the sampling technique (i.e. dry/wet preservation of the sample) more than the devices themselves.

The principle strength of the considered two techniques is the ease of aerosol sample collection and storage. FNA can be used also to study directly liquid samples, as we did for pure seawater samples (without any intermediate dilution). In case of aerosol samples, it was considered that substrate used to collect aerosols could be transported and stored without any strict procedural precautions. A systematic study of substrates exposed to varying storage times and conditions shows little variation in resulting INP counts as described in [174]. However we did not verify this assumption for seaspray samples, due to a lack of time.

The principal limitation of both DFPC and FNA technique is that they suffer from long and time intensive analysis which are limited to one mechanism at the time (only immersion freezing for FNA and deposition or condensation freezing for DFPC). Furthermore, after analysis, a part of the instrumentation must be prepared for reuse in a labour intensive cleaning process. For FNA we single used the eppendorf tubes and the tip cones (tip cones were used with a syringe to distribute the liquid sample inside the eppendorf tubes). Periodically, we used UV radiation to sterilise a part of the set up (including the filter holder and the connecting tubes). Thus the ratio of sampling time to processing time is one area of focus for continuous incremental improvement.

5.3 Ice Nucleating properties at the GAW station Cimone Mountain

Two field campaigns were performed during May 2014 and October 2015 at the high mountain Observatory Mt. Cimone (2165 m a.s.l.). A very simple experimental approach was adopted: aerosol was collected on a filter and simultaneosly characterised for its size distribution with an optical particle counter.

The campaign was influenced by a Saharan Dust transport Event (SDE) which was compared to «clean» days (NSE). In addition, the results were related to the observations conducted in parallel at a closed rural site (San Pietro Capo Fiume).

Overall, we observed lower INP concentration at the high observatory site in comparison to the rural site. This effect is justified by the lower aerosols concentrations at the remote site. In

addition, the rural site is surrounded by grassland and crop field, thus we can not exclude a possible influence of soil dust particle, that could have increased the INP concentration of the rural site. Further tests need to be performed in order to verify such assumption.

During the SDE that occurred in May 2014, a reduction of the aerosol activated fraction was observed at Mt. Cimone and, to a lower extent, at San Pietro Capo Fiume, suggesting, for this event, a limited ice nucleating activity for Saharan dust particles. To explain this, we suggested that our measurements was affected: i) either by modifications of the Saharan dust surface properties during transport in the atmosphere ("aging processes"), ii) either by the fact that measurements were performed at relatively high temperatures for the activation of mineral dust (−18 °C).

Laboratory studies (in Boose 2016 [19]) performed on the effect of atmospheric aging processes on desert dust particles showed contradicting conclusions: i) a reduction of the ice nucleating efficiency of certain species, especially K-feldspar minerals, when exposed to condensation of sulphuric acid [19]; ii) an increasing of the ice nucleation ability of certain dusts exposed to condensation of ammonia (Salam et al., 2007 [132]) or treated with ozone (Kanji et al., 2013 [133]). In Boose 2016 [19] it is indicated that Saharan dust particles have no activity above the Portable Ice Nucleation Chamber (PINC) detection limit for temperatures warmer than −20 °C. In addition, Boose et al., 2017 suggested that industrial pollution from the North African coastal region can lead to an increase in the ice nucleation efficiency of the Saharan dust. Our results do not support the indication that desert dust from Sahara is more efficient after aging/transport. In addition, measurements performed in February 2014 during another SDE could be distinct at −18 °C activation temperature, suggesting an ice nucleating capability of certain desert dust species also at this temperature (even if the effect was more important at −22 °C activation temperature).

5.4 Ice nucleation properties of ice nuclei in the Arctic marine environment

Ocean is an important source of aerosols on a global scale (as more than two thirds of the Earth's surface is covered by the sea) and then it is important to identify its ice nucleating capabilities. As shown in the forth chapter of this manuscript, we measured the Arctic seaspray capacity to nucleate ice (refers to Figure 4.34).

The seaspray considered in this study was laboratory generated through a state of art marine aerosol generator (MAG) which allows sufficient concentrations of aerosols to appreciate variations in the ice nucleation properties of sea sprays generated from different seawater samples. The use of an aerosol generator to isolate sea spray from other sources, it is a steadily increasing field of research, driven also by the contribution of CAICE center and the efforts of K. Prather.

In our work, measurements of ice nuclei number per unit volume (in the air and in the water) and ice nuclei surface active density (in the air) were found to compare well with earlier studies of marine ice nuclei collected near the ocean during oceanographic campaigns ([154], [245], [72], [153]). This agreement shows that the presence of ice nuclei in the marine boundary layer comes mainly from marine aerosols and that the usage of a MAG system does not alter the

ice nucleating properties of primary marine aerosol (PMA), beyond the observed spread found in natural PMA samples. Through the adopted MAG it was possible to generate enough aerosols to perform at the same time the PMA chemical characterisation.

We showed evidences that the availability of chemical elements, such as soluble calcium and magnesium, might be determinant for the transfer of certain IN species from the sea (water) to the air (sea spray). When calcium in the PM1 seaspray increased, we noticed an apparent 'depression' in the sodium mass detected also in the seaspray. This results was accompanied by an augmentation of ice nuclei per unit air volume activated under immersion freezing -at temperature warmer than -18 °C- and collected through the steam jet aerosol collector. This increment was not visible with DFPC instrument that showed a better agreement with FNA ice nuclei number concentrations only in the second part of the campaign. Considering the freezing temperatures of activation in the sea spray, reported in Figure 4.11, and starting already around -6 °C, we suggest that a part of the seaspray has a biological origin, in relation to these warmer temperature of activation ().

We registered a weak dependence among the concentration of ice nuclei in the seaspray to the ones in the seawater. Thus we bring a few elements that may invalidate the parametrisation suggested by Wilson et al., 2015, [72]. This last is an empirical fit for the number of ice nuclei -from droplet freezing measurements- per mass of total organic carbon, both measured in the marine surface microlayer. As noted by other authors, [154], [150], this parametrisation has been developed for sea surface microlayer samples, and it does not necessary reflects the concentration of INP in the seaspray emitted into the atmosphere.

Our study focused also on INP measurements directly in bulk seawater samples. These samples were collected from a parallel mesocosm experience in which control seawater was compared to polluted seawater (intentionally enriched in ammonium sulphate and ammonium nitrate). For the first time, our study has recorded a decrease in the INP number concentration per unit water volume in the polluted seawater (with respect to the "clean" seawater). We showed also the possible effect of seawater temperature that was anticorrelated to INP concentration in the seawater.

The PARCS-MACA project aimed to combine also information coming from the marine biology. These data are still under analysis and in the near future will be combined to our data to eventually deduce a new parametrisation. In the meanwhile, we suggested a few hypothesis:

- soluble INP species could be related to "CSP and TEP" which provide macro-molecules that could behave as possible Ice Nuclei. However, this organic matter is dissolved in seawater, and need a 'bond' to be effectively transferred. A possible ligand element is Calcium (/Magnesium), as shown in the work of Wei-Chun Chin 2008 [283].

- a source of insoluble INP species may be connected to the availability of carbonaceous shell residues, as in the decay of Aemiliana Huxley (a phytoplancton species). A recent work of Trainic et al., 2018 [275] has indicate the efficient transfer of Aemiliana Huxley residues to the atmosphere after a virus attack (as Aemiliana Huxley can undergo apoptosis, when attacked by virus/bacteria, to preserve the entire community). The shells are mainly empty (i.e. light) and can float at the air/sea interface and be easily ejected to the air (see [275]). More tests need to be performed to verify this last assumption.

- the possible presence of carbonaceous shells -made of $CaCO_3$- can interfere with normal protocols adopted for carbon organics/inorganics measurements.

Differences among DFPC and FNA measured concentrations, appeared only in one part of the campaign, reinforcing the idea of different INP species in the marine environment. In the first part of the campaign, FNA results show a significant correlation of ice nuclei per unit air volume and the concentration of soluble calcium in the seaspray. We suggested that this ice nuclei are likely to be due to soluble species, organised around a calcium ligand, which might be better preserved in liquid -with respect to dry- conditions. To confirm these results, further tests should be performed to identify the best preservation method for sea spray samples (in a dry or wet shape).

Our results are valuables because not only they characterise INP in the Arctic primary marine aerosol, but also because they provides indication which could aid the understanding of marine environments. These information provide the basis for comprehensive modelling efforts.

5.5 Achievement

Through this thesis, the mapping of the ice nuclei properties at different geographical sites could be achieved, and also the promotion of the cooperation among the Italian ISAC-CNR Institute and the French LaMP-CNR laboratory. In particular, a collaboration agreement was signed (protocol number CNR-154623 and CNRS-0003955 of 07/12/2016) for the sharing of samples and technical knowledge among common campaigns related to ice nuclei measurements.

Through this collaboration, I could deploy both the Italian and the French techniques and, most of all, I could participate personally to the Arctic measurement campaign PARCS-MACA (an involvement not foreseen at the early beginning of the PhD). As a result, the Italian DFPC instrument could be used for the first time in the Arctic - thus increasing its visibility and starting a new ongoing line of researches in this sector - while the French group could benefit from the characterisation of samples at colder temperatures (e.g. -22 and -25 °C obtained through DFPC).

By participating at the PARCS-MACA campaign, I was involved directly in the field -by installing/uninstalling the instruments and collecting the samples- and I learnt a number of protocols that are usually dedicated to biological samples, as flash freezing, aseptic laboratory techniques and dry ice cold transportation. I could use these protocols in a latter campaign in which I was recruited after PARCS-MACA (the Mediterranean oceanographic cruise Peacetime). For the sake of brevity, the results from Peacetime campaign are not presented in this study, but they were also part of the PhD research activities.

5.6 Implication of our findings

The results from this thesis are valuable as they yield atmospheric INP data in location never or rarely covered by past measurements. These data will contribute to a global perspective on atmospheric INP distribution and variability by nourishing atmospheric databases under the 'BACCHUS framework', as well as the 'Research In Svalbard portal'.

The BACCHUS database aims at a holistic understanding of ice nucleation processes on a global scale and it is analogous to ACTRIS-2 database which is dedicated to cloud condensation nuclei and aerosol particle data. The Research In Svalbard portal is focused on all the processes related to Svalbard climate and it is a relevant component of the Integrated Arctic-Earth Observing System. These database can be used for the quantification of the spatial and temporal variability of INP concentrations and help global and regional modelling studies of ice-containing clouds. Together with other atmospheric INP observations, our data will aid to reduce the uncertainty in the description of aerosol-cloud-climate interactions.

On a more fundamental basis, we have added elements to the understanding of the ice nucleation ability of marine aerosols in the atmosphere. Our in situ studies of sea-spray and seawater in the Arctic region gives a more narrow constrain of the ice nucleation ability of primary marine aerosols (PMA) in this location and period of the year.

DFPC has proven to reliably measure INP concentrations under various thermodynamic conditions, while FNA was helpful in the detection range of biological interest. The direct comparison of these two apparatus and the overall comparison with literature, have yielded indication on the limitations of the adopted sampling techniques (especially with regard to the preservation of seawater samples) and it yielded a few indication on the dual nature of marine ice nuclei. We provide a protocol for the storage and preservation of seawater samples. In addition, we suggested more tests to identify a possible degradation of dry filter samples -with respect to liquid vials- affecting the preservation of soluble INP species.

5.7 Perspective

A summary by points is listed below on the ongoing and future field studies (already planned or likely to be done in the near future) that will increase our comprehension on atmospheric ice nuclei.

- Ice nuclei concentration in primary marine aerosol should be characterised in several other locations, to appreciate spatial variation and to dishern the prevalent parameters governing them. To this purpose, LaMP-CNRS has partecipated to further campaigns covering the Mediterranean sea (international oceanographic campaign Peacetime) and the Southern hemisphere (the French initiative Sea2Cloud and the Tangaroa oceanographic Antartic cruise). The analysis of these samples is still under treatment.

- It is fundamental to check the temporal variation of the locations that have been already covered. To this purpose, a line of research has been activated by ISAC-CNR in order to characterise INP time series at both Cimone Mountain and the Ny Alesund station in the next future.

- Dedicated experiments should be performed to state whether the preservation of aerosols samples (of which seaspray) at $+4/-20/-80$ can affect the detection of ice nuclei, especially with regard of biological samples (i.e. containing proteins).

- It is fundamental to state whether pollutant will indirectly increase or decrease INP activity.

In relation the the last point, we report below the main conclusion expressed in the final deliverable (number D5.9) of the European Bacchus project: « *In summary, the results obtained during BACCHUS confirm earlier results that biological particles are the best INP, initiating ice nucleation already at temperatures larger than* $-10\,^{\circ}C$*. Dust particles are almost everywhere (together with haze and smoke) and control heterogeneous ice formation in the temperature range for about* -18 *to* $-35\,^{\circ}C$*. In the absence of dust, INP at a remote North Atlantic coastal site were largely comprised of organic carbon and/or heat labile material from biological activity but sea spray aerosols also contributed. No evidence was found for INP from anthropogenic activity to be an important source for INP. In summary, anthropogenic activities mainly affect CCN concentrations while they only indirectly affect INP concentrations.*»

Therefore, we expect that in future years, the INP research community will investigate deeply the indirect effect of anthropogenic emissions (i.e. the possible effect of pollutants on INP populations) not only in the atmosphere but also in the oceans. On the basis of our work, we suggest that pollutants can:

- i) either modify the surface tension of seawater which have a primary role in bubble bursting process. Thus, pollutant can increase or decrease the concentration of particles released in the atmosphere from the oceans. Furthermore, in case of insoluble acquatic nano-pollutants, there is the possibility that they can be emitted themselves. In this case they could behave like vessels for the transfer of sticky organic matter or virus/bacteria.

- ii) either modify the acidity or alkalinity of cloud liquid droplets which in turn seems to affect the expression of ice nuclei in both biological (see Attard et al., 2012 [284]) and inorganic species (see Kumar et al., 2018 [134]).

Such studies could be a step forward to assess the coupling biosphere-aerosol-cloud-climate, which in turn are necessary to improve Earth System Models and will provide indications to policy makers and Air/Water Quality regulations.

Appendix A

Bergeron–Findeisen process

In his 1911 publication *The Thermodynamics of the Atmosphere* Wegener noted that ice crystals invariably grow at the expense of super-cooled droplets, due to the fact that crystals have a lower equilibrium vapour pressure. He then suggested that raindrops might result from the competition between ice crystals and super-cooled cloud droplets. In 1933, Tor Bergeron contributed to this theory by developing a theoretical explanation of the process by which precipitation may form within a mixed phase cloud and Walter Findeisen further developed it. The Bergeron–Findeisen–Wegener theory (also referred to with the same names in a different order) is commonly called the ice process of precipitation, and formerly, ice-crystal theory. Thus, within a mixture of liquid droplets and ice crystals (provided that the total water content is sufficiently high) the ice crystals would gain mass by vapour deposition at the expense of the liquid drops that would loose mass by evaporation. Upon attaining sufficient weight, the ice crystals would fall as snow and further undergo several transitions -accretion, melting, and/or evaporation- before reaching the ground. This process requires a small number of ice crystals with respect to the large amount of supercooled liquid droplets. The Wegener-Bergeron-Findeisen process is an extremely powerful microphysical mechanism that can cause rapid transformation of cloud macrophysical and radiative properties (see the review of Storelvmo and Tan, 2015 [285]).

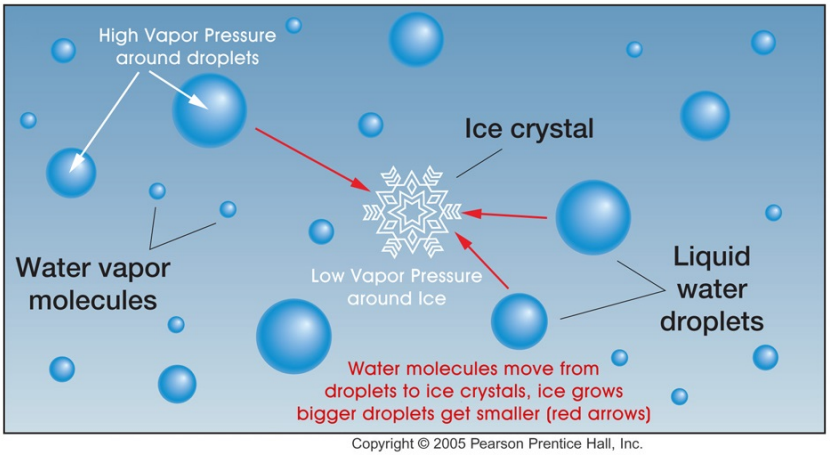

Figure A.1: Schematisation of the growth of ice crystals by diffusion of water vapour through the Wegener-Bergeron-Findeisen process. Image modified from Pearson Prentice Hall 2005, Inc.

Appendix B

Image analysis for dfpc

Once the ice crystals have developed on the filter (after 15/20 min of exposition to saturated vapours) an image is recorded through the camera. If the number of crystal is low, the count is visually made. In case of higher concentrations, an automatic software is employed to count the white dots (i.e. the ice crystals). The images need to be treated in case of noise or to account for the proximity of certain ice crystals. At the beginning, ImageJ was used to elaborate each images and to count them. During this thesis, a code was developed under Matlab R 2018a to improve the image analysis and the counting.

The main step of the code are the followings: passage to a binary image; erosion; counting; memorize crystals boundary; textbox the number. An example of operation is reported below. Open Matlab and import the figure (command "imread"). Convert the RGB format to a grey level scale (command rgb2gray). Select the disc corresponding to the sampled area (corresponding to a smaller diameter D' than the entire filter, to account only for the surface which is exposed to the aerosols collection). Erase the image content outside the area of interest. Plot circles around the crystals in yellow and display them on the background of the original image. In the final image, it is possible to underline the corona that has been rejected.

If the noise is not reduced, the grid traced on the filter can be taken for a crystal. An example is reported in Figure B.3. To reduce this noise, a threshold level should be carefully determined. To this purpose, the maximum intensity of the recorded signal should be considered and the threshold level may be settled to half of the maximum. In a few cases, a more acceptable threshold is the $\pm 10\%$ of the the maximum pixel intensity.

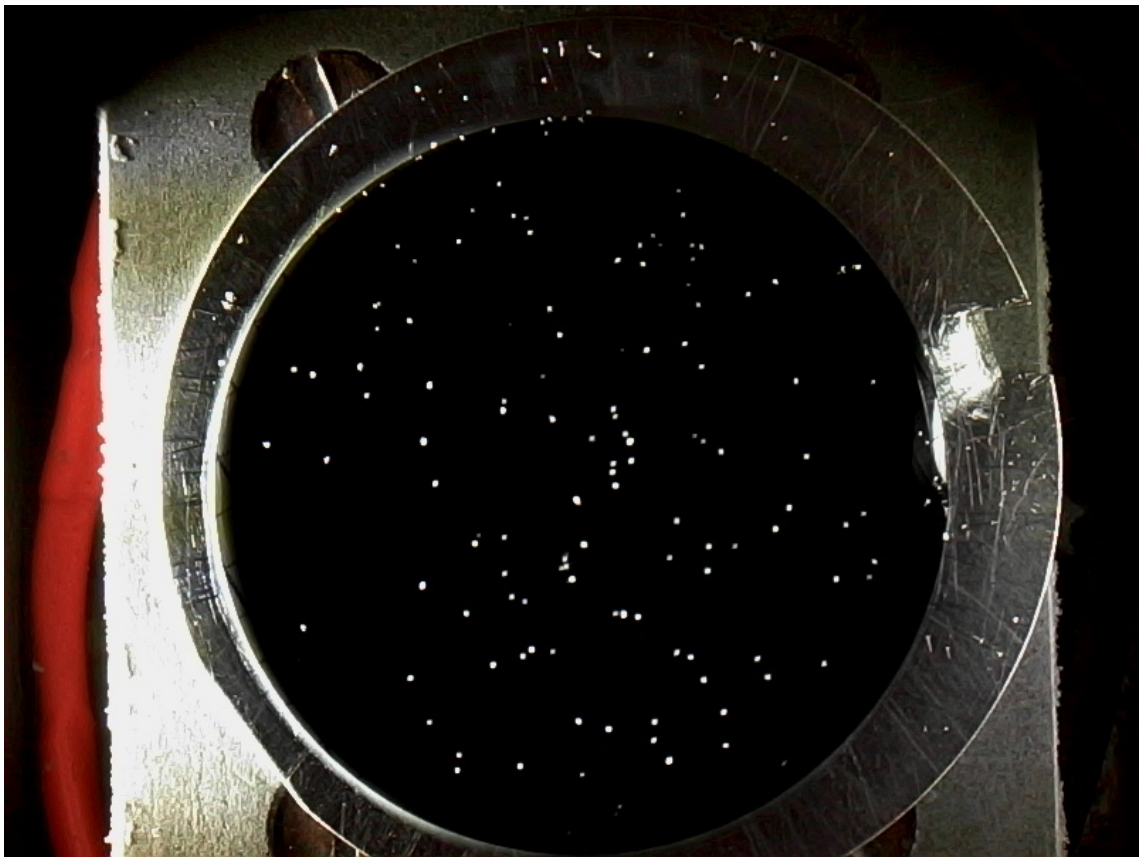

Figure B.1: Picture taken from the usb camera on the PM10 filter from Cimone Montain campaign (sampled on October the 8^{th} 2015, afternoon) and processed inside the DFPC. Ice crystals are seen as white dots as they reflect the light which is pointed on the filter from a led source fixed at the left of the image. It can be seen that the combined structure filter plus metal plate is placed on the Peltier cooler support.

Figure B.2: Figure B.1 after the selection with ImageJ which is used also to center the filter and measur its diameter in pixel units. This picture is saved as 'Image.bmp' in a Matlab folder for subsequent analysis.

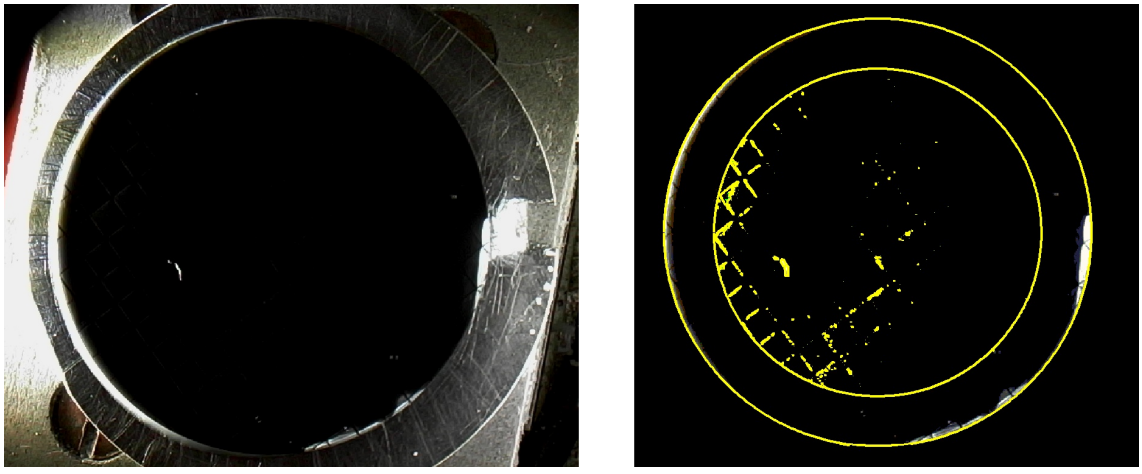

Figure B.3: Example of the interference of the background on the counting of the white dots.

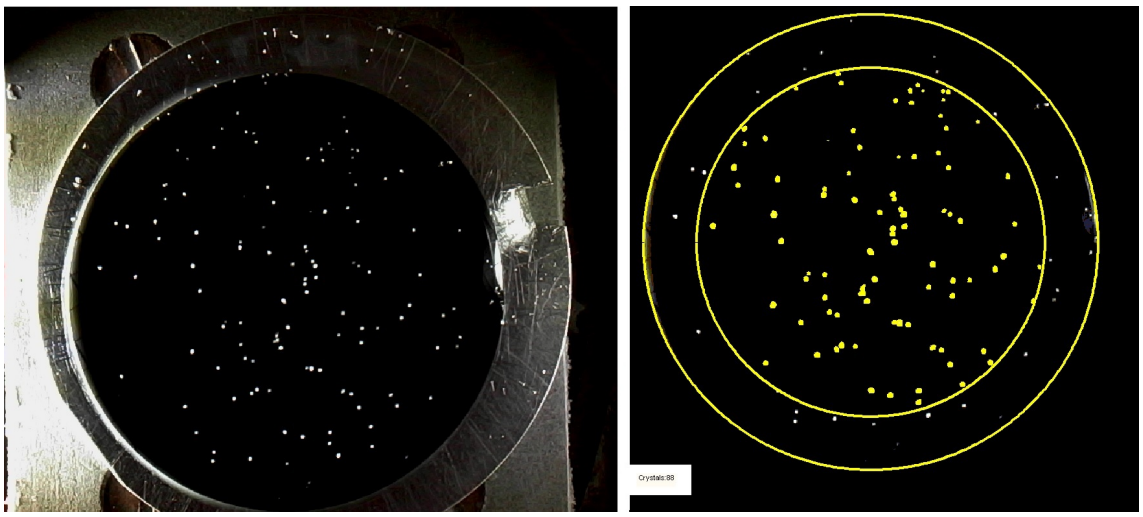

Figure B.4: Image before and after the analysis performed with the code reported here. The filter reported here is a PM_{10} sampled on the 08/10/2015-h17 and activated at T=−22°C.

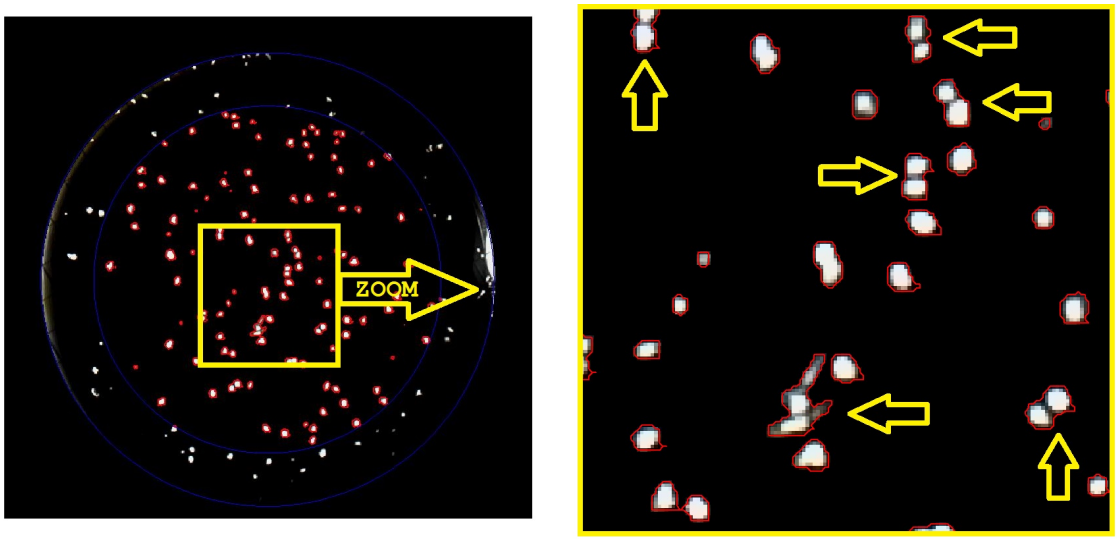

Figure B.5: Zoom to highlights the capability of the developed code to distinguish between ice crystals developed in a close region. The filter reported here is the same reported in Figure B.6.

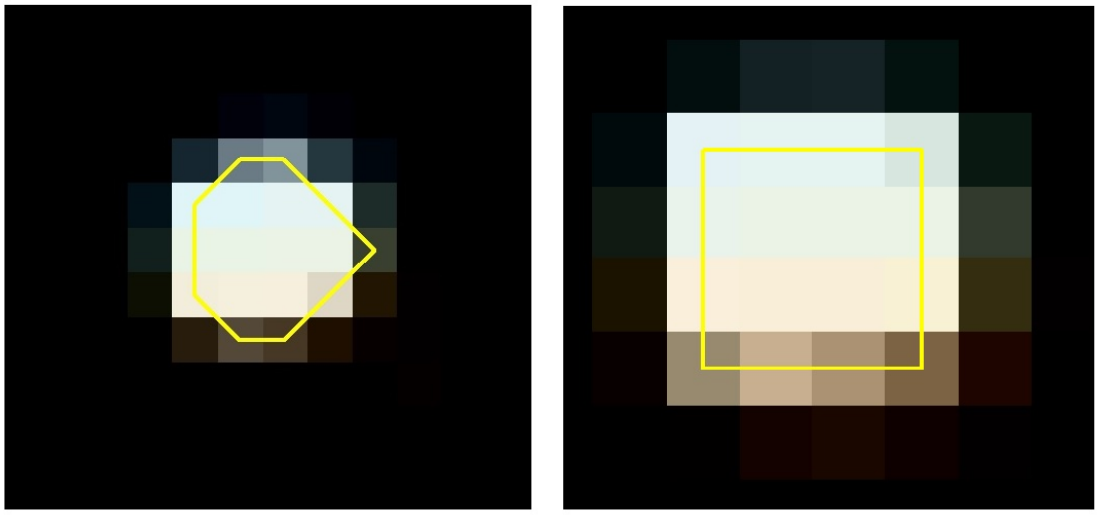

Figure B.6: Zoom on the shape of two ice crystals, as drawn by the software which has considered variation on the pixel intensity. The diameter is around 5 pixels, correspondent for these pictures to 440 μm.

Appendix C

Source Code

Presented below is the code that has been conceived to enumerate the ice crystals grown on a black substrate inside the dfpc chamber (as presented in Appendix A). The code was run under the Imaging Tool Box of Matlab. It was written with a basic number of functions in order to run also under old versions (as Matlab 2008) but it can work also under recent ones. In general, no ice crystals grow in the external disc. Indeed, the air stream can not pass through this zone, and then no aerosol particle should be present. However, a few ice crystals may appear in the external region (see C.2) but they should not be taken into consideration. We believe that these crystals are due to impurities released by the filter holder in the compression region (see Figure C.1) concomitant to the metal rings. This part should be always cleaned with alcohol, but under field campaign this step is not always performed and then it can provide fake counts if this is not excluded. The code was conceived to isolate the region of interest, to account for photo lighting inhomogeneities, and to memorize the crystals positions in an array matrix.

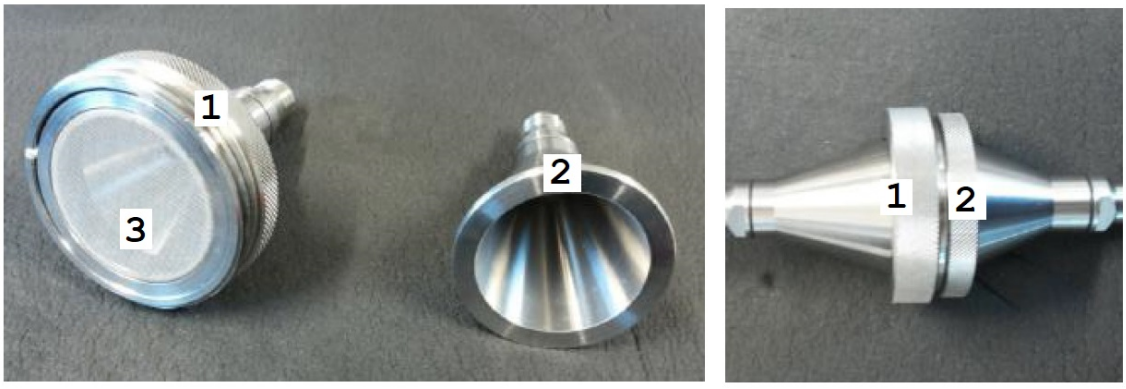

Figure C.1: Filter Holder open (left) and closed (right). The filter is inserted on the metal grid (3) while the metal rings (1) and (2) are screwed in. The external area of the filter is in contact with the metal rings to ensure the sealing. Photo credit Matteo Piazza.

```
%%%%%%%%%%%%%%
%%%%%%%%%%%%%%
%% Nicosia A., 2016 %%%%
%%%%%%%%%%%%%%
%%%%%%%%%%%%%%
```

clear all; % clean the command window

I=imread ('Image.bmp');

% load the image of the filter in a bmp format. The filter should have been previously centred inside a black frame 600X600.

I1=rgb2gray(I); % convert the image from RGB to a grey scale

Rout= single (500/2);

%replace this value with the correct radius –in pixel- of the filter's image. This value can be evaluated easily with ImageJ or similar software. In our measurements it ranged from 400 to 600 pixels, in relation to the usb camera distance to obtain the focus .

RinReal= single (Rout*36)/47;

% define the internal radius of the disc that will be analysed (taking away the external disc in which the air has not passed through during the sampling). The value 36 refers to the grid diameter (expressed in cm) employed in this study and related to available surface area in which the aerosol pass trhough. For some filter holder models this value may be higher. The number 47 is the diameter of the filter expressed in cm. Redefine these quantities if necessary.

Rin= single (Rout*36.88)/47; % extend the previous disc to account for a few crystals that may fall outside the region of interest during the pre-treatment. Estimation of ice crystals diameters were of about 0.44 micron, then we consider twice this value (id est 0.88 micron is the lenght of two adjacent ice crystals) as extra diameter for the disc of interest.

R2= Rin * Rin ;

I2=I1; %I2 contains just the selected disc while the outer region is cancelled

z=0;

for i=0:1:599;

x=i-300;

for j=0:1:599;

y=300-j;

z=x*x+y*y;

if z > (Rin * Rin) %everything outside the disc is cancelled (i.e. is equal to zero)

I2(i+1,j+1)=0;

end

end

end

%%%%%%%%%%%%%%%%%%%%%%%%%%%

%% noise reduction and passage to a binary image %%

%%%%%%%%%%%%%%%%%%%%%%%%%%%

Max=single(max(I2(:))); % find the maximum intensity of the signal in I2 in the range [0,255]

M=single((Max/1000)); % convert Max to a number in the range [0,1]

level=single(M-M*0.1); % consider just the 10

I3=im2bw(I2, level); % I3 is a binary image and the threshold is fixed to 'level'

%%%%%%%%%%%%%%%

%% Erosion %%%%%%%%

%%%%%%%%%%%%%%%

```
se = strel('disk',0); % the radius of the disk should be maintained as lower as possible
Ieroded = imerode(I3,se);
%%%%%%%%%%%%%%%
%% Counting %%%%%%%%
%%%%%%%%%%%%%%%%%
I4 = bwlabel(Ieroded,8);
% It returns the matrix I4 containing labels for the connected objects measured from Ieroded
[I4,num] = bwlabel(Ieroded,8);
[B,L,N,A] = bwboundaries(Ieroded);
%%%%%%%%%%%%%%%
%% Final Image %%%%%%
%%%%%%%%%%%%%%%%%
mFigure = figure()
imshow(I); hold on;
for k=1:length(B),
if(~sum(A(k,:)))
boundary = Bk;
plot(boundary(:,2),...
boundary(:,1),'y','LineWidth',3);
for l=find(A(:,k))'
boundary = Bl;
plot(boundary(:,2),...
boundary(:,1),'g','LineWidth',2);
end
end
end
hold on;
teta = -pi:0.01:pi;
plot(300+ RinReal*cos(teta),300+ RinReal *sin(teta), 'y','LineWidth',1),
plot(300+Rout*cos(teta),300+ Rout *sin(teta), 'y','LineWidth',1),
hold off;
mTextBox = uicontrol('style','text'); % write the number of crystals in the same frame
t.FontSize = 16;
s = strcat('Crystals:' , num2str(num));
set(mTextBox,'String', s)
%%%%%%%%%%%%
%%%%%%%%%%%%
```

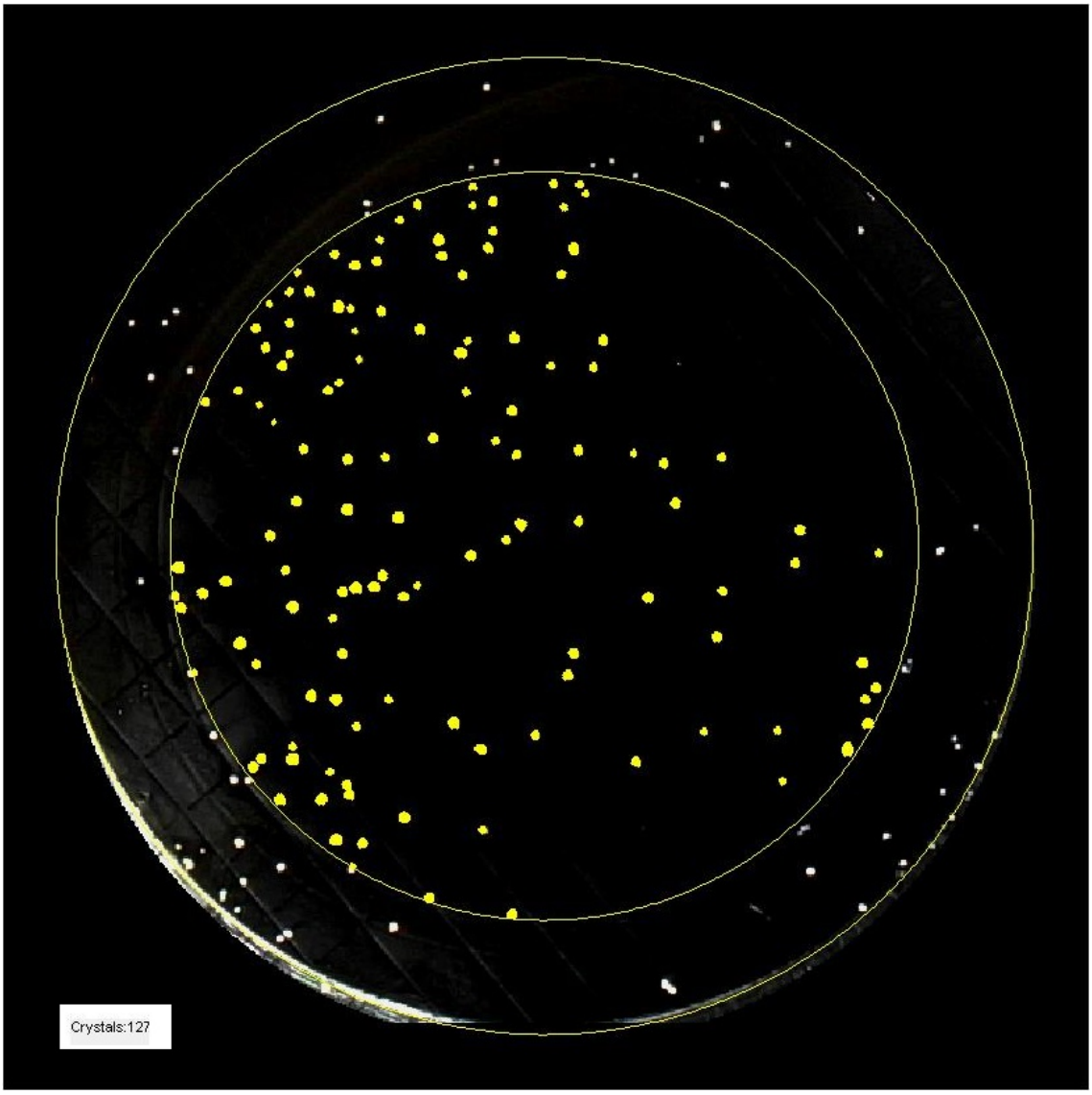

Figure C.2: A figure showing the results of the code. The software has selected the disc of interest and it has estimated the number of crystals only in this region. In addition, each crystal counted has been coloured in yellow, to visually evaluate the population of white dots left apart (corrisponding to impurities and treated as noise). The number of counting is reported in the left corner downside.

Appendix D

Particle Size Distribution from OPC and DMPS

To estimate the particle size distribution of sea spray aerosol (and calculate its total surface area for unit volume), it is current practise to dry the aerosol and to assume that the particles are spherical, in order to measured an electrical mobility particle diameter or an optical particle diameter. However, in nature sea spray particles are more likely to be cubical, especially under low relative humidity, while they growth as spheres under higher relative humidity (RH>40%). The growth factor of marine aerosols depend on both the relative humidity and both the amount of hygroscopic and non hygroscopic material carried by the particles (Snider et al., 2007 [286]). The ratio among hygroscopic and non hygroscopic material is not a fixed quantity, and may vary from one marine aerosols to another and posteriori correction may be erroneous. In our set up, we decide to measure both the dried and the undried Particle Size Distribution.

Figure D.2 reports the PSD of the dried aerosols measured by DMPS (neutralised through an Xray advanced aerosol neutralizer, TSI), while the original hydrated nascent sea spray was measured by OPC (WELAS 2100, Palas). We notice that the two instruments fairly agree below 240 nm, while DMPS overestimate OPC in the interval 240-425 nm. DMPS data have been corrected for multiple charge influence in the inversion routine, so we exclude the influence of multiple charges. We exclude also a major influence of the hygroscopicity of inorganic sea salt particles for the following two reasons:

- the presence of hydrates can lower the hygroscopic growth of inorganic sea salt of about 8–15% than pure sodium chloride (as explained in Zieger et al., 2017 [287]).
- the difference among a wet/dry aerosol measured through an optical system would have the effect to translate the peaks towards larger size, and increase the concentration of coarse particles. In our case, Figure D.2 shows a rapid decrease of the wet aerosols with respect to the dried one.

In literature, differences among the optical and the mobility electrical diameter have been reported when the shape of the aerosols particles were not spherical and if their refractive index were too different from the ones considered during calibration (with PSL latex spheres). Considering the specific generation processes adopted in this study, it is plausible to assume that the primary

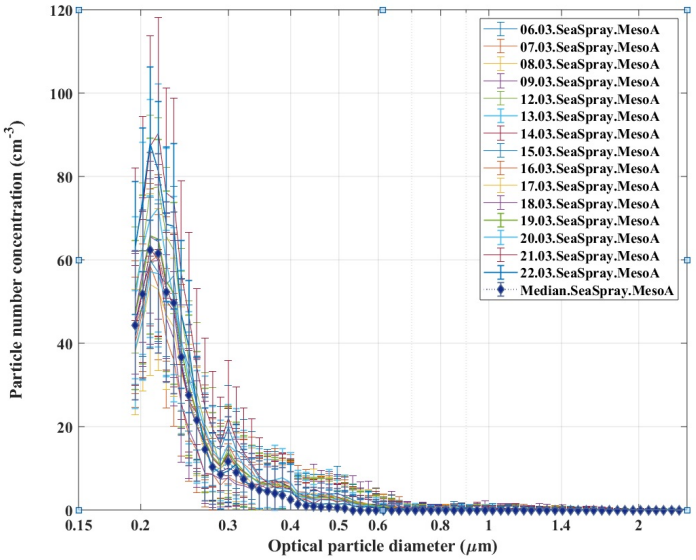

Figure D.1: Particle Size Distribution of the primary marine aerosol generated, measured by the Optical Particle Counter WELAS.

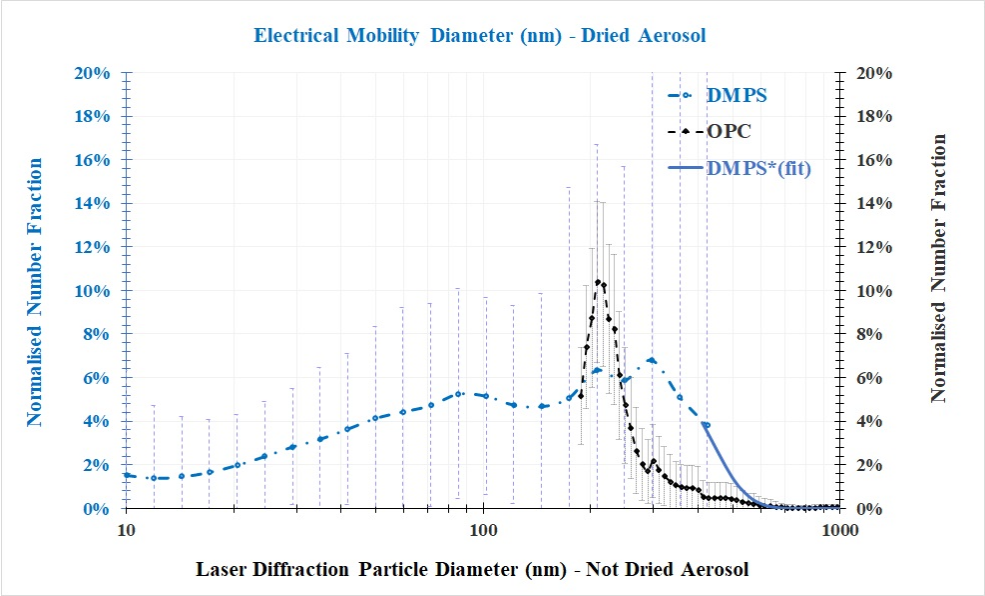

Figure D.2: Comparison among the two average Particle Size Distribution from the WELAS OPC and the custom made DMPS.

marine aerosol generated was charged, and that several aggregates might have occurred, thus affecting the OPC measurements.

Acronyms

AIDA Aerosol Interactions and Dynamics of the Atmosphere. 37

AMS Aerosols Mass Spectrometer. 26, 28

BACCHUS Impact of Biogenic versus Anthropogenic emissions on Clouds and Climate: towards a Holistic UnderStanding Background international project. 41, 42

CCN Cloud Condensation Nuclei. 2, 9

CNR National Research Council. 20

CNRS National Center for Scientific Research. 20

CNT Classical Nucleation Theory. 4, 5, 6

CPC Condensation Particle Counter. 87, 88

DFPC Dynamic Filter Processing Chamber. 20, 26, 31, 32, 33, 35, 36, 37, 41, 66, 71, 73, 82, 83, 94, 110, 115

DMPS Differential Mobility Particle Sizer. 87, 88, 126

$\mathbf{f_{IN}}$ Activation Fraction. 25, 32, 33

FNA Freezing Nucleation Apparatus. vii, 20, 26, 29, 66, 71, 72, 73, 75, 79, 82, 84, 94, 101, 110

FRIDGE FRankfurt Isothermal static Diffusion chambEr. 33

IN Ice Nuclei. 44, 46, 53

INP Ice Nuclei Particles. 2, 3, 4, 6, 7, 9, 11, 15, 19, 20, 21, 23, 31

ISAC-CNR Institute of Atmospheric Sciences and Climate of the Italian National Research Council. 20, 33

LINDA LED based Ice Nucleation Detection Apparatus. 29

MC Mountain Cimone. vi, 42, 43, 50, 51, 53, 55

MPC Mixed Phase Cloud. 1, 2, 3, 11, 17

MPS Mobility Particle Sizer Spectrometer. 26, 28, 31, 33, 87

$\mathbf{n}_s$ size equivalent Ice Nucleation Active Surface-site density. 24, 25, 26, 32, 38

OA Organic Aerosol. 13

OM Organic Matter. 13, 14

OPC Optical Particle Counter. 26, 28, 31, 33, 87, 89, 126, 125

PBL Planetray Boundary Layer. 53, 55

PCF Pore Condensation followed by Freezing. 17

PMA Primary Marine Aerosol. 71, 86, 87

PSD Particle Size Distribution. 87, 92, 125, 126

PTOF Particle Time-Of-Flight. 28

$\mathbf{S_i}$ Saturation ratio with respect to Ice. 7, 8, 25

$\mathbf{S_w}$ Saturation ratio with respect to Water. 4, 7, 8, 25, 26, 31, 33, 37, 38

SCLWD Super-Cooled Liquid Water Droplets. 4

SJAC Steam Jet Aerosol Collector. 71, 73

SOA Secondary Organic Aerosol. 14

SPC San Pietro Capofiume. vi, 42, 43, 46, 48, 49, 50, 51, 53

T freezing Temperature. 4, 25, 26, 31, 33, 37

VOC Volatile organic compounds. 8

Bibliography

[1] B. Stevens and S. Bony. Water in the atmosphere. *Physics Today*, 66(6):29–34, 2013.

[2] C. J. Stubenrauch, W. B. Rossow, S. Kinne, S. Ackerman, G. Cesana, H. Chepfer, L. Di Girolamo, B. Getzewich, A. Guignard, A. Heidinger, B. C. Maddux, W. P. Menzel, P. Minnis, C. Pearl, S. Platnick, C. Poulsen, J. Riedi, S. Sun-Mack, A. Walther, D. Winker, S. Zeng, and G. Zhao. Assessment of global cloud datasets from satellites: Project and database initiated by the gewex radiation panel. *Bulletin of the American Meteorological Society*, 94(7):12219–12238, 2013.

[3] A. I. Flossmann and W. Wobrock. Will pollution reduce precipitations? *Air Pollution Modeling and its Application XXI. NATO Science for Peace and Security Series C: Environmental Security*, Springer, Dordrecht:549–557, 2011.

[4] J. Sillmann, T. Thorarinsdottir, N. Keenlyside, N. Schaller, L. V. Alexander, G. Hegerl, S. I. Seneviratne, R. Vautard, X. Zhang, and F. W. Zwiers. Understanding, modeling and predicting weather and climate extremes: Challenges and opportunities. *Weather and Climate Extremes*, 18:65–74, 2017.

[5] T. Deshler. Chemistry of the atmosphere. Observations for Chemistry (In Situ): Particles. *Encyclopedia of Atmospheric Sciences, Academic Press*, pages 379–386, 2015.

[6] J. Rosinski, P. L. Haagenson, C. T. Nagamoto, B. Quintana, F. Parungo, and S. D. Hoyt. Ice-forming nuclei in air masses over the Gulf of Mexico. *Journal of Aerosol Science*, 19(5):539–551, 1988.

[7] S. M. Burrows, C. Hoose, U. Pöschl, and M. G. Lawrence. Ice nuclei in marine air: Biogenic particles or dust? *Atmospheric Chemistry and Physics*, 2013.

[8] H. R. Pruppacher and J. Klett. *Microphysics of Clouds and Precipitation*. Dordrecht, Kluwer Academic Publishers, 1997.

[9] T. Hiron and A. I. Flossmann. A Study of the Role of the Parameterization of Heterogeneous Ice Nucleation for the Modeling of Microphysics and Precipitation of a Convective Cloud.

[10] I. Gultepe, A. J. Heymsfield, P. R. Field, and D. Axisa. Ice-Phase Precipitation. *Meteorological Monographs*, 2017.

[11] P. J. DeMott, O. Möhler, O. Stetzer, G. Vali, Z. Levin, M. D. Petters, M. Murakami, T. Leisner, U. Bundke, H. Klein, Z. A. Kanji, R. Cotton, H. Jones, S. Benz, M. Brinkmann, D. Rzesanke, H. Saathoff, M. Nicolet, A. Saito, B. Nillius, H. Bingemer, J. Abbatt, K. Ardon, E. Ganor, D. G. Georgakopoulos, and C. Saunders. Resurgence in ice nuclei measurement research. *Bulletin of the American Meteorological Society*, 2011.

[12] A. I. Flossmann and W. Wobrock. A review of our understanding of the aerosol-cloud interaction from the perspective of a bin resolved cloud scale modelling. *Atmospheric Research*, 97(4):478 – 497, 2010.

[13] K. T. O and R. Wood. An approximation for homogeneous freezing temperature of water droplets. *Atmospheric Chemistry and Physics*, 21(15):31867–31889, 2015.

[14] C. Vega, J. L. F. Abascal, and P. G. Debenedetti. Physics and chemistry of water and ice. *Physical Chemistry Chemical Physics*, 2011.

[15] D. Rosenfeld and W. L. Woodley. Deep convective clouds with sustained supercooled liquid water down to -37.5°C. *Nature*, 2000.

[16] Y. Hu, S. Rodier, K. M. Xu, W. Sun, J. Huang, B. Lin, P. Zhai, and D. Josset. Occurrence, liquid water content, and fraction of supercooled water clouds from combined CALIOP/IIR/MODIS measurements. *Journal of Geophysical Research Atmospheres*, 2010.

[17] D. Lamb and J. Verlinde. *Physics and chemistry of clouds*. Cambridge University Press, Cambridge, 2011.

[18] C. Nanev. *Theory of Nucleation. Handbook of Crystal Growth: Second Edition*. 1:315–358, 2015.

[19] Y. Boose. *Field and laboratory studies of atmospheric ice nucleating particles*. PhD thesis, ETH Zurich, 2016.

[20] J. M. Wallace and P. V. Hobbs. *Atmospheric Science: An Introductory Survey*. Elsevier, 2006.

[21] T. Koop, B. Luo, A. Tsias, and T. Peter. Water activity as the determinant for homogeneous ice nucleation in aqueous solutions. *Nature*, 406(611), 2000.

[22] M. J. Bangert. *Interaction of Aerosol, Clouds, and Radiation on the Regional Scale*. PhD thesis, Karlsruher Instituts für Technologie, 2012.

[23] N. H. Fletcher, P. Squires, and Bowen E. G. *The physics of rainclouds.* University press Cambridge, London., 1962.

[24] E. K. Bigg. The formation of atmospheric ice crystals by the freezing of droplets. *Quarterly Journal of the Royal Meteorological Society*, 1953.

[25] E. K. Bigg. The supercooling of water. *Proceedings of the Physical Society. Section B*, 1953.

[26] G. Vali. Sizes of Atmospheric Ice Nuclei. *Nature*, 212:384, 1966.

[27] G. Vali, P. J. DeMott, O. Möhler, and T. F. Whale. Technical note: A proposal for ice nucleation terminology. *Atmospheric Chemistry and Physics*, 15(18):10263–10270, 2015.

[28] N. H.. Fletcher. Active Sites and Ice Crystal Nucleation. *Journal of Atmospheric Sciences*, 26(6):1266–1271, 1969.

[29] C. Marcolli, S. Gedamke, T. Peter, and B. Zobrist. Efficiency of immersion mode ice nucleation on surrogates of mineral dust. *Atmospheric Chemistry and Physics*, 2007.

[30] C. Marcolli. Deposition nucleation viewed as homogeneous or immersion freezing in pores and cavities. *Atmospheric Chemistry and Physics*, 2014.

[31] P. J. Connolly, O. Möhler, P. R. Field, H. Saathoff, R. Burgess, T. Choularton, and M. Gallagher. Studies of heterogeneous freezing by three different desert dust samples. *Atmospheric Chemistry and Physics*, 9(8):2805–2824, 2009.

[32] F. Lüönd, O. Stetzer, A. Welti, and U. Lohmann. Experimental study on the ice nucleation ability of size-selected kaolinite particles in the immersion mode. *Journal of Geophysical Research*, 115(D14), 2010.

[33] D. Niedermeier, R. A. Shaw, S. Hartmann, H. Wex, T. Clauss, J. Voigtländer, and F. Stratmann. Heterogeneous ice nucleation: Exploring the transition from stochastic to singular freezing behaviour. *Atmospheric Chemistry and Physics*, 11(16):8767–8775, 2011.

[34] M. Niemand, O. Möhler, B. Vogel, H. Vogel, C. Hoose, P. Connolly, H. Klein, H. Bingemer, P. J. DeMott, J. Skrotzki, and T. Leisner. A Particle-Surface-Area-Based Parameterization of Immersion Freezing on Desert Dust Particles. *Journal of the Atmospheric Sciences*, 2012.

[35] J. H. Seinfeld and S. N. Pandis. *Atmospheric chemistry and physics from air pollution to climate change, Second Edition.* Wiley, 2006.

[36] T. Young. An Essay on the Cohesion of Fluids. *Philosophical Transactions of the Royal Society of London*, 1805.

[37] M. J. Jamieson, C. E. Nicholson, and S. J. Cooper. First Study on the Effects of Interfacial Curvature and Additive Interfacial Density on Heterogeneous Nucleation. Ice Crystallization in Oil-in-Water Emulsions and Nanoemulsions with Added 1-Heptacosanol. *Crystal Growth & Design*, 5(2):451–459, 2005.

[38] Z. A. Kanji, L. A. Ladino, H. Wex, Y. Boose, M. Burkert-Kohn, D. J. Cziczo, and M. Krämer. Overview of Ice Nucleating Particles. *Meteorological Monographs*, 2017.

[39] T. Zolles, J. Burkart, T. Häusler, B. Pummer, R. Hitzenberger, and H. Grothe. Identification of ice nucleation active sites on feldspar dust particles. *Journal of Physical Chemistry A*, 2015.

[40] R. Rogers and M. K. Yau. *A short course in cloud physics.* Oxford, New York: Pergamon Press, 1989.

[41] M. P. Meyers, P. J. DeMott, and W. R. Cotton. New Primary Ice-Nucleation Parameterizations in an Explicit Cloud Model. *Journal of Applied Meteorology*, 1992.

[42] V. T. J. Phillips, P. J. DeMott, and C. Andronache. An Empirical Parameterization of Heterogeneous Ice Nucleation for Multiple Chemical Species of Aerosol. *Journal of the Atmospheric Sciences*, 2008.

[43] C. Hoose, J. E. Kristjánsson, and S. M. Burrows. How important is biological ice nucleation in clouds on a global scale? *Environmental Research Letters*, 2010.

[44] U. Lohmann and J. Feichter. Global indirect aerosol effects: a review. *Atmospheric Chemistry and Physics Discussions*, 2004.

[45] T. Storelvmo. Aerosol Effects on Climate via Mixed-Phase and Ice Clouds. *The Annual Review of Earth and Planetary Sciences is online at earth.annualreviews.org*, 45:199–222, 2017.

[46] O. Boucher, D. Randall, P. Artaxo, C. Bretherton, G. Feingold, P. Forster, V.-M. Kerminen, Y. Kondo, H. Liao, U. Lohmann, P. Rasch, S. K. Satheesh, S. Sherwood, B. Stevens, and X. Y. Zhang. *Clouds and aerosols*, pages 571–657. Cambridge University Press, Cambridge, UK, 2013.

[47] P. J. DeMott, A. J. Prenni, X. Liu, S. M. Kreidenweis, M. D. Petters, C. H. Twohy, M. S. Richardson, T. Eidhammer, and D. C. Rogers. Predicting global atmospheric ice nuclei distributions and their impacts on climate. *Proceedings of the National Academy of Sciences*, 2010.

[48] M. D. Tarn, S. N. F. Sikora, G. C. E. Porter, D. O'Sullivan, M. Adams, T. F. Whale, A. D. Harrison, J. Vergara-Temprado, T. W. Wilson, J. Shim, and B. J. Murray. The study of atmospheric ice-nucleating particles via microfluidically generated droplets. *Microfluidics and Nanofluidics*, 2018.

[49] C. Hoose and O. Möhler. Heterogeneous ice nucleation on atmospheric aerosols: A review of results from laboratory experiments. *Atmospheric Chemistry and Physics*, 2012.

[50] L. B. Hande, C. Engler, C. Hoose, and I. Tegen. Seasonal variability of Saharan desert dust and ice nucleating particles over Europe. *Atmospheric Chemistry and Physics*, 2015.

[51] V. J. Schaefer. The Formation of Ice Crystals in the Laboratory and the Atmosphere. *Chemical Reviews*, 44(2):291–320, 1949.

[52] J. Cozic, S. Mertes, B. Verheggen, D. J. Cziczo, S. J. Gallavardin, S. Walter, U. Baltensperger, and E. Weingartner. Black carbon enrichment in atmospheric ice particle residuals observed in lower tropospheric mixed phase clouds. *Journal of Geophysical Research Atmospheres*, 2008.

[53] M. Kamphus, M. Ettner-Mahl, T. Klimach, F. Drewnick, L. Keller, D. J. Cziczo, S. Mertes, S. Borrmann, and J. Curtius. Chemical composition of ambient aerosol, ice residues and

cloud droplet residues in mixed-phase clouds: Single particle analysis during the cloud and aerosol characterization experiment (CLACE 6). *Atmospheric Chemistry and Physics*, 2010.

[54] D. J. Cziczo, K. D. Froyd, C. Hoose, E. J. Jensen, M. Diao, M. A. Zondlo, J. B. Smith, C. H. Twohy, and D. M. Murphy. Clarifying the Dominant Sources and Mechanisms of Cirrus Cloud Formation. *Science*, 340(6138):1320–1324, 2013.

[55] P. J. DeMott, K. Sassen, M. R. Poellot, D. Baumgardner, D. C. Rogers, S. D. Brooks, A. J. Prenni, and S. M. Kreidenweis. African dust aerosols as atmospheric ice nuclei. *Geophysical Research Letters*, 2003.

[56] J. M. Creamean, K. J. Suski, D. Rosenfeld, A. Cazorla, P. J. DeMott, R. C. Sullivan, A. B. White, F. M. Ralph, P. Minnis, J. M. Comstock, J. M. Tomlinson, and K. A. Prather. Dust and biological aerosols from the Sahara and Asia influence precipitation in the Western U.S. *Science*, 2013.

[57] C. Chou, O. Stetzer, E. Weingartner, Z. Jurányi, Z. A. Kanji, and U. Lohmann. Ice nuclei properties within a Saharan dust event at the Jungfraujoch in the Swiss Alps. *Atmospheric Chemistry and Physics*, 2011.

[58] M. Kumai. Identification of Nuclei and Concentrations of Chemical Species in Snow Crystals Sampled at the South Pole. *Journal of the Atmospheric Sciences*, 33(5):833–841, 1976.

[59] J. D. Atkinson, B. J. Murray, M. T. Woodhouse, T. F. Whale, K. J. Baustian, K. S. Carslaw, S. Dobbie, D. O'Sullivan, and T. L. Malkin. The importance of feldspar for ice nucleation by mineral dust in mixed-phase clouds. *Nature*, 498:355, 2013.

[60] J. D. Yakobi-Hancock, L. A. Ladino, and J. P. D. Abbatt. Feldspar minerals as efficient deposition ice nuclei. *Atmospheric Chemistry and Physics*, 2013.

[61] D. J. Cziczo, K. D. Froyd, S. J. Gallavardin, O. Möhler, S. Benz, H. Saathoff, and D. M. Murphy. Deactivation of ice nuclei due to atmospherically relevant surface coatings. *Environmental Research Letters*, 2009.

[62] C. M. Archuleta, P. J. DeMott, and S. M. Kreidenweis. Ice nucleation by surrogates for atmospheric mineral dust and mineral dust/sulfate particles at cirrus temperatures. *Atmospheric Chemistry and Physics*, 2005.

[63] T. C. Bond, S. J. Doherty, D. W. Fahey, P. M. Forster, T. Berntsen, B. J. Deangelo, M. G. Flanner, S. Ghan, B. Kärcher, D. Koch, S. Kinne, Y. Kondo, P. K. Quinn, M. C. Sarofim, M. G. Schultz, M. Schulz, C. Venkataraman, H. Zhang, S. Zhang, N. Bellouin, S. K. Guttikunda, P. K. Hopke, M. Z. Jacobson, J. W. Kaiser, Z. Klimont, U. Lohmann, J. P. Schwarz, D. Shindell, T. Storelvmo, S. G. Warren, and C. S. Zender. Bounding the role of black carbon in the climate system: A scientific assessment. *Journal of Geophysical Research Atmospheres*, 2013.

[64] S. D. Brooks, K. Suter, and L. Olivarez. Effects of Chemical Aging on the Ice Nucleation Activity of Soot and Polycyclic Aromatic Hydrocarbon Aerosols. *The Journal of Physical Chemistry A*, 118(43):10036–10047, 2014.

[65] C. Chou, Z. A. Kanji, O. Stetzer, T. Tritscher, R. Chirico, M. F. Heringa, E. Weingartner, A. S.H. Prévôt, U. Baltensperger, and U. Lohmann. Effect of photochemical ageing on the ice nucleation properties of diesel and wood burning particles. *Atmospheric Chemistry and Physics*, 2013.

[66] M. D. Petters, M. T. Parsons, A. J. Prenni, P. J. Demott, S. M. Kreidenweis, C. M. Carrico, A. P. Sullivan, G. R. McMeeking, E. Levin, C. E. Wold, J. L. Collett, and Hans Moosmüller. Ice nuclei emissions from biomass burning. *Journal of Geophysical Research Atmospheres*, 2009.

[67] P. J. DeMott, Y. Chen, S. M. Kreidenweis, D. C. Rogers, and D. E. Sherman. Ice formation by black carbon particles. *Geophysical Research Letters*, 1999.

[68] O. Möhler, C. Linke, H. Saathoff, M. Schnaiter, R. Wagner, A. Mangold, M. Krämer, and U. Schurath. Ice nucleation on flame soot aerosol of different organic carbon content. *Meteorologische Zeitschrift*, 2005.

[69] M. Dymarska, B. J. Murray, L. Sun, M. L. Eastwood, D. A. Knopf, and A. K. Bertram. Deposition ice nucleation on soot at temperatures relevant for the lower troposphere. *Journal of Geophysical Research Atmospheres*, 2006.

[70] Z. A. Kanji and J. P. D. Abbatt. Laboratory studies of ice formation via deposition mode nucleation onto mineral dust and n-hexane soot samples. *Journal of Geophysical Research Atmospheres*, 2006.

[71] D. A. Knopf, P. A. Alpert, and B. Wang. The Role of Organic Aerosol in Atmospheric Ice Nucleation: A Review. 2018.

[72] T. W. Wilson, L. A. Ladino, P. A. Alpert, M. N. Breckels, I. M. Brooks, Browse J., S. M. Burrows, K. S. Carslaw, J. A. Huffman, Christopher J., W. P. Kilthau, R. H. Mason, Mcfiggans G., L. A. Miller, J. J. Najera, Polishchuk E. , Rae S. , C. L. Schiller, Meng S. , J. Vergara Temprado, T. F. Whale, J. P. S. Wong, Wurl O., J. D. Yakobi-Hancock, J. P. D. Abbatt, J. Y. Aller, A. K. Bertram, D. A. Knopf, and B. J. Murray. A marine biogenic source of atmospheric ice-nucleating particles. *Nature*, 525(7568):234, 2015.

[73] K. J. Baustian, M. E. Wise, E. J. Jensen, G. P. Schill, M. A. Freedman, and M. A. Tolbert. State transformations and ice nucleation in amorphous (semi-)solid organic aerosol. *Atmospheric Chemistry and Physics*, 2013.

[74] B. J. Murray, T. W. Wilson, S. Dobbie, Z. Cui, S. M. R. K. Al-Jumur, O. Möhler, M. Schnaiter, R. Wagner, S. Benz, M. Niemand, H. Saathoff, V. Ebert, S. Wagner, and B. Kärcher. Heterogeneous nucleation of ice particles on glassy aerosols under cirrus conditions. *Nature Geoscience*, 3:233, 2010.

[75] J. E. Shilling, T. J. Fortin, and M. A. Tolbert. Depositional ice nucleation on crystalline organic and inorganic solids. *Journal of Geophysical Research Atmospheres*, 2006.

[76] T. W. Wilson, B. J. Murray, R. Wagner, O. Möhler, H. Saathoff, M. Schnaiter, J. Skrotzki, H. C. Price, T. L. Malkin, S. Dobbie, and S. M.R.K. Al-Jumur. Glassy aerosols with a range of compositions nucleate ice heterogeneously at cirrus temperatures. *Atmospheric Chemistry and Physics*, 2012.

[77] B. Zobrist, C. Marcolli, T. Koop, B. P. Luo, D. M. Murphy, U. Lohmann, A. A. Zardini, U. K. Krieger, T. Corti, D. J. Cziczo, S. Fueglistaler, P. K. Hudson, D. S. Thomson, and T. Peter. Oxalic acid as a heterogeneous ice nucleus in the upper troposphere and its indirect aerosol effect. *Atmospheric Chemistry and Physics*, 2006.

[78] D. M. Lienhard, A. J. Huisman, U. K. Krieger, Y. Rudich, C. Marcolli, B. P. Luo, D. L. Bones, J. P. Reid, A. T. Lambe, M. R. Canagaratna, P. Davidovits, T. B. Onasch, D. R. Worsnop, S. S. Steimer, T. Koop, and T. Peter. Viscous organic aerosol particles in the upper troposphere: Diffusivity-controlled water uptake and ice nucleation? *Atmospheric Chemistry and Physics*, 2015.

[79] V. R. Després, J. A. Huffman, S. M. Burrows, A. S. Corinna, H.and Safatov, G. Buryak, J. Fröhlich-Nowoisky, W. Elbert, M. O. Andreae, U. Pöschl, and R. Jaenicke. Primary biological aerosol particles in the atmosphere: A review. 2012.

[80] L. R. Maki and K. J. Willoughby. Bacteria as Biogenic Sources of Freezing Nuclei. *Journal of Applied Meteorology*, 1978.

[81] R. C. Schnell and G. Vali. Biogenic Ice Nuclei: Part I. Terrestrial and Marine Sources. *Journal of the Atmospheric Sciences*, 1976.

[82] K. Diehl, C. Quick, S. Matthias-Maser, S.K. Mitra, and R. Jaenicke. The ice nucleating ability of pollen: Part I: Laboratory studies in deposition and condensation freezing modes. *Atmospheric Research*, 58(2):75–87, 2001.

[83] K. Diehl, S. Matthias-Maser, R. Jaenicke, and S. K. Mitra. The ice nucleating ability of pollen:: Part II. Laboratory studies in immersion and contact freezing modes. *Atmospheric Research*, 61(2):125–133, 2002.

[84] D. O'Sullivan, B. J. Murray, T. L. Malkin, T. F. Whale, N. S. Umo, J. D. Atkinson, H. C. Price, K. J. Baustian, J. Browse, and M. E. Webb. Ice nucleation by fertile soil dusts: Relative importance of mineral and biogenic components. *Atmospheric Chemistry and Physics*, 2014.

[85] I. Coluzza, J. Creamean, M. Rossi, H. Wex, P. Alpert, V. Bianco, Y. Boose, C. Dellago, L. Felgitsch, J. Fröhlich-Nowoisky, H. Herrmann, S. Jungblut, Z. Kanji, G. Menzl, B. Moffett, C. Moritz, A. Mutzel, U. Pöschl, M. Schauperl, J. Scheel, E. Stopelli, F. Stratmann, H. Grothe, and D. Schmale. Perspectives on the Future of Ice Nucleation Research: Research Needs and Unanswered Questions Identified from Two International Workshops. *Atmosphere*, 2017.

[86] D. O'Sullivan, B. J. Murray, J. F. Ross, and M. E. Webb. The adsorption of fungal ice-nucleating proteins on mineral dusts: A terrestrial reservoir of atmospheric ice-nucleating particles. *Atmospheric Chemistry and Physics*, 2016.

[87] D. Gurian-Sherman and S. E. Lindow. Bacterial ice nucleation: significance and molecular basis. *The FASEB Journal*, 7(14):1338–1343, 1993.

[88] C. E. Morris, D. G. Georgakopoulos, and D. C. Sands. Ice nucleation active bacteria and their potential role in precipitation. *Journal de Physique IV (Proceedings)*, 2004.

[89] C. E. Morris, D. C. Sands, B. A. Vinatzer, C. Glaux, C. Guilbaud, A. Buffière, S. Yan, H. Dominguez, and B. M. Thompson. The life history of the plant pathogen Pseudomonas syringae is linked to the water cycle. *The ISME Journal*, 2008.

[90] T. P. Wright, J. D. Hader, G. R. McMeeking, and M. D. Petters. High relative humidity as a trigger for widespread release of ice nuclei. *Aerosol Science and Technology*, 2014.

[91] G. Langer. Analysis of Results from Second International Ice Nucleus Workshop with Emphasis on Expansion Chambers, NCAR Counters, and Membrane Filters. *Journal of Applied Meteorology*, 12(6):991–999, 1973.

[92] U. Bundke, B. Nillius, R. Jaenicke, T. Wetter, H. Klein, and H. Bingemer. The fast Ice Nucleus chamber FINCH. *Atmospheric Research*, 2008.

[93] O. Möhler, O. Stetzer, S. Schaefers, C. Linke, M. Schnaiter, R. Tiede, H. Saathoff, M. Krämer, A. Mangold, P. Budz, P. Zink, J. Schreiner, K. Mauersberger, W. Haag, B. Kärcher, and U. Schurath. Experimental investigation of homogeneous freezing of sulphuric acid particles in the aerosol chamber AIDA. *Atmospheric Chemistry and Physics*, 3(1):211–223, 2003.

[94] T. Tajiri, K. Yamashita, M. Murakami, A. Saito, K. Kusunoki, N. Orikasa, and L. Lilie. A Novel Adiabatic-Expansion-Type Cloud Simulation Chamber. *Journal of the Meteorological Society of Japan. Ser. II*, 91:687–704, 2013.

[95] R. Al-Naimi and C. P. R. Saunders. Measurements of natural deposition and condensation-freezing ice nuclei with a continuous flow chamber. *Atmospheric Environment (1967)*, 19(11):1871–1882, 1985.

[96] D. C. Rogers, P. J. DeMott, S. M. Kreidenweis, and Y. Chen. A continuous-flow diffusion chamber for airborne measurements of ice nuclei. *Journal of Atmospheric and Oceanic Technology*, 2001.

[97] E. K. Bigg. Ice forming nuclei in the high Arctic. *Tellus, Series B: Chemical and Physical Meteorology*, 1996.

[98] H. Klein, W. Haunold, U. Bundke, B. Nillius, T. Wetter, S. Schallenberg, and H. Bingemer. A new method for sampling of atmospheric ice nuclei with subsequent analysis in a static diffusion chamber. *Atmospheric Research*, 96(2):218–224, 2010.

[99] G. Langer and J. Rodgers. An experimental study of the detection of ice nuclei on membrane filters and other substrata. *Journal of applied meteorology*, 14:560–570, 1975.

[100] K. Ardon-Dryer, Z. Levin, and R. P. Lawson. Characteristics of immersion freezing nuclei at the South Pole station in Antarctica. *Atmospheric Chemistry and Physics*, 2011.

[101] C. Budke and T. Koop. BINARY: An optical freezing array for assessing temperature and time dependence of heterogeneous ice nucleation. *Atmospheric Measurement Techniques*, 2015.

[102] D. Knopf and P. Alpert. Water activity based model of heterogeneous ice nucleation kinetics for freezing of water and aqueous solution droplets. *Faraday discussions*, 165:513–534, 2013.

[103] B. J. Murray, S. L. Broadley, T. W. Wilson, J. D. Atkinson, and R. H. Wills. Heterogeneous freezing of water droplets containing kaolinite particles. *Atmospheric Chemistry and Physics*, 2011.

[104] G. Vali. Repeatability and randomness in heterogeneous freezing nucleation. *Atmospheric Chemistry and Physics*, 2008.

[105] G. Vali, D. Rogers, G. Gordon, C. P. R. Saunders, M. Reischel, and R. Black. Aerosol and nucleation research in support of NASA cloud physics experiments in space outline. Technical report, 1978.

[106] M. L. Corrin, H. W. Edwards, and J. A. Nelson. The Surface Chemistry of Condensation Nuclei: II. The Preparation of Silver Iodide Free of Hygroscopic Impurities and Its Interaction with Water Vapor. *Journal of the Atmospheric Sciences*, 21(5):565–567, 1964.

[107] E. Sanz, C. Vega, J. R. Espinosa, R. Caballero-Bernal, J. L. F. Abascal, and C. Valeriani. Homogeneous Ice Nucleation at Moderate Supercooling from Molecular Simulation. *Journal of the American Chemical Society*, 135(40):15008–15017, 2013.

[108] M. Matsumoto, S. Saito, and I. Ohmine. Molecular dynamics simulation of the ice nucleation and growth process leading to water freezing. *Nature*, 416:409, 2002.

[109] L. Lupi and V. Molinero. Does Hydrophilicity of Carbon Particles Improve Their Ice Nucleation Ability? *The Journal of Physical Chemistry A*, 118(35):7330–7337, 2014.

[110] L. Lupi, A. Hudait, and V. Molinero. Heterogeneous Nucleation of Ice on Carbon Surfaces. *Journal of the American Chemical Society*, 136(8):3156–3164, 2014.

[111] J. C. Johnston and V. Molinero. Crystallization, Melting, and Structure of Water Nanoparticles at Atmospherically Relevant Temperatures. *Journal of the American Chemical Society*, 134(15):6650–6659, 2012.

[112] E. B. Moore and V. Molinero. Is it cubic? Ice crystallization from deeply supercooled water. *Phys. Chem. Chem. Phys.*, 13(44):20008–20016, 2011.

[113] S. J. Cox, S. M. Kathmann, B. Slater, and A. Michaelides. Molecular simulations of heterogeneous ice nucleation. I. Controlling ice nucleation through surface hydrophilicity. *The Journal of Chemical Physics*, 142(18):184704, 2015.

[114] S. J. Cox, S. M. Kathmann, B. Slater, and A. Michaelides. Molecular simulations of heterogeneous ice nucleation. II. Peeling back the layers. *The Journal of Chemical Physics*, 142(18):184705, 2015.

[115] S. J. Cox, S. M. Kathmann, J. A. Purton, M. J. Gillan, and A. Michaelides. Non-hexagonal ice at hexagonal surfaces: the role of lattice mismatch. *Phys. Chem. Chem. Phys.*, 14(22):7944–7949, 2012.

[116] J. Y. Yan and G. N. Patey. Heterogeneous Ice Nucleation Induced by Electric Fields. *The Journal of Physical Chemistry Letters*, 2(20):2555–2559, 2011.

[117] J. Y. Yan and G. N. Patey. Molecular Dynamics Simulations of Ice Nucleation by Electric Fields. *The Journal of Physical Chemistry A*, 116(26):7057–7064, 2012.

[118] J. Y. Yan and G. N. Patey. Ice nucleation by electric surface fields of varying range and geometry. *The Journal of Chemical Physics*, 139(14):144501, 2013.

[119] P. Pedevilla, S. J. Cox, B. Slater, and A. Michaelides. Can Ice-Like Structures Form on Non-Ice-Like Substrates? The Example of the K-feldspar Microcline. *The Journal of Physical Chemistry C*, 120(12):6704–6713, 2016.

[120] Y. Bi, R. Cabriolu, and T. Li. Heterogeneous ice nucleation controlled by the coupling of surface crystallinity and surface hydrophilicity. *Journal of Physical Chemistry C*, 2016.

[121] A. Kiselev, F. Bachmann, P. Pedevilla, S. J Cox, A. Michaelides, D. Gerthsen, and T. Leisner. Active sites in heterogeneous ice nucleation the example of K-rich feldspars. *Science*, 355(6323):367–371, 2017.

[122] N. Fukuta and R. C. Schaller. Ice Nucleation by Aerosol Particles. Theory of Condensation-Freezing Nucleation. *Journal of the Atmospheric Sciences*, 39(3):648–655, 1982.

[123] H. Wex, P. J. Demott, Y. Tobo, S. Hartmann, M. Rösch, T. Clauss, L. Tomsche, D. Niedermeier, and F. Stratmann. Kaolinite particles as ice nuclei: Learning from the use of different kaolinite samples and different coatings. *Atmospheric Chemistry and Physics*, 2014.

[124] N. Hiranuma, O. Möhler, K. Yamashita, T. Tajiri, A. Saito, A. Kiselev, N. Hoffmann, C. Hoose, E. Jantsch, T. Koop, and M. Murakami. Ice nucleation by cellulose and its potential contribution to ice formation in clouds. *Nature Geoscience*, 8:273, 2015.

[125] R. Wagner, A. Kiselev, O. Möhler, H. Saathoff, and I. Steinke. Pre-activation of ice-nucleating particles by the pore condensation and freezing mechanism. *Atmospheric Chemistry and Physics*, 2016.

[126] N. Hoffmann, D. Duft, A. Kiselev, and T. Leisner. Contact freezing efficiency of mineral dust aerosols studied in an electrodynamic balance: quantitative size and temperature dependence for illite particles. *Faraday Discuss.*, 165:383–390, 2013.

[127] N. Hoffmann, A. Kiselev, D. Rzesanke, D. Duft, and T. Leisner. Experimental quantification of contact freezing in an electrodynamic balance. *Atmospheric Measurement Techniques*, 2013.

[128] B. Nagare, C. Marcolli, A. Welti, O. Stetzer, and U. Lohmann. Comparing contact and immersion freezing from continuous flow diffusion chambers. *Atmospheric Chemistry and Physics*, 2016.

[129] P. Seifert, A. Ansmann, S. Groß, V. Freudenthaler, B. Heinold, A. Hiebsch, I. Mattis, J. Schmidt, F. Schnell, M. Tesche, U. Wandinger, and M. Wiegner. Ice formation in ash-influenced clouds after the eruption of the Eyjafjallajkull volcano in April 2010. *Journal of Geophysical Research Atmospheres*, 2011.

[130] S. K. Sihvonen, G. P. Schill, N. A. Lyktey, D. P. Veghte, M. A. Tolbert, and M. A. Freedman. Chemical and Physical Transformations of Aluminosilicate Clay Minerals Due to Acid Treatment and Consequences for Heterogeneous Ice Nucleation. *The Journal of Physical Chemistry A*, 118(38):8787–8796, 2014.

[131] G. Kulkarni, M. Nandasiri, A. Zelenyuk, J. Beranek, N. Madaan, A. Devaraj, V. Shutthanandan, S. Thevuthasan, and T. Varga. Effects of crystallographic properties on the ice nucleation properties of volcanic ash particles. *Geophysical Research Letters*, 2015.

[132] A. Salam, U. Lohmann, and G. Lesins. Ice nucleation of ammonia gas exposed montmorillonite mineral dust particles. *Atmospheric Chemistry and Physics*, 2007.

[133] Z. A. Kanji, A. Welti, C. Chou, O. Stetzer, and U. Lohmann. Laboratory studies of immersion and deposition mode ice nucleation of ozone aged mineral dust particles. *Atmospheric Chemistry and Physics*, 2013.

[134] A. Kumar, C. Marcolli, B. Luo, and T. Peter. Ice nucleation activity of silicates and aluminosilicates in pure water and aqueous solutions - Part 1: The K-feldspar microcline. *Atmospheric Chemistry and Physics*, 2018.

[135] B. G. Pummer, C. Budke, S. Augustin-Bauditz, D. Niedermeier, L. Felgitsch, C. J. Kampf, R. G. Huber, K. R. Liedl, T. Loerting, T. Moschen, M. Schauperl, M. Tollinger, C. E. Morris, H. Wex, H. Grothe, U. Pöschl, T. Koop, and J. Fröhlich-Nowoisky. Ice nucleation by water-soluble macromolecules. *Atmospheric Chemistry and Physics*, 2015.

[136] M. Joly, P. Amato, L. Deguillaume, M. Monier, C. Hoose, and A. M. Delort. Quantification of ice nuclei active at near 0 °c temperatures in low-altitude clouds at the Puy de Dôme atmospheric station. *Atmospheric Chemistry and Physics*, 2014.

[137] P. Amato, M. Joly, C. Schaupp, E. Attard, O. Möhler, C. E. Morris, Y. Brunet, and A. M. Delort. Survival and ice nucleation activity of bacteria as aerosols in a cloud simulation chamber. *Atmospheric Chemistry and Physics*, 2015.

[138] H. A. Constantinidou. Atmospheric dispersal of ice nucleation-active bacteria: The role of rain. 80:934, 1990.

[139] O. Möhler, S. Benz, H. Saathoff, M. Schnaiter, R. Wagner, J. Schneider, S. Walter, V. Ebert, and S. Wagner. The effect of organic coating on the heterogeneous ice nucleation efficiency of mineral dust aerosols. *Environmental Research Letters*, 2008.

[140] C. E. Morris, F. Conen, Alex H. J., V. Phillips, U. Pöschl, and D. C. Sands. Bioprecipitation: A feedback cycle linking Earth history, ecosystem dynamics and land use through biological ice nucleators in the atmosphere. *Global Change Biology*, 2014.

[141] J. Fröhlich-Nowoisky, T. C. J. Hill, B. G. Pummer, P. Yordanova, G. D. Franc, and U. Pöschl. Ice nucleation activity in the widespread soil fungus Mortierella alpina. *Biogeosciences*, 2015.

[142] S. Pouleur, C. Richard, J.-G. Martin, and H. Antoun. Ice Nucleation Activity in Fusarium acuminatum and Fusarium avenaceumt. pages 2960–2964, 1992.

[143] S. Augustin, H. Wex, D. Niedermeier, B. Pummer, H. Grothe, S. Hartmann, L. Tomsche, T. Clauss, J. Voigtländer, K. Ignatius, and F. Stratmann. Immersion freezing of birch pollen washing water. *Atmospheric Chemistry and Physics*, 2013.

[144] B. G. Pummer, H. Bauer, J. Bernardi, S. Bleicher, and H. Grothe. Suspendable macromolecules are responsible for ice nucleation activity of birch and conifer pollen. *Atmospheric Chemistry and Physics*, 2012.

[145] S. Hartmann, S. Augustin, T. Clauss, J. Voigtländer, D. Niedermeier, H. Wex, and F. Stratmann. Immersion freezing of ice nucleating active protein complexes. *Atmospheric Chemistry and Physics Discussions*, 2012.

[146] S. Augustin-Bauditz, H. Wex, C. Denjean, S. Hartmann, J. Schneider, S. Schmidt, M. Ebert, and F. Stratmann. Laboratory-generated mixtures of mineral dust particles with biological substances: Characterization of the particle mixing state and immersion freezing behavior. *Atmospheric Chemistry and Physics*, 2016.

[147] R. B. Rangel-Alvarado, Y. Nazarenko, and P. A. Ariya. Snow-borne nanosized particles: Abundance, distribution, composition, and significance in ice nucleation processes. *J. Geophys. Res. Atmos.*, 120(22):760–11, 2015.

[148] W. D. Hamilton and T. M. Lenton. Spora and Gaia: how microbes fly with their clouds. *Ethology Ecology & Evolution*, 10(1):1–16, 1998.

[149] J. Vergara-Temprado, B. J. Murray, T. W. Wilson, D. O'Sullivan, J. Browse, K. J. Pringle, K. Ardon-Dryer, A. K. Bertram, S. M. Burrows, D. Ceburnis, P. J. Demott, R. H. Mason, C. D. O'Dowd, M. Rinaldi, and K. S. Carslaw. Contribution of feldspar and marine organic aerosols to global ice nucleating particle concentrations. *Atmospheric Chemistry and Physics*, 2017.

[150] W. T. K. Huang, L. Ickes, I. Tegen, M. Rinaldi, D. Ceburnis, and U. Lohmann. Global relevance of marine organic aerosols as ice nucleating particles. *Atmospheric Chemistry and Physics Discussions*, 2017:1–34, 2017.

[151] S. M. Burrows, W. Elbert, M. G. Lawrence, and U. Pöschl. Bacteria in the global atmosphere - Part 1: Review and synthesis of literature data for different ecosystems. 2009.

[152] A. Sesartic, U. Lohmann, and T. Storelvmo. Bacteria in the ECHAM5-HAM global climate model. *Atmospheric Chemistry and Physics*, 2012.

[153] V. E. Irish, P. Elizondo, J. Chen, C. Chou, J. Charette, M. Lizotte, L. A. Ladino, T. W. Wilson, M. Gosselin, B. J. Murray, E. Polishchuk, J. P. D. Abbatt, L. A. Miller, and A. K. Bertram. Ice-nucleating particles in canadian arctic sea-surface microlayer and bulk seawater. *Atmospheric Chemistry and Physics*, 17(17):10583–10595, 2017.

[154] C. S. McCluskey, J. Ovadnevaite, M. Rinaldi, J. Atkinson, F. Belosi, D. Ceburnis, S. Marullo, T. C. J. Hill, U. Lohmann, Z. A. Kanji, C. O'Dowd, S. M. Kreidenweis, and P. J. DeMott. Marine and Terrestrial Organic Ice-Nucleating Particles in Pristine Marine to Continentally Influenced Northeast Atlantic Air Masses. *Journal of Geophysical Research: Atmospheres*, 123(11):6196–6212.

[155] G. Vali. *The Third International Workshop on Ice Nucleus Measurements*. University of Wyoming, 1976.

[156] B. J. Mason. The physics of clouds. Clarendon press: Oxford university press, (2nd ed.), 1971. *Quarterly Journal of the Royal Meteorological Society* :98(417):708-708.

[157] N. Hiranuma, S. Augustin-Bauditz, H. Bingemer, C. Budke, J. Curtius, A. Danielczok, K. Diehl, K. Dreischmeier, M. Ebert, F. Frank, N. Hoffmann, K. Kandler, A. Kiselev, T. Koop, T. Leisner, O. Möhler, B. Nillius, A. Peckhaus, D. Rose, S. Weinbruch, H. Wex, Y. Boose, P. J. Demott, J. D. Hader, T. C.J. Hill, Z. A. Kanji, G. Kulkarni, E. J.T. Levin, C. S. McCluskey, M. Murakami, B. J. Murray, D. Niedermeier, M. D. Petters, D. O'Sullivan, A. Saito, G. P. Schill, T. Tajiri, M. A. Tolbert, A. Welti, T. F. Whale, T. P. Wright, and K. Yamashita. A comprehensive laboratory study on the immersion freezing behavior of illite NX particles: A comparison of 17 ice nucleation measurement techniques. *Atmospheric Chemistry and Physics*, 2015.

[158] B. J. Murray, D. O'Sullivan, J. D. Atkinson, and M. E. Webb. Ice nucleation by particles immersed in supercooled cloud droplets. 2012.

[159] F. Belosi, M. Piazza, A. Nicosia, and G. Santachiara. Influence of supersaturation on the concentration of ice nucleating particles. *Tellus B: Chemical and Physical Meteorology*, 70(1):1454809, 2018.

[160] N. Sabbagh-Kupelwieser, A. Maisser, and W. W. Szymanski. From micro- to nanosized particles: Selected characterization methods and measurable parameters. *Particuology*, 9(3):193–203, 2011.

[161] H. Grimm and D. J. Eatough. Aerosol measurement: The use of optical light scattering for the determination of particulate size distribution, and particulate mass, including the semi-volatile fraction. *Journal of the Air and Waste Management Association*, 2009.

[162] A. Nicosia, L. Manodori, A. Trentini, I. Ricciardelli, D. Bacco, V. Poluzzi, L. Di Matteo, and F. Belosi. Field study of a soft x-ray aerosol neutralizer combined with electrostatic classifiers for nanoparticle size distribution measurements. 37, 2017.

[163] J. T Jayne, D. C. Leard, X. Zhang, P. Davidovits, K. A. Smith, C. E. Kolb, and D. R. Worsnop. Development of an Aerosol Mass Spectrometer for Size and Composition Analysis of Submicron Particles. *Aerosol Science & Technology*, 33:49–70, 2000.

[164] J. L. Jimenez, J. T. Jayne, Q. Shi, C. E. Kolb, D. R. Worsnop, I. Yourshaw, J. H. Seinfeld, R. C. Flagan, X. Zhang, K. A. Smith, J. W. Morris, and P. Davidovits. Ambient aerosol sampling using the Aerodyne Aerosol Mass Spectrometer. *J. Geophys. Res*, 108(D7):8425, 2003.

[165] J. D. Allan, M. R. Alfarra, K. N. Bower, P. I. Williams, M. W. Gallagher, J. L. Jimenez, A. G. Mcdonald, E. Nemitz, M. R Canagaratna, J. T. Jayne, H. Coe, and D. R. Worsnop. Quantitative sampling using an Aerodyne aerosol mass spectrometer 2. Measurements of fine particulate chemical composition in two U.K. cities. *J. Geophys. Res*, 108(D3):4091, 2003.

[166] J. D. Allan, A. E. Delia, H. Coe, K. N. Bower, M. R. Alfarra, J. L. Jimenez, A. M. Middlebrook, F. Drewnick, T. B. Onasch, M. R. Canagaratna, Jo. T. Jayne, and D. R. Worsnop. A generalised method for the extraction of chemically resolved mass spectra from Aerodyne aerosol mass spectrometer data. *Journal of Aerosol Science*, 35(7):909–922, 2004.

[167] F. Conen, C. E. Morris, J. Leifeld, M. V. Yakutin, and C. Alewell. Biological residues define the ice nucleation properties of soil dust. *Atmospheric Chemistry and Physics*, 11(18):9643–9648, 2011.

[168] M. Joly, E. Attard, M. Sancelme, L. Deguillaume, C. Guilbaud, C. E. Morris, P. Amato, and A. M. Delort. Ice nucleation activity of bacteria isolated from cloud water. *Atmospheric Environment*, 2013.

[169] E. Stopelli, F. Conen, C. Guilbaud, J. Zopfi, C. Alewell, and C. E. Morris. Ice nucleators, bacterial cells and pseudomonas syringae in precipitation at jungfraujoch. *Biogeosciences*, 14(5):1189–1196, 2017.

[170] G. Pouzet, E. Peghaire, M. Aguès, J. L. Baray, F. Conen, and P. Amato. Atmospheric processing and variability of biological ice nucleating particles in precipitation at Opme, France. *Atmosphere*, 2017.

[171] E. Stopelli, F. Conen, L. Zimmermann, C. Alewell, and C. E. Morris. Freezing nucleation apparatus puts new slant on study of biological ice nucleators in precipitation. *Atmospheric Measurement Techniques*, 7(1):129–134, 2014.

[172] D. K. Perovich. Complex yet translucent: the optical properties of sea ice. *Physica B: Condensed Matter*, 338(1-4):107–114, 2003.

[173] G. Vali. Quantitative evaluation of experimental results an the heterogeneous freezing nucleation of supercooled liquids. *Journal of the Atmospheric Sciences*, 28(3):402–409, 1971.

[174] J. Schrod, A. Danielczok, D. Weber, M. Ebert, E. S. Thomson, and H. G. Bingemer. Re-evaluating the Frankfurt isothermal static diffusion chamber for ice nucleation. *Atmospheric Measurement Techniques*, 2016.

[175] F. Belosi, G. Santachiara, and F. Prodi. Ice-forming nuclei in Antarctica: New and past measurements. *Atmospheric Research*, 2014.

[176] F. Belosi, M. Rinaldi, S. Decesari, L. Tarozzi, A. Nicosia, and G. Santachiara. Ground level ice nuclei particle measurements including Saharan dust events at a Po Valley rural site (San Pietro Capofiume, Italy). *Atmospheric Research*, 2017.

[177] M. Rinaldi, G. Santachiara, A. Nicosia, M. Piazza, S. Decesari, S. Gilardoni, M. Paglione, P. Cristofanelli, A. Marinoni, P. Bonasoni, and F. Belosi. Atmospheric Ice Nucleating Particle measurements at the high mountain observatory Mt. Cimone (2165 m a.s.l., Italy). *Atmospheric Environment*, 2017.

[178] A. Nicosia, M. Piazza, G. Santachiara, and F. Belosi. Heterogeneous nucleation of ice in the atmosphere. In *Journal of Physics: Conference Series*, 2017.

[179] P. J. DeMott, O. Möhler, D. J. Cziczo, N. Hiranuma, M. D. Petters, S. S. Petters, F. Belosi, Bingemer H. G., S. D. Brooks, C. Budke, M. Burkert-Kohn, K. N. Collier, A. Danielczok, O. Eppers, L. Felgitsch, S. Garimella, H. Grothe, P. Herenz, T. C. J. Hill, K. Höhler, Z. A. Kanji, A. Kiselev, T. Koop, T. B. Kristensen, K. Krüger, G. Kulkarni, E. J. T. Levin, B. J. Murray, A. Nicosia, D. O'Sullivan, A. Peckaus, M.J. Polen, H. C. Price, N. Reicher, D. A. Rothenberg, Y. Rudich, G. Santachiara, T. Schiebel, J. Schrod, T. M. Seifried, F. Stratmann, R.C. Sullivan, K. J. Suski, M. Szakáll, H. P. Taylor, R. Ullrich, J. Vergara-Temprado, R. Wagner, T. F. Whale, D. Weber, A. Welti, T. W. Wilson, and M. J.and Zenker J. Wolf. Overview of results from the fifth international workshop on ice nucleation part 2 (fin-02): Laboratory intercomparisons of ice nucleation measurements. *Atmospheric Measurement Techniques Discussions*, 2018:1–44, 2018.

[180] G. Santachiara, L. Di Matteo, F. Prodi, and F. Rinaldi2017. Atmospheric particles acting as Ice Forming Nuclei in different size ranges. *Atmospheric Research*, 2010.

[181] G. Santachiara, F. Belosi, and F. Prodi. Ice crystal precipitation at Dome C site (East Antarctica). *Atmospheric Research*, 2016.

[182] G. Santachiara, F. Prodi, A. Nicosia, and F. Belosi. Discrepancy between Ice Particles and Ice Nuclei in Mixed Clouds: Critical Aspects. 7:287–297, 2017.

[183] H. M. Jones, M. J. Flynn, P. J. Demott, and O. Möhler. Manchester Ice Nucleus Counter (MINC) measurements from the 2007 International workshop on Comparing Ice nucleation Measuring Systems (ICIS-2007). *Atmospheric Chemistry & Physics*, 11:53–65, 2011.

[184] F. Belosi, J. Schrod, A. Nicosia, G. Santachiara, F. Prodi, D. Weber, and H. Bingemer. Off line-measurement of ice-nucleating particles, *EAC European Aerosol Conference, Tours France, September 4-9, 2016*, Poster presentation number P1-AAS-AAP-077.

[185] U. Baltensperger, H. W. Gäggeler, D. T. Jost, M. Lugauer, M. Schwikowski, E. Weingartner, and P. Seibert. Aerosol climatology at the high-alpine site Jungfraujoch, Switzerland. *Journal of Geophysical Research: Atmospheres*, 1997.

[186] P. Bonasoni, F. Evangelisti, U. Bonafe, F. Ravegnani, F. Calzolari, A. Stohl, L. Tositti, O. Tubertini, and T. Colombo. Stratospheric ozone intrusion episodes recorded at Mt. Cimone during the VOTALP project: Case studies. *Atmospheric Environment*, 2000.

[187] M. Lugauer, U. Baltensperger, M. Furger, H. W. Gäggeler, D. T. Jost, S. Nyeki, and M. Schwikowski. Influences of vertical transport and scavenging on aerosol particle surface area and radon decay product concentrations at the Jungfraujoch (3454 m above sea level). *Journal of Geophysical Research Atmospheres*, 2000.

[188] A. Marinoni, P. Cristofanelli, F. Calzolari, F. Roccato, U. Bonafè, and P. Bonasoni. Continuous measurements of aerosol physical parameters at the Mt. Cimone GAW Station (2165 m asl, Italy). *Science of The Total Environment*, 391(2-3):241–251, 2008.

[189] J. Schrod, D. Weber, J. Drücke, C. Keleshis, M. Pikridas, M. Ebert, B. Cvetković, S. Nickovic, E. Marinou, H. Baars, A. Ansmann, M. Vrekoussis, N. Mihalopoulos, J. Sciare, J. Curtius, and H. G. Bingemer. Ice nucleating particles over the Eastern Mediterranean measured by unmanned aircraft systems. *Atmospheric Chemistry and Physics*, 17(7), 2017.

[190] A. Gagin. The Ice Phase in Winter Continental Cumulus Clouds. *Journal of the Atmospheric Sciences*, 32(8):1604–1614, 1975.

[191] Y. Levi and D. Rosenfeld. Ice Nuclei, Rainwater Chemical Composition, and Static Cloud Seeding Effects in Israel. *Journal of Applied Meteorology*, 35(9), 1996.

[192] K. Ardon-Dryer and Z. Levin. Ground-based measurements of immersion freezing in the eastern Mediterranean. *Atmospheric Chemistry and Physics*, 2014.

[193] M. Rinaldi, A. Nicosia, G. Santachiara, S. Decesari, M. Paglione, S. Sandrini, S. Gilardoni, P. Cristofanelli, A. Marinoni, P. Bonasoni, M. C. Facchini, and F. Belosi. Ice Nuclei measurements across Europe within BACCHUS, 2017.

[194] P. Cristofanelli, T.C. Landi, F. Calzolari, R. Duchi, A. Marinoni, M. Rinaldi, and P. Bonasoni. Summer atmospheric composition over the Mediterranean basin: Investigation on transport processes and pollutant export to the free troposphere by observations at the WMO/GAW Mt. Cimone global station (Italy, 2165 m a.s.l.). *Atmospheric Environment*, 141:139–152, 2016.

[195] E. K. Bigg. Measurement of concentrations of natural ice nuclei. *Atmospheric Research*, 25(5):397–408, 1990.

[196] E. K. Bigg, S. C. Mossop, R. T. Meade, and N. S. C. Thorndike. The Measurement of Ice Nucleus Concentrations by Means of Millipore Filters. *Journal of Applied Meteorology*, 2(2):266–269, 1963.

[197] G. G. Lala and J. E. Jiusto. Numerical Estimates of Humidity in a Membrane–Filter Ice Nucleus Chamber. *Journal of Applied Meteorology*, 11(4):674–683, 1972.

[198] C. M. Stevenson. An improved millipore filter technique for measuring the concentrations of freezing nuclei in the atmosphere. *Quarterly Journal of the Royal Meteorological Society*, 94(399):35–43, 1968.

[199] D. A. Knopf and T. Koop. Heterogeneous nucleation of ice on surrogates of mineral dust. *Journal of Geophysical Research Atmospheres*, 2006.

[200] B. Wang and D. A. Knopf. Heterogeneous ice nucleation on particles composed of humic-like substances impacted by O3. *Journal of Geophysical Research Atmospheres*, 2011.

[201] B. Wang, A. Laskin, T. Roedel, M. K. Gilles, R. C. Moffet, A. V. Tivanski, and D. A. Knopf. Heterogeneous ice nucleation and water uptake by field-collected atmospheric particles below 273 K. *Journal of Geophysical Research Atmospheres*, 2012.

[202] R. C. Schnell, R. F. Pueschel, and D. L. Wellman. Ice nucleus characteristics of Mount St. Helens effluents. *Journal of Geophysical Research: Oceans*, 87(C13):11109–11112, 1982.

[203] Jiang, H., Y. Yin, and Yang, L., and Yang, S., Su, H., and Chen, K. The characteristics of atmospheric ice nuclei measured at different altitudes in the Huangshan Mountains in Southeast China. *Advances in Atmospheric Sciences*, 31(2):396–406, 2014.

[204] F. Conen, S. Rodríguez, C. Hüglin, S. Henne, E. Herrmann, N. Bukowiecki, and C. Alewell. Atmospheric ice nuclei at the high-altitude observatory Jungfraujoch, Switzerland. *Tellus, Series B: Chemical and Physical Meteorology*, 2015.

[205] R. J. Cotton and P. R. Field. Ice nucleation characteristics of an isolated wave cloud. *Quarterly Journal of the Royal Meteorological Society*, 2002.

[206] P. R. Field, R. J. Cotton, D. Johnson, K. Noone, P. Glantz, P. H. Kaye, E. Hirst, R. S. Greenaway, C. Jost, R. Gabriel, T. Reiner, M. Andreae, C. P. R. Saunders, A. Archer, T. Choularton, M. Smith, B. Brooks, C. Hoell, B. Bandy, and A. Heymsfield. Ice nucleation in orographic wave clouds: Measurements made during INTACC. *Quarterly Journal of the Royal Meteorological Society*, 127(575):1493–1512, 2001.

[207] J. Rosinski and G. Morgan. Cloud condensation nuclei as a source of ice-forming nuclei in clouds. *Journal of Aerosol Science*, 22(2):123–133, 1991.

[208] J. Bertrand, J. Baudet, and J. Dessens. Seasonal Variations and Frequency Distributions of Ice Nuclei Concentrations at Abidjan, West Africa. *Journal of Applied Meteorology*, 12(7):1191–1195, 1973.

[209] E. K. Bigg and G. T. Miles. The Results of Large–Scale Measurements of Natural Ice Nuclei. *Journal of the Atmospheric Sciences*, 21(4):396–403, 1964.

[210] H. Jiang, Y. Yin, H. Su, Y. Shan, and R. Gao. The characteristics of atmospheric ice nuclei measured at the top of Huangshan (the Yellow Mountains) in Southeast China using a newly built static vacuum water vapor diffusion chamber. *Atmospheric Research*, 2015.

[211] P. V. Hobbs and J. D. Locatelli. Ice Nucleus Measurements at Three Sites in Western Washington. *Journal of the Atmospheric Sciences*, 27(1):90–100, 1970.

[212] B. F. Ryan and W. D. Scott. Ice Nuclei and the Onset of Rainfall. *Journal of the Atmospheric Sciences*, 26(3):611–612, 1969.

[213] E. K. Bigg, S. Soubeyrand, and C. E. Morris. Persistent after-effects of heavy rain on concentrations of ice nuclei and rainfall suggest a biological cause. *Atmospheric Chemistry and Physics*, 2015.

[214] J. A. Huffman, A. J. Prenni, P. J. Demott, C. Pöhlker, R. H. Mason, N. H. Robinson, J. Fröhlich-Nowoisky, Y. Tobo, V. R. Després, E. Garcia, D. J. Gochis, E. Harris, I. Müller-Germann, C. Ruzene, B. Schmer, B. Sinha, D. A. Day, M. O. Andreae, J. L. Jimenez, M. Gallagher, S. M. Kreidenweis, A. K. Bertram, and U. Pöschl. High concentrations of biological aerosol particles and ice nuclei during and after rain. *Atmospheric Chemistry and Physics*, 2013.

[215] A. J. Prenni, Y. Tobo, E. Garcia, P. J. DeMott, J. A. Huffman, C. S. McCluskey, S. M. Kreidenweis, J. E. Prenni, C. Pöhlker, and U. Pöschl. The impact of rain on ice nuclei populations at a forested site in Colorado. *Geophysical Research Letters*, 2013.

[216] K. Hara, T. Maki, F. Kobayashi, M. Kakikawa, M. Wada, and A. Matsuki. Variations of ice nuclei concentration induced by rain and snowfall within a local forested site in Japan. *Atmospheric Environment*, 127:1–5, 2016.

[217] R. C. Schnell and G. Vali. Atmospheric Ice Nuclei from Decomposing Vegetation. *Nature*, 236:163, 1972.

[218] A. L. Buck. New equations for computing vapor pressure and enhancement factor. *Journal of Applied Meteorology*, 20:1527–1532, 1981.

[219] J. M. Prospero. Long-range transport of mineral dust in the global atmosphere: Impact of african dust on the environment of the southeastern united states. *Proceedings of the National Academy of Sciences*, 104:15917–15927, 1999.

[220] Z. Levin, A. Teller, E. Ganor, and Y. Yin. On the interactions of mineral dust, sea-salt particles, and clouds: A measurement and modeling study from the Mediterranean Israeli Dust Experiment campaign. *Journal of Geophysical Research D: Atmospheres*, 2005.

[221] S. Henne, M. Furger, and A. S. H. Prévôt. Climatology of mountain venting-induced elevated moisture layers in the lee of the alps. *Journal of Applied Meteorology*, 44(5):620–633, 2005.

[222] C. Carbone, S. Decesari, M. Paglione, L. Giulianelli, M. Rinaldi, A. Marinoni, P. Cristofanelli, A. Didiodato, P. Bonasoni, S. Fuzzi, and M. C. Facchini. 3-year chemical composition of free tropospheric pm1 at the mt. cimone gaw global station – south europe – 2165 m a.s.l. *Atmospheric Environment*, 87:218–227, 2014.

[223] M. Rinaldi, S. Gilardoni, M. Paglione, S. Sandrini, S. Fuzzi, P. Massoli, P. Bonasoni, P. Cristofanelli, A. Marinoni, V. Poluzzi, and S. Decesari. Organic aerosol evolution and transport observed at mt. cimone (2165 m a.s.l.), italy, during the pegasos campaign. *Atmospheric Chemistry and Physics*, 2015.

[224] I. Ricciardelli, D. Bacco, M. Rinaldi, G. Bonafè, F. Scotto, A. Trentini, G. Bertacci, P. Ugolini, C. Zigola, F. Rovere, C. Maccone, C. Pironi, and V. Poluzzi. A three-year investigation of daily pm2.5 main chemical components in four sites: the routine measurement program of the supersito project (po valley, italy). *Atmospheric Environment*, 152:418–430, 2017.

[225] W. T. Morgan, J. D. Allan, K. N. Bower, E. J. Highwood, D. Liu, G. R. McMeeking, M. J. Northway, P. I. Williams, R. Krejci, and H. Coe. Airborne measurements of the spatial distribution of aerosol chemical composition across europe and evolution of the organic fraction. *Atmospheric Chemistry and Physics*, 10:4065–4083, 2010.

[226] A. F. Stein, R. R. Draxler, G. D. Rolph, B. J.B. Stunder, M. D. Cohen, and F. Ngan. Noaa's hysplit atmospheric transport and dispersion modeling system. 2015.

[227] G. Rolph, A. Stein, and B. Stunder. Real-time Environmental Applications and Display sYstem: READY. *Environmental Modelling & Software*, 95:210–228, 2017.

[228] A. J. Prenni, J. Y. Harrington, T. Michael, P. J. DeMott, A. Avramov, C. N. Long, S. M. Kreidenweis, P. Q. Olsson, and J. Verlinde. Can ice-nucleating aerosols affect arctic seasonal climate? *Bulletin of the American Meteorological Society*, 88(4):541–550, 2007.

[229] M. C. Serreze and R. G. Barry. Processes and impacts of Arctic amplification: A research synthesis. *Global and Planetary Change*, 77(1–2):85–96, 2011.

[230] J. E. Walsh. Intensified warming of the arctic: Causes and impacts on middle latitudes. *Global and Planetary Change*, 117:52–63, 2014.

[231] J. A. Curry, J. L. Schramm, and E. E. Ebert. Impact of clouds on the surface radiation balance of the Arctic Ocean. *Meteorology and Atmospheric Physics*, 51(3):197–217, 1993.

[232] J. E. Walsh and W. L. Chapman. Arctic cloud-radiation-temperature associations in observational data and atmospheric reanalyses. *Journal of Climate*, 1998.

[233] J. A. Screen and I. Simmonds. The central role of diminishing sea ice in recent Arctic temperature amplification. *Nature*, 464:1334, 2010.

[234] D. Ghatak and J. Miller. Implications for Arctic amplification of changes in the strength of the water vapor feedback. *Journal of Geophysical Research Atmospheres*, 2013.

[235] A. Costa, J. Meyer, A. Afchine, A. Luebke, G. Günther, J. R. Dorsey, M. W. Gallagher, A. Ehrlich, M. Wendisch, D. Baumgardner, H. Wex, and M. Krämer. Classification of arctic, midlatitude and tropical clouds in the mixed-phase temperature regime. *Atmospheric Chemistry and Physics*, 17(19):12219–12238, 2017.

[236] M. Wendisch, M. Brückner, J.P. Burrows, S. Crewell, K. Dethloff, K. Ebell, C. Lüpkes, A. Macke, J. Notholt, J. Quaas, A. Rinke, and I. Tegen. Understanding causes and effects of rapid warming in the arctic. *EOS*, 98. *Eos*, 98, 2017.

[237] National SOLAS networks 2017 annual reports and future activities.

[238] F. Vidussi, B. Mostajir, E. Fouilland, E. Le Floc'h, J. Nouguier, C. Roques, P. Got, D. Thibault-Botha, T. Bouvier, and M. Troussellier. Effects of experimental warming and increased ultraviolet b radiation on the mediterranean plankton food web. *Limnology and Oceanography*, 56(1):206–218.

[239] A. N. Schwier, C. Rose, E. Asmi, A. M. Ebling, W. M. Landing, S. Marro, M. L. Pedrotti, A. Sallon, F. Iuculano, S. Agusti, A. Tsiola, P. Pitta, J. Louis, C. Guieu, F. Gazeau, and K. Sellegri. Primary marine aerosol emissions from the Mediterranean Sea during pre-bloom and oligotrophic conditions: Correlations to seawater chlorophyll a from a mesocosm study. *Atmospheric Chemistry and Physics*, 2015.

[240] A. N. Schwier, K. Sellegri, S. Mas, B. Charrière, J. Pey, C. Rose, B. Temime-Roussel, J.-L. Jaffrezo, D. Parin, D. Picard, M. Ribeiro, G. Roberts, R. Sempéré, N. Marchand, and B. D'Anna. Primary marine aerosol physical flux and chemical composition during a nutrient enrichment experiment in mesocosms in the mediterranean sea. *Atmospheric Chemistry and Physics*, 17(23):14645–14660, 2017.

[241] E. Fuentes, H. Coe, D. Green, G. De Leeuw, G. McFiggans, and E. Fuentes Lopez. On the impacts of phytoplankton-derived organic matter on the properties of the primary marine aerosol - part 1: Source fluxes. *Atmospheric Chemistry and Physics*, 10(19):9295–9317, 2010.

[242] G. C. Roberts and A. Nenes. A continuous-flow streamwise thermal-gradient ccn chamber for atmospheric measurements. *Aerosol Science and Technology*, 39(3):206–221, 2005.

[243] M. Müller, C. George, and B. D'Anna. Enhanced spectral analysis of C-TOF Aerosol Mass Spectrometer data: Iterative residual analysis and cumulative peak fitting. *International Journal of Mass Spectrometry*, 306(1):1–8, 2011.

[244] R. C. Schnell. Ice nuclei produced by laboratory cultured marine phytoplankton. *Geophysical Research Letters*, 2(11):500–502, 1975.

[245] P. J. DeMott, T. C. J. Hill, C. S. McCluskey, K. A. Prather, D. B. Collins, R. C. Sullivan, M. J. Ruppel, R. H. Mason, V. E. Irish, T. Lee, C. Y. Hwang, T. S. Rhee, J. R. Snider,

G. R. McMeeking, S. Dhaniyala, E. R. Lewis, J. J. B. Wentzell, J. Abbatt, C. Lee, C. M. Sultana, A. P. Ault, J. L. Axson, M. Diaz Martinez, I. Venero, G. Santos-Figueroa, M. D. Stokes, G. B. Deane, O. L. Mayol-Bracero, V. H. Grassian, T. H. Bertram, A. K. Bertram, B. F. Moffett, and G. D. Franc. Sea spray aerosol as a unique source of ice nucleating particles. *Proceedings of the National Academy of Sciences*, 113(21):5797–5803.

[246] C. S. McCluskey, T. C. J. Hill, F. Malfatti, C. M. Sultana, C. Lee, M. V. Santander, C. M. Beall, K. A. Moore, G. C. Cornwell, D. B. Collins, K. A. Prather, T. Jayarathne, E. A. Stone, F. Azam, S. M. Kreidenweis, and P. J. DeMott. A dynamic link between ice nucleating particles released in nascent sea spray aerosol and oceanic biological activity during two mesocosm experiments. *Journal of the Atmospheric Sciences*, 74(1):151–166, 2017.

[247] X. Wang, G. B. Deane, K. A. Moore, O. S. Ryder, M. D. Stokes, C. M. Beall, D. B. Collins, M. V. Santander, S. M. Burrows, C. M. Sultana, and K. A. Prather. The role of jet and film drops in controlling the mixing state of submicron sea spray aerosol particles. *Proceedings of the National Academy of Sciences*, 2017.

[248] P. K. Quinn, D. B. Collins, V. H. Grassian, K. A. Prather, and T. S. Bates. Chemistry and Related Properties of Freshly Emitted Sea Spray Aerosol. 115(10):4383–4399, 2015.

[249] M. Ebert A. Worringen L. Schütz Zimmermann, F. and S. Weinbruch. Environmental scanning electron microscopy (ESEM) as a new technique to determine the ice nucleation capability of individual atmospheric aerosol particles. *Atmospheric Environment*, 41:8219–8227, 2007.

[250] D. A. Orsini, Y. Ma, A. Sullivan, B. Sierau, K. Baumann, and R. J. Weber. Refinements to the particle-into-liquid sampler (PILS) for ground and airborne measurements of water soluble aerosol composition. *Atmospheric Environment*, 37(9-10):1243–1259, 2003.

[251] R. C. Schnell and G. Vali. Freezing nuclei in marine waters. *Tellus*, 27(3):321–323, 1975.

[252] C. S. Mccluskey. *Evidence for a biological control on emissions of marine ice nucleating particles: laboratory, field and modeling results*. PhD thesis, Colorado State University, 2017.

[253] B. D. Johnson and P. J. Wangersky. Seawater filtration: Particle flow and impaction considerations. *Limnology and Oceanography*, 1985.

[254] M. C. Facchini, M. Rinaldi, S. Decesari, C. Carbone, E. Finessi, M. Mircea, S. Fuzzi, D. Ceburnis, R. Flanagan, E. D. Nilsson, G. de Leeuw, M. Martino, J. Woeltjen, and C. D. O'Dowd. Primary submicron marine aerosol dominated by insoluble organic colloids and aggregates. *Geophysical Research Letters*, 35(L17814), 2008.

[255] E. Fuentes, H. Coe, D. Green, G. De Leeuw, and G. McFiggans. Laboratory-generated primary marine aerosol via bubble-bursting and atomization. *Atmospheric Measurement Techniques*, 3(1):141–162, 2010.

[256] R. L. Modini, B. Harris, and Z. D. Ristovski. The organic fraction of bubble-generated, accumulation mode Sea Spray Aerosol (SSA). *Atmospheric Chemistry and Physics*, 2010.

[257] J. Zábori, M. Matisans, R. Krejci, E. D. Nilsson, and J. Ström. Artificial primary marine aerosol production: A laboratory study with varying water temperature, salinity, and succinic acid concentration. *Atmospheric Chemistry and Physics*, 2012.

[258] K. A. Prather, T. H. Bertram, V. H. Grassian, G. B. Deane, M. D. Stokes, P. J. DeMott, L. I. Aluwihare, B. P. Palenik, F. Azam, J. H. Seinfeld, R. C. Moffet, M. J. Molina, C. D. Cappa, F. M. Geiger, G. C. Roberts, L. M. Russell, A. P. Ault, J. Baltrusaitis, D. B. Collins, C. E. Corrigan, L. A. Cuadra-Rodriguez, C. J. Ebben, S. D. Forestieri, T. L. Guasco, S. P. Hersey, M. J. Kim, W. F. Lambert, R. L. Modini, W. Mui, B. E. Pedler, M. J. Ruppel, O. S. Ryder, N. G. Schoepp, R. C. Sullivan, and D. Zhao. Bringing the ocean into the laboratory to probe the chemical complexity of sea spray aerosol. *Proceedings of the National Academy of Sciences*, 2013.

[259] D. B. Collins, D. Zhao, M. J. Ruppel, G. B. Deane, M. D. Stokes, P. J. DeMott, C. Lee, R. L. Modini, L. M. Russell, and K. A. Prather. Evaluating the properties of sea spray aerosols produced in the laboratory: Comparisons with controlled breaking waves. *AIP Conference Proceedings*, 1527(551), 2013.

[260] C. O'Dowd, D. Ceburnis, J. Ovadnevaite, J. Bialek, D. B. Stengel, M. Zacharias, U. Nitschke, S. Connan, M. Rinaldi, S. Fuzzi, S. Decesari, M. C. Facchini, S. Marullo, R. Santoleri, A. Dell'Anno, C. Corinaldesi, M. Tangherlini, and R. Danovaro. Connecting marine productivity to sea-spray via nanoscale biological processes: Phytoplankton Dance or Death Disco? *Scientific Reports*, (5):14883, 2015.

[261] B. Gantt and N. Meskhidze. Wind speed dependent size-resolved parameterization for the organic enrichment of sea spray. *Atmospheric Chemistry and Physics Discussions*, 11:425–452, 2011.

[262] J. Ovadnevaite, D. Ceburnis, M. Canagaratna, H. Berresheim, J. Bialek, G. Martucci, D. R. Worsnop, and C. O'Dowd. On the effect of wind speed on submicron sea salt mass concentrations and source fluxes. *Journal of Geophysical Research Atmospheres*, 117(D16201), 2012.

[263] C. O'Dowd, M. C. Facchini, F. Cavalli, D. Ceburnis, M. Mircea, S. Decesari, S. Fuzzi, Y. J. Yoon, and J.-P. Putaud. Biogenically driven organic contributions to marine aerosol. *Nature*, (431):676–680, 2004.

[264] M. V. Orellana, P. A. Matrai, C. Leck, C. D. Rauschenberg, A. M. Lee, and E. Coz. Marine microgels as a source of cloud condensation nuclei in the high Arctic. *Proceedings of the National Academy of Sciences of the United States of America*, 108(33):13612–7, 2011.

[265] C. Oppo, S. Bellandi, N. Degli Innocenti, A. M. Stortini, G. Loglio, E. Schiavuta, and R. Cini. Surfactant components of marine organic matter as agents for biogeochemical

fractionation and pollutant transport via marine aerosols. *Marine Chemistry*, 63(3):235 – 253, 1999.

[266] M. E. Salter, E. Hamacher-Barth, C. Leck, J. Werner, C. M. Johnson, I. Riipinen, E. D. Nilsson, and P. Zieger. Calcium enrichment in sea spray aerosol particles. *Geophysical Research Letters*, 43(15):8277–8285, 2016.

[267] R. Cini, R. Udisti, G. Piccardi, G. Loglio, N. Degli Innocenti, A. M. Stortini, B. Pampaloni, and U. Tesei. A Simple Model for K and Ca Enrichment Interpretation in Antarctic Snow. *International Journal of Environmental Analytical Chemistry*, 71(3-4):265–287, 1998.

[268] K. Okada, Y. Ishizaka, T. Masuzawa, and K. Isono. Chlorine Deficiency in Coastal Aerosols. *Journal of the Meteorological Society of Japan*, 56(5):501–506.

[269] P. E. Wilkniss and D. J. Bressan. Fractionation of the Elements F, C1, Na, and K at the Sea-Air Interface. 77(27), 1972.

[270] N. Takegawa, Y. Miyazaki, Y. Kondo, Y. Komazaki, T. Miyakawa, J. L. Jimenez, J. T. Jayne, D. R. Worsnop, J. D. Allan, and R. J. Weber. Characterization of an Aerodyne Aerosol Mass Spectrometer (AMS): Intercomparison with other aerosol instruments. *Aerosol Science and Technology*, 39(8):760–770, 2005.

[271] F. Cavalli, M. Viana, K. E. Yttri, J. Genberg, and J. P. Putaud. Toward a standardised thermal-optical protocol for measuring atmospheric organic and elemental carbon: The EUSAAR protocol. *Atmospheric Measurement Techniques*, 3(1):79–89, 2010.

[272] G. Aymoz, J. L. Jaffrezo, D. Chapuis, J. Cozic, and W. Maenhaut. Seasonal variation of PM10main constituents in two valleys of the French Alps. I: EC/OC fractions. *Atmospheric Chemistry and Physics*, 7(3):661–675, 2007.

[273] M. Rinaldi, S. Decesari, E. Finessi, L. Giulianelli, C. Carbone, S. Fuzzi, C. D. O'Dowd, D. Ceburnis, and M. C. Facchini. Primary and Secondary Organic Marine Aerosol and Oceanic Biological Activity: Recent Results and New Perspectives for Future Studies. *Advances in Meteorology*, 2010(ID:310682):10 pages, 2010.

[274] A. Karanasiou, E. Diapouli, F. Cavalli, K. Eleftheriadis, M. Viana, A. Alastuey, X. Querol, and C. Reche. On the quantification of atmospheric carbonate carbon by thermal/optical analysis protocols. *Atmospheric Measurement Techniques*, 4:2409–2419, 2011.

[275] M. Trainic, I. Koren, S. Sharoni, M. Frada, L. Segev, Y. Rudich, and A. Vardi. Infection Dynamics of a Bloom-Forming Alga and Its Virus Determine Airborne Coccolith Emission from Seawater. *iScience*, 2018.

[276] C. S. Mccluskey, P. J. Demott, T. C. J. Hill, A. Rauker, J. Ovadnevaite, D. Ceburnis, C. O'Dowd, R. Humphries, M. Keywood, A. Protat, M. Harvey, E. R. Lewis, C. Y. Hwang, T. Lee, and S. M. Kreidenweis. Abundance and characteristics of ice nucleating particles in remote coastal and oceanic regions. *Proceedings of the 20th International Conference on Nucleation and Atmospheric Aerosols, 25-30.6.2017, Helsinki*, pages 255–257, 2017.

[277] P. A. Baron and K. Willeke. Aerosol measurement : principles, techniques, and applications , 2nd Edition. 2005.

[278] J. Vergara-Temprado, B. J. Murray, T. W. Wilson, D. O'Sullivan, J. Browse, K. J. Pringle, K. Ardon-Dryer, A. K. Bertram, S. M. Burrows, D. Ceburnis, P. J. Demott, R. H. Mason, C. D. O'Dowd, M. Rinaldi, and K. S. Carslaw. Contribution of feldspar and marine organic aerosols to global ice nucleating particle concentrations. *Atmospheric Chemistry and Physics*, 17(5):3637–3658, 2017.

[279] U. Lohmann, M. Burkert, A. Ansmann, C. Facchini, M. Kanakidou, P. Stier, R. Makkonen, J. Schmale, A. Gilgen, G. Eirund, A. Welti, M. Sporre, and T. Berntsen. *BACCHUS Impact of Biogenic versus Anthropogenic emissions on Clouds and Climate: towards a Holistic UnderStanding.* Project ID: 603445. Deliverable number D5.8: Final summary for policy makers. Technical report, 2018.

[280] E. Bodenschatz, S. P. Malinowski, R. A. Shaw, and F. Stratmann. Can we understand clouds without turbulence? *Science,* 327(5968):970-971. 2010.

[281] M. Rinaldi, F. Belosi, A. Nicosia, G. Santachiara, S. Decesari, and M. C. Facchini. Ice Nucleating Particles at Mace Head during the 2015 BACCHUS campaign through off-line measurements. *Geophysical Research Abstracts*, 18:12160, 2016.

[282] M. Rinaldi, S. Gilardoni, M. Paglione, S. Sandrini, S. Decesari, N. Z., A. Marinoni, P. Cristofanelli, P. Bonasoni, P. Ielpo, K. Fossum, G. P. Gobbi, and M. C. Facchini. Physico-chemical characterization of Mediterranean background aerosol at the Capogranitola observatory (Sicily). *Geophysical Research Abstracts*, 19:16201, 2017.

[283] W.-C. Chin, M. V. Orellana, and P. Verdugo. Spontaneous assembly of marine dissolved organic matter into polymer gels. *Nature*, 391:568–572, 1998.

[284] E. Attard, H. Yang, A. M. Delort, P. Amato, U. Pöschl, C. Glaux, T. Koop, and C. E. Morris. Effects of atmospheric conditions on ice nucleation activity of Pseudomonas. *Atmospheric Chemistry and Physics*, 12(22):10667–10677, 2012.

[285] T. Storelvmo and I. Tan. The Wegener-Bergeron-Findeisen process - Its discovery and vital importance for weather and climate. *Meteorologische Zeitschrift*, 24(4):455–461, 2015.

[286] J. R. Snider and M. D. Petters. Optical particle counter measurement of marine aerosol hygroscopic growth. *Atmospheric Chemistry and Physics*, 8(7):1949–1962, 2008.

[287] P. Zieger, O. Väisänen, J. C. Corbin, D. G. Partridge, S. Bastelberger, M. Mousavi-Fard, B. Rosati, M. Gysel, U. K. Krieger, C. Leck, A. Nenes, I. Riipinen, A. Virtanen, and M. E. Salter. Revising the hygroscopicity of inorganic sea salt particles. *Nature Communications*, 8:15883, 2017.